NASA CONTRACTOR REPORT

NASA CR-1297

NASA CR-1297

MODEL TESTS OF JET-INDUCED LIFT EFFECTS ON A VTOL AIRCRAFT IN HOVER

by P. K. Shumpert and J. G. Tibbetts

Prepared by
LOCKHEED-GEORGIA COMPANY
Marietta, Ga.
for Langley Research Center

NATIONAL AERONAUTICS AND SPACE ADMINISTRATION • WASHINGTON, D. C. • MARCH 1969

NASA CR-1297

MODEL TESTS OF JET-INDUCED LIFT EFFECTS ON A VTOL AIRCRAFT IN HOVER

By P. K. Shumpert and J. G. Tibbetts

Prepared under Contract No. NAS 1-7891 by
LOCKHEED-GEORGIA COMPANY
Marietta, Ga.

for Langley Research Center

NATIONAL AERONAUTICS AND SPACE ADMINISTRATION

For sale by the Clearinghouse for Federal Scientific and Technical Information
Springfield, Virginia 22151 – CFSTI price $3.00

Page Intentionally Left Blank

Page Intentionally Left Blank

ABSTRACT

Lift losses and jet decay profiles were measured for 18 nozzle configurations and various airframe configurations at nozzle pressure ratios from 1.4 to 2.3 and at heights from landing gear height to infinity. Outboard-hinged nozzle doors greatly increased the lift losses except near the ground. Increasing nozzle lateral spacing reduced the near-ground losses. Other changes had lesser lift effects.

The lift losses out of ground effect correlated well with a jet decay parameter which reflected the amount of jet mixing and the corresponding strength of the induced flow field. After correcting for the effects of differences in the jet decay parameter, the results of the present tests also correlated well with the results of a previous NASA test program (NASA TN D-3166) which used a similar model.

Page Intentionally Left Blank

MODEL TESTS OF JET-INDUCED LIFT EFFECTS

ON A VTOL AIRCRAFT IN HOVER

by P. K. Shumpert and J. G. Tibbetts
Lockheed-Georgia Company

SUMMARY

Jet-induced interference effects were investigated for a jet aircraft in hovering flight using a scale model with numerous nozzle configurations and model components. Interference loads and jet decay data were obtained in and out of ground effect to determine the effects of various parameters on interference loads and to assess a technique for correlating lift loss with jet decay characteristics.

Most of the configurations showed a lift loss out of ground effect of approximately 2 to 3 percent. Of the nozzle parameters and airframe components tested, nozzle lateral spacing and the addition of outboard-hinged nozzle doors had the greatest effect on lift interference.

It was found that lift losses could be correlated using an empirical expression based on the maximum jet decay rate, the jet length to the point of maximum decay rate, and the planform-to-total-nozzle area ratio. The correlation, however, was quite sensitive to the fairing of the velocity-distance curve in the region of the maximum decay rate. The scatter could be reduced materially by refairings that are still consistent with the measured data.

INTRODUCTION

To evaluate the performance of a proposed jet VTOL aircraft, detailed knowledge is required of the losses in thrust due to the powerplant installation in the airframe. These losses include those common to conventional jet aircraft such as inlet and nozzle losses, plus losses due to hot gas ingestion and to jet-induced lift loss. The purposes of the investigation reported herein were to provide additional experimental information on the jet-induced lift loss problem for a number of lift system arrangements and airframe configurations, and to correlate the lift losses with the jet decay characteristics downstream of the nozzles.

When a lifting jet discharges through the lower surface of a fuselage, a loss in lift is encountered with the aircraft out of ground effect. This is the result of a reduction in pressure over the aircraft lower fuselage, nacelle

and wing surfaces produced by the entrainment of ambient air by the exhaust jets. When in the proximity of the ground, both the sign and magnitude of the jet-induced lift loads depend on the aircraft height above the ground, on the aircraft external configuration, and on the lift system arrangement.

Investigations of jet-induced interference effects have been reported in references 1 through 8 for a number of aircraft configurations. However, a systematic investigation of the parameters believed to have a significant effect on VTOL aircraft lift performance has not previously been conducted.

The present investigation was accomplished using a scale model of a jet VTOL aircraft with a fuselage-mounted lift system with 18 nozzle configurations and various airframe configurations. The test program was designed to determine the effect of a number of parameters on lift interference both in and out of ground effect during hover conditions. The effect of nozzle pressure ratio at a constant nozzle area was one of the parameters investigated. In addition, nozzle geometry has been shown according to other investigators to be an important factor in determining VTOL lift loss. Consequently, the effects of nozzle out-board and aft inclination, number of nozzles, nozzle aspect ratio, aircraft-planform-to-nozzle area ratio, and nozzle spacing were investigated in this program. The effects of wing height relative to the lower surface of the fuselage and of flap deployment were also investigated. The effects of various airframe components (empennage, landing gear and doors, and nozzle closure doors) were also investigated since they affect the flow field around an aircraft and may have a significant effect on lift interference. Other parameters which were investigated include nozzle pressure ratio at constant thrust, nozzle area at constant nozzle pressure ratio, and roll and pitch attitudes.

The program was further designed to investigate the correlation between lift losses and jet decay characteristics. Reference 1 indicates that induced lift loss is a fairly simple function of the maximum jet decay rate, the jet length to the point of maximum decay rate, and the planform-to-total-nozzle area ratio, and shows that interference loads with different nozzle configurations and wing planforms can be correlated by a relationship involving these parameters. The present study indicates the applicability of this relationship to a wider range of configuration variables than have heretofore been investigated.

To determine the relationship between lift loss and jet decay profile, the decay pattern of the maximum dynamic pressure of the jet was measured for each nozzle configuration to a distance of about 10 equivalent nozzle diameters from the nozzles. For two of the nozzle configurations, the dynamic pressure decay profile was measured with the ground plane in place. The effect on interference loads of changing the jet decay profile by making internal changes upstream of the nozzle was also determined.

A substantial portion of the lift data presented herein were obtained during earlier Lockheed-sponsored tests in 1965. All of the jet decay data were obtained during the 1968 program. All tests covered a nozzle pressure ratio range of approximately 1.4 to 2.3. Lift, drag, and side force data were recorded out of ground effect and at height-to-wing-span ratios from 0.1 to 2.0.

SYMBOLS

Measurements for this investigation were taken in the U. S. Customary System of Units. Equivalent values are indicated herein in the International System. Details concerning the use of the International System, together with physical constants and conversion factors, are given in reference 9.

A_g area of gap between nozzles and fuselage, sq in. (sq cm)

A_j total nozzle area, sq in. (sq cm)

b wing span, in. (cm). b = 42.0 in. (107.0 cm), model scale

D diameter of individual nozzle, in. (cm)

D_e equivalent diameter of total nozzle area, in. (cm)

h height, normal to ground plane, to intersection of resultant thrust vector and fuselage lower surface, in. (cm)

$\Delta L'$ increment of lift component normal to model waterline plane due to jet-induced interference, lb (N)

ΔL increment of lift due to jet-induced interference, lb (N)

ΔL_g gap correction to ΔL, lb (N). $\Delta L_g = \Delta P_c(A_g) \cos \alpha$

ΔL_c ΔL, corrected for effect of nozzle gap, lb (N). $\Delta L_c = \Delta L + \Delta L_g$

P ambient static pressure, psia (N/sq cm)

P_c cavity pressure inside model fuselage, in. H_2O (cm H_2O)

$P_{t,n}$ nozzle exit total pressure, psia (N/sq cm)

$P_{t,x}$ maximum total pressure measured at distance x downstream of nozzle, psia (N/sq cm)

ΔP_c pressure differential across model fuselage, in. H_2O (cm H_2O). $\Delta P_c = P_c - P$

q_n compressible dynamic pressure at nozzle exit, psi (N/sq cm). $q_n = P_{t,n} - P$

q_x maximum compressible dynamic pressure at distance x downstream of nozzle, psi (N/sq cm). $q_x = P_{t,x} - P$

S model planform area, sq in. (sq cm)

T	resultant jet thrust in the lift direction, lb (N)
T'	summation of jet thrusts along individual nozzle centerlines, lb (N)
x	normal distance from nozzle exit to point downstream, in. (cm)
X	longitudinal distance between centers of adjacent nozzles at nozzle exit plane, in. (cm)
Y	lateral distance between model centerline and center of nozzle at nozzle exit plane, in. (cm)
α	pitch angle, deg. Positive, nose up
δ	ratio of ambient pressure to sea level standard pressure
θ	included wall angle of conical nozzle, deg
ϕ	roll angle, deg. Positive, right wing down

Subscripts:

i	point of maximum rate of jet decay
max	maximum

MODEL, APPARATUS, AND PROCEDURE

Model

The test set-up, shown in figure 1, represents an approximately 14-percent scale model of a jet VTOL aircraft with a fuselage-mounted lift system. The model geometry is shown in figure 2. The basic configuration consisted of the fuselage, the nacelles, and a moderately low wing with 0° flaps. Other configurations incorporated the empennage, landing gear, landing gear doors, nozzle doors, and wings with 40° flaps. Two configurations with the wing at the bottom of the fuselage were also tested. The low-wing configurations are shown in figure 3. The model external configurations and nozzle configurations are both defined in table 1.

The model was inverted to facilitate changes in ground plane height and out-of-ground-effect testing. The model was supported on load cells, described later, and was mounted about one wing span from the ground.

A plenum chamber and nozzle assembly, shown in figure 4, were located in the cavity of the model as shown in figure 5, and were supported independently of the model to isolate interference loads from nozzle thrust. Air at ambient temperature was supplied to the plenum chamber through a 4.5-inch (11.45-cm) diameter pipe passing longitudinally through the nose of the model. The plenum

chamber was supported at its aft end by a 0.50-inch (1.27-cm) diameter strut passing through the top of the model. (Unless otherwise noted, "top" and "bottom" as used herein refer to the aircraft rather than the test set-up.) The gaps around the air supply line and the support strut were approximately 0.25 inches (0.64 cm) and 0.38 inches (0.95 cm) wide, respectively.

The various nozzle configurations were mounted in rectangular plates attached to the bottom of the plenum chamber. For each nozzle configuration, a corresponding cover plate, shown in figures 6 and 7, was attached to the bottom of the fuselage. The gaps between the nozzles and the cover plates were approximately 0.19 inches (0.48 cm) wide. Turning vanes were attached to the plenum side of the nozzle plates, as shown in figure 8, to aid in establishing an approximately uniform flow distribution and velocity profile in the nozzles.

Test Set-Up

Figure 1(a) shows the ground plane simulator, which consisted of an 8-foot-square plywood sheet, supported at the corners by vertical posts. The height of the ground plane was adjusted by a chain and sprocket at each corner and was read directly on a steel tape. The ground plane simulator was mounted on casters so that it could be removed for out-of-ground-effect testing.

Interference loads were obtained using the six-component force-measuring system shown in figure 9. The force-measuring system was designed to measure all loads and moments on the model with three lift load cells, two side load cells, and one drag load cell. Lift, drag, and side force load cells were installed at the tail of the model, lift and side force load cells at the right wingtip, and a lift load cell alone at the left wingtip. Each load cell consisted of a strain gage mounted on a steel bar to measure the bending moment and thus the applied load. For the lift loss tests, the strain gage signals were routed through a channel selector box and were read on a visual indicator. The lift-measuring strain gage system in particular was calibrated at intervals during the test program to insure confidence in the data.

The load cells were fastened to the corners of a horizontal triangular frame attached to the top of the model, rather than to the model itself. Rods with self-aligning bearing ends were installed between the frame and the load cells to eliminate unwanted force components. The load cells were mounted on posts which could be adjusted to position the model accurately.

The jet decay characteristics of the various configurations were obtained using a total pressure rake, shown in figure 10, with 29 probes arranged in a line and connected to a 50-tube manometer board. The rake was located at the end of a horizontal boom attached to a 4-inch-square steel post anchored to the ground. The boom could be rotated about the support post to traverse the jet wake, and could be raised and lowered by a chain and sprocket to obtain surveys at various heights. The rake could be rotated about the longitudinal axis of the boom to align the probes with non-vertical wakes. Locks were provided to maintain rigidity during testing. The positions of the probes relative to the model were determined from an angular scale on the vertical post. Steel tapes were used for height and lateral position measurements.

The airflow to the nozzles were controlled by an electrically-actuated butterfly valve and was measured by means of an orifice-type flowmeter. The orifice upstream pressure was read on a bourdon gage, the orifice pressure differential on a U-tube manometer, and the plenum chamber pressure on a single-tube manometer. Thermocouples were located in the plenum chamber and upstream of the orifice, and were connected through a channel selector box to a visual readout temperature indicator.

To establish the relationship between plenum chamber pressure and nozzle exit total pressure, a rake containing 25 total pressure probes, shown in figure 11, was used to survey the exits of all nozzles on the right side of the model and one on the left side, to check for symmetry. The probes were connected to the 50-tube mercury manometer board and the data were recorded photographically.

The pressure in the model cavity surrounding the plenum chamber differed from the ambient pressure because of the gaps around the nozzles and supports, and the resulting induced flow. The cavity pressure was measured on a U-tube manometer.

Procedure

To determine nozzle thrust, the 25-probe nozzle exit rake was used to obtain nozzle exit pressure ratio as a function of the plenum chamber pressure ratio. The equation for the specific thrust of a convergent nozzle with isentropic flow was then used to obtain a calibration of thrust against nozzle pressure ratio for each nozzle configuration. The measured airflow, as a function of nozzle pressure ratio, was then used to obtain the total thrust.

The model height measured normal to the ground plane was taken as the distance from the ground plane to the point where the resultant thrust vector, determined from the nozzle geometry, passed through the fuselage bottom surface. The tests were conducted with the ground plane normal to the resultant thrust vector except when testing for the effects of roll and pitch attitude.

To obtain the jet dynamic pressure decay data close to the model, the maximum dynamic pressure of each jet on the right side of the model was recorded at each distance from the model. The average of these values was used as the maximum dynamic pressure at that distance. At some distance from the model the jets usually coalesced so that a jet core could not be identified for each nozzle. Discrete cores formed by the coalescence of two or more jets could be distinguished, however, and the maximum dynamic pressures of these cores were averaged to obtain the maximum dynamic pressure at that position.

Since the tests were conducted out of doors, testing was discontinued when wind velocities were high enough to significantly affect the recorded data.

PRESENTATION OF RESULTS

The thrusts of all nozzle configurations, corrected for atmospheric pressure, are shown in figure 12 as a function of nozzle exit pressure ratio. The data points are not shown for the thrust curve which applies to the majority of the nozzle configurations, since all of the applicable data fall within ± 2 percent of the curve.

The jet decay data for all 18 nozzle configurations are presented in figure 13 for an infinite height-to-wing-span ratio. The effect of height on the jet profiles is shown in figures 14 and 15. For the latter figures, only one nozzle was surveyed on each configuration- the right center of nozzle configuration 7a and the right rear of nozzle configuration 22. The jet decay profiles show the ratio of local total pressure minus ambient pressure to nozzle exit total pressure minus ambient pressure as a function of the ratio of distance downstream of the nozzle exit to equivalent nozzle diameter.

The basic lift loss data, showing the lift increment normal to the model waterline, are presented in figures 16 through 33 as a function of nozzle pressure ratio, with height-to-wing-span ratio as a parameter. These data have been normalized to standard atmospheric pressure but the gap correction, discussed later, has not been applied. In addition, a correction for nozzle aft cant (if any) must be applied to obtain true hover lift increment parallel to the resultant thrust vector. These corrections have been applied in the comparison curves, discussed later, which show the effects of nozzle and airframe configuration variables on lift loss.

Aft cant of the nozzles may also cause a small jet-induced interference force to be exerted on the drag load cell, and one component of this drag force acts parallel to the resultant nozzle thrust and thus contributes to hover lift. However, the measured drag-link jet-induced forces were found to be so small that their components in the resultant nozzle thrust direction were negligible.

The basic lift data, figures 16 through 33, are arranged in order of nozzle configuration number, with the model configuration number in ascending order for each nozzle configuration. A listing of these figures and the comparison and correlation figures derived from them, is presented in the following section.

Two groups of comparison, correlation, and correction figures are presented. Figures 34 through 46 contain those curves which do not directly indicate the effect of a particular configuration or attitude parameter. Included in this group are comparisons of data from the 1965 and 1968 programs, data relating to the correction for the effect of the gap between the airframe model and the nozzles and plenum supports, curves showing the effect of nozzle pressure ratio, and figures relating to the correlation of lift loss with jet decay characteristics.

The second group, figures 47 through 60, shows the effects of the configuration and attitude parameters that were investigated. The data are presented

as percent lift loss versus height-to-wing-span ratio at a nozzle pressure ratio of 2.0 except for figure 57, which shows the effect of nozzle area and pressure ratio at a constant thrust. A listing of the configuration and attitude comparison curves and the basic lift loss curves from which they are derived is presented at the end of this section.

All of the curves of figures 46 through 60 have been corrected for the effect of nozzle aft cant angle (if any), and the effect of the nozzle-to-model gap has been applied to the curves of figures 46 through 58. These effects are recognized so that the curves show the lift loss that is felt along the resultant thrust vector that is normal to the ground, not what acts normal to the model waterline as in the case of the basic lift loss curves.

DISCUSSION

General

Repeatability.- To insure the continuity of the 1965 and 1968 test programs and to provide an indication of the validity of both programs, three of the configurations investigated in 1965 were included in the 1968 program. Figure 34 shows how the lift interference loads compare for the two programs. The average deviation of the faired curves for the 1965 and 1968 data from a mean curve of the two is approximately 4 percent of the lift loss.

In addition, several repeat runs were made during both the 1965 and 1968 programs. Figure 27(b) presents data from a repeat run for comparison with the original run of figure 27(a), while repeat data at specific heights are shown

by the flagged symbols of figures 18(f), 32(c), and 32(d). The repeatability may be seen to be approximately ±2 percent of the lift loss.

Lift curve break.- One of the basic lift curves, figure 18(f), is notable in that, for this particular nozzle/model combination, nozzle configuration 2 and model configuration 6, a definite break in the lift loss curve for a height-to-wing-span ratio of 0.211 occurs between nozzle pressure ratios of 1.70 and 1.84. The lift loss increases smoothly with increasing pressure ratio on each side of the break, but a sharp reduction in lift loss occurs as the pressure ratio increases through this range. Crossplots at pressure ratios above and below the break are presented in figure 35. The break is less apparent in figure 35.

This sudden change in lift loss is a real effect, and was duplicated in a repeat test. Other VTOL jet-induced flow effect test programs have shown similar instabilities of the induced flow field at certain conditions, although not in such a clear and well-defined manner. The cause of the break is not understood.

Gap correction.- The gaps between the fuselage of the model and the air supply pipe, the plenum chamber support strut, and the nozzles allow the jets to induce a flow of air through the fuselage. The absolute pressure in the fuselage cavity is thus somewhat higher than it would be if inflow were prevented. Valid load cell measurements could not be obtained with the gaps sealed. Therefore, since the cavity pressure with sealed inflow gaps can be expected to be approximately equal to the external pressure that would be felt on nozzle seals if such seals were installed, the difference between the sealed and unsealed measured cavity pressures was multiplied by the nozzle gap area, and the product was used as the gap correction force increment.

Cavity pressures were measured for all configurations during the 1968 lift loss tests, and the out-of-ground-effect results are shown in figure 35. However, cavity pressures with the inflow gaps sealed were measured only for nozzle configurations 2, 3a, and 7a at all heights, and for 3 and 12 at an infinite height. The results at infinite height are shown in figure 37 as the ratio of sealed to unsealed cavity pressure.

It was necessary to estimate the sealed cavity pressures for the other configurations. Attempts were made to relate the pressure difference or the pressure ratio, sealed to unsealed, at a given height and nozzle pressure ratio, to the gap-to-nozzle area ratio. These attempts, however, were unsuccessful.

The method adopted to determine a gap correction was to take the faired curve of figure 37 as the ratio of the sealed to unsealed cavity pressure for all configurations with the ground plane removed and to calculate an out-of-ground-effect lift loss correction for each configuration, using this ratio and the gap area and measured unsealed cavity pressure for the particular configuration. This lift loss correction was then applied at all height-to-wing-span ratios as a constant increment. Figure 38 indicates that the error resulting from this procedure is less than 2 percent of the actual lift loss for the three configurations for which complete cavity pressure data are available. In figure

38 the numerator of the ordinate is the lift loss that has been corrected for gap effect by the use of the sealed and unsealed cavity pressures actually measured at each height. The denominator is the lift loss obtained using the constand-increment approximation just described. Figure 38 is presented for a nozzle pressure ratio of 2.0, but the curves for other pressure ratios are similar.

Effect of nozzle pressure ratio.- The effect of nozzle pressure ratio on percent lift loss for one nozzle and model configuration over the range of ground plane heights investigated is shown in figure 39. An increase in pressure ratio is seen to result in a decrease in percent lift loss for all ground plane heights. It was found that this effect is similar for all the configurations investigated. Consequently, the comparison data presented to show the effects of other parameters are shown for only one nozzle pressure ratio. Figure 40 indicates the effect of pressure ratio on percent lift loss for all configurations out of ground effect.

The nozzle pressure ratio effect just discussed is for a constant nozzle area, with the thrust varying in accordance with the pressure ratio. The effect of varying the pressure ratio and nozzle area simultaneously in order to hold a constant thrust is discussed later, in connection with the discussion of the effects of configuration variables.

Correlation of Lift Loss With Jet Decay Characteristics

One of the purposes of the present program was to investigate the validity of the lift loss correlation presented in reference 1, which can be written as follows:

$$\Delta L/T = k \sqrt{S/A_j} \sqrt{-\left[\frac{\partial(q_x/q_n)}{\partial(x/D_e)}\right]_{max} \Big/ \left(\frac{x}{D_e}\right)_i}$$

In this equation the constant of proportionality, k, depends on airframe variables and components, such as wing height, flaps, landing gear, and nozzle doors; the first radical accounts for the relative area of the airframe planform and the nozzles; and the second radical, the jet decay parameter, accounts for the rapidity of the jet mixing process and the corresponding strength of the induced flow field. The jet decay parameter is intended to be independent of airframe characteristics and to be affected primarily by the nozzle configuration, with perhaps some effect of nozzle pressure ratio and aircraft height.

Out of ground effect results.- Figures 41 through 43 present the percent lift loss divided by the area ratio radical, as a function of the jet decay parameter for all configurations. Figure 41 covers the basic model, without flaps, empennage, landing gear, or nozzle doors; figure 42 an essentially complete aircraft; and figure 43 the low-wing configurations. The effect of pressure ratio is shown in each figure.

The data agree quite well with a straight line passing through the origin as predicted by the correlating equation presented above. The results of the tests of reference 1, shown on figure 43, agree reasonably well with the results of the present tests with similar airframe configurations and pressure ratios. At a given value of the jet decay parameter, the low-wing configurations (model configurations 10 and 11) have significantly higher lift losses than the midwing configurations (model configurations 1 and 5), as would be expected. The validity of the correlation presented in reference 1 appears to be well supported by the results of the present program.

Scatter of data.- The scatter of the data of figures 41 through 43 is believed to result primarily from the uncertainty of the maximum slopes of the jet decay profiles, although nozzle configuration may have a small effect. It was found that the data points of figures 41 through 43 could be shifted horizontally by significant amounts, simply by refairing the jet decay curves. Figure 44 shows one such refairing, as well as the original curve. The corresponding original and revised points on the correlation curve are shown by the open and solid symbols of figure 41(c) for nozzle configuration 3. It was found that most of the other points could be similarly shifted, using refairings that were still consistent with the measured jet decay pressures.

To provide a further check on the validity of the correlation of reference 1, one of the nozzle configurations was tested with altered jet decay characteristics. The alteration was accomplished by installing inserts upstream of the nozzle exits in nozzle configuration 7a to produce nozzle configuration 7b. The jet decay characteristics of these configurations are plotted in figures 13(j) and 13(k). No data points are shown in figure 13(k) because the curves have been crossplotted from data taken at other values of nozzle pressure ratio.

According to the correlation of reference 1, the lift loss data of nozzle configuration 7b should correlate with the other data of figure 41. Moreover, the deviation of the 7a and 7b data from the regression line should be less than the average deviation of the remaining data, since all other effects of nozzle configuration are eliminated. Finally, nozzle configuration 7b should have a larger jet decay parameter and a higher lift loss than nozzle configuration 7a. All of these effects may be observed in figure 41, indicating that jet mixing and decay indeed have significant effects on lift loss and that the jet decay parameter provides a good correlation.

Correction for nozzle pressure ratio.- Figures 41 through 43 show that there is a nozzle pressure ratio effect in the correlation based on the equation presented above from reference 1. A modification has therefore been made to the correlation equation to recognize this effect, and the revised equation can be written as follows:

$$\Delta L/T = k_1 \sqrt{S/A_j}\ (P_{t,n}/P)^{-.64} \sqrt{-\left[\frac{\partial(q_x/q_n)}{\partial(x/D_e)}\right]_{max} \Big/ \left(\frac{x}{D_e}\right)_i}$$

The constant of proportionality, k_1, is now dependent only on the model configuration. The modified form of the correlation equation has been applied to the data of figures 41 through 43 and the results are presented in figure 45. The symbols on figure 45 are not data points but are points used to identify data obtained from the regression lines of figures 41, 42, and 43 at a jet decay parameter of 0.5 and at each nozzle pressure ratio presented. As is shown, the nozzle pressure ratio raised to a constant power multiplied by the jet decay parameter provides a good correlation with a single straight line passing through the origin for each model configuration. It is to be noted that model configurations 10 and 11 are the same except for planform shape, and reference 1 shows that there is essentially no effect of planform shape at a constant planform-to-total-nozzle area ratio.

In ground effect.- The effect of ground proximity on the jet profiles is shown in figures 14 and 15 for nozzle configurations 7a and 22 respectively. The data indicate that ground proximity has little effect on jet decay. A tabulation of jet decay parameters based on data from figures 14 and 15 is presented in table 2. It shows that at a given nozzle pressure ratio, the jet decay parameter varies by only 7 percent or less over the full range of ground plane heights investigated. As is shown in figure 39, the jet-induced lift loss results are influenced by ground proximity. However, the characteristics of lift loss as a function of height vary widely with nozzle and model configurations, as will be shown later in the discussion. Thus the correlation of reference 1 appears to be valid only out of ground effect.

Comparison of Lockheed and NASA Data

In order to provide a comparison between the present investigation and that of reference 1, the lift loss of a configuration simulating a scaled-up version of one of the models of reference 1 was investigated. The two configurations were similar in that each had a delta wing, a planform-to-total-nozzle area ratio of 49.5, and four nozzles with similar spacings. Figure 46 indicates some difference between the lift loss data of reference 1 and that of this investigation for the similar models. The jet decay parameter of the present investigation, however, was about 22 percent larger than that of reference 1 out of ground effect at a pressure ratio of 2.08. Based on the correlation discussed previously, therefore, the lift loss data of reference 1 in figure 46 have been scaled up 22 percent to provide a more meaningful comparison of the two sets of data. The agreement may be seen to be quite good, considering the differences in size, model component details, model mounting, and instrumentation. It should be noted that the data of reference 1 at the planform-to-total-nozzle area ratio used in this comparison does not include height-to-wing-span ratios below approximately 0.35. However, at other planform-to-total-nozzle area ratios of the same model, the general shape of the percent lift loss curves of reference 1 is similar to that of this investigation shown in figure 46.

Effect of Configuration Variables

Survey of lift loss results.- All of the nozzle and model configurations showed a lift degradation at all pressure ratios and heights. Out of ground

effect, the lift losses were quite similar for all configurations- 2 to 3 percent of the lift component of the resultant nozzle thrust, for example, at a pressure ratio of 2.0. The ground plane was observed to influence lift interference on all configurations up to a height-to-wing-span ratio of at least 2.0, the maximum value investigated other than infinity. Above a height-to-wing-span ratio of about 0.5, the percent lift loss curves for all configurations showed similar characteristics, with a smooth and gradual decrease toward the value at infinity. Below a height of one-half wing span, the lift interference effects were highly dependent on the nozzle and model configuration. The favorable lift interference effect which was observed for many of the configurations when near the ground can probably be attributed to the impact of jet fountains on the under surfaces of the model. Such fountains are created when jets spread out radially on the ground and impinge on each other.

Of the nozzle configuration parameters investigated, the lateral spacing of the nozzle had the greatest effect on lift interference, especially near landing gear height, where increasing the lateral spacing 70 percent decreased the lift loss 93 percent. The nozzle closure doors had the greatest influence of all of the airframe components tested. Adding nozzle doors outboard of the nozzles increased the lift loss by a factor of from 2 to 3 except at height-to-wing-span ratios of less than about 0.25.

To show the effects of nozzle variables, airframe components, and other parameters on lift interference, the lift data are compared below for configurations and test conditions which show the effect of varying a particular parameter. In most cases the data are presented as percent lift loss versus height-to-wing-span ratio at a pressure ratio of 2.0.

Effect of outboard cant.- Figure 47 shows the effect of canting the nozzles 10° outboard, compared to nozzles directed parallel to the plane of symmetry. Four-, six-, and eight-nozzle configurations are shown. With four nozzles, outboard cant has practically no effect, although no outboard cant is slightly better at infinite height. With eight nozzles there is again little difference over most of the height range, but outboard cant markedly improves lift at the lower altitudes. With six nozzles the situation is quite different; no outboard cant is better by almost 1 percent of resultant nozzle thrust over almost the complete height range. Only quite near the ground does outboard cant show a fountain effect that makes it superior. The seemingly anomalous behavior of the six-nozzle configuration has not been explained.

Effect of aft cant.- The influence of nozzle aft cant on lift interference is shown in figure 48. With the nozzles angled out 10° from the plane of symmetry, aft cant is detrimental at all heights, although the effect is small. With no outboard cant, aft cant has essentially no effect except near the ground, where increasing the aft cant from 0° to 10° diminishes the favorable fountain effect.

Effect of number of nozzles.- Figure 49 shows the effect of varying the number of nozzles, with the total nozzle area held constant. Out of ground effect, decreasing the number of nozzles reduces the lift loss, which is to be expected from the decreased jet mixing surface area, entrainment, and induced

flow of ambient air. The percent lift loss for the eight-nozzle configuration is about one and one-half times that of the four-nozzle configuration. Thus the lift loss in this case is approximately proportional to the jet perimeter.

As height is reduced, the above trend begins to reverse and is completely reversed below a height-to-wing-span ratio of about 0.15. The change may be associated with the downward fountains that form in a group of more than four nozzles. With four nozzles, the upward fountain in the center stagnates on the fuselage, and the fountain flow is then free to leave the system, flowing out horizontally between the nozzles. Adding another pair of nozzles, however, tends to block a portion of the horizontal outflow. This portion of the air is forced back downward, giving an additional upward reaction on the fuselage. As additional pairs of nozzles are added, more downward fountains form, resulting in the sequence of curves shown in figure 49.

Effect of longitudinal and lateral spacing.- The most significant effect of nozzle spacing occurs in the height-to-wing-span ratio range from about 0.1 to about 0.3. In this range, as may be seen from figures 50 and 51, increasing the spacing reduces the lift loss; outside this range there is essentially no effect. The load occurring on the lower fuselage area between the nozzles in close ground proximity is greatly influenced by the impinging fountain flow from a portion of the jets being deflected off the ground. As the nozzle spacing increases, the favorable load on the fuselage from the fountain flow produces less jet-induced interference lift loss.

Effect of wing height.- The effect of lowering the wing from its basic moderately-low position to the level of the bottom of the fuselage is shown in figure 52. There is very little difference in lift loss over most of the height range. Near the ground, however, the low wing and the ground form a channel in which the static pressure of the spreading jets is reduced considerably below the ambient pressure, masking the fountain effect, and causing a serious lift loss.

Effect of airframe components.- Figure 53 shows the effects of various airframe components. In figure 53, the flaps, landing gear, and empennage have been added to the basic model, first separately and then in combination. Above a height of about 0.2 wing spans, deploying the flaps reduces the lift loss slightly, probably by impeding induced flow on the lower surfaces of the wings. The other components have little or no effect in this range. Near the ground the main change is the reduction in lift loss that occurs when all components are added simultaneously. It is not known why the combination shows an improvement that is not apparent for any of the individual components.

Figure 54 compares outboard-hinged nozzle closure doors with inboard-hinged doors and no doors, for two nozzle configurations. The outboard-hinged doors cause a dramatic increase in lift loss resulting in an increase of two to three times that for the configuration with no doors at heights above about 0.3 wing spans. Lift losses with inboard-hinged doors are not greatly different from those with no doors. The outboard doors apparently act like the mixing section of an ejector and cause a substantial reduction in the static pressure on the bottom of the fuselage. At lower heights a sizable ground effect reduces the

lift loss with outboard-hinged doors to values comparable to those of the other two configurations. The favorable ground effect probably results from the downward deflection of the fountains by the doors, and the corresponding upward reaction on the fuselage.

The effects of deploying the flaps, landing gear, and inboard-hinged nozzle doors on the lift loss of a complete aircraft with the empennage installed are shown in figure 55. All of the curves are quite similar, generally falling within a band having a width of about 1 percent of the resultant nozzle thrust. Model configuration 9 does, however, show a definite lift dip at a height-to-wing-span ratio of approximately 0.12. It appears from the other curves that with the landing gear extended, a more realistic configuration at this height, the dip is eliminated regardless of the positions of the flaps and doors. The landing gear itself presumably causes some upward fountaining, and the landing gear doors may turn portions of the various fountains back downward.

Effect of nozzle area.- Figure 56 shows the effect of varying the total nozzle area to be small, both for four nozzles and for eight nozzles. The large-area and small-area curves are quite close to each other at all heights, for both numbers of nozzles. The maximum relative change in percent lift loss occurs for the four-nozzle configuration out of ground effect, where a one-third reduction in total nozzle area (and thrust) produces about a 25-percent reduction in percent lift loss.

Effect of pressure ratio at constant thrust.- The configurations used to show the effect of total nozzle area on lift loss may also be used to show the effect of pressure ratio at constant thrust. The results, presented in figure 57, are quite similar to the curves showing the effect of nozzle area, and indicate that pressure ratio at constant thrust, like nozzle area at varying thrust, has a minor effect.

Effect of nozzle aspect ratio.- The effect of nozzle aspect ratio is shown in figure 58. The circular nozzle is seen to be superior at all heights except over a small range near the ground. Out of ground effect the lift loss with an elongated nozzle is about 25 percent more than that with a circular nozzle, which is to be expected because of the increased jet perimeter of the elongated nozzle. Both nozzle configurations experience a favorable fountain effect near the ground, but that associated with the elongated nozzle is larger and gives this configuration superior performance at heights of 0.1 to 0.2 wing spans. The greater apparent fountain effect presumably results from the increased model surface area bounded by the jets and the more solid boundary created by the elongated jet, which tend to better contain the reflected jets and thus increase the pressure exerted on the model.

Effect of attitude.- Figures 59 and 60 show the effect of roll and pitch on the percent lift loss for two nozzle configurations. Nozzle configuration 21 (figure 60) is quite insensitive to attitude at all heights, the curves showing a spread of about 2 percent of resultant nozzle thrust component, normal to the ground, over the full 15° range on each axis. Nozzle configuration 8 (figure 59) is slightly more sensitive to both types of motion.

CONCLUDING REMARKS

Model tests of the jet-induced lift losses of a direct-lift VTOL aircraft with fuselage-mounted engines have been conducted at hover over a nozzle pressure ratio range of approximately 1.4 to 2.3 and a height range from landing gear height to infinity. Eighteen nozzle configurations and a number of individual and combined airframe modifications were tested. In addition to lift losses, the decay profiles of the jets were measured so that the lift losses could be correlated with the mixing and entrainment characteristics of the jets out of ground effect.

Most of the configurations showed a lift loss out of ground effect of approximately 2 to 3 percent. Increasing the lateral spacing of the nozzles reduces the lift loss in close ground proximity since larger lift loads are produced on the lower fuselage area between the nozzles by the impinging fountain flow from a portion of the jet being deflected off the ground. Adding outboard-hinged nozzle doors drastically increased the lift losses at the higher height-to-wing-span ratios by serving as the mixing section of an ejector. Moving the wing from the moderately-low to the low position greatly increased the lift loss near the ground. With the total nozzle area held constant, increasing the number of nozzles decreased the lift losses near the ground by creating downward fountains but increased the lift losses above about 0.2 wing spans by increasing the jet mixing area. Few of the other changes had significant effects on lift loss.

The lift loss data correlated well with the jet decay parameter obtained from reference 1 and, as would be expected, the low-wing configurations showed higher lift losses than the mid-wing configurations at the same value of the jet decay parameter. It was found that this correlation could be modified to include the effects of nozzle pressure ratio. In addition, differences in the magnitude of the jet decay parameter accounted for the major part of the apparent discrepancy between the lift losses measured on similar models in the present program and in the program reported in reference 1.

Lockheed-Georgia Company
Marietta, Georgia
July 2, 1968

REFERENCES

1. Gentry, Garl L.; and Margason, Richard J.: Jet-Induced Lift Losses on VTOL Configurations Hovering In and Out of Ground Effect. NASA TN D-3166, 1966.

2. McLemore, H. Clyde: Jet-Induced Lift Loss of Jet VTOL Configurations in Hovering Condition. NASA TN D-3435, 1966.

3. Otis, James H., Jr.: Induced Interference Effects on a Four-Jet VTOL Configuration With Various Wing Planforms in the Transition Speed Range. NASA TN D-1400, 1962.

4. Spreemann, Kenneth P.; and Sherman, Irving R.: Effects of Ground Proximity on the Thrust of a Simple Downward-Directed Jet Beneath a Flat Surface. NACA TN 4407, 1958.

5. Hammond, Alexander D.; and McLemore, H. Clyde: Hot-Gas Ingestion and Jet Interference Effects for Jet V/STOL Aircraft. Presented to Flight Mechanics Panel of AGARD (Göttingen, West Germany), Sept. 13-15, 1967.

6. Schade, Robert O.: Ground Interference Effects. NASA TN D-727, 1961.

7. Vogler, Raymond D.: Effects of Various Arrangements of Slotted and Round Jet Exits on the Lift and Pitching-Moment Characteristics of a Rectangular-Base Model at Zero Forward Speed. NASA TN D-660, 1961.

8. Wyatt, L. A.: Static Tests of Ground Effect on Planforms Fitted With a Centrally-Located Round Lifting Jet. C. P. No. 749, Brit. A.R.C., 1964.

9. Mechtly, E. A.: The International System of Units - Physical Constants and Conversion Factors. NASA SP-7012, 1964.

Table 1. - Model external and nozzle configurations.

Model config		Nozzle config	X/D, Y/D, Fwd, D	A_j, sq cm	D, cm	X/D	Y/D	Outb'd cant, deg	Aft cant, deg	S/A_j	A_g/A_j
1	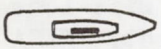	1	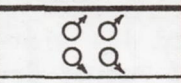	67.65	4.64	1.70	1.00	10	10	66.0	.62
		1a	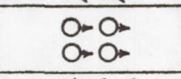	67.65	4.64	1.70	1.00	0	10	66.0	.43
2	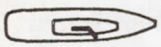	2	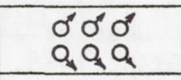	67.65	3.79	1.70	1.00	10	10	66.0	.80
3	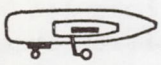	3	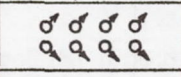	67.65	3.28	1.70	1.00	10	10	66.0	.95
		3a	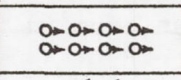	67.65	3.28	1.70	1.00	0	10	66.0	.60
4	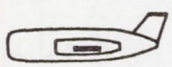	4	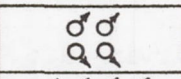	45.65	3.79	1.70	1.00	10	10	99.0	.80
		5	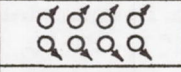	90.20	3.79	1.70	1.00	10	10	49.5	.80
5	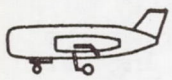	6	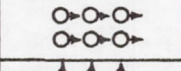	67.65	3.79	1.70	1.00	0	10	66.0	.80
6	 Outb'd	7	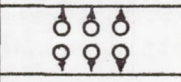	67.65	3.79	1.70	1.00	10	0	66.0	.80
		7a	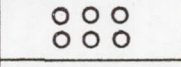	67.65	3.79	1.70	1.00	0	0	66.0	.62
7	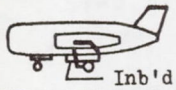 Inb'd	7b*	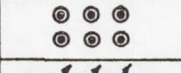	67.65	3.79	1.70	1.00	0	0	66.0	.62
		8		67.65	**	1.70	1.00	10	10	66.0	.84
8	 Inb'd	9	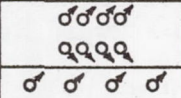	67.65	3.28	1.50	1.00	10	10	66.0	.95
9	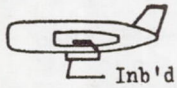 Inb'd	10	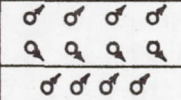	67.65	3.28	2.00	1.00	10	10	66.0	.95
		12	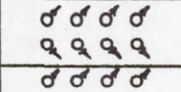	67.65	3.28	1.70	1.35	10	10	66.0	.95
10		13	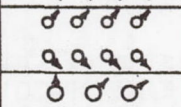	67.65	3.28	1.70	1.70	10	10	66.0	.95
11	 Delta wing	21	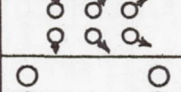	73.65	3.96	***	1.19	10	****	60.7	.71
		22		90.20	5.36	4.00	.75	0	0	49.5	.43

* Same as 7a except plug inserts were installed in each nozzle. Plugs were flat disks 1.78 cm in diameter located 1.7 cm upstream of nozzle exit plane.

** Elongated nozzle - 1.26 cm radius at ends with centers 2.52 cm apart.

*** Fwd, center and aft nozzle angles of 0°, 9.75° and 17.0° respectively.

**** Between fwd and center, X/D = 1.88; between center and aft, X/D = 1.85.

Table 2.- Effect of ground plane height and nozzle pressure ratio on jet decay parameter.

(a) Nozzle configuration 7a.

$$\sqrt{-\left[\frac{\partial(q_x/q_n)}{\partial(x/D_e)}\right]_{max}} \Big/ \left(\frac{x}{D_e}\right)_i$$

$P_{t,n}/P$ / h/b	1.40	1.70	2.00	2.30
∞	.439	.430	.422	.415
.570	.424	.417	.410	.402
.498	.450	.439	.429	.420
.368	.453	.446	.440	.433
.237	.437	.427	.418	.409

(b) Nozzle configuration 22.

$$\sqrt{-\left[\frac{\partial(q_x/q_n)}{\partial(x/D_e)}\right]_{max}} \Big/ \left(\frac{x}{D_e}\right)_i$$

$P_{t,n}/P$ / h/b	1.40	1.70	2.00	2.30
∞	.436	.425	.415	.406
.570	.432	.422	.413	.404
.498	.430	.420	.411	.402
.368	.422	.416	.410	.405
.237	.438	.424	.411	.401

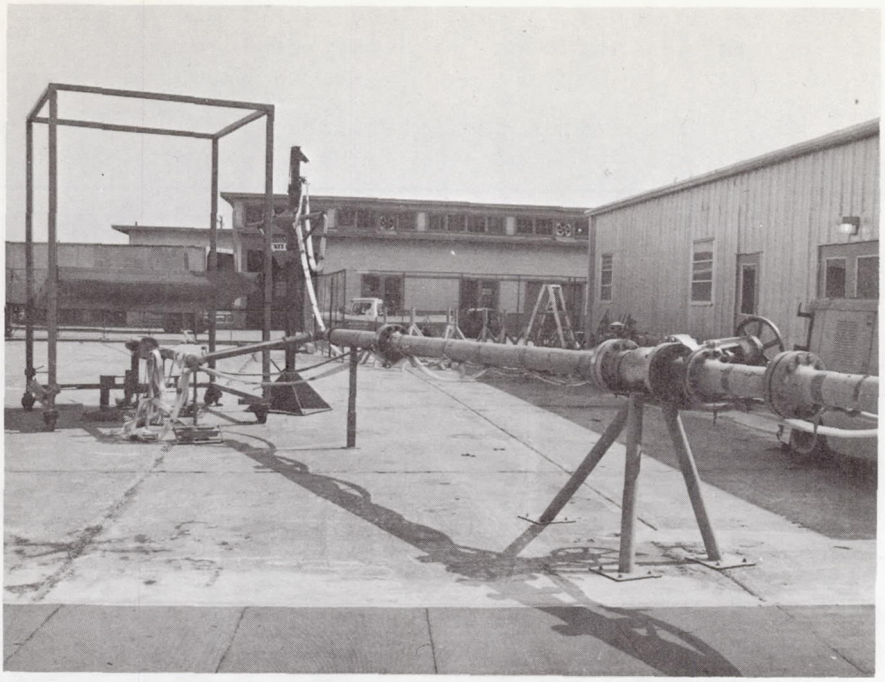

(a) Overall view of test set-up.

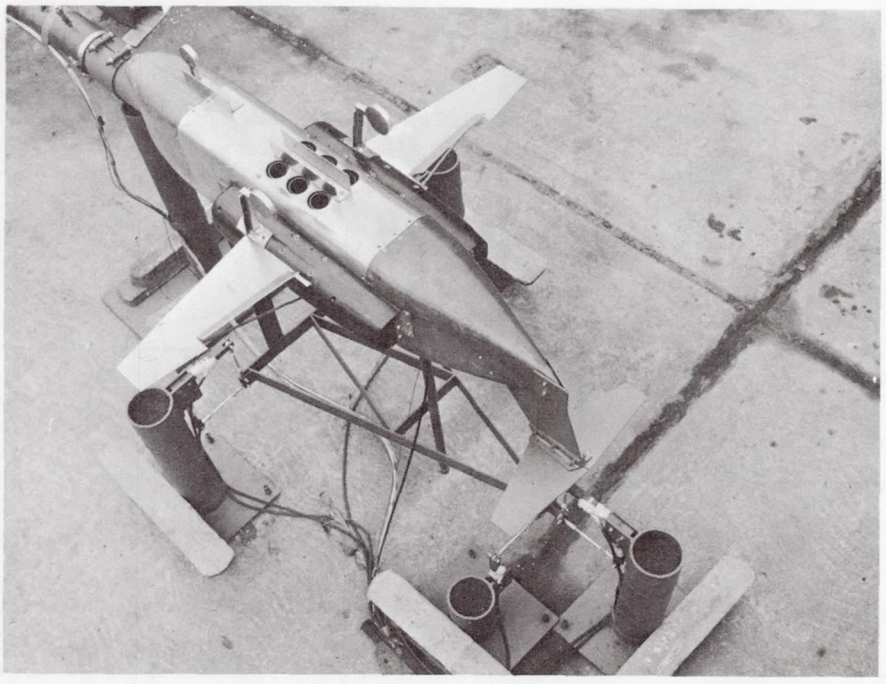

(b) Inverted model mounted on force-measuring system.

Figure 1.- Test set-up.

TABLE A.- FUSELAGE CONTOURS

FUSELAGE STATION	WATERLINE (UPPER) ① *	BUTT LINE ③ *	RADIUS
0.00	33.89	0.00	
1.40	35.45	2.60	1.09
2.67	36.11	3.64	1.78
5.22	37.07	5.14	2.75
10.31	38.14	7.05	3.79
15.39	38.78	8.27	4.43
23.03	39.26	9.31	4.91
30.66	39.44	9.67	5.09
TO	↓	↓	↓
90.08	39.44	9.67	5.09
97.71	38.93	9.21	4.81
105.34	37.66	7.63	4.02
112.98	35.62	5.60	2.95
120.61	33.08	3.51	1.88
128.24	29.95	1.45	0.76
130.79	28.83	0.74	0.38
133.33	26.72	0.00	

*FUSELAGE CONTOUR SYMMETRIC ABOUT WL 25.45 AND BL 0.00

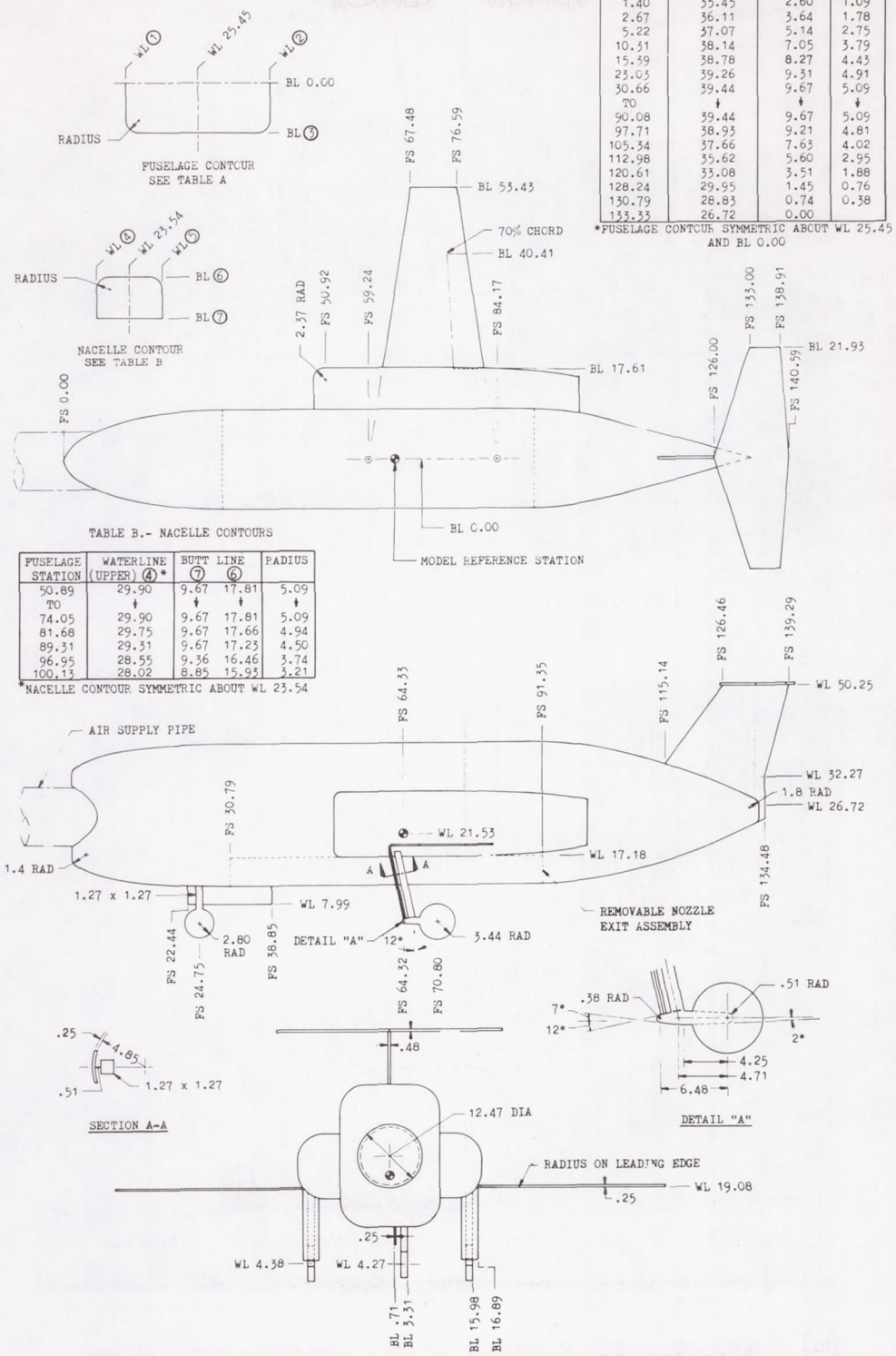

Figure 2.- Geometry of the model. All dimensions in centimeters.

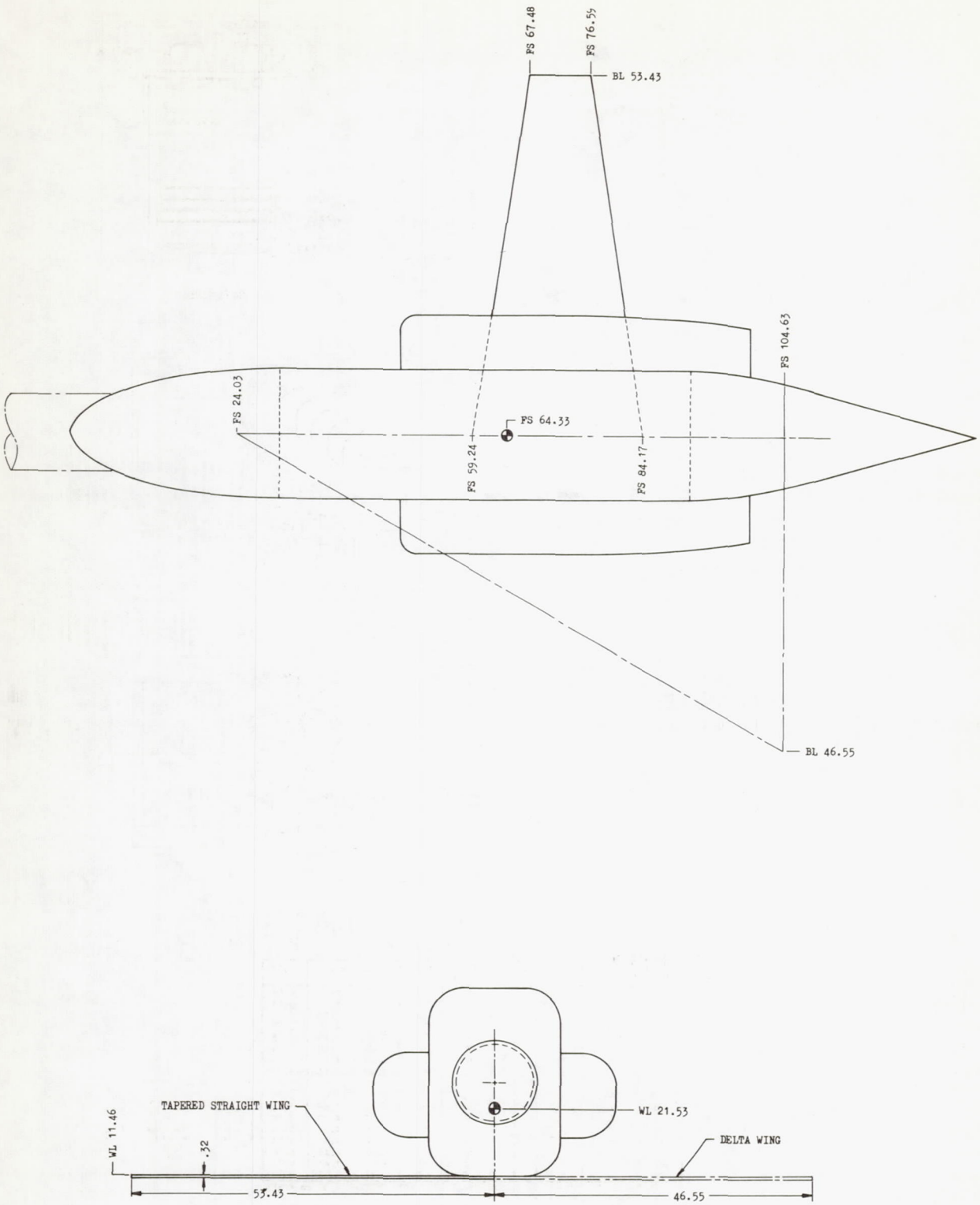

Figure 3.- Geometry of the low-wing configurations. All dimensions in centimeters.

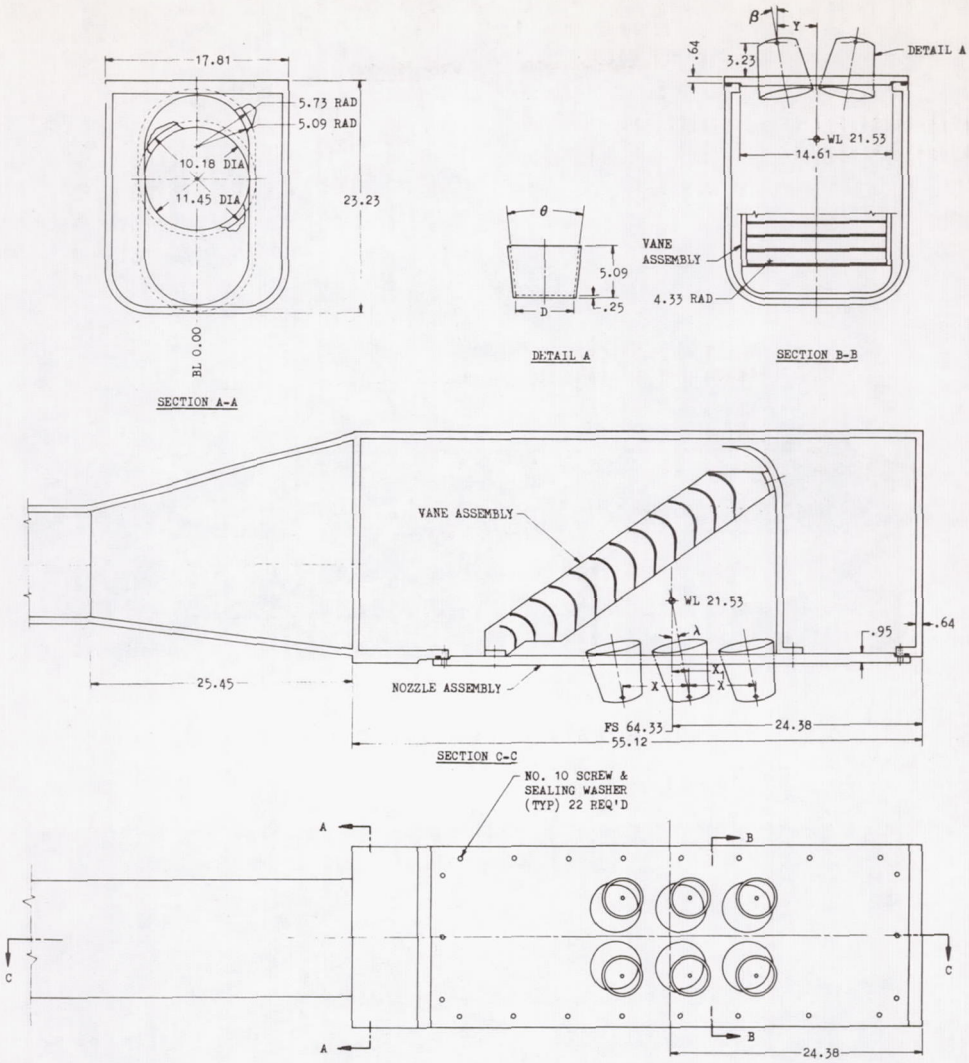

NOZZLE CONFIGURATION DIMENSIONS

NOZZLE CONFIG	NUMBER NOZZLES	D, cm	θ, deg	β, deg	λ, deg	X, cm	X_1, cm	Y, cm
1	4	4.64	12	10	10	7.90	5.61	4.64
1a	4	4.64	↓	0	10	7.90	5.61	4.64
2	6	3.79		10	10	6.45	1.65	3.79
3	8	3.28		10	10	5.58	4.45	3.28
3a	8	3.28		0	10	5.58	4.45	3.28
4	4	3.79		10	10	6.45	4.88	3.79
5	8	3.79		10	10	6.45	4.88	3.79
6	6	3.79		0	10	6.45	1.65	3.79
7	6	3.79		10	0	6.45	0	3.79
7a	6	3.79		0	0	6.45	0	3.79
8	6	*		10	10	6.45	1.65	3.79
9	8	3.28		10	10	4.92	4.12	3.28
10	8	3.28		10	10	6.56	4.94	3.28
12	8	3.28		10	10	5.58	4.45	4.43
13	8	3.28		10	10	5.58	4.45	5.58
21	6	3.96		10	**	***	1.42	4.71
22	4	5.36		0	0	21.45	10.73	4.02

* ELONGATED NOZZLE - 1.76 cm RADIUS AT ENDS WITH CENTERS 2.52 cm APART. EQUIVALENT DIAMETER OF 3.79 cm.

** FWD, CENTER AND AFT NOZZLE ANGLES OF 0, 9.75 and 17.0 RESPECTIVELY.

*** BETWEEN FWD AND CENTER, X = 7.43; BETWEEN CENTER AND AFT, X = 7.2

Figure 4.- Geometry of the plenum chamber, turning vanes, and nozzle assemblies. All dimensions in centimeters.

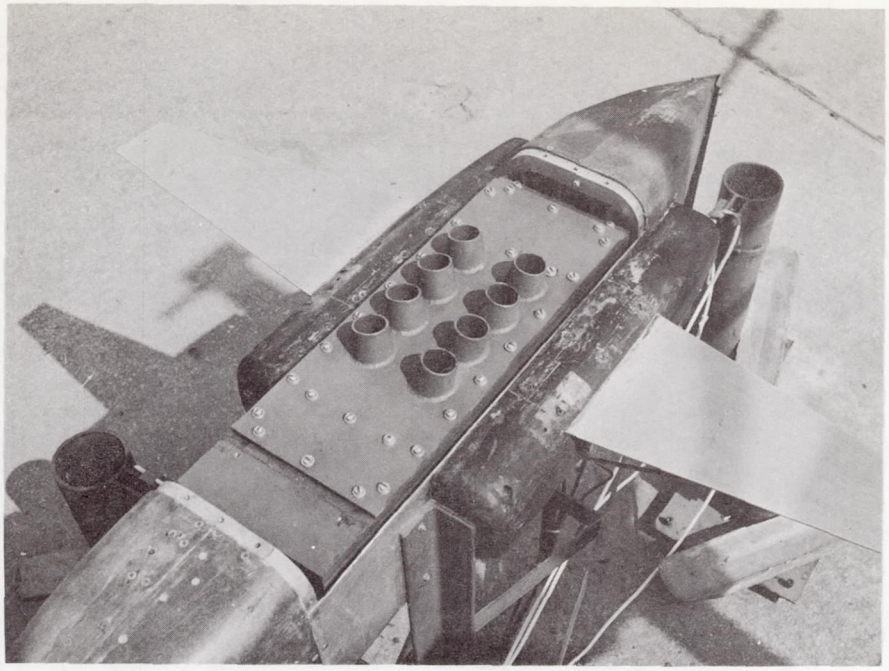

(a) Nozzle assembly in place.

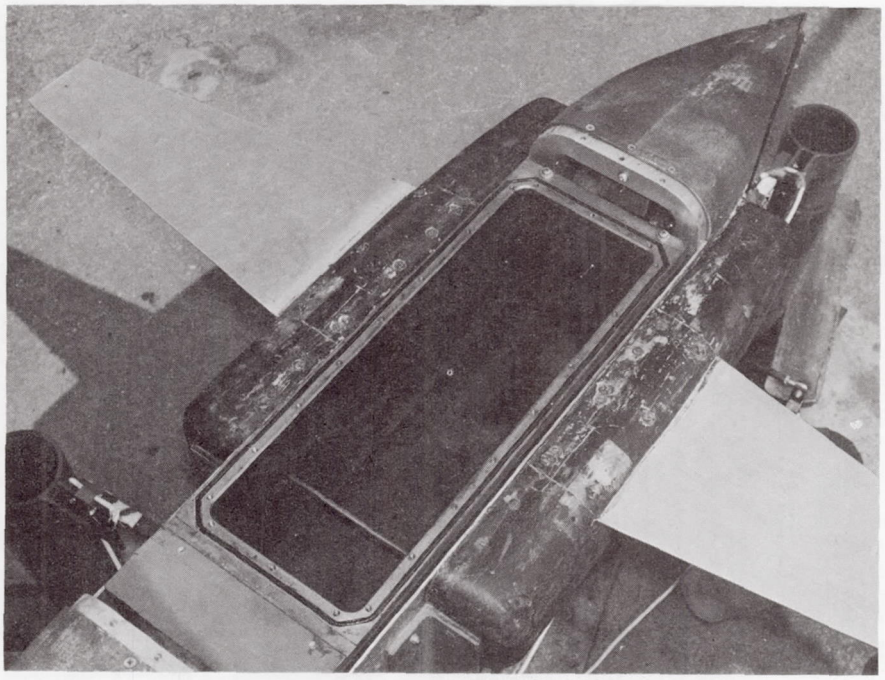

(b) Nozzle assembly removed.

Figure 5.- Plenum chamber in model cavity.

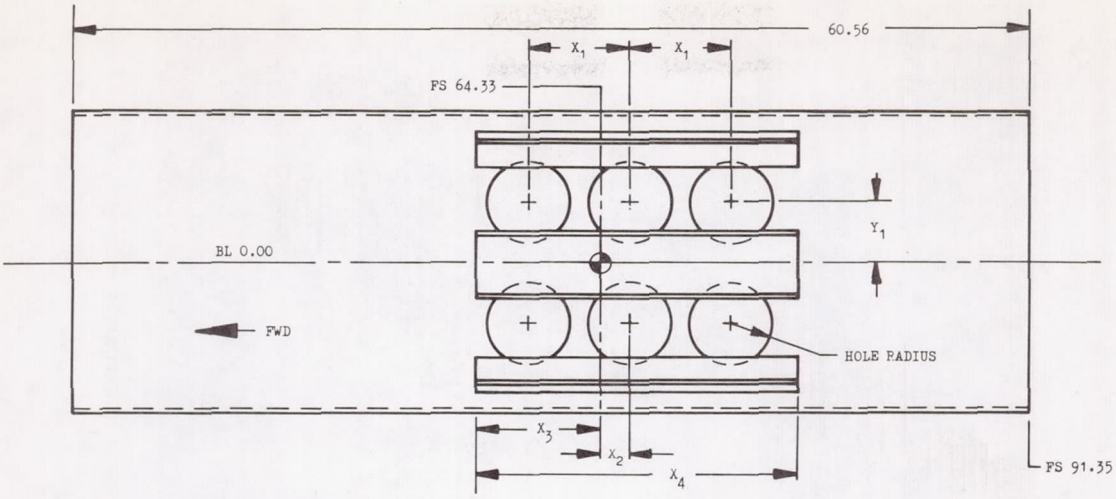

PLAN VIEW

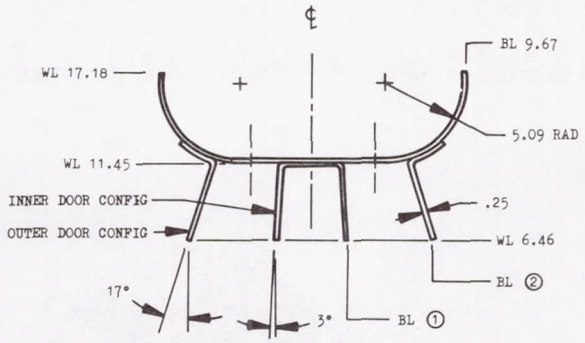

END VIEW

REMOVABLE NOZZLE EXIT ASSEMBLY DIMENSIONS

NOZZLE CONFIG	NUMBER HOLES	HOLE DIA, cm	Y_1, cm	X_1, cm	X_2, cm	X_3, cm	X_4, cm	BL ①	BL ②
1	4	5.90	4.78	7.90	5.74				
1a	4	5.55	4.64	7.90	5.74				
2	6	5.09	3.93	6.45	1.79	7.79	20.36	1.98	7.71
3	8	4.58	3.42	5.58	4.58				
3a	8	4.15	3.28	5.58	4.58				
4	4	5.09	3.93	6.45	5.01				
5	8	5.09	3.93	6.45	5.01				
6	6	5.09	3.79	6.45	1.79				
7	6	5.09	3.93	6.45	0				
7a	6	4.84	3.79	6.45	0				
8	6	*	3.93	6.45	1.79	7.79	20.36	2.67	7.00
9	8	4.58	3.42	4.92	1.67				
10	8	4.58	3.42	6.56	5.07				
12	8	4.58	4.57	5.58	4.58				
13	8	4.58	5.69	5.58	4.56				
21	6	**	4.82	***	1.50	9.16	21.63	2.74	
22	4	6.41	4.02	21.45	10.73				

* ELONGATED HOLE - 1.88 cm RADIUS AT ENDS WITH CENTERS 2.54 cm APART.
** FWD HOLES, 5.09 cm; CENTER AND AFT HOLES, 5.34 cm.
*** BETWEEN FWD AND CENTER, X_1 = 7.56; BETWEEN CENTER AND AFT, X_1 = 7.42.

Figure 6.- Geometry of removable fuselage cover plate. All dimensions in centimeters.

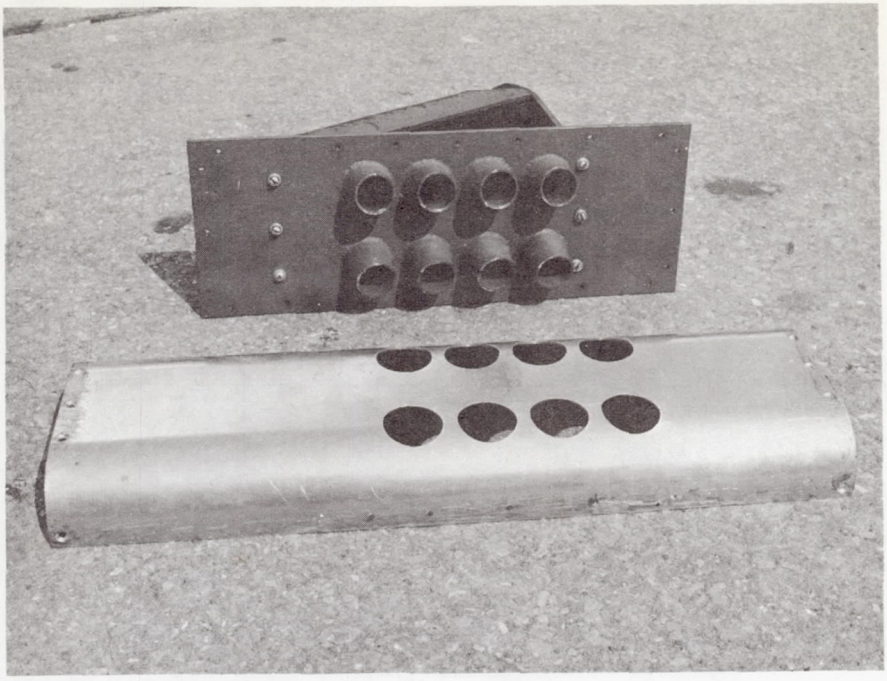

Figure 7.- Nozzle assembly with matching cover plate.

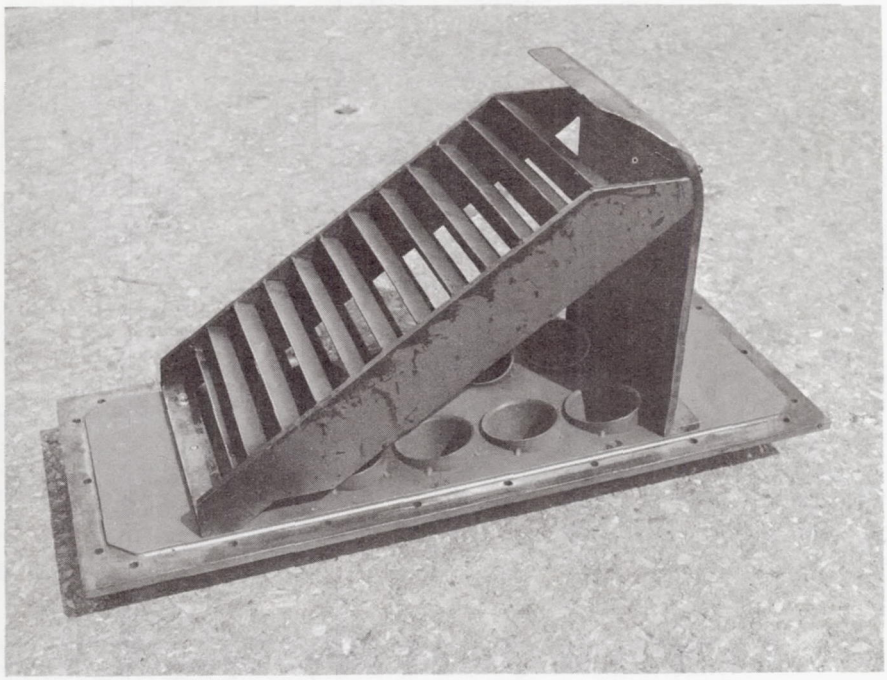

Figure 8.- Turning vanes.

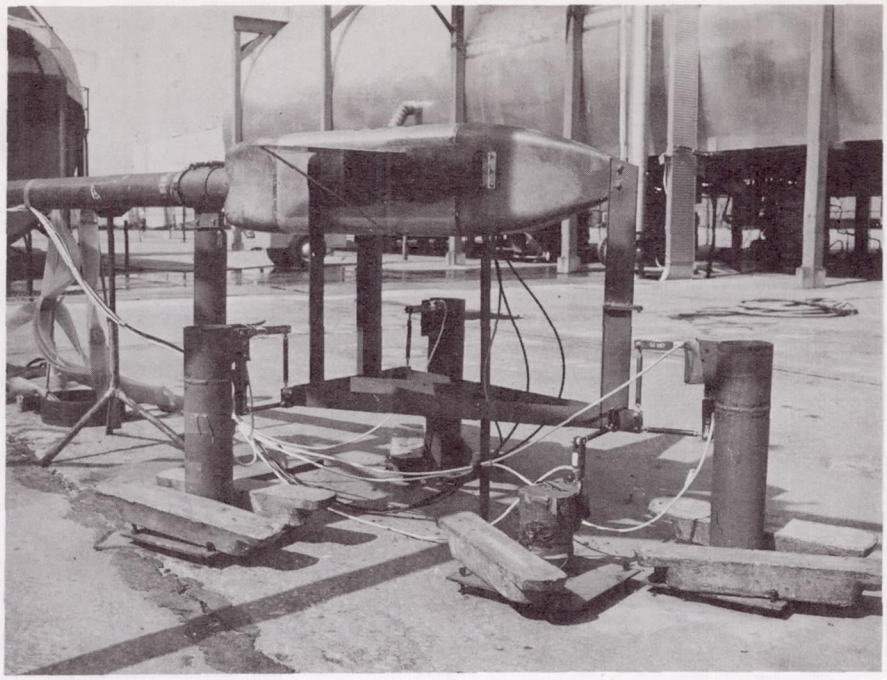

(a) Overall view.

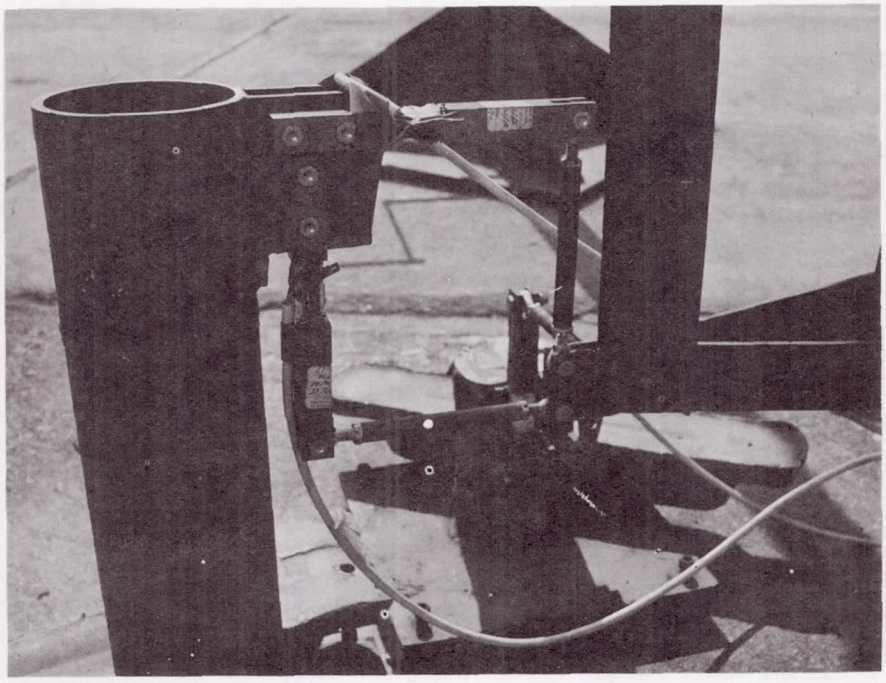

(b) Aft load cells.

Figure 9.- Six-component force-measuring system.

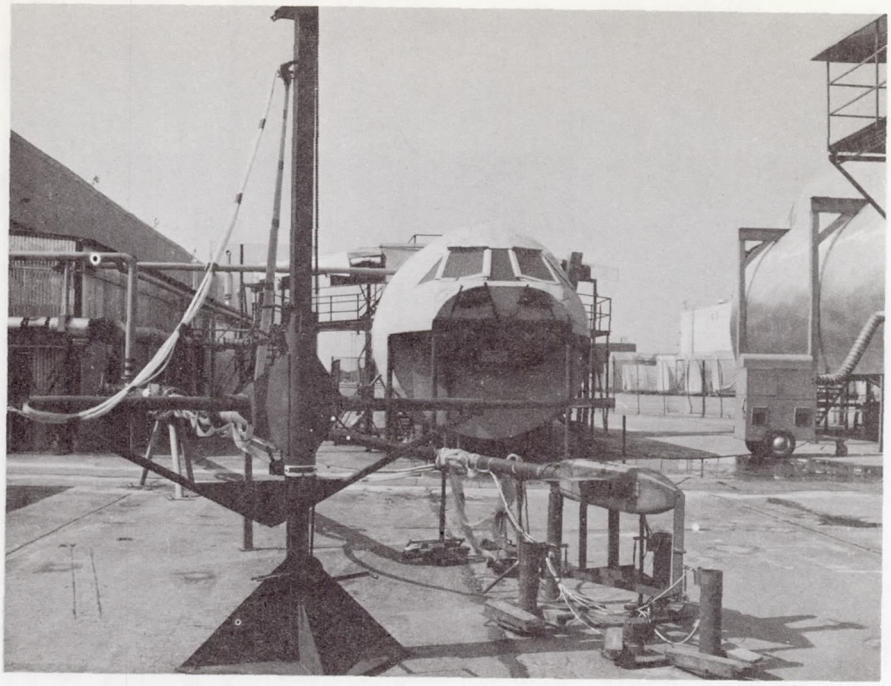

(a) Support.

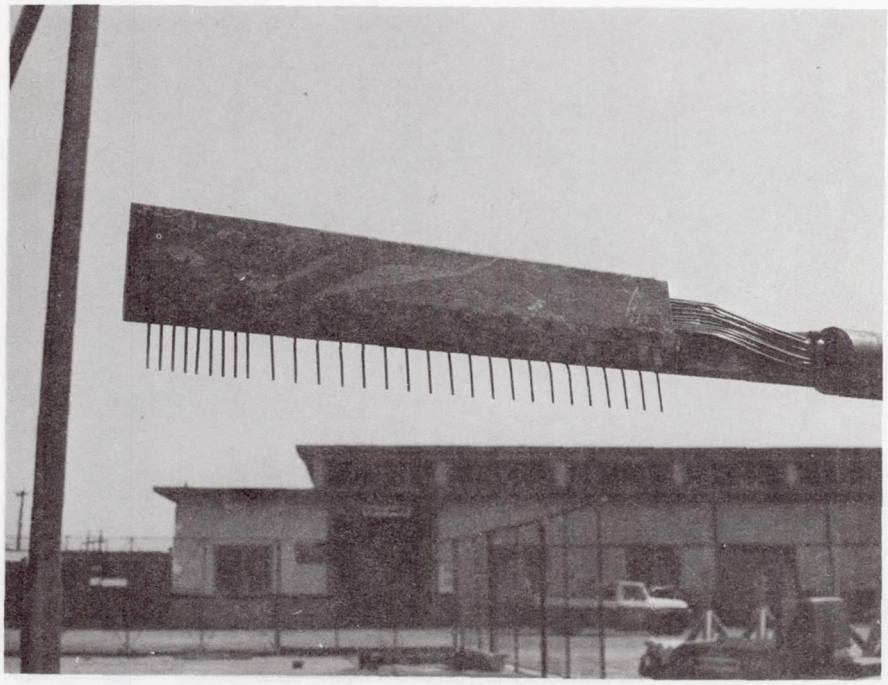

(b) Rake.

Figure 10.- Jet decay rake.

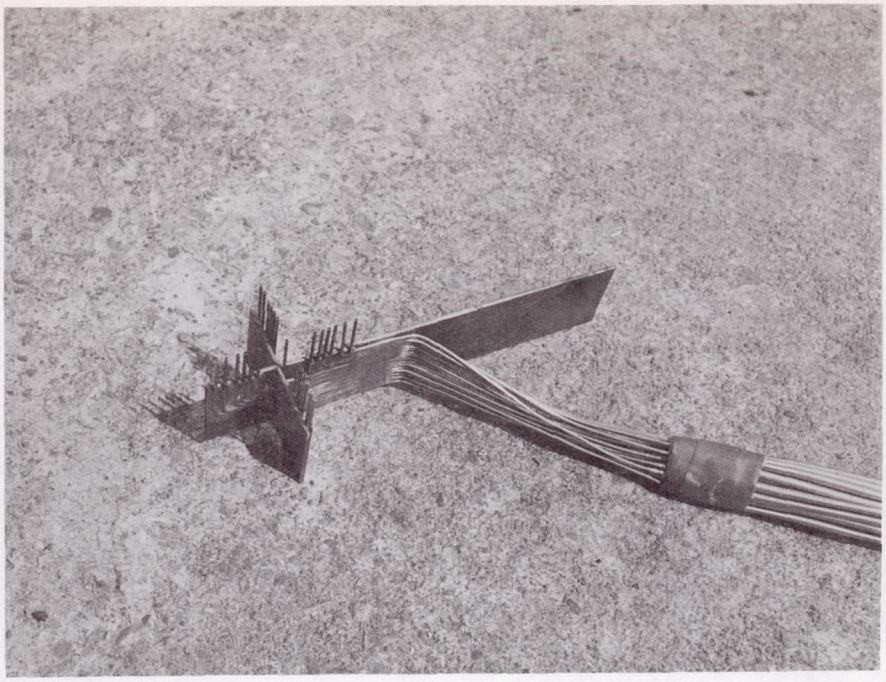

(a) Rake.

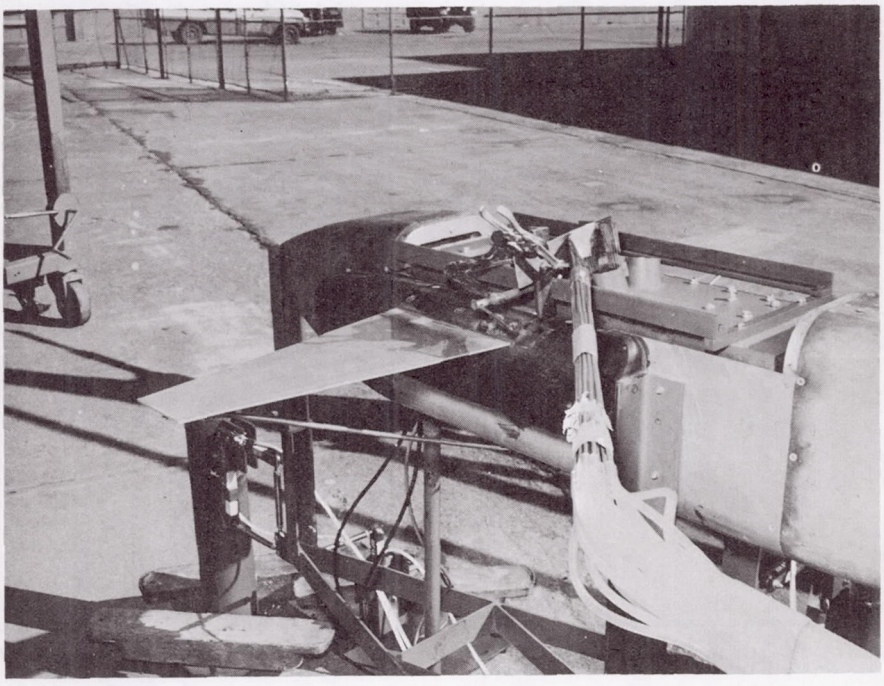

(b) Rake on support frame, in position for test.

Figure 11.- Nozzle exit survey rake.

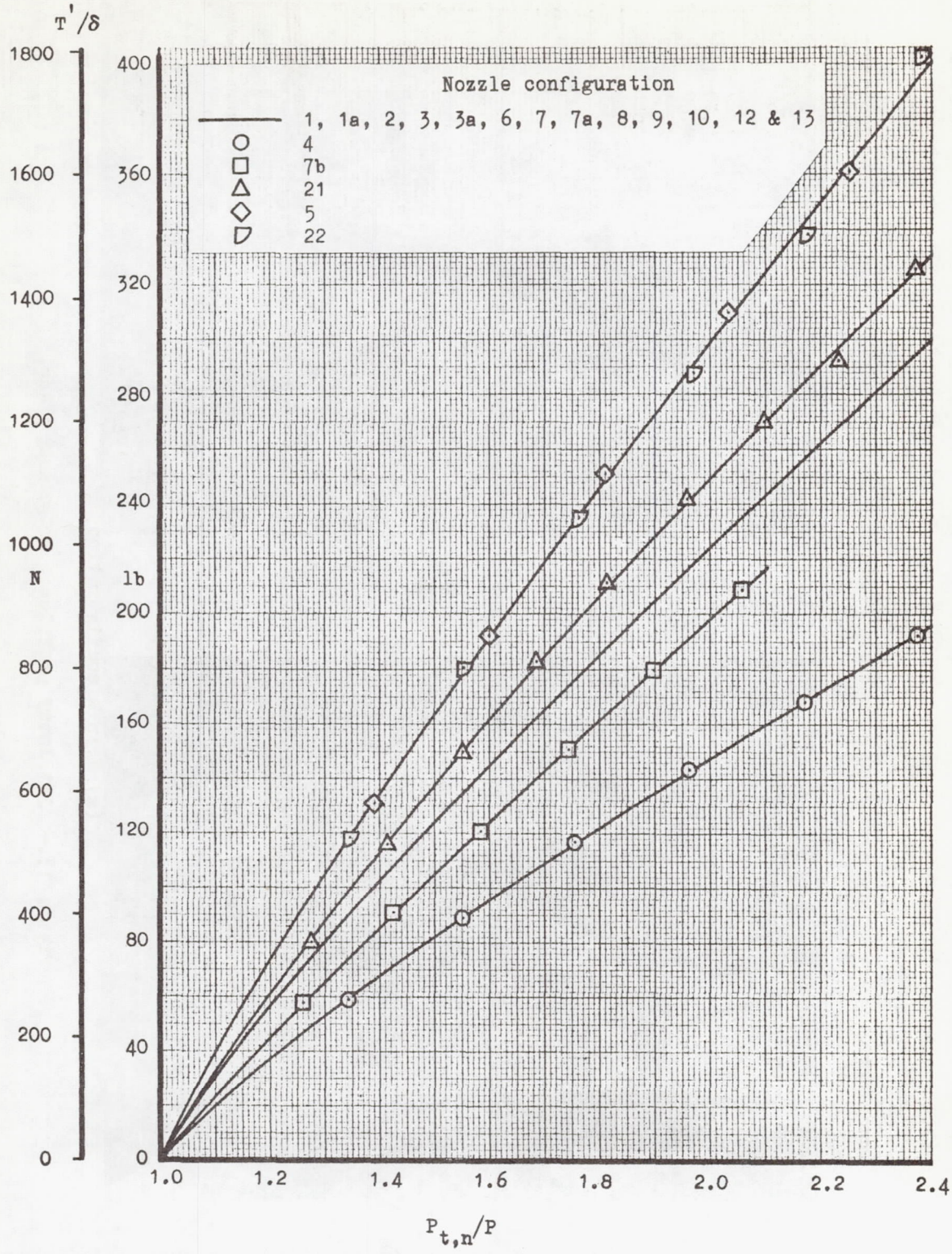

Figure 12.- Nozzle thrust.

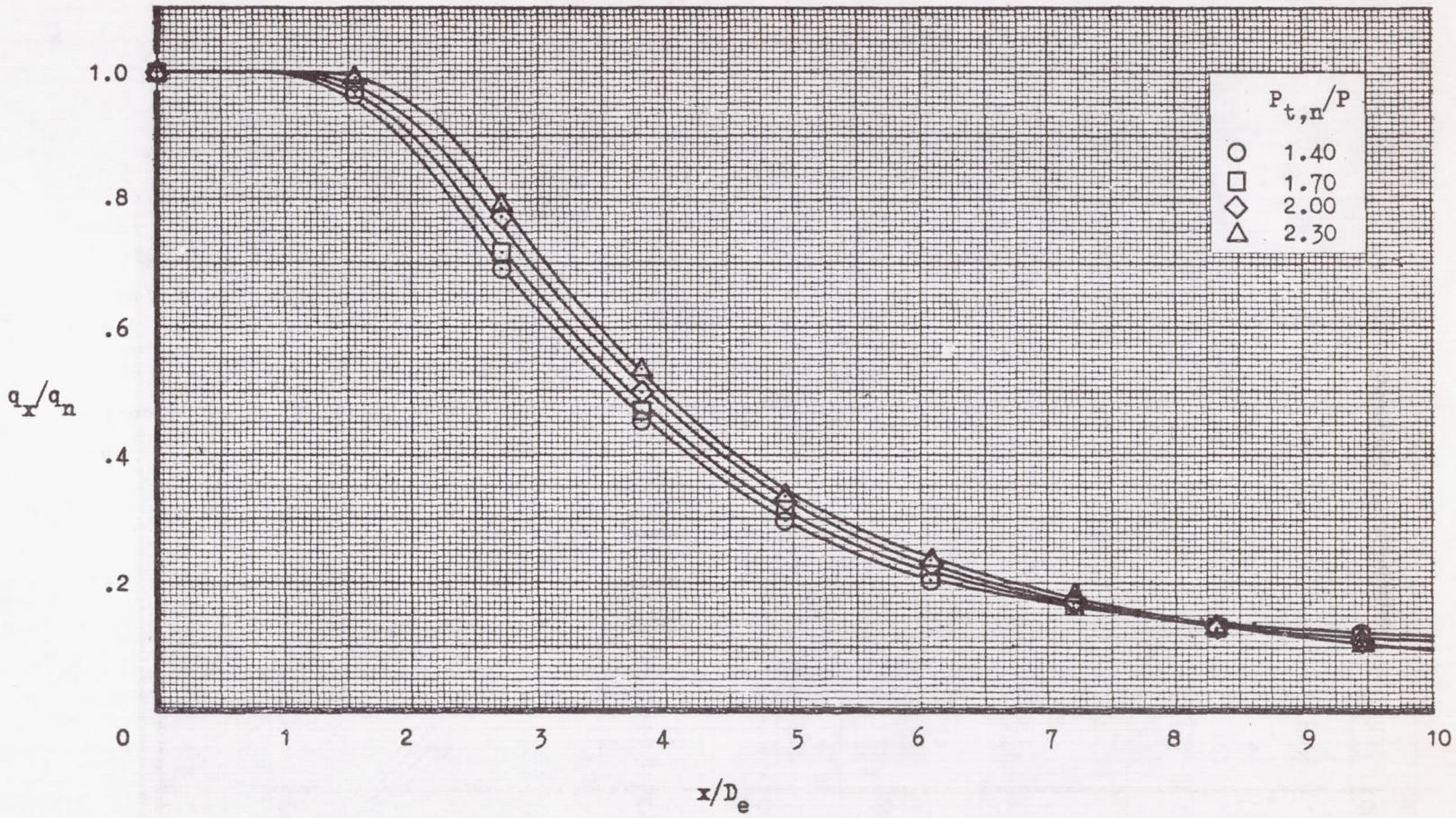

(a) Nozzle configuration 1.

Figure 13.- Jet decay profiles. No ground plane.

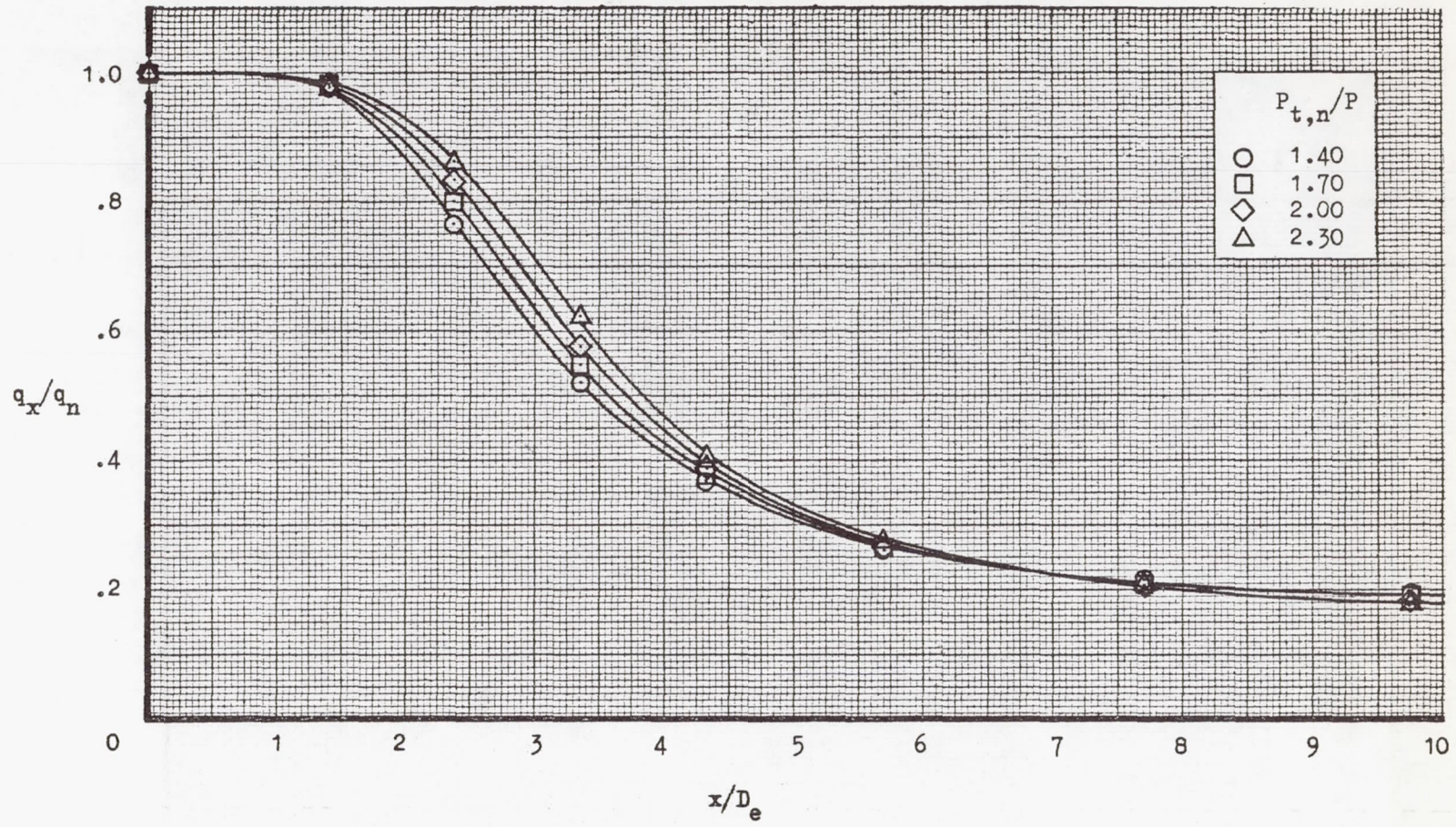

(b) Nozzle configuration 1a.

Figure 13.- Continued.

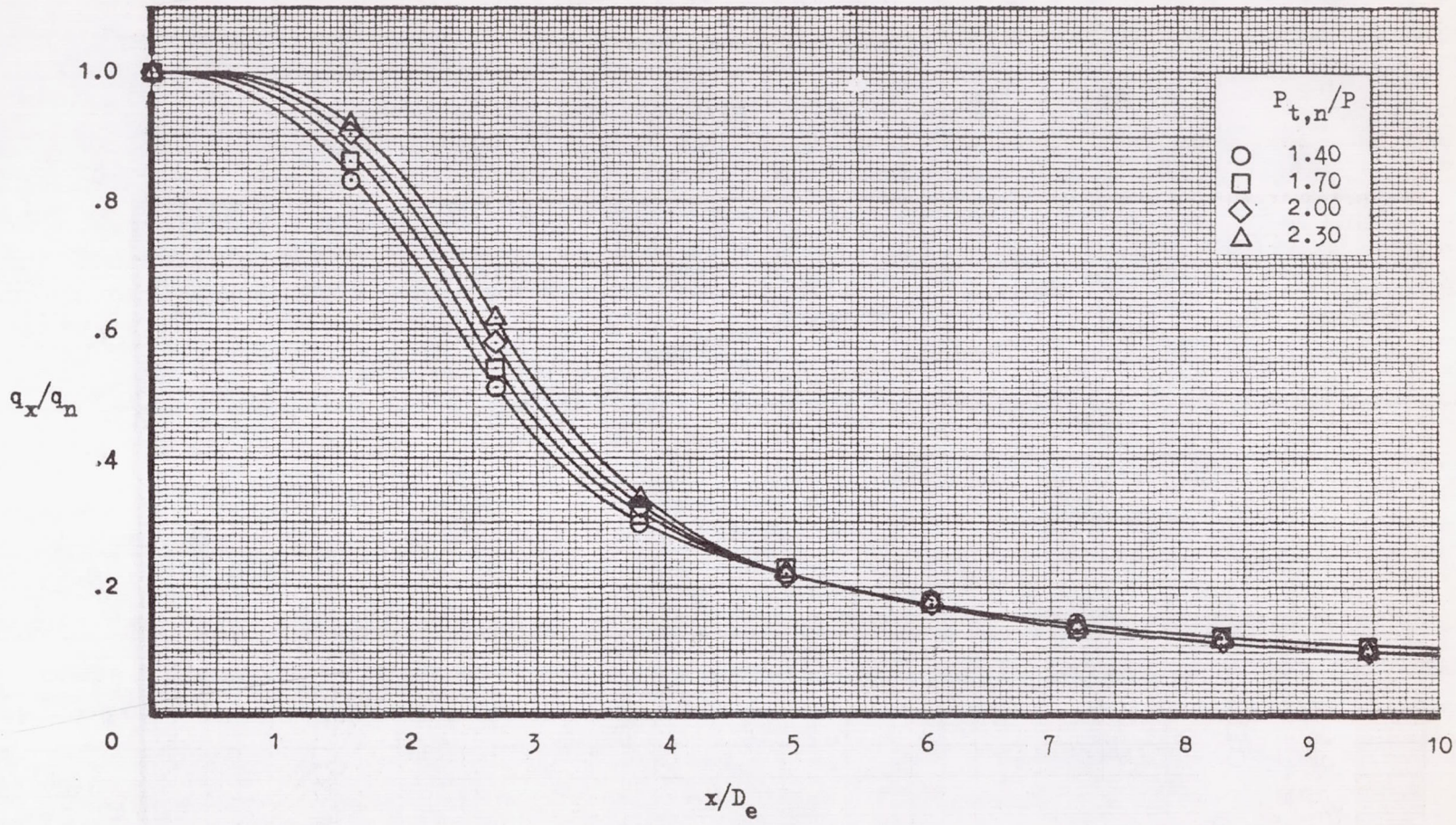

(c) Nozzle configuration 2.

Figure 13.- Continued.

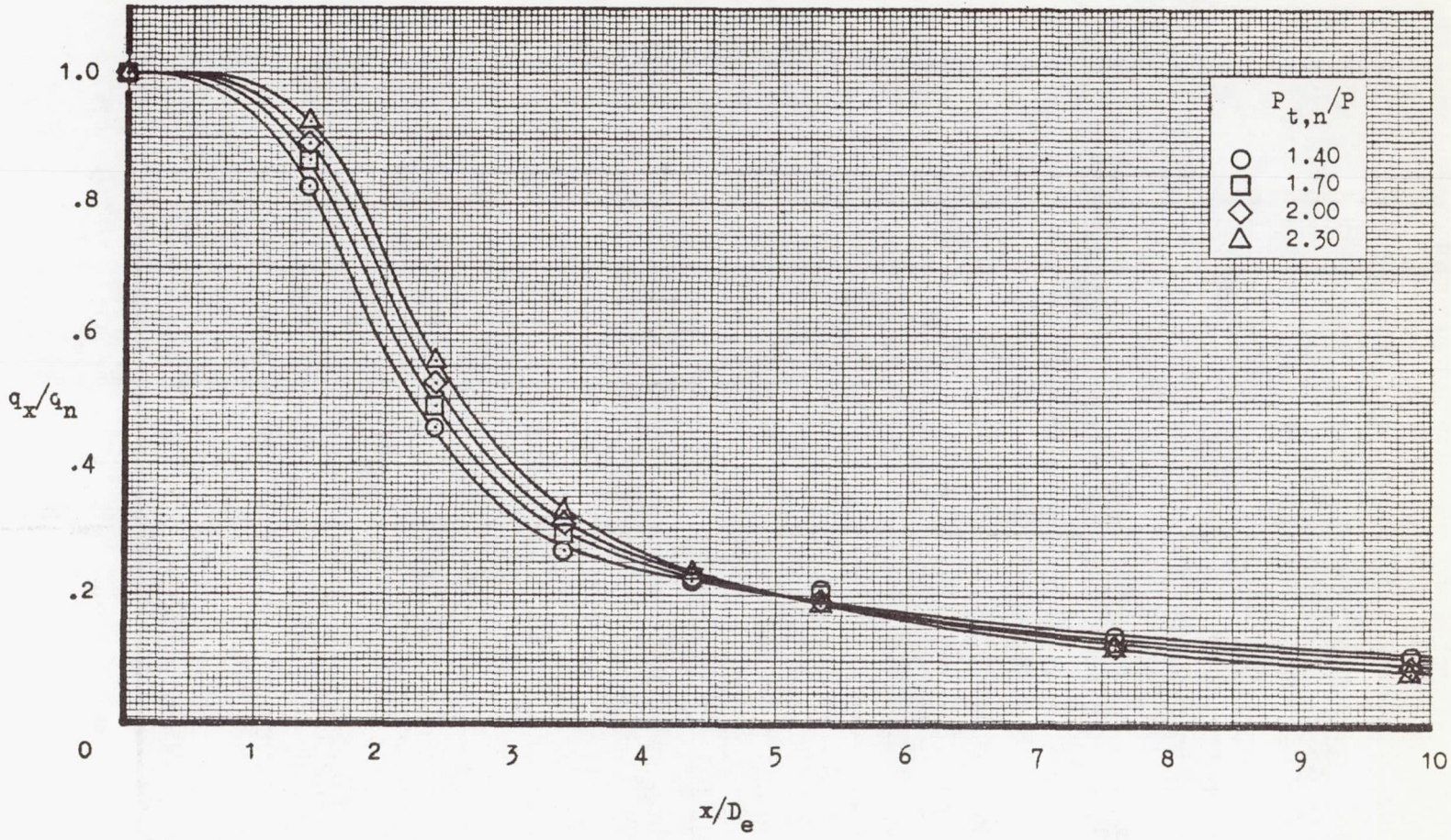

(d) Nozzle configuration 3.

Figure 13.- Continued.

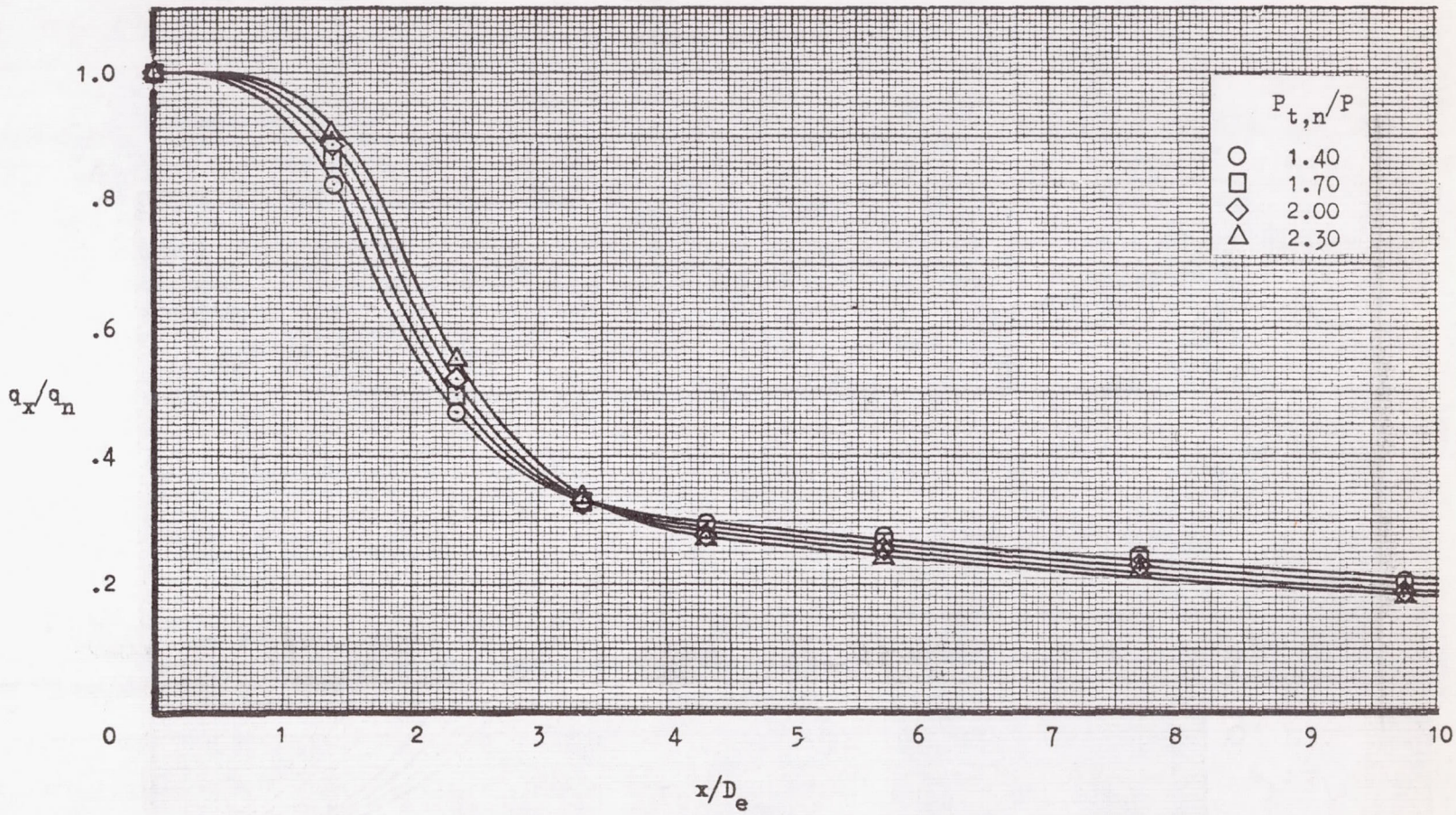

(e) Nozzle configuration 3a.

Figure 13.- Continued.

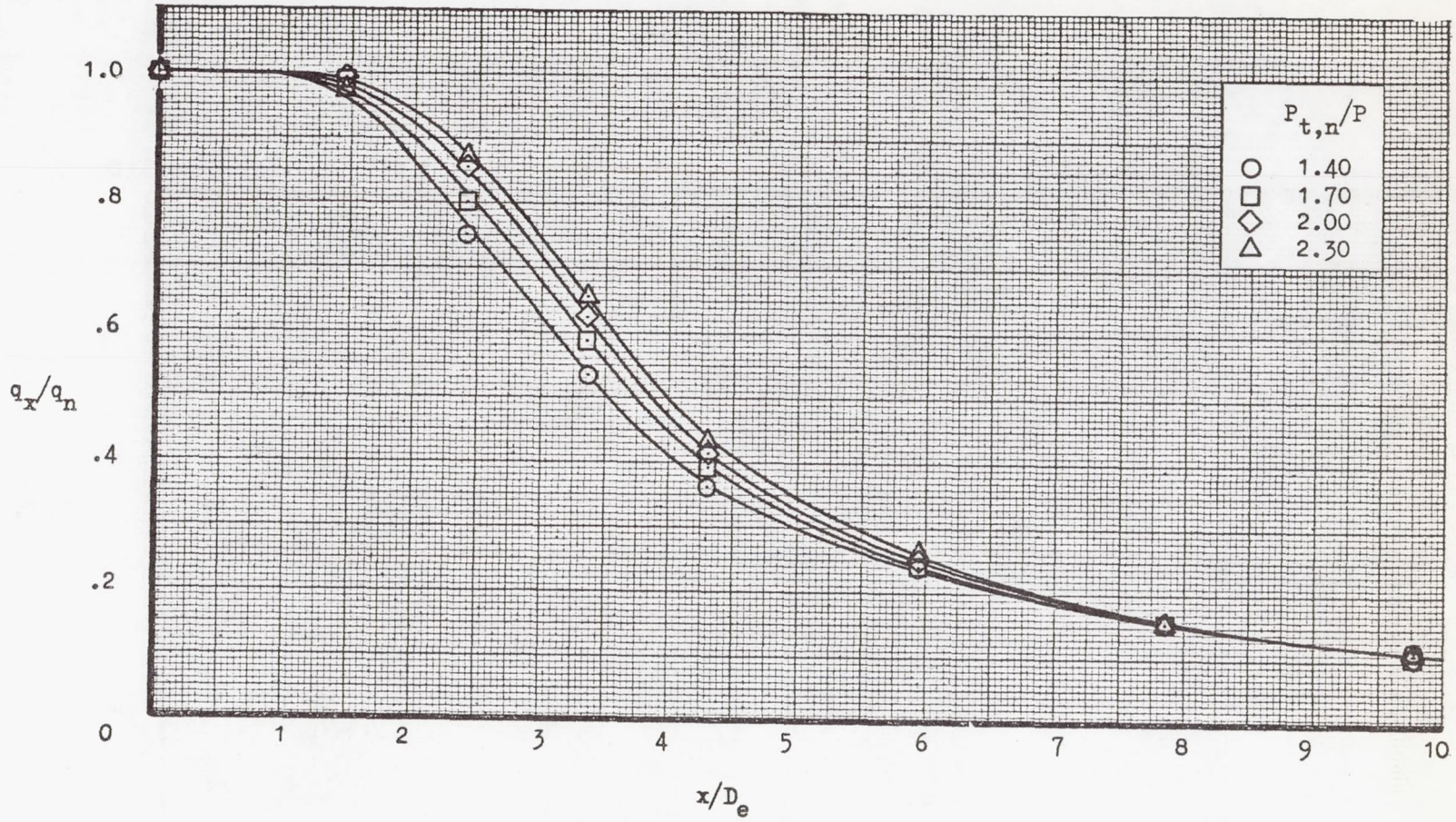

(f) Nozzle configuration 4.

Figure 13.- Continued.

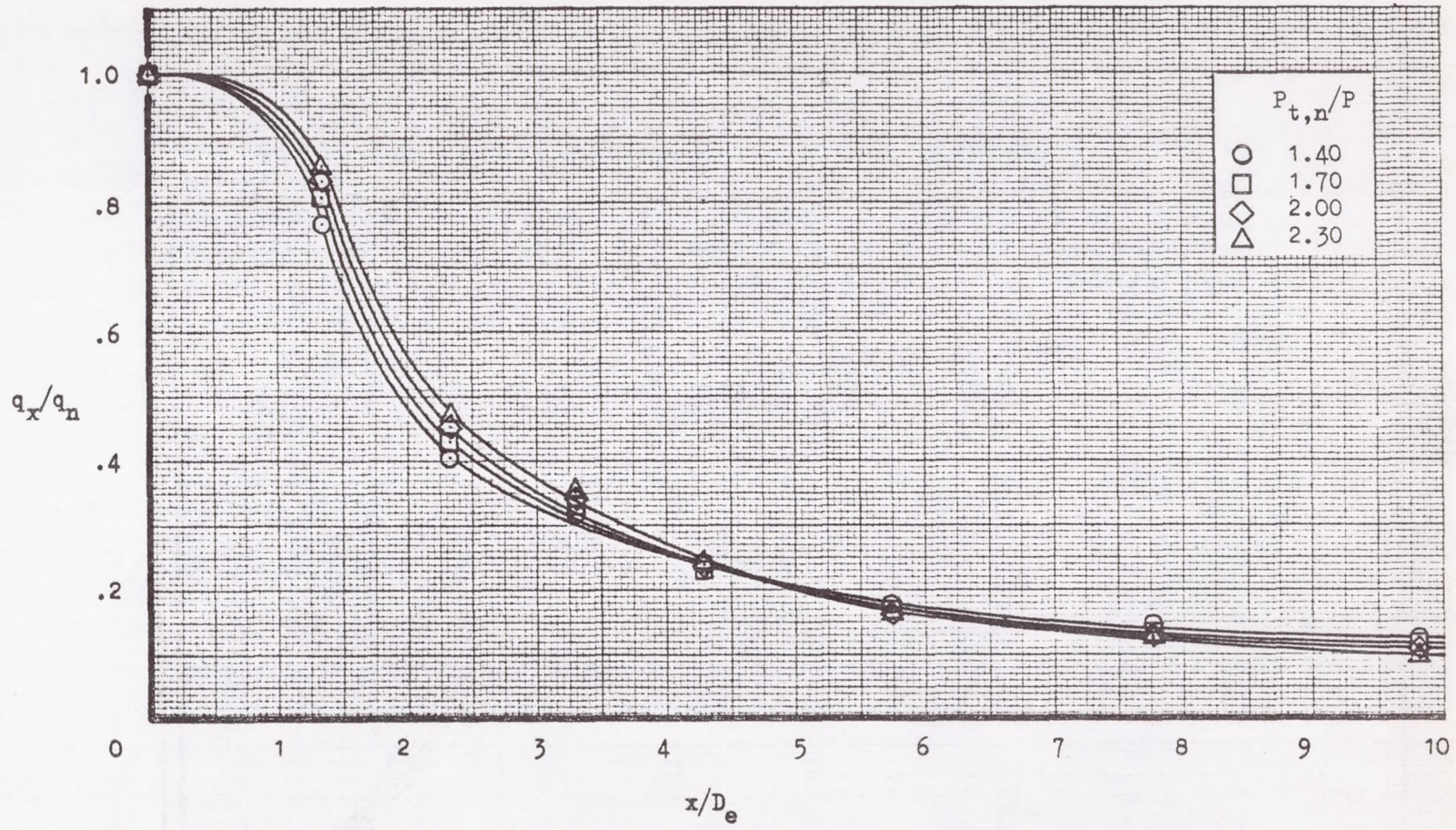

(g) Nozzle configuration 5.

Figure 13.- Continued.

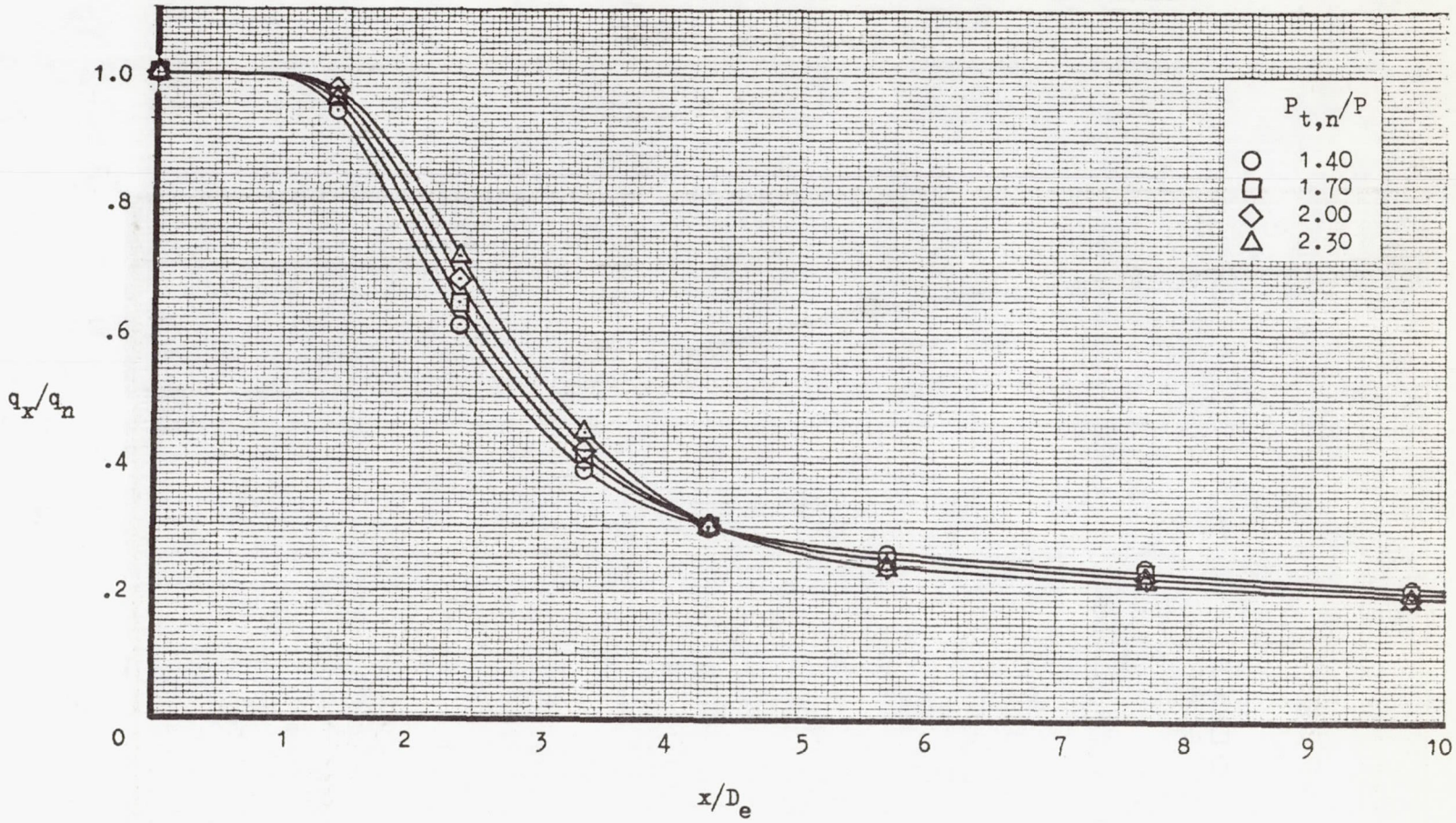

(h) Nozzle configuration 6.

Figure 13.- Continued.

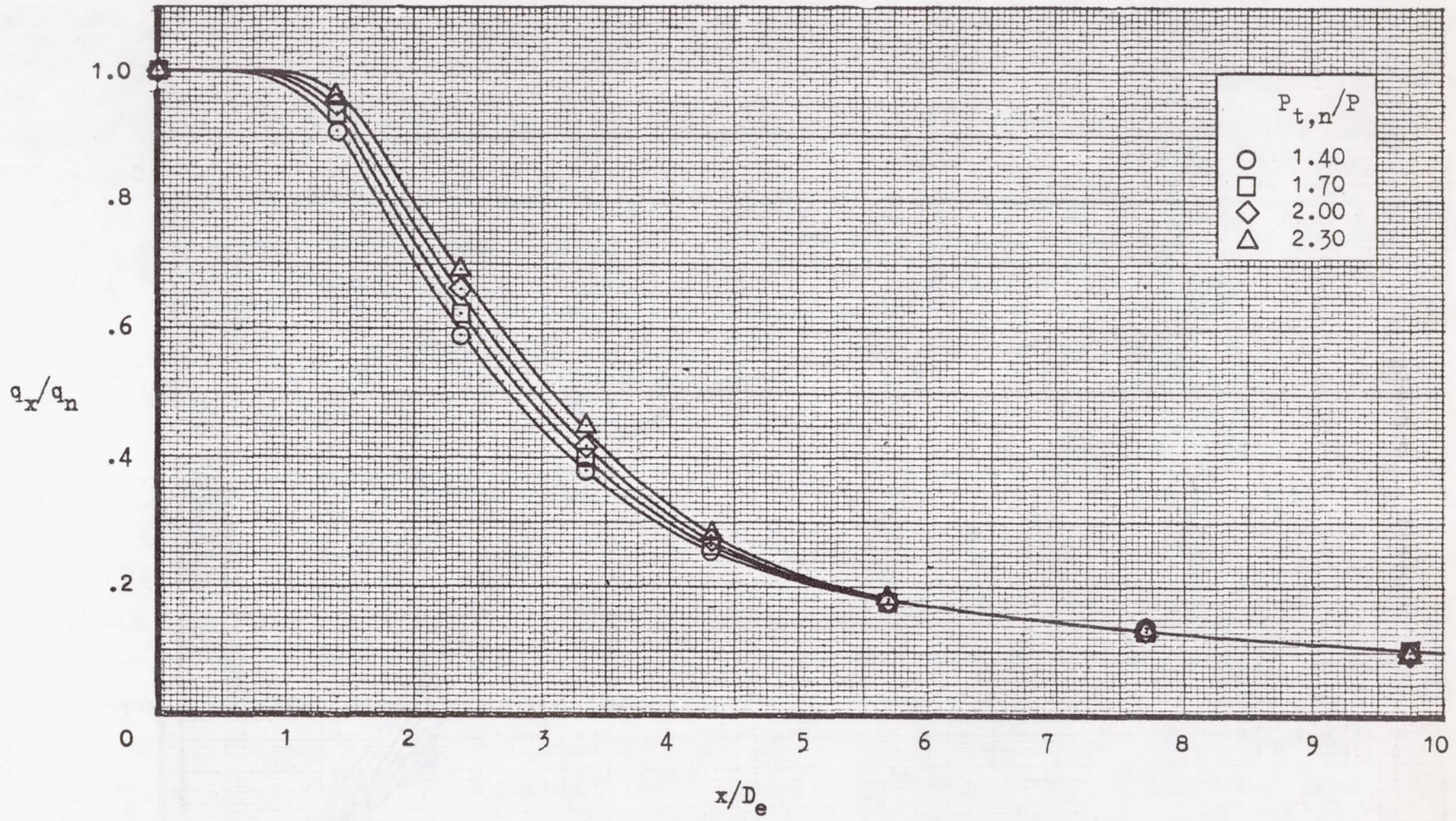

(i) Nozzle configuration 7.

Figure 13.- Continued.

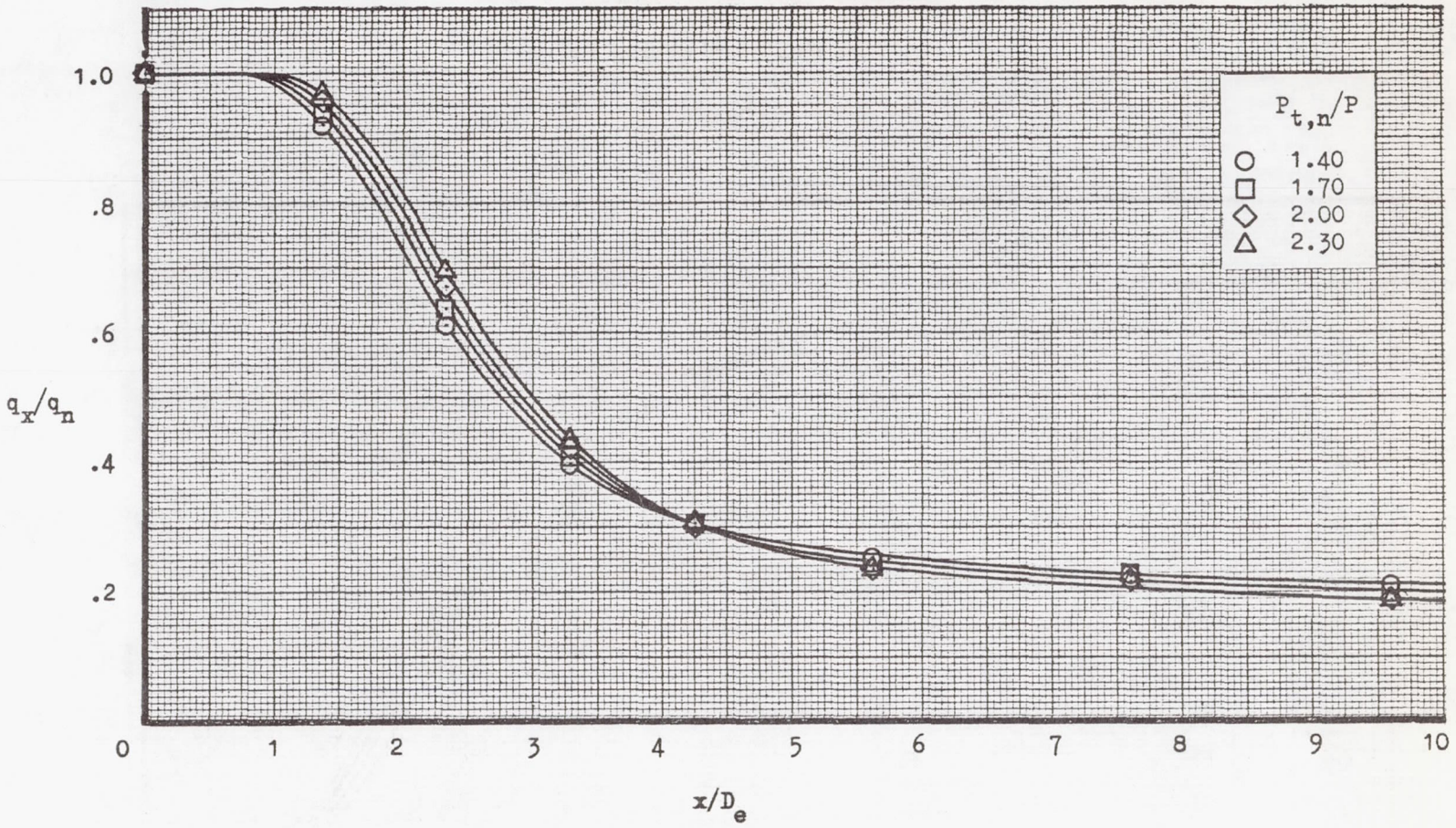

(j) Nozzle configuration 7a.

Figure 13.- Continued.

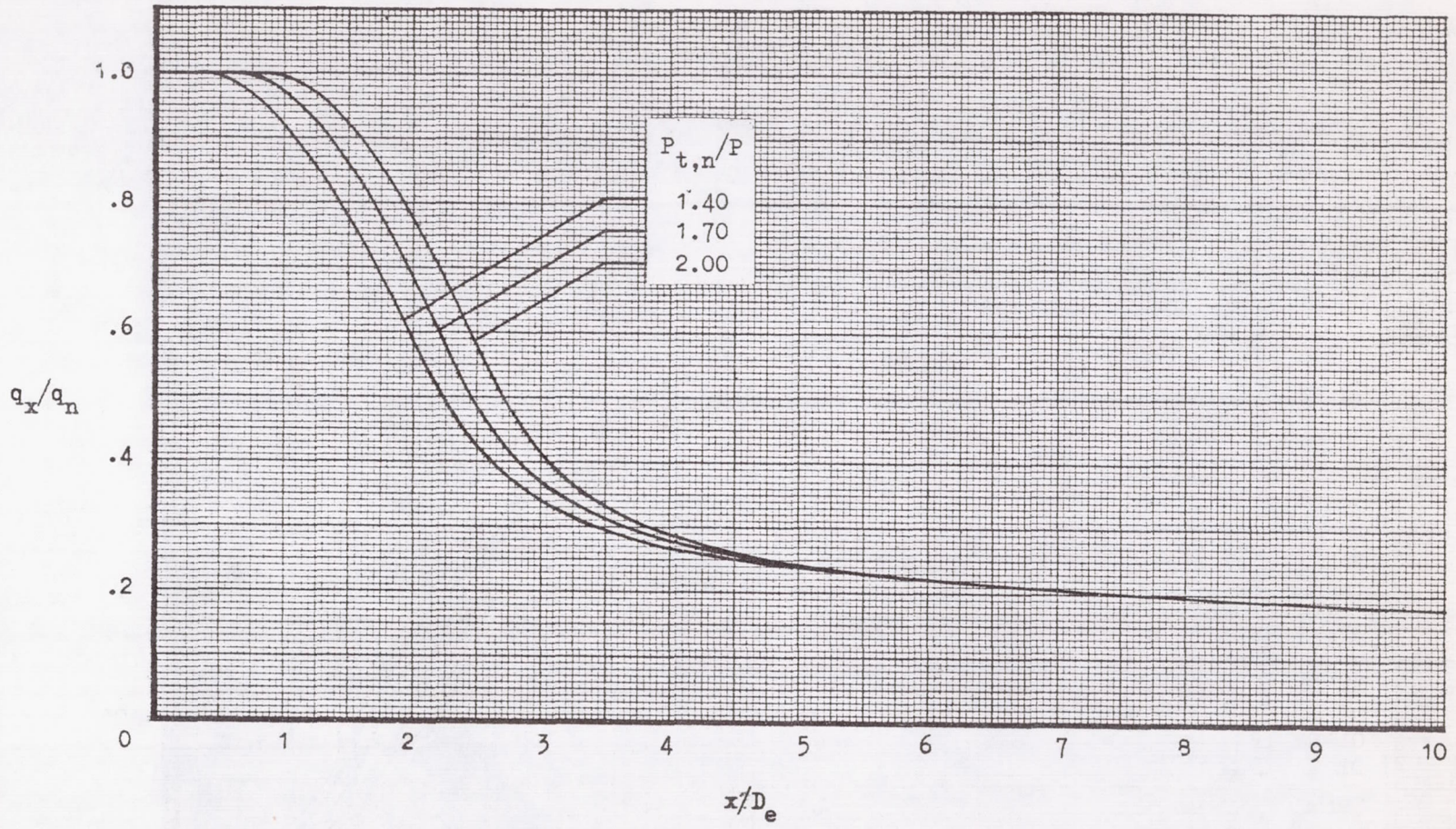

(k) Nozzle configuration 7b.

Figure 13.- Continued.

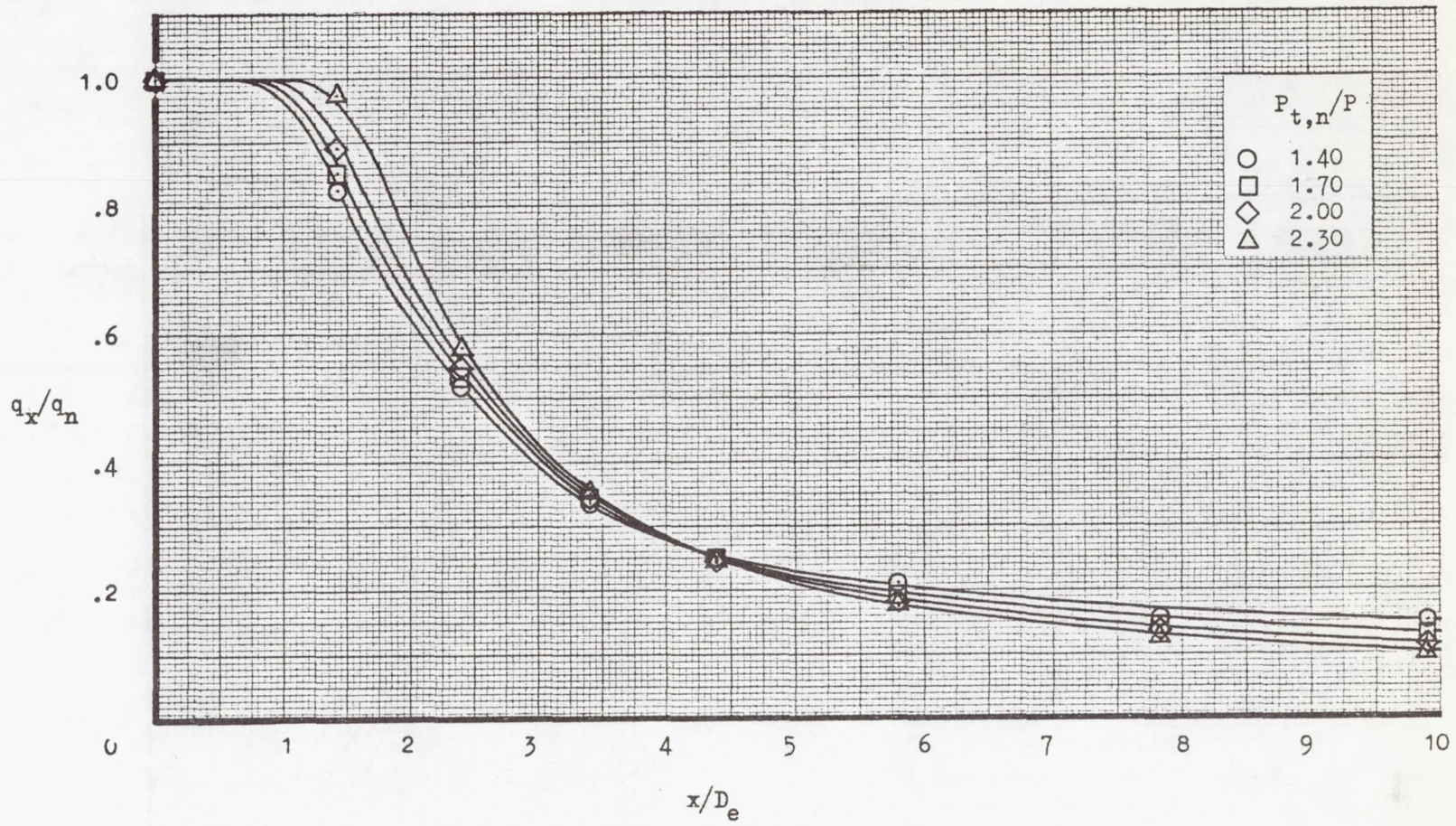

(l) Nozzle configuration 8.

Figure 13.- Continued.

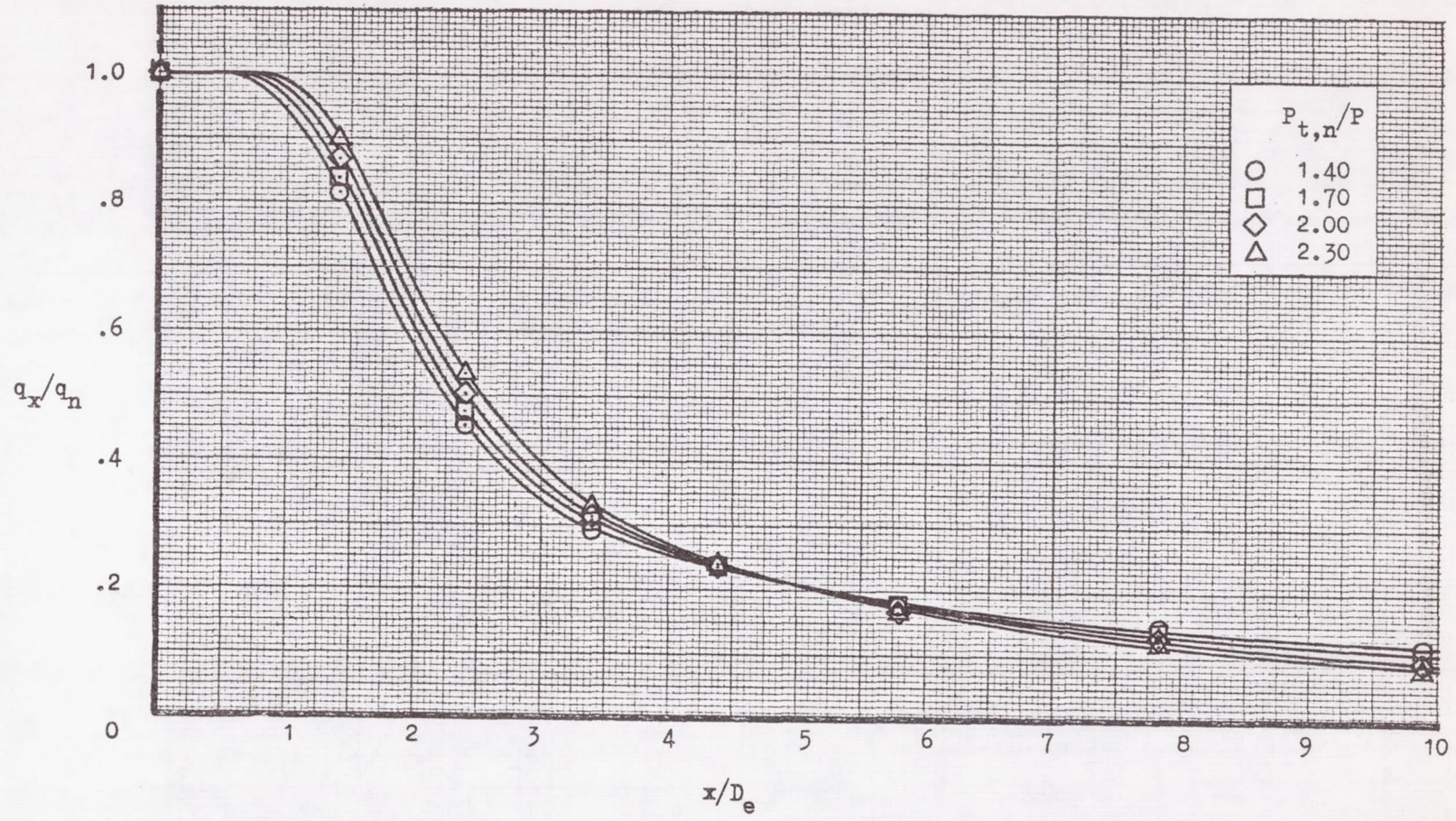

(m) Nozzle configuration 9.

Figure 13.- Continued.

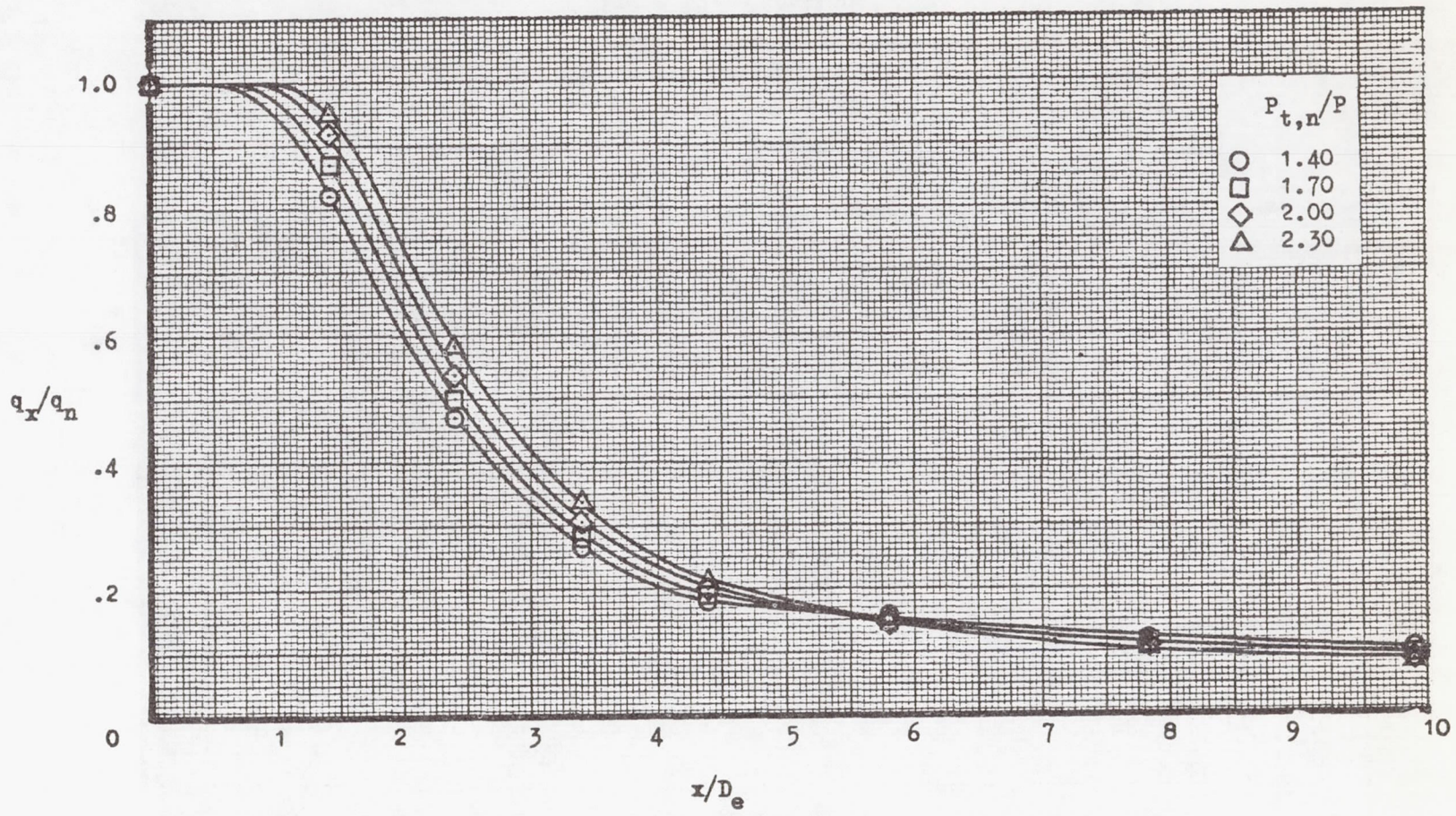

(n) Nozzle configuration 10.

Figure 13.- Continued.

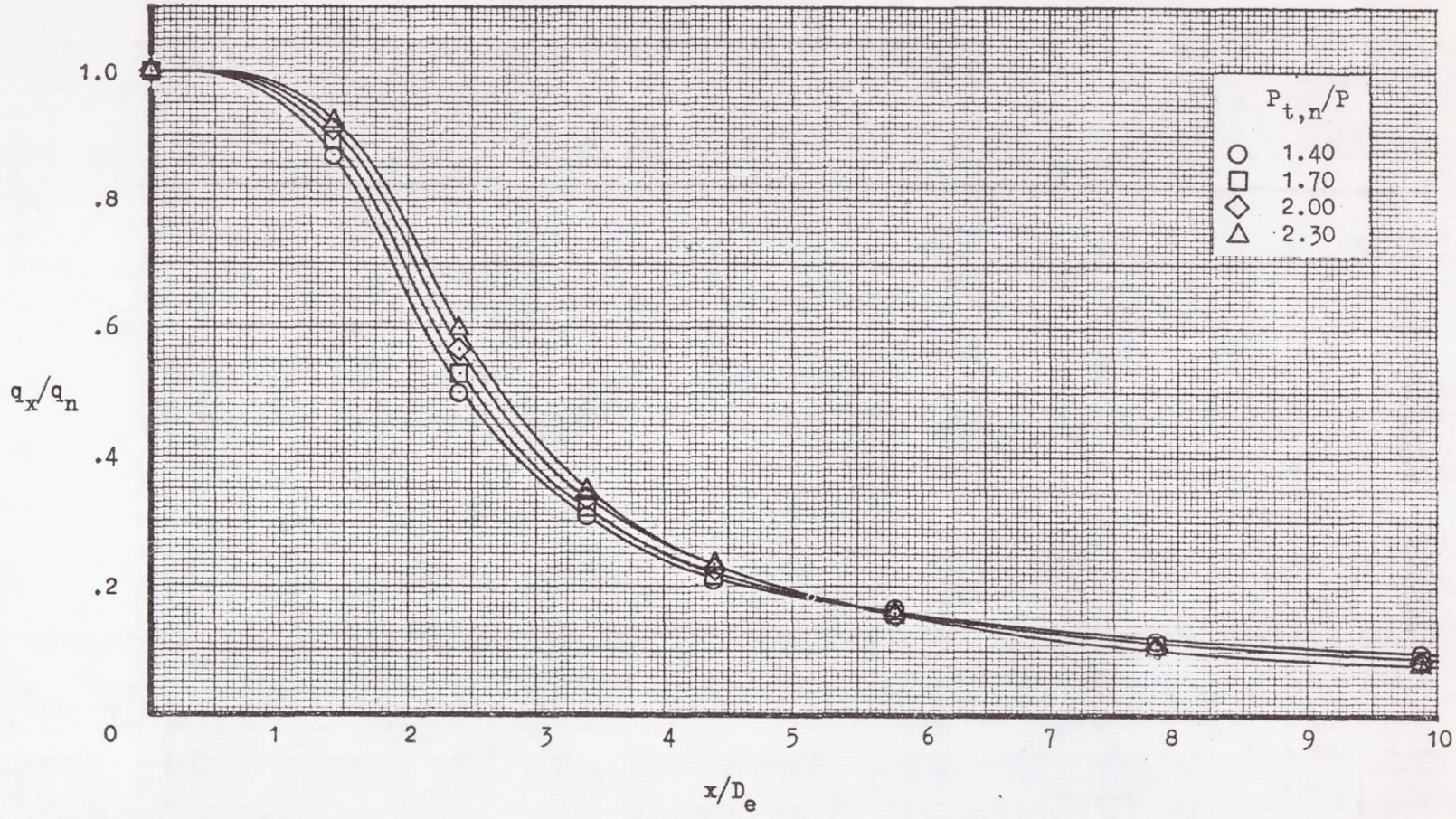

(o) Nozzle configuration 12.

Figure 13.- Continued.

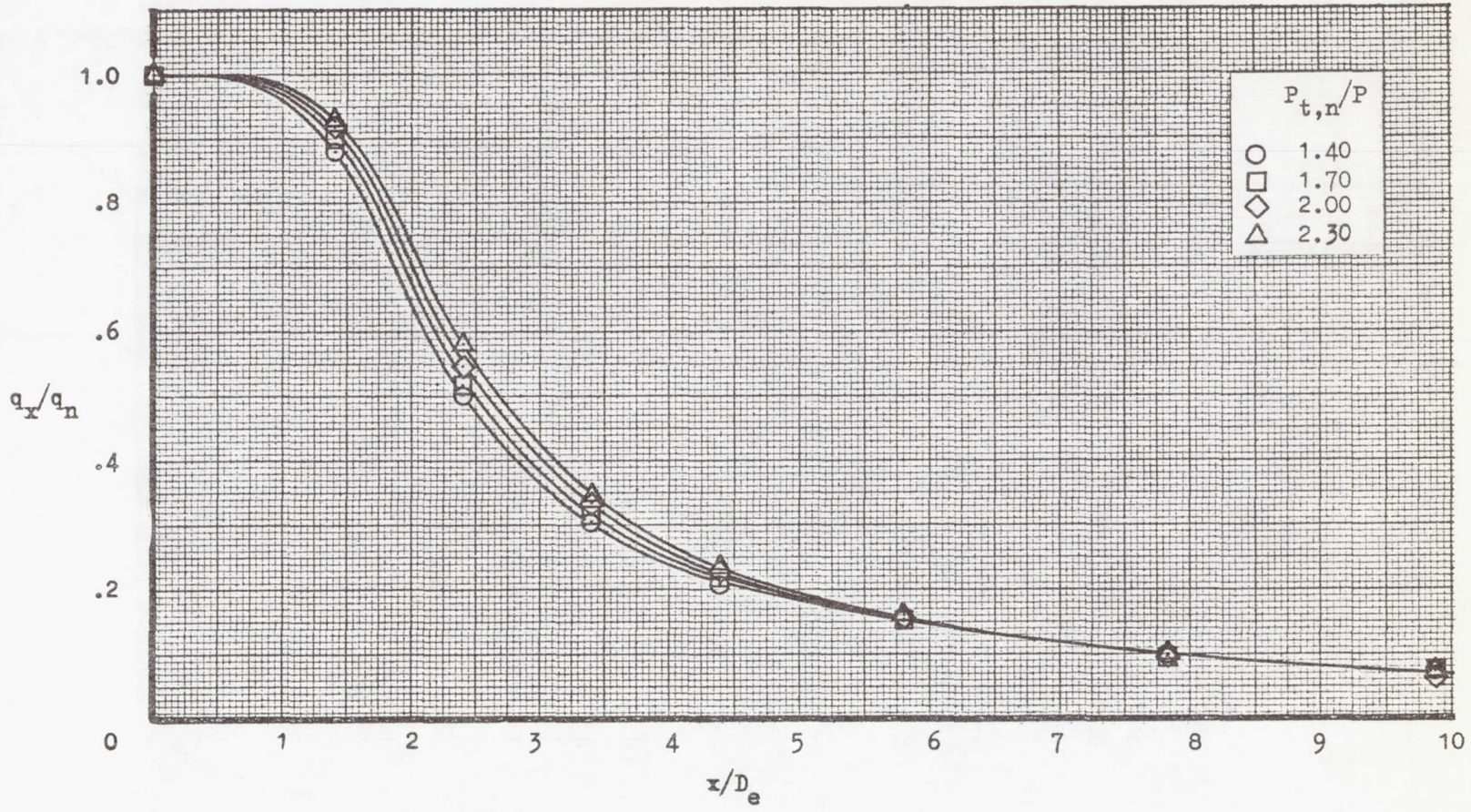

(p) Nozzle configuration 13.

Figure 13.- Continued.

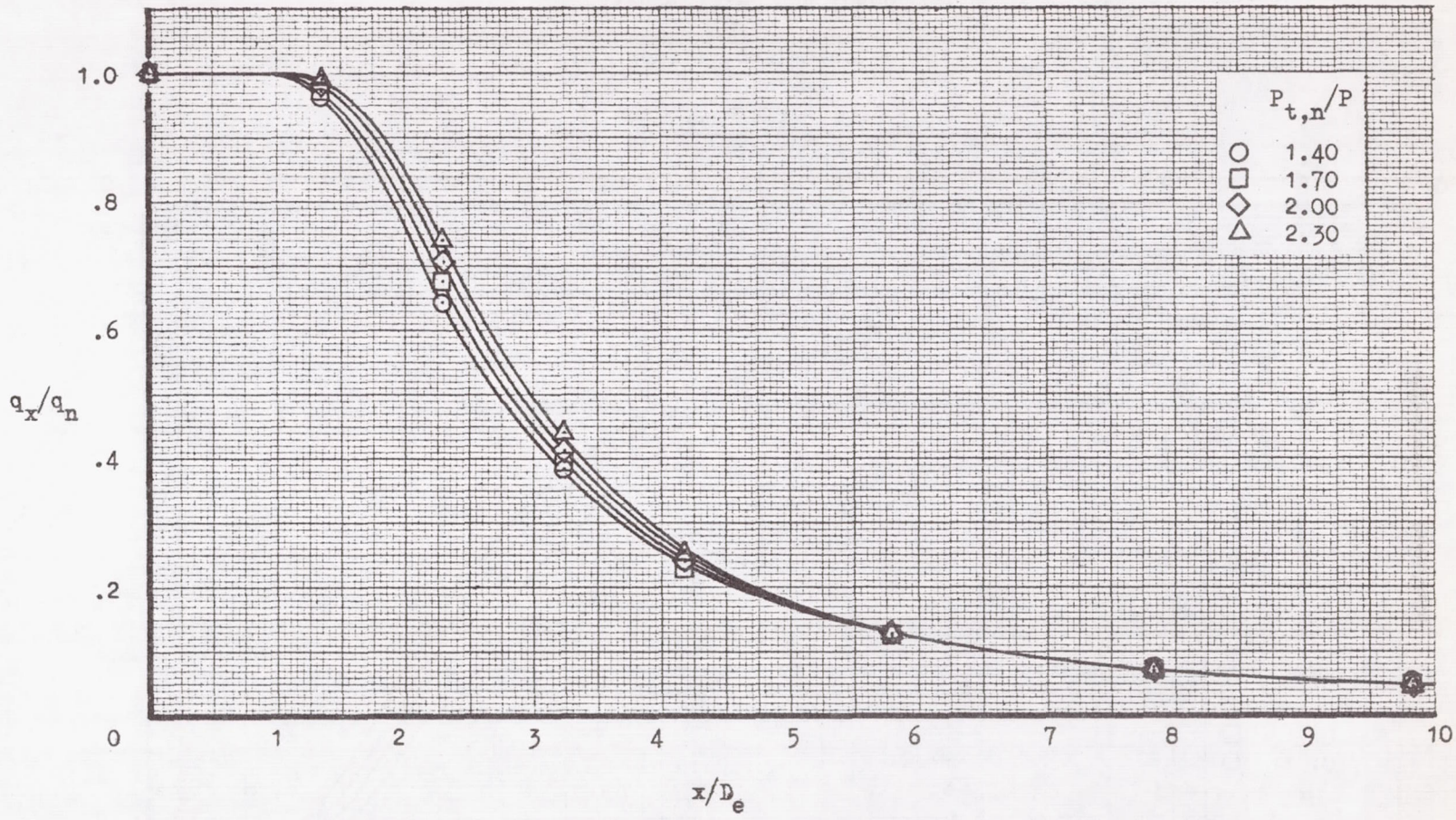

(q) Nozzle configuration 21.

Figure 13.- Continued.

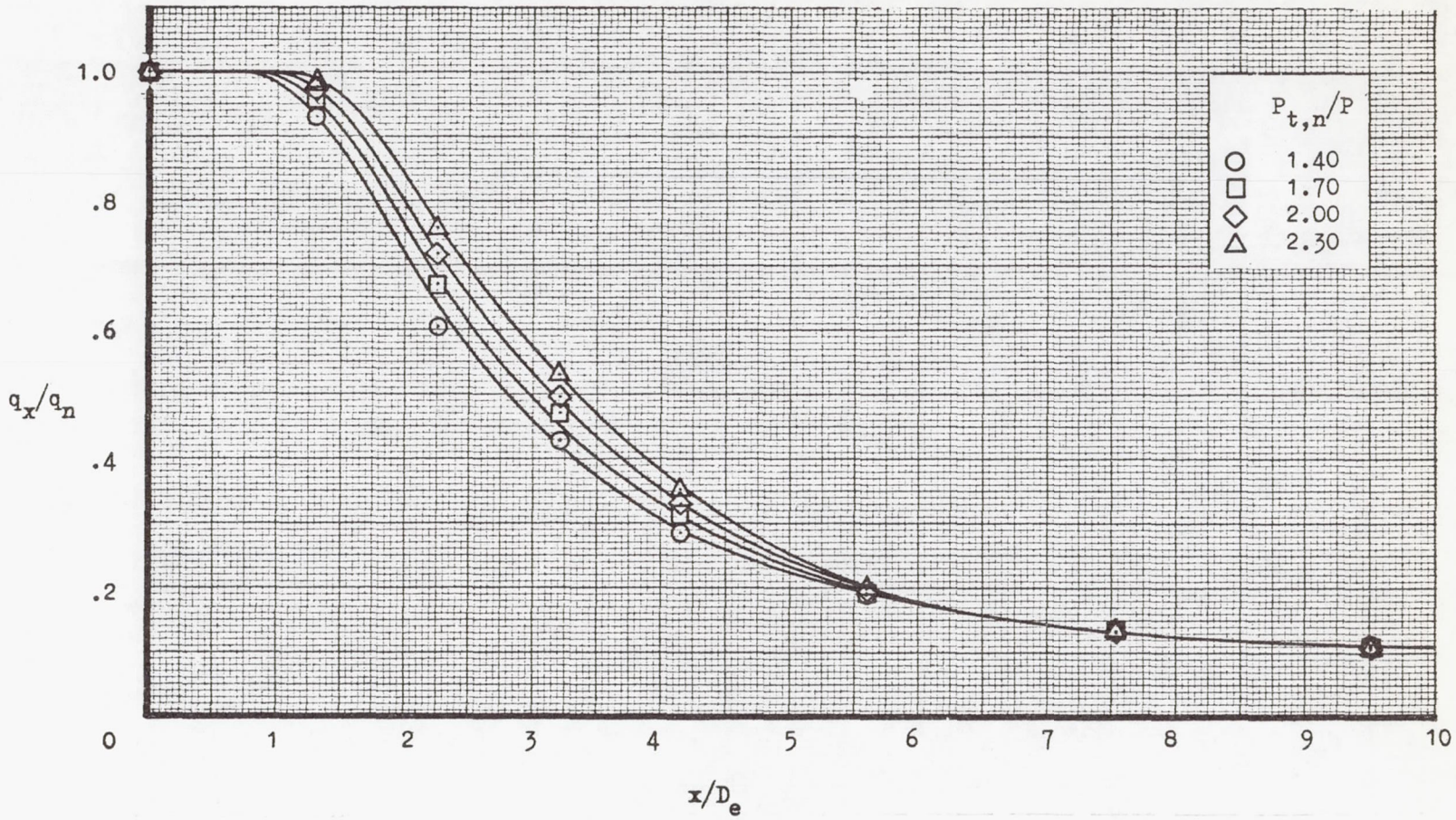

(r) Nozzle configuration 22.

Figure 13.- Concluded.

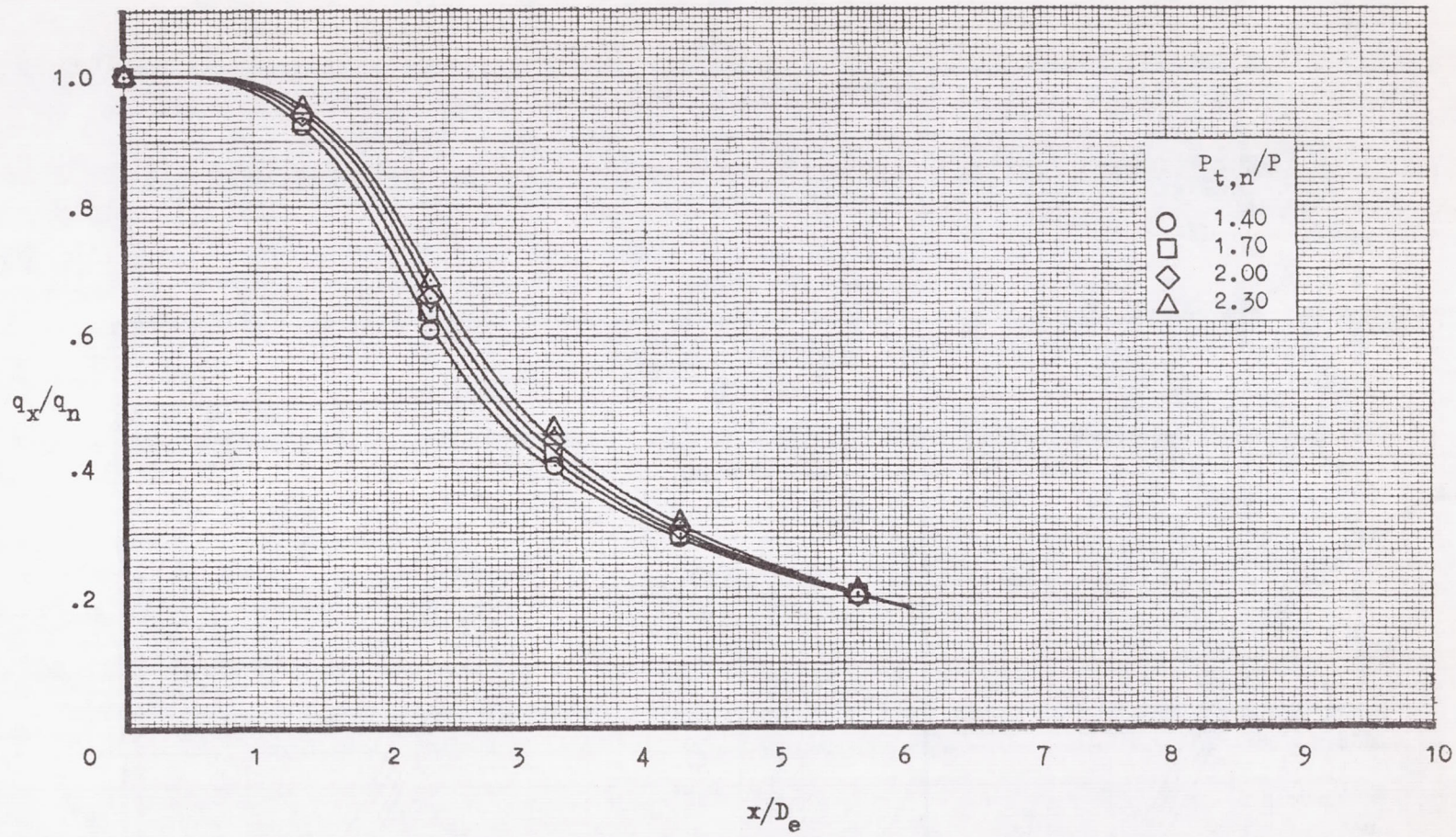

(a) $h/b = \infty$

Figure 14.- Effect of ground plane on jet decay. Nozzle configuration 7a.

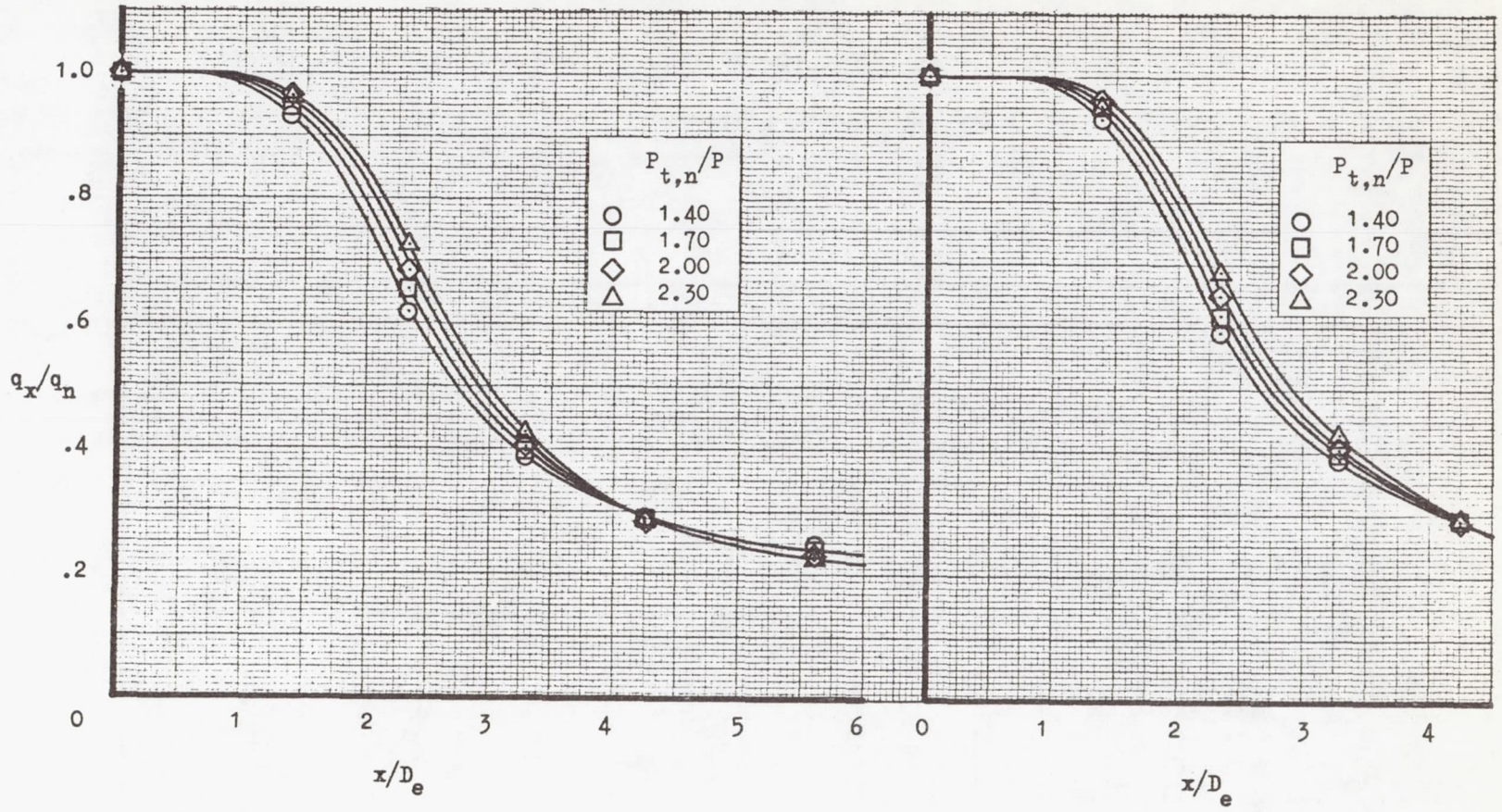

(b) h/b = 0.570

(c) h/b = 0.498

Figure 14.- Continued.

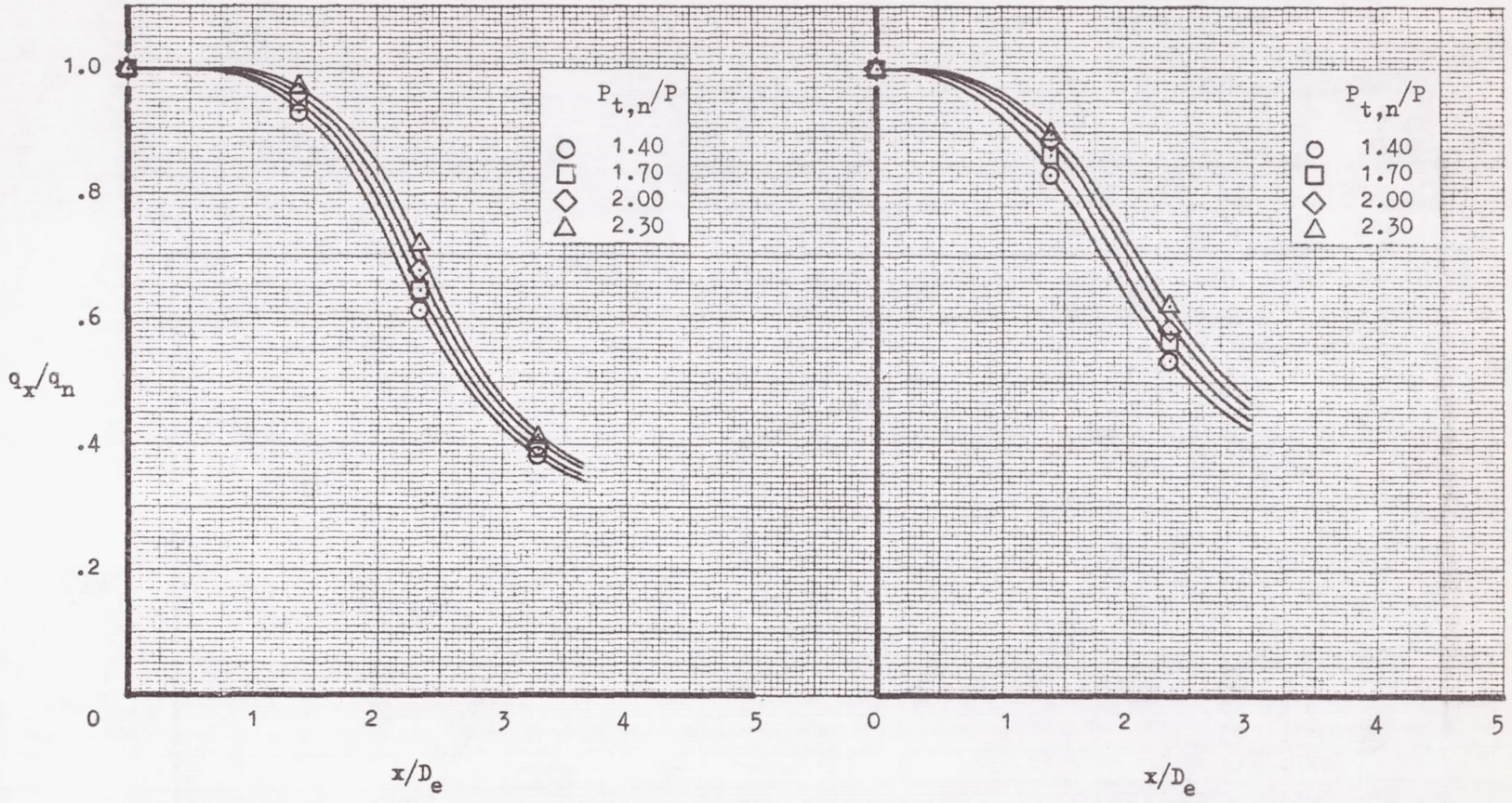

(d) h/b = 0.368

(e) h/b = 0.237

Figure 14.- Concluded.

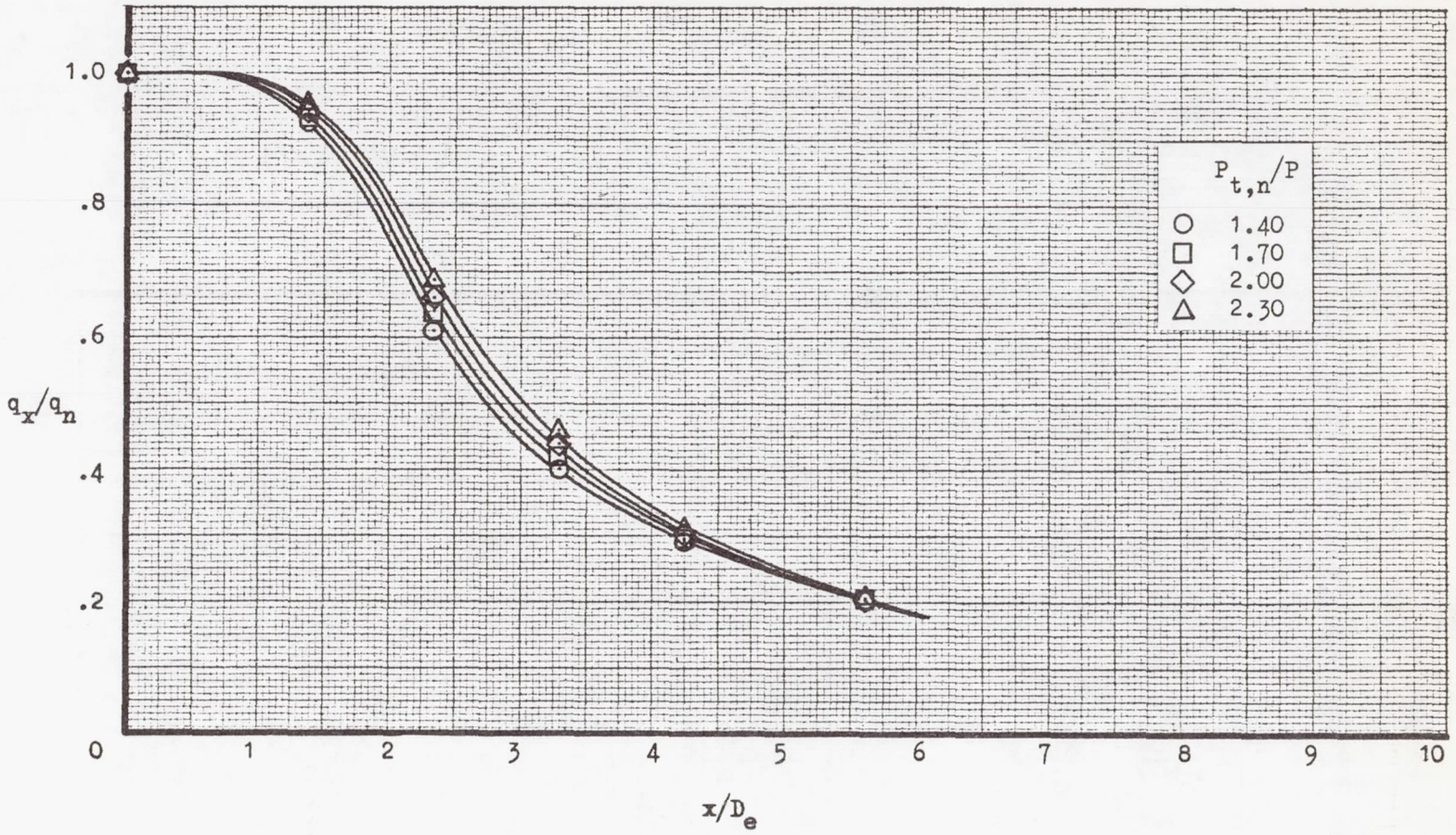

(a) $h/b = \infty$

Figure 15.- Effect of ground plane on jet decay. Nozzle configuration 22.

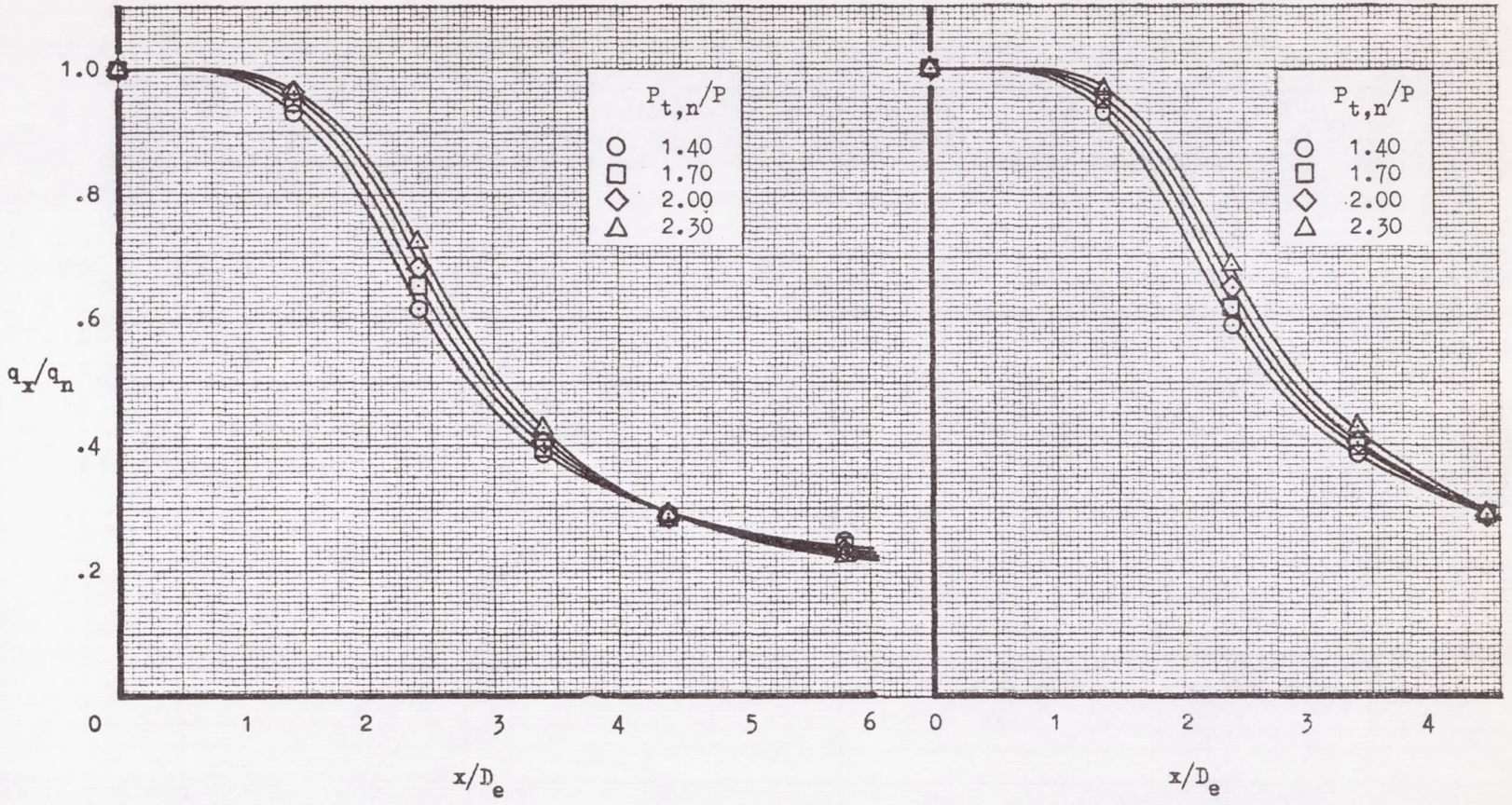

(b) h/b = 0.570

(c) h/b = 0.498

Figure 15.- Continued.

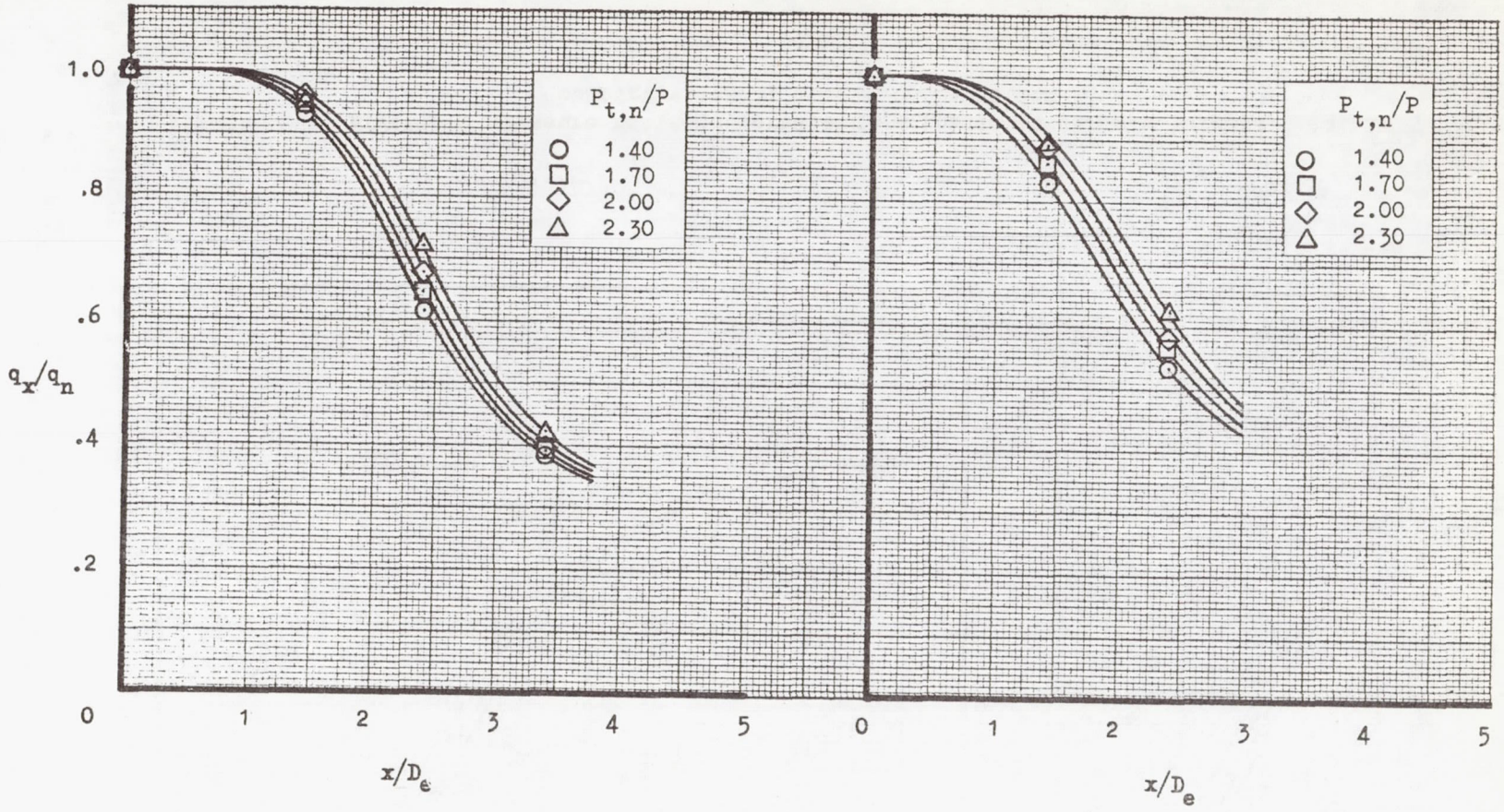

(d) h/b = 0.368

(e) h/b = 0.237

Figure 15.- Concluded.

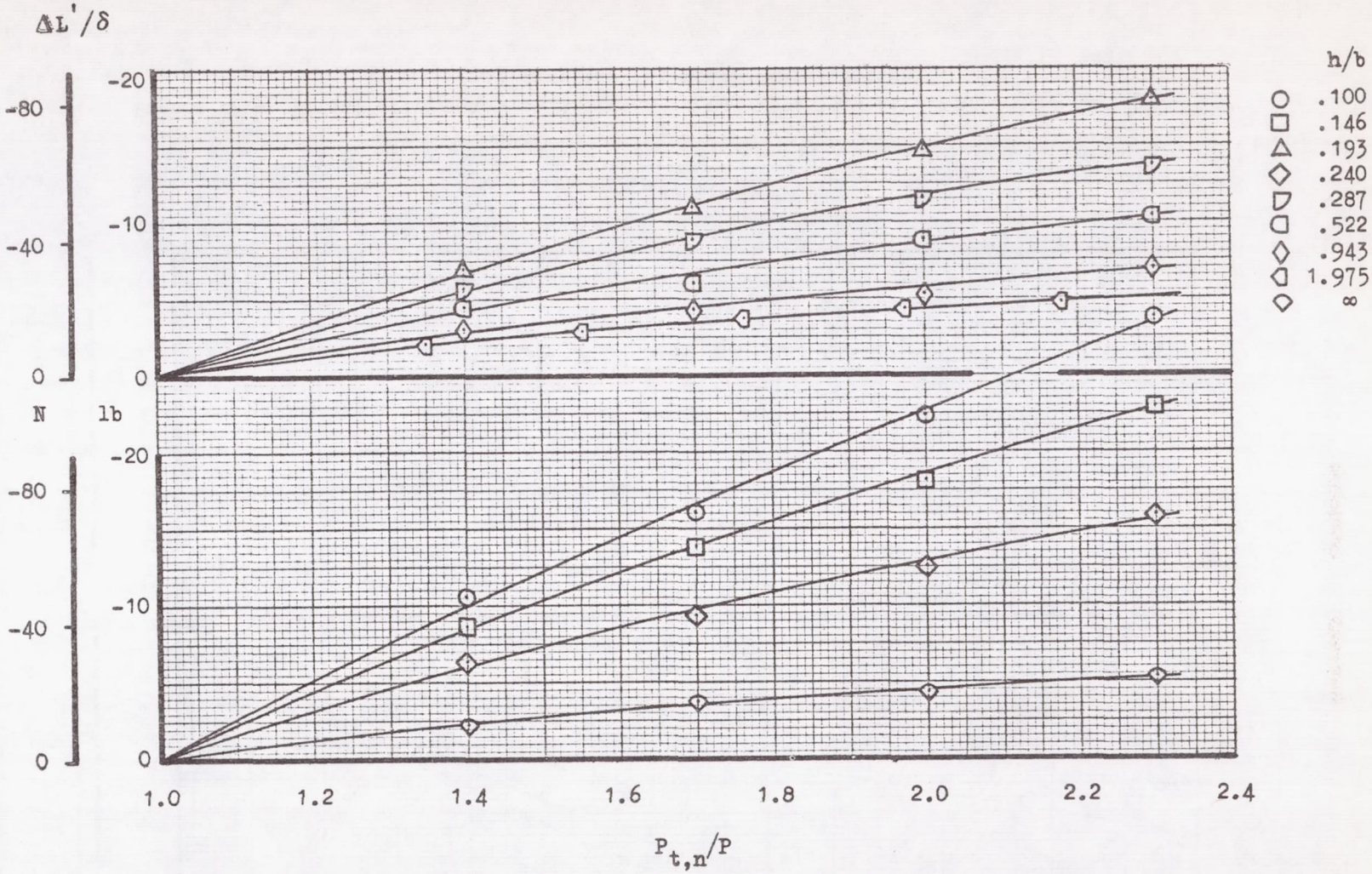

Figure 16.- Effect of pressure ratio on corrected lift loss at various heights. Nozzle configuration 1; model configuration 1.

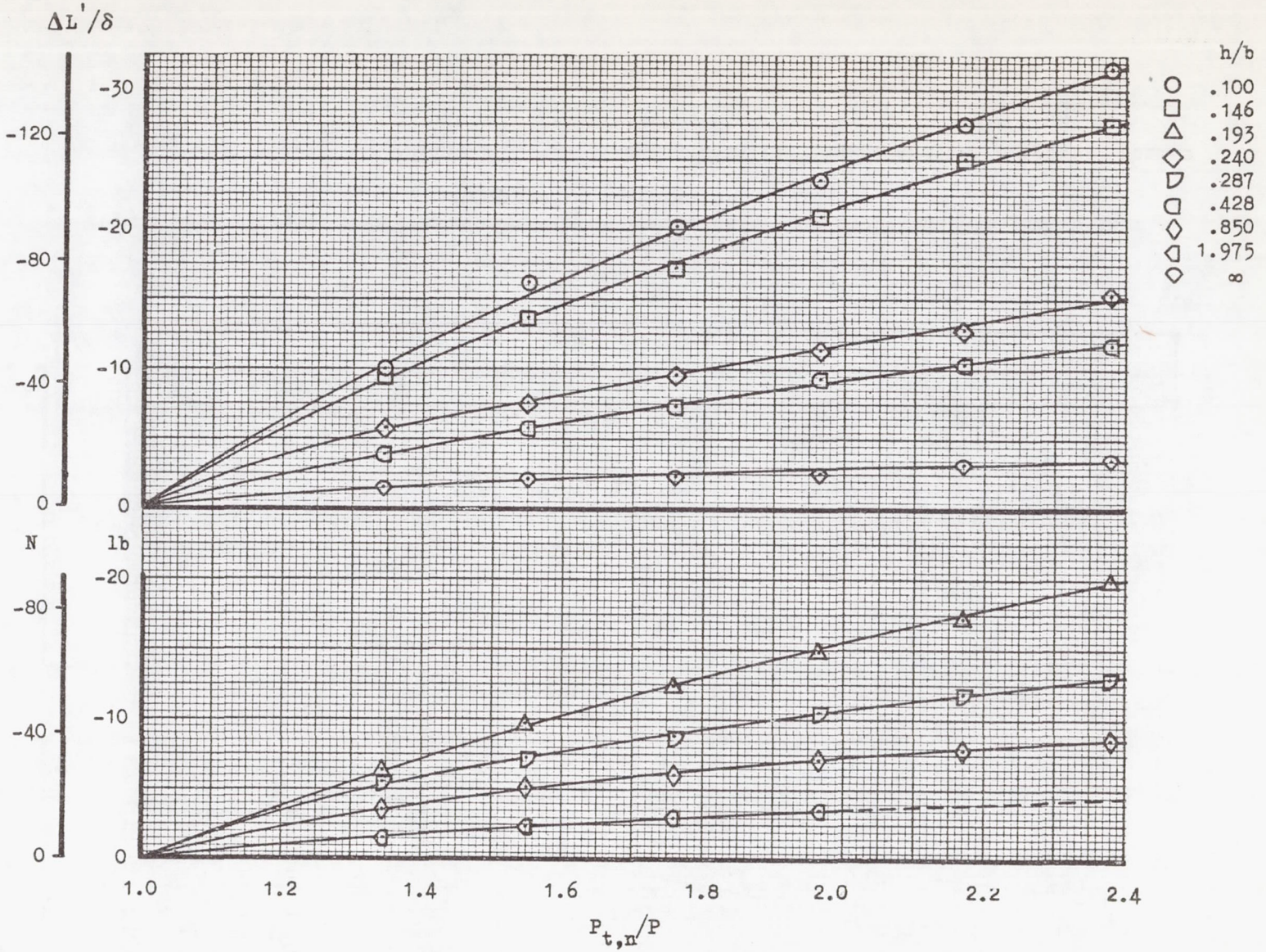

Figure 17.- Effect of pressure ratio on corrected lift loss at various heights. Nozzle configuration 1a; model configuration 1.

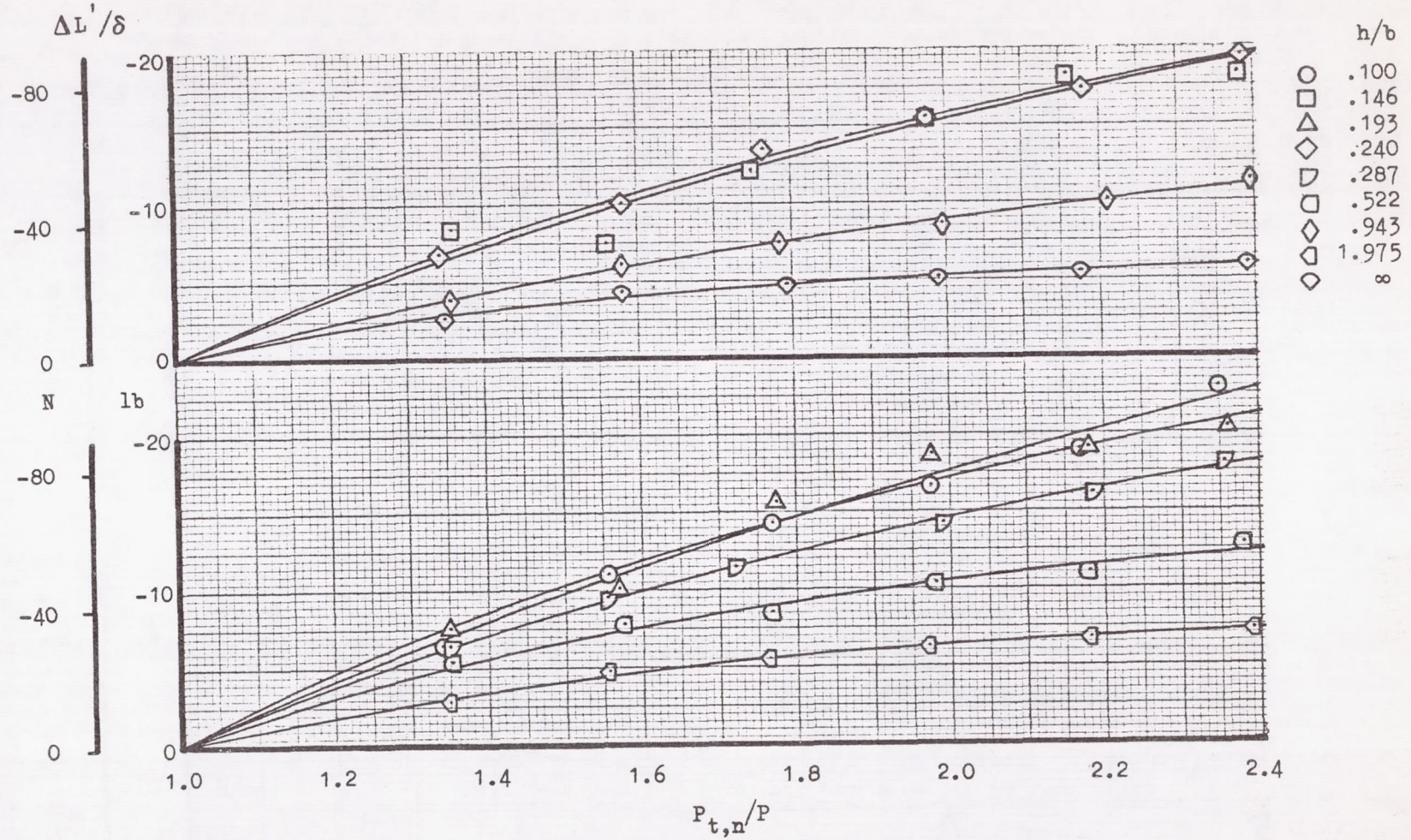

(a) Model configuration 1.

Figure 18.- Effect of pressure ratio on corrected lift loss at various heights. Nozzle configuration 2.

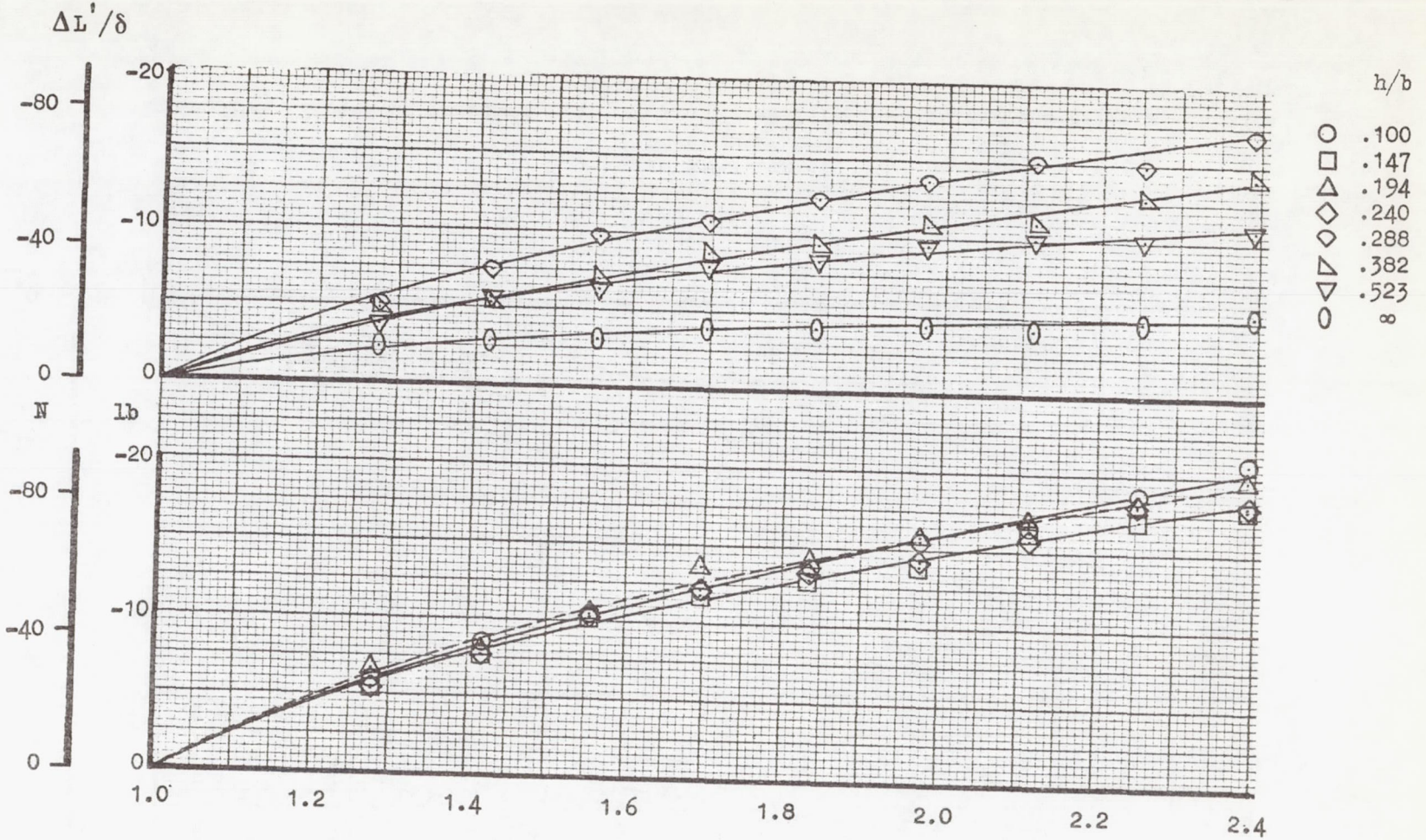

(b) Model configuration 2.

Figure 18.— Continued.

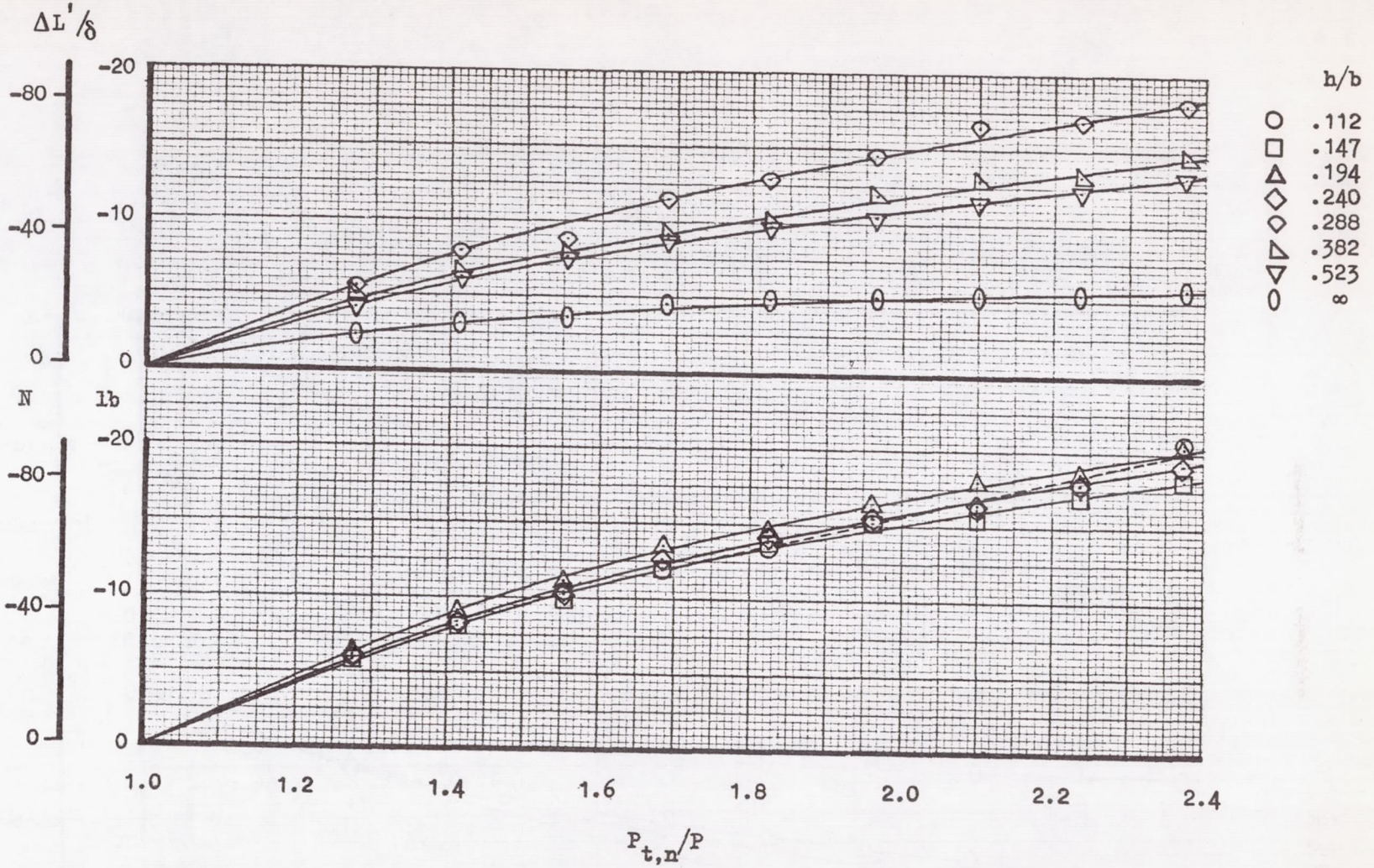

(c) Model configuration 3.

Figure 18.- Continued.

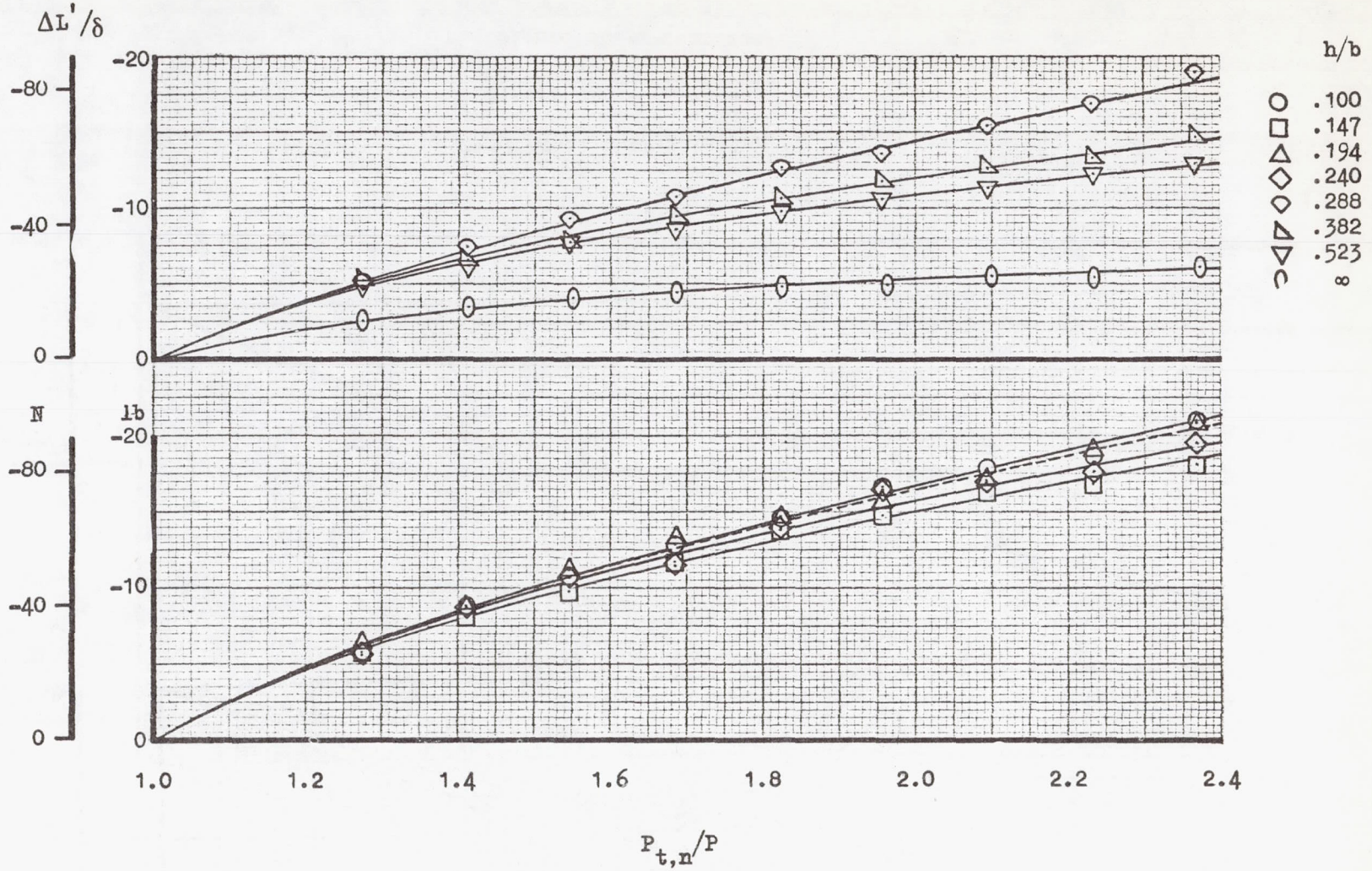

(d) Model configuration 4.

Figure 18.- Continued.

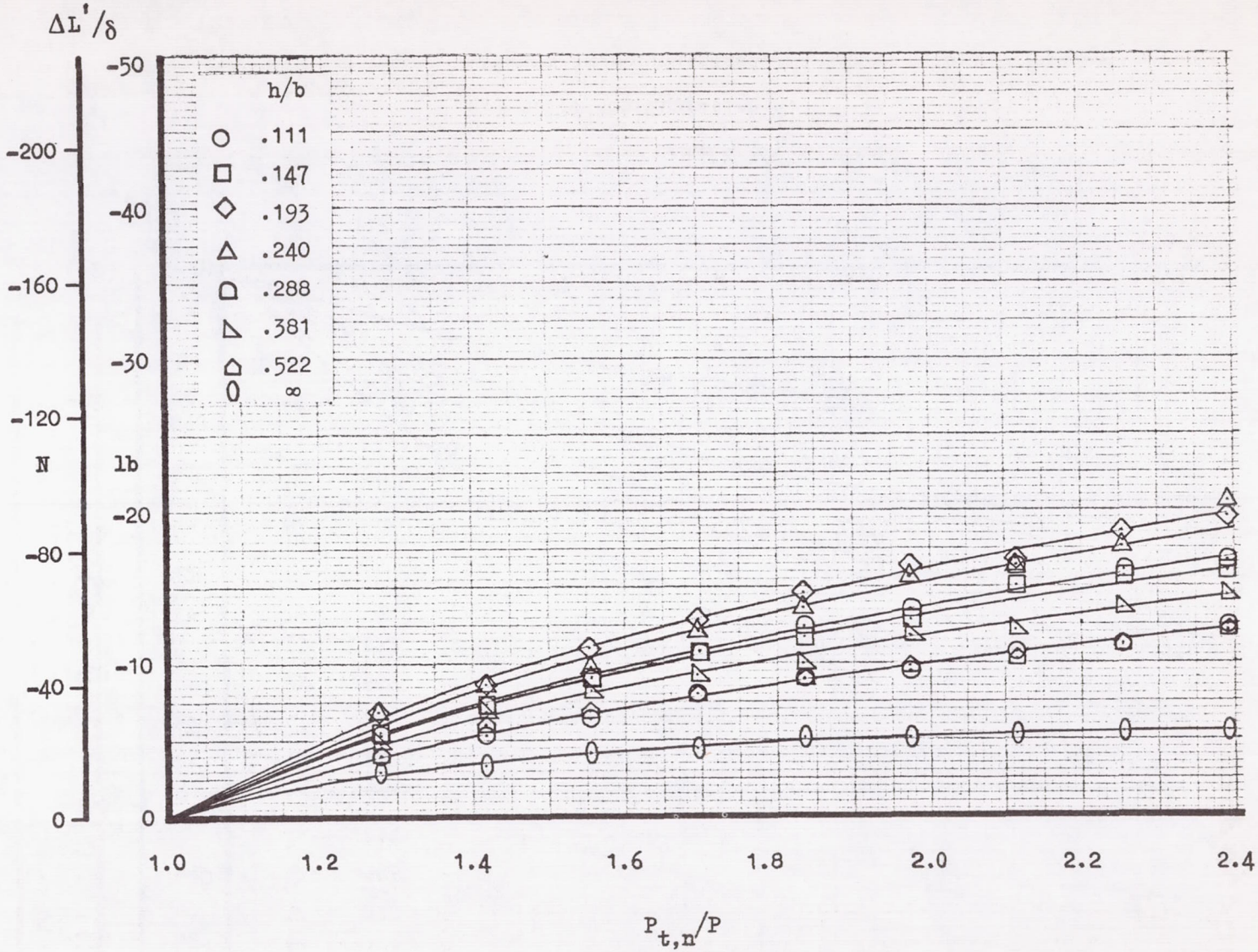

(e) Model configuration 5.

Figure 18.- Continued.

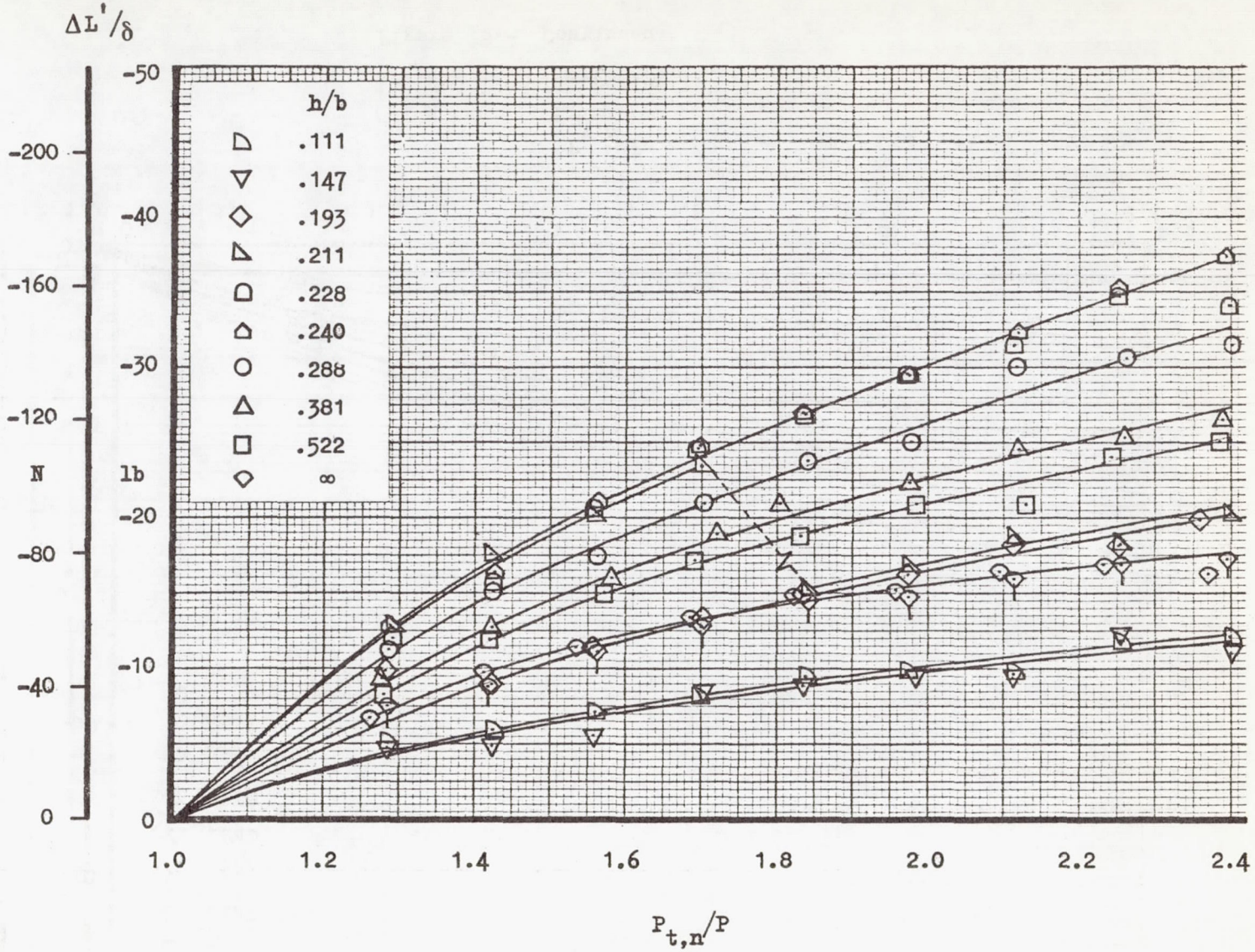

(f) Model configuration 6.

Figure 18.- Continued.

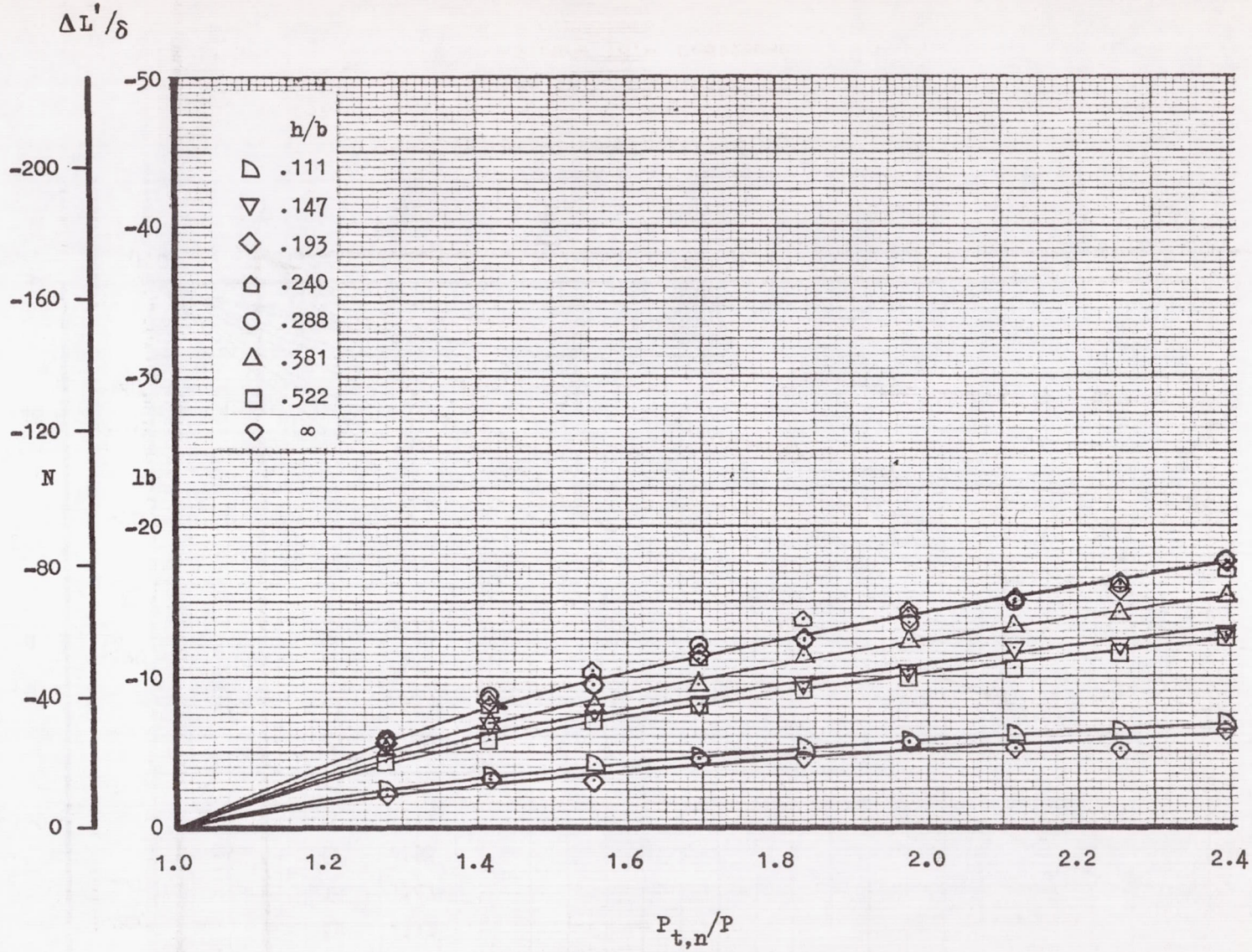

(g) Model configuration 7.

Figure 18.- Continued.

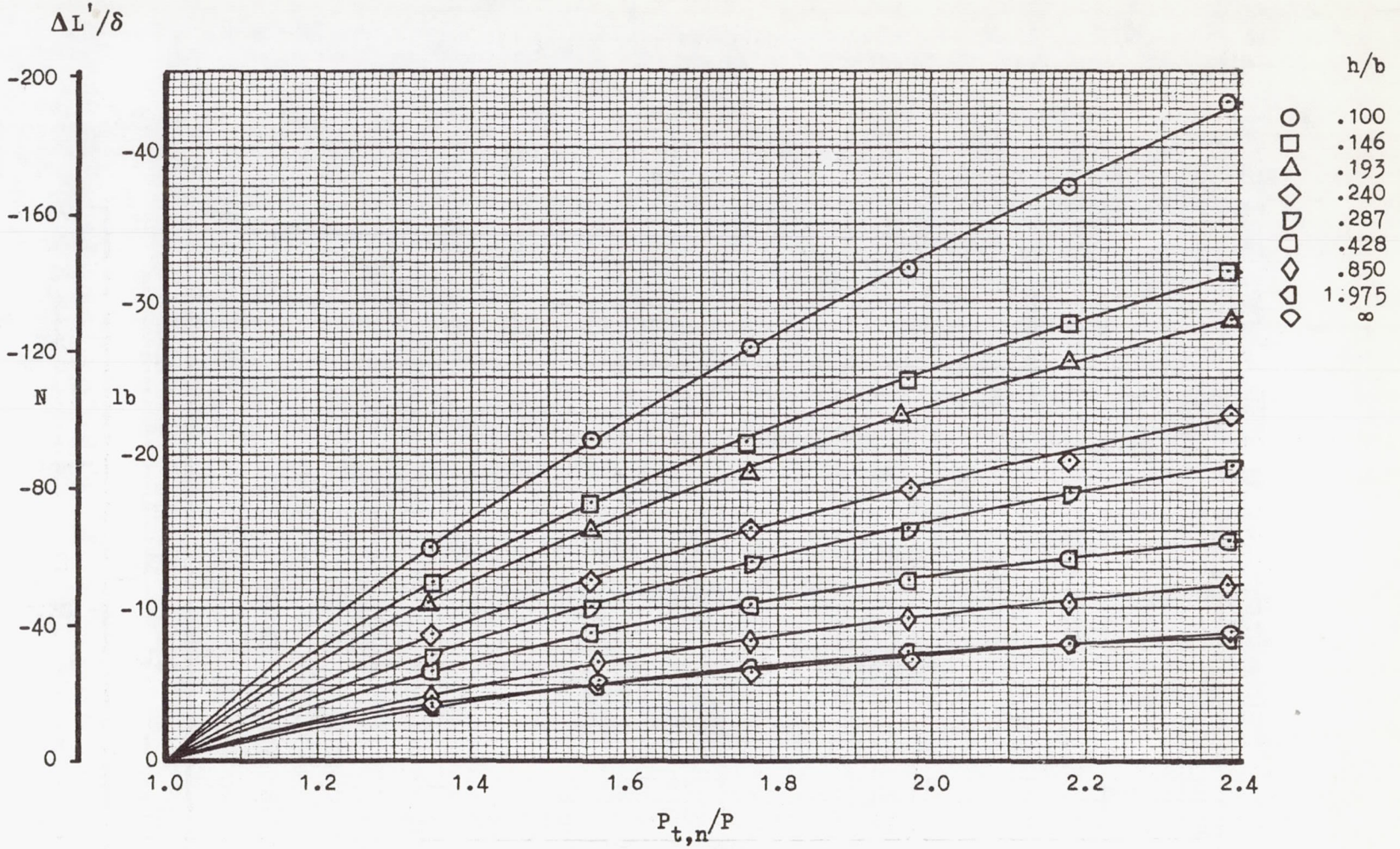

(h) Model configuration 10.

Figure 18.- Concluded.

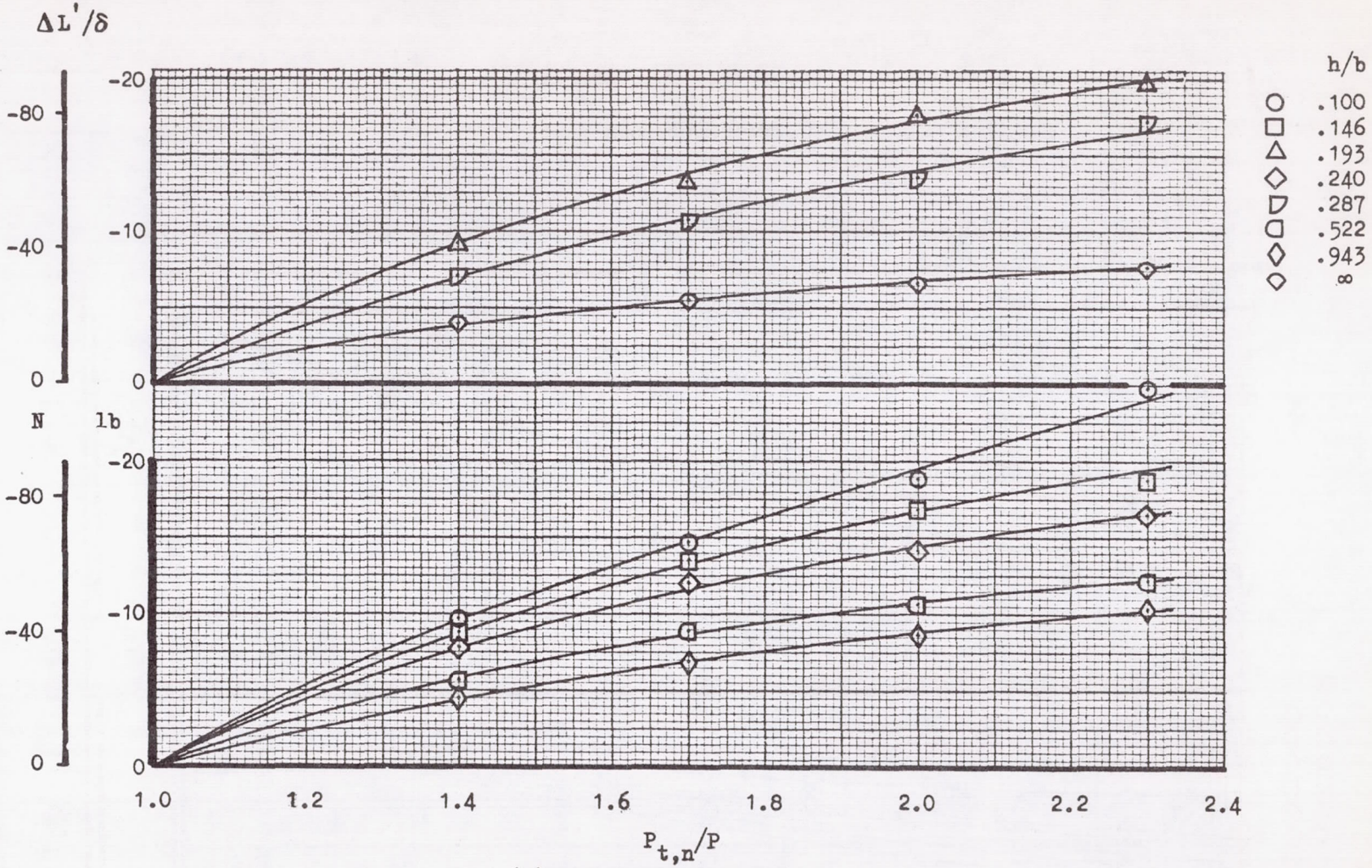

(a) Model configuration 1.

Figure 19.- Effect of pressure ratio on corrected lift loss at various heights. Nozzle configuration 3.

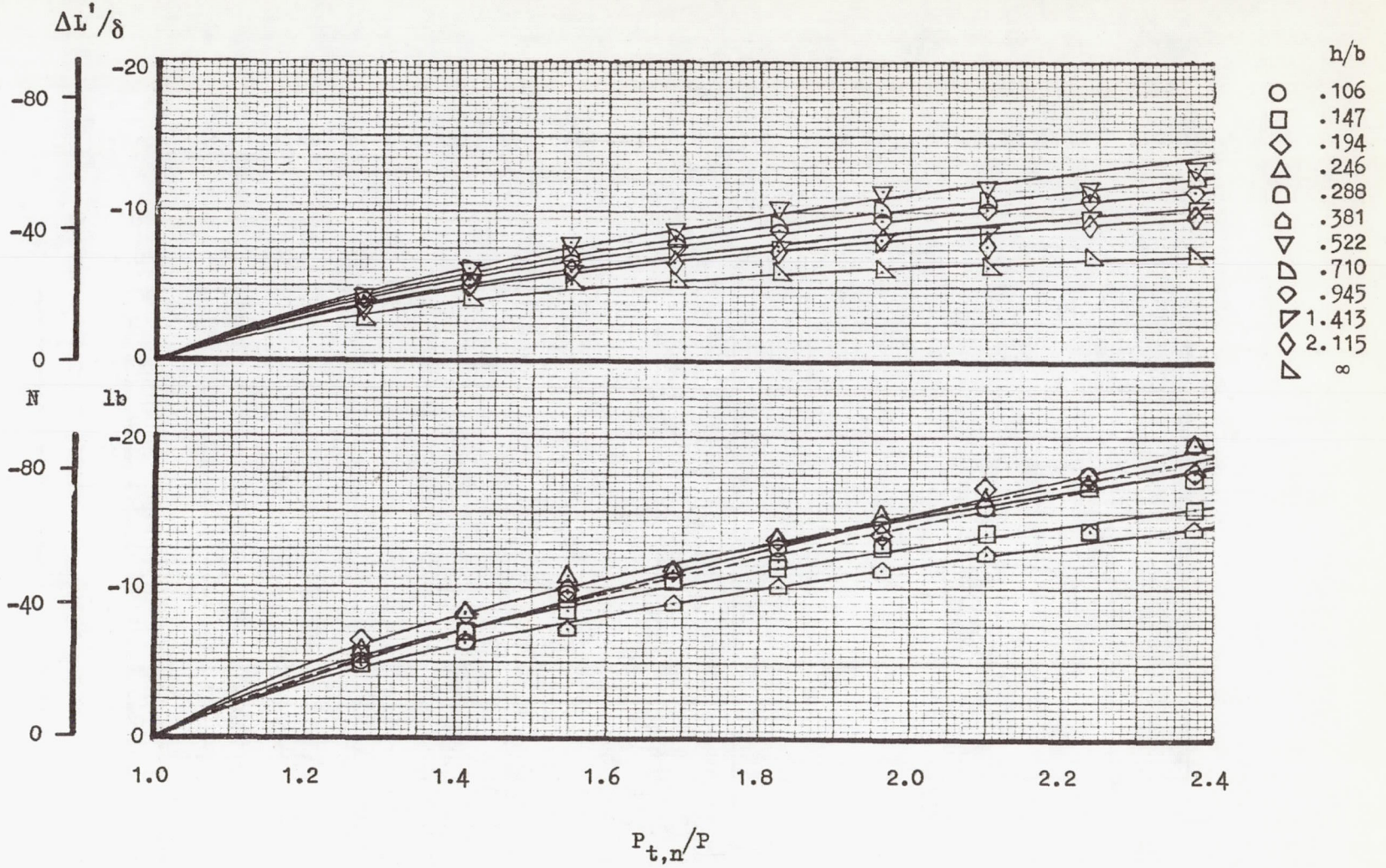

(b) Model configuration 5.

Figure 19.- Concluded.

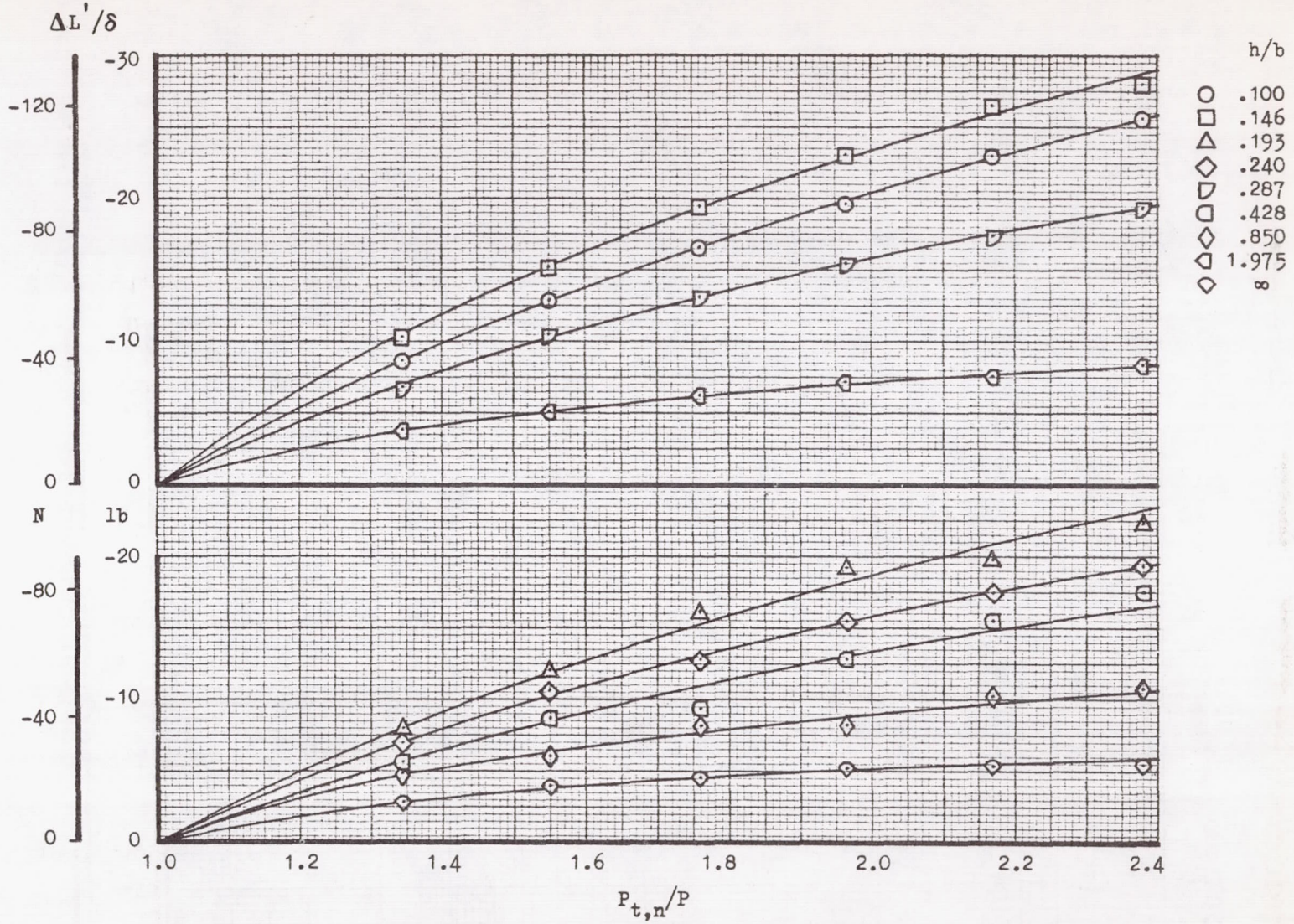

Figure 20.- Effect of pressure ratio on corrected lift loss at various heights. Nozzle configuration 3a; model configuration 1.

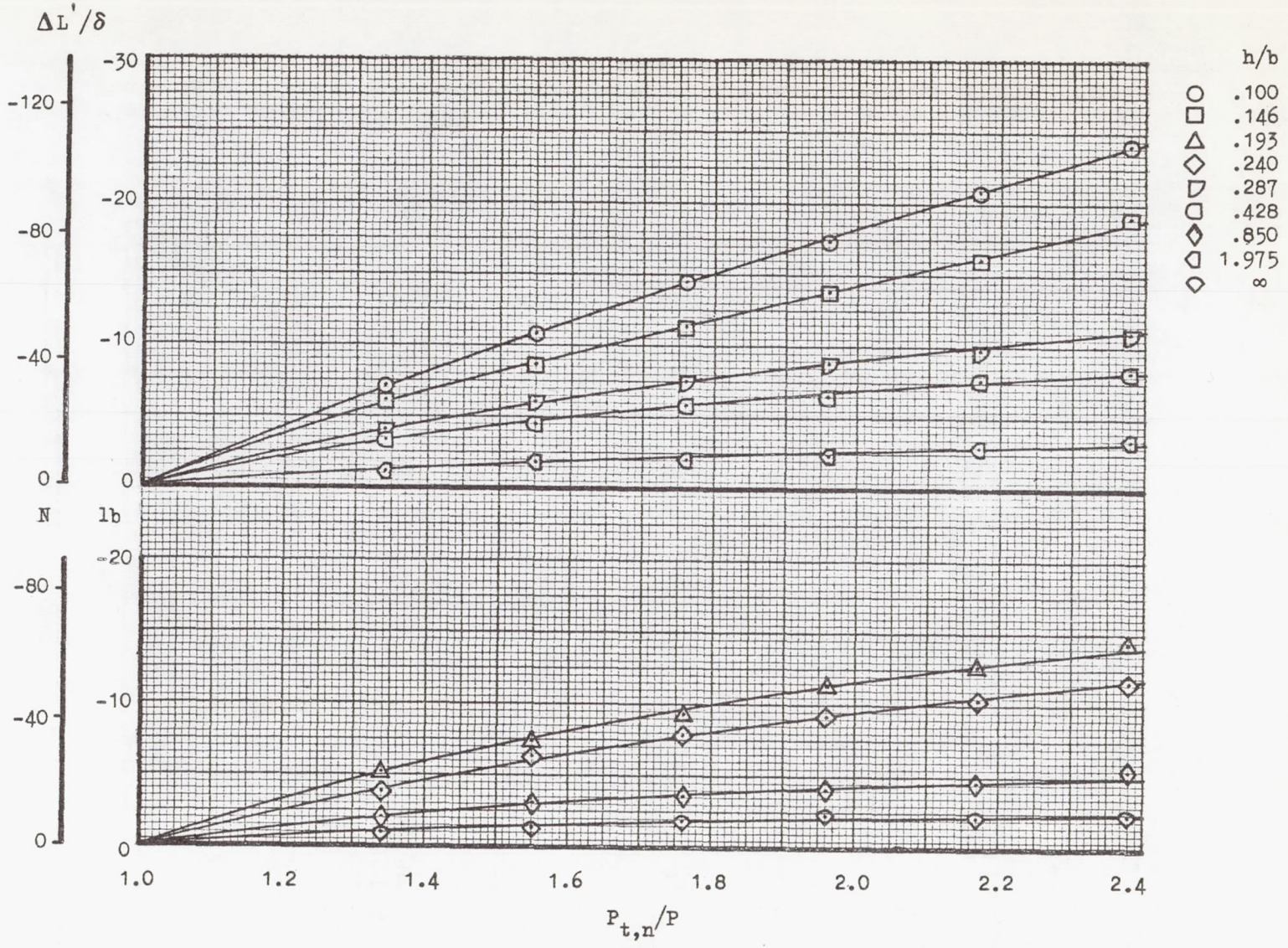

Figure 21.- Effect of pressure ratio on corrected lift loss at various heights. Nozzle configuration 4; model configuration 1.

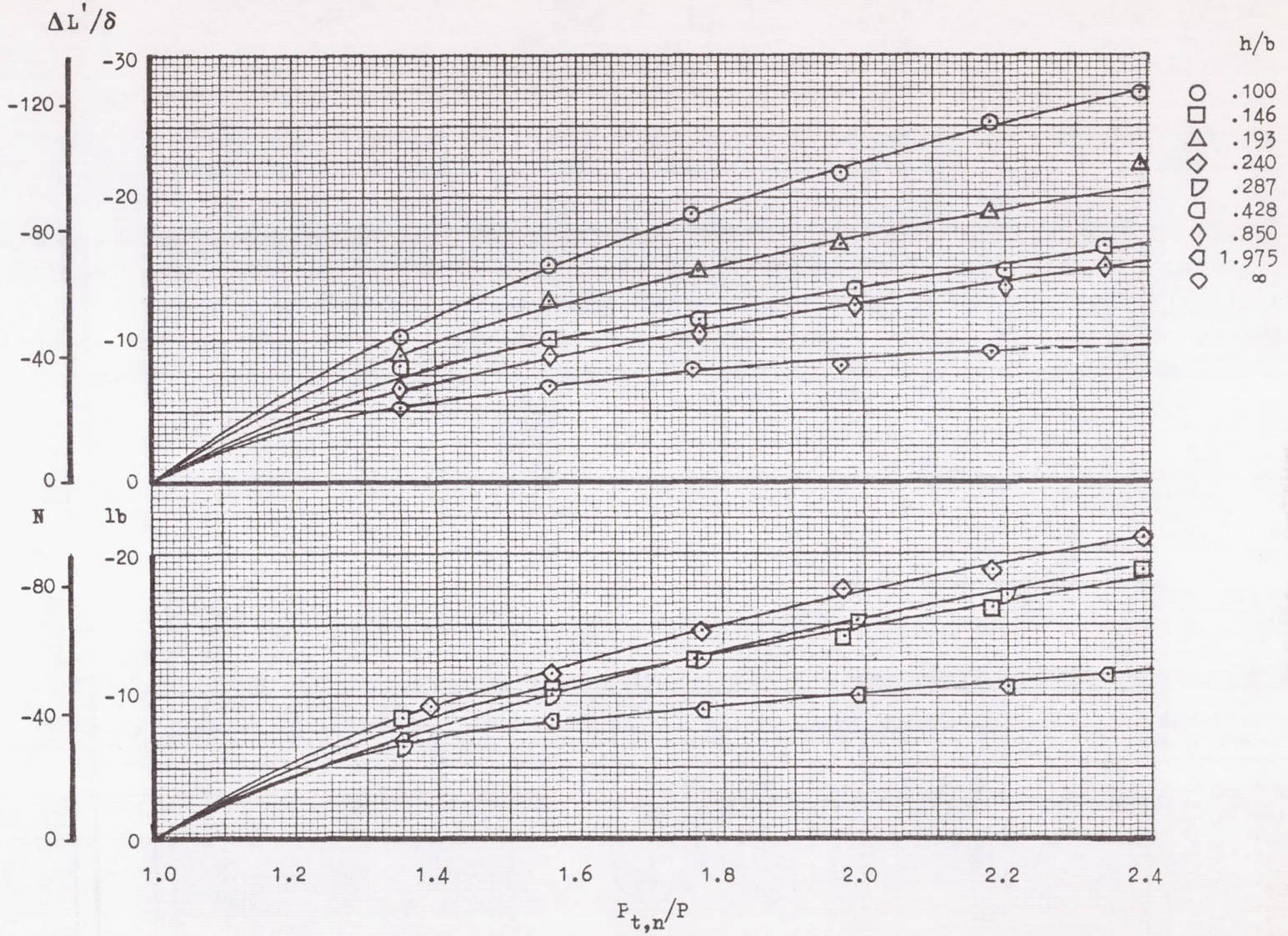

Figure 22.- Effect of pressure ratio on corrected lift loss at various heights. Nozzle configuration 5; model configuration 1.

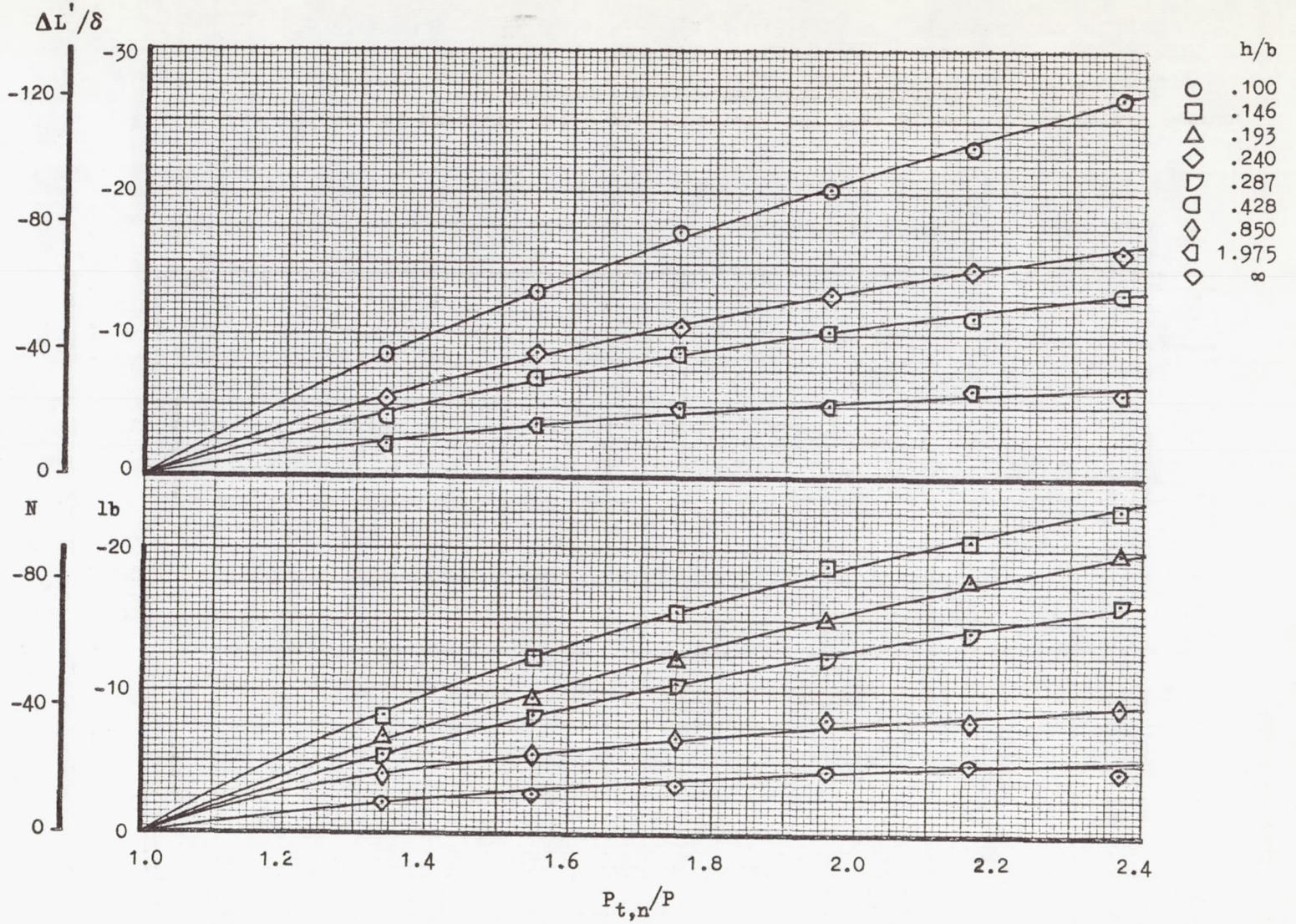

Figure 23.- Effect of pressure ratio on corrected lift loss at various heights. Nozzle configuration 6; model configuration 1.

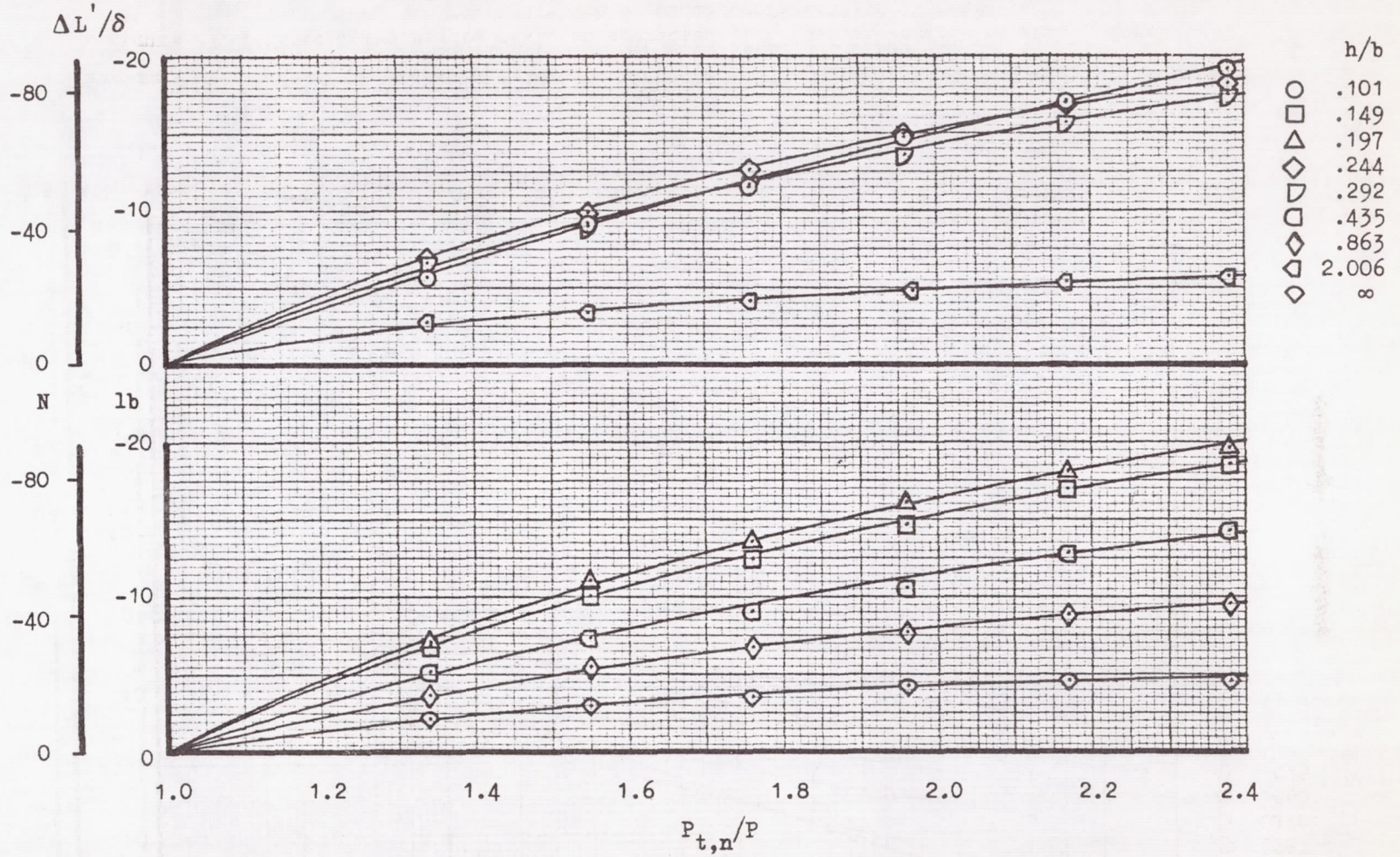

Figure 24.- Effect of pressure ratio on corrected lift loss at various heights. Nozzle configuration 7; model configuration 1.

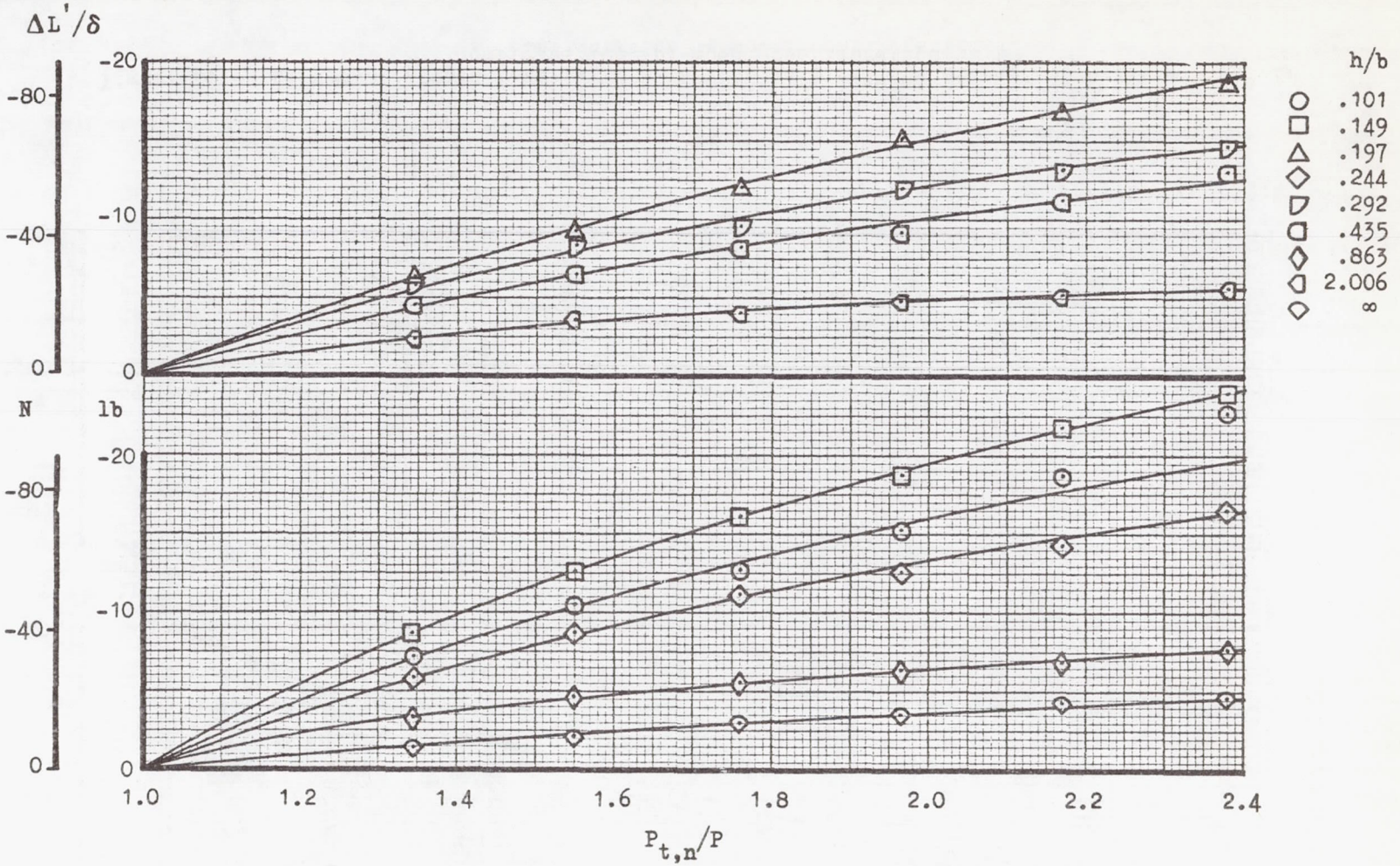

Figure 25.- Effect of pressure ratio on corrected lift loss at various heights. Nozzle configuration 7a; model configuration 1.

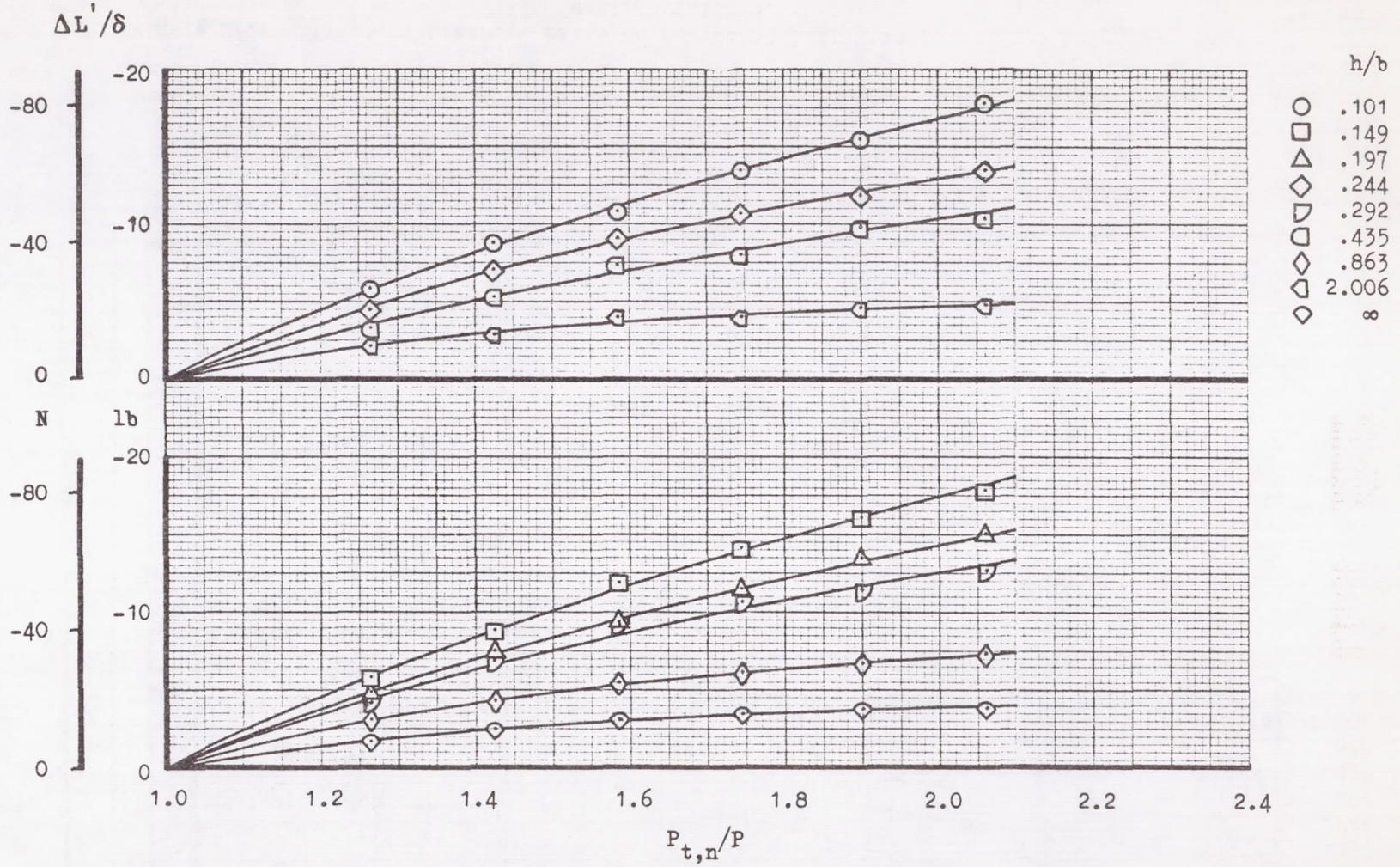

Figure 26.- Effect of pressure ratio on corrected lift loss at various heights. Nozzle configuration 7b; model configuration 1.

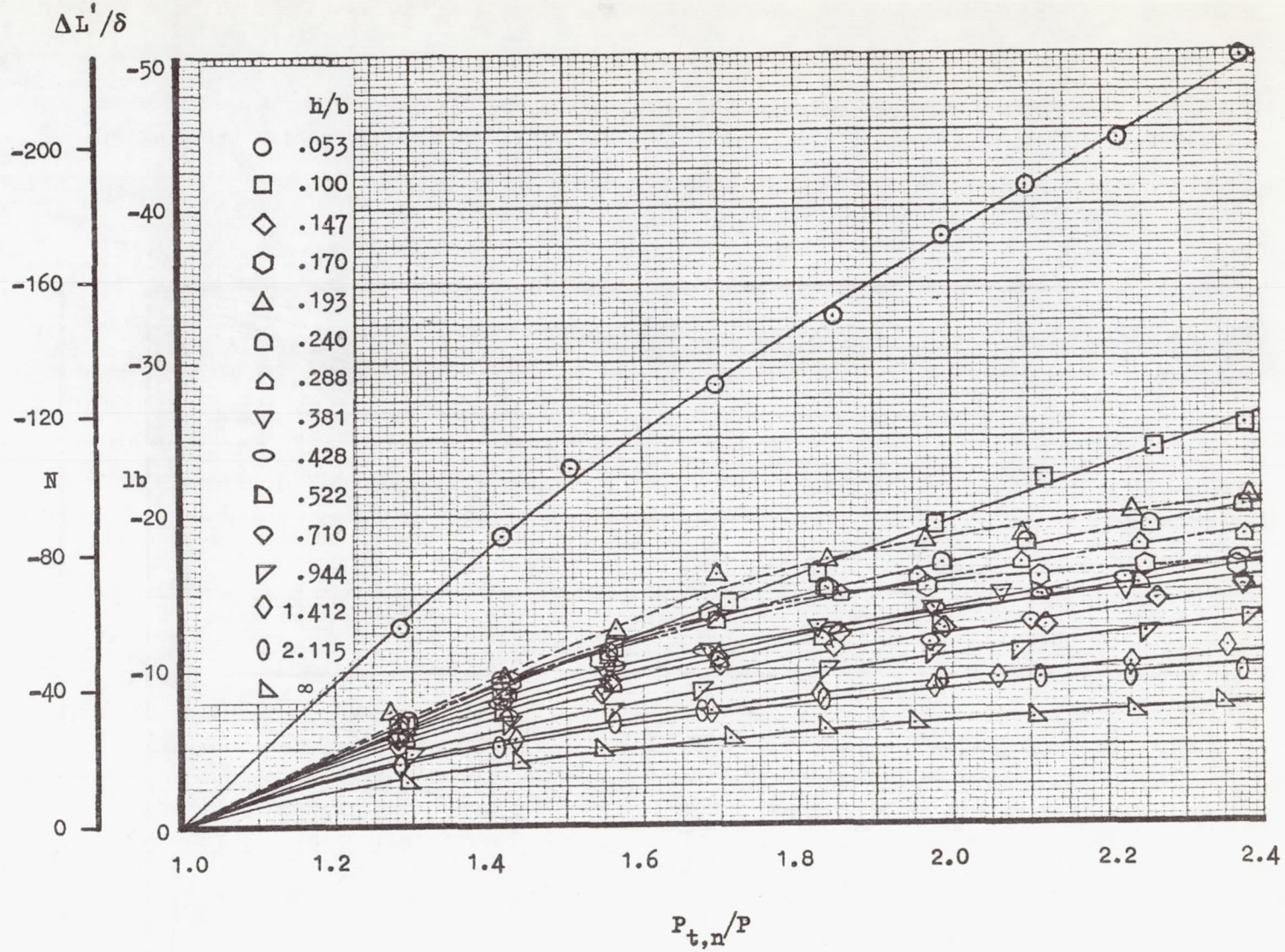

(a) Model configuration 1.

Figure 27.- Effect of pressure ratio on corrected lift loss at various heights. Nozzle configuration 8.

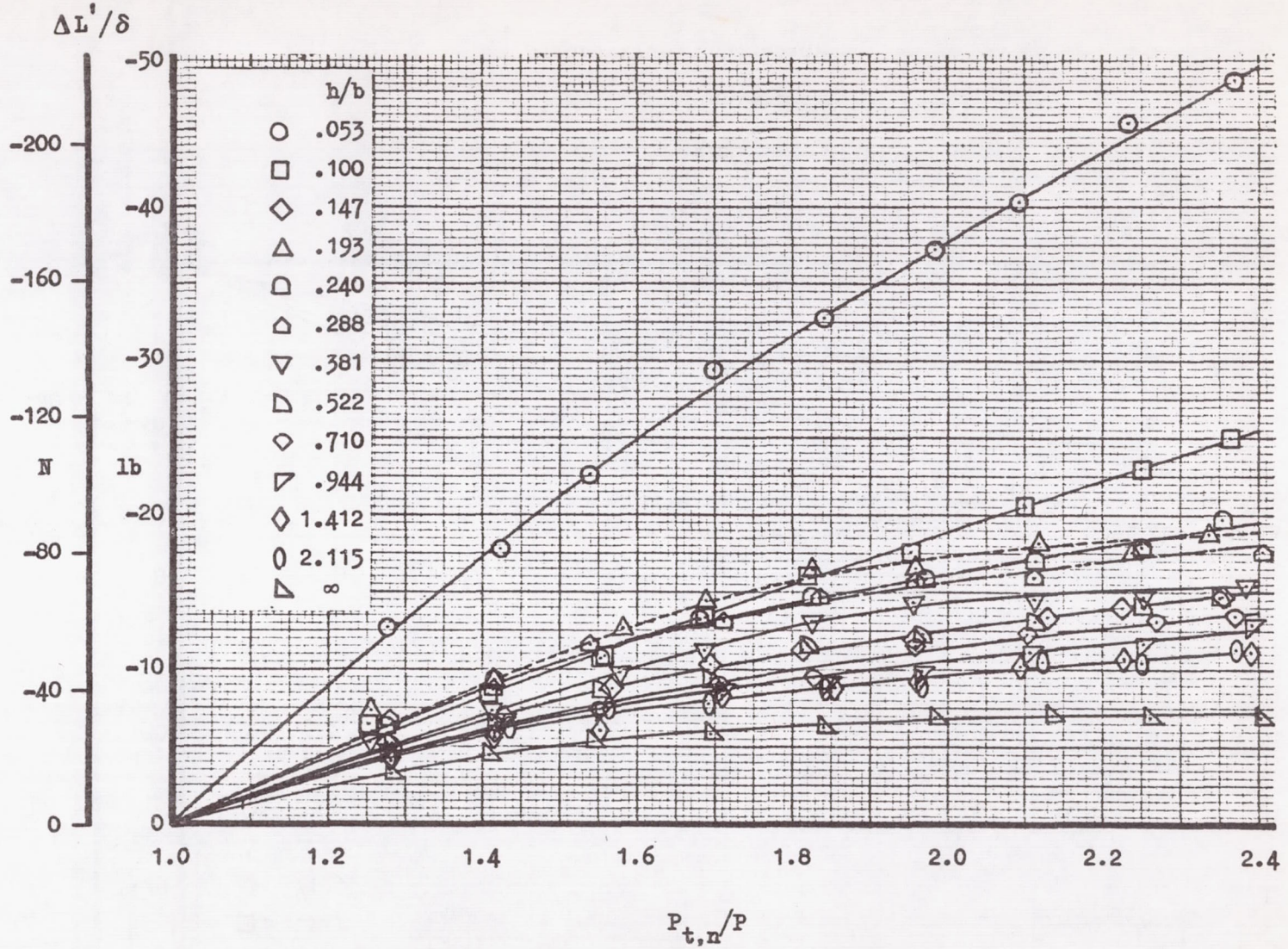

(b) Model configuration 1; repeat data.

Figure 27.- Continued.

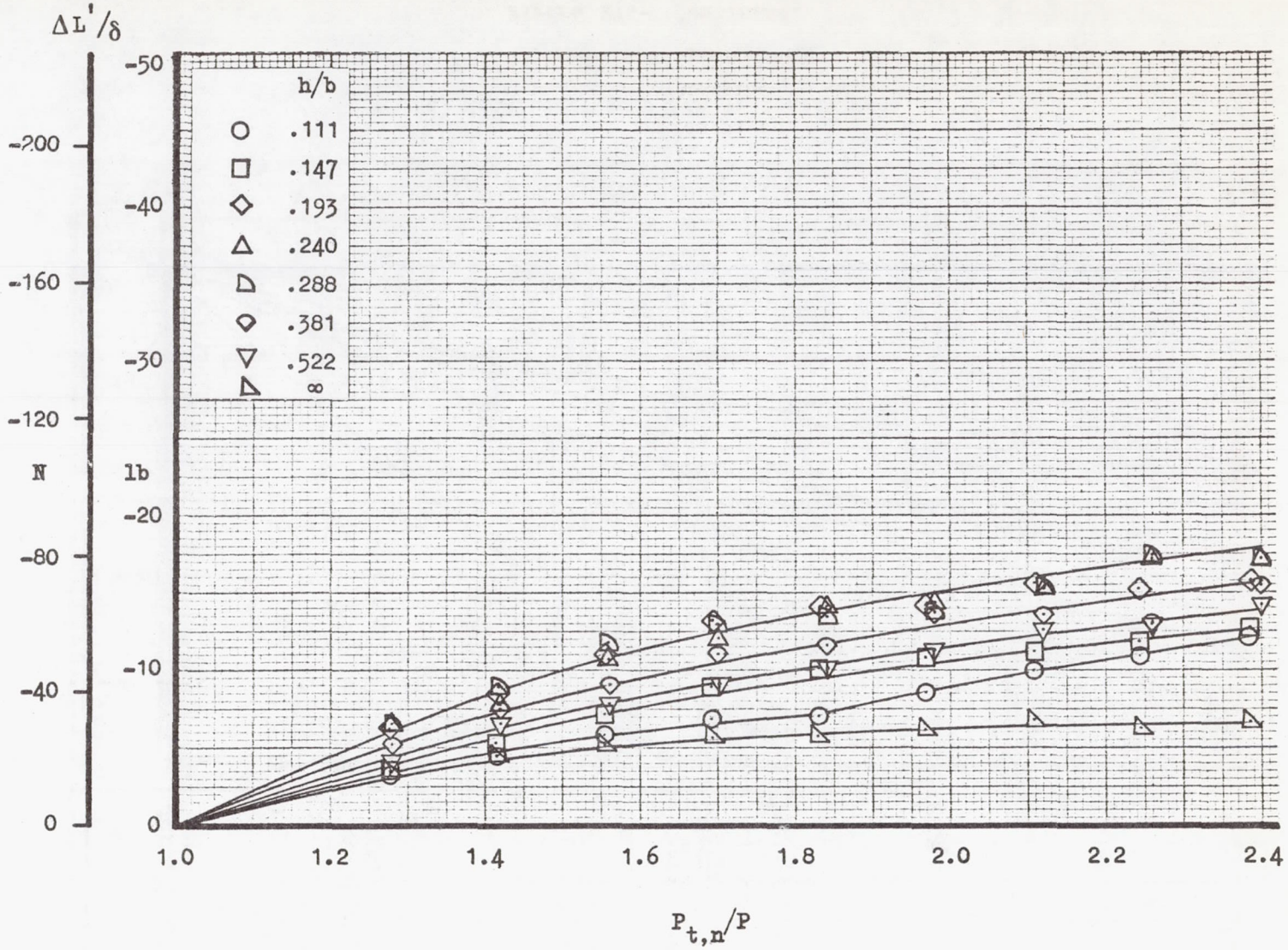

(c) Model configuration 5.

Figure 27.- Continued.

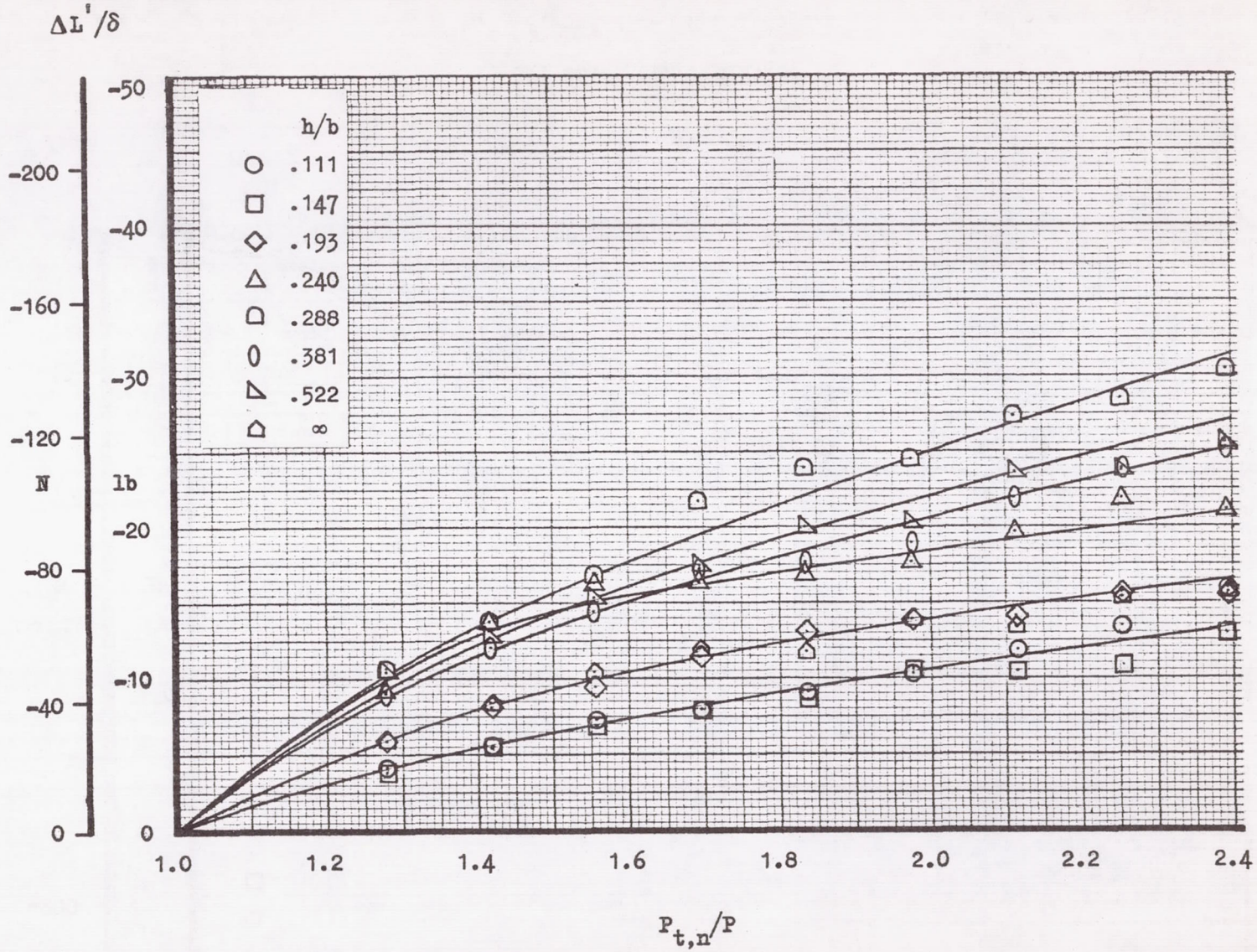

(d) Model configuration 6.

Figure 27.- Continued.

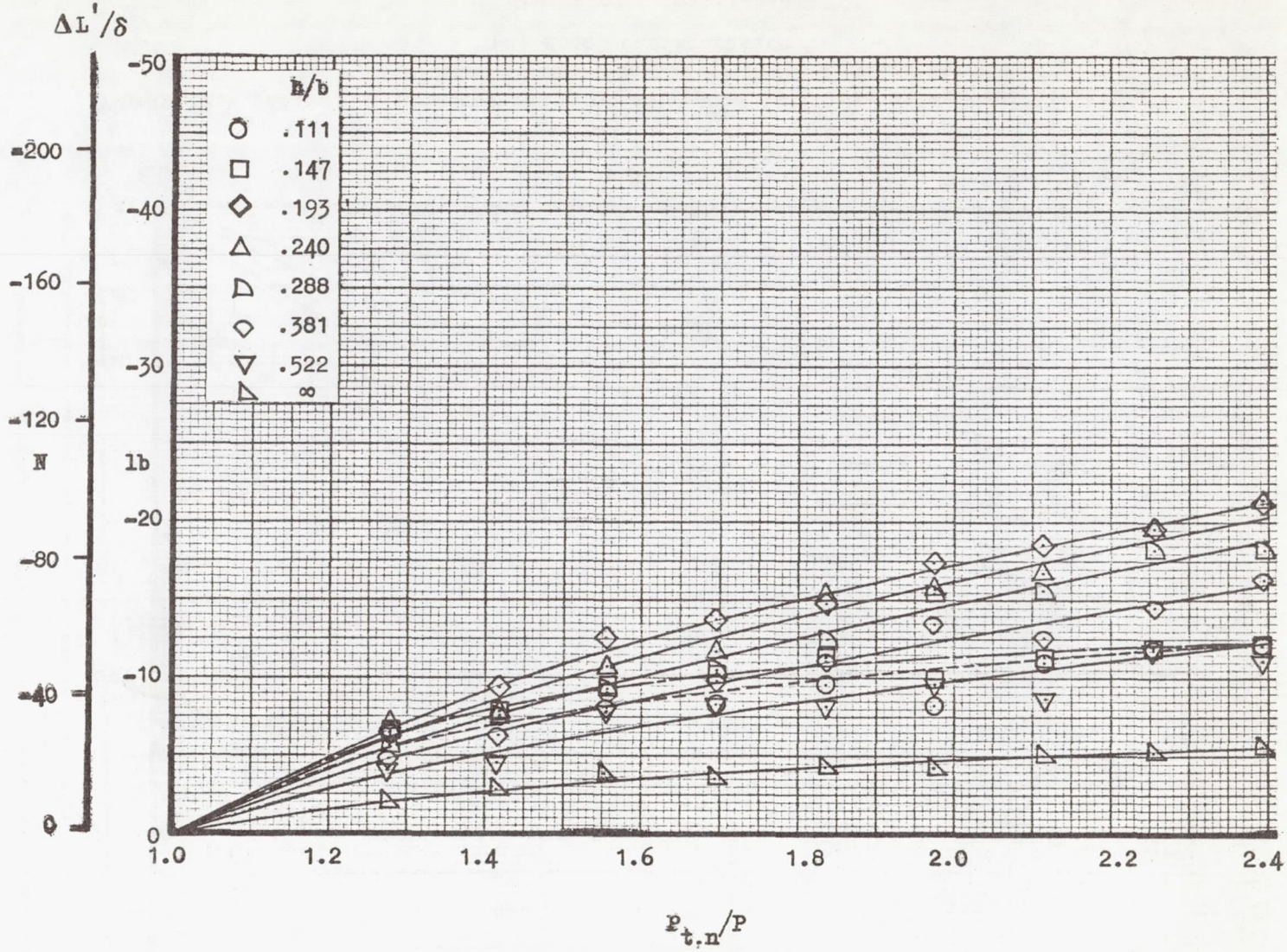

(e) Model configuration 7.

Figure 27.- Concluded.

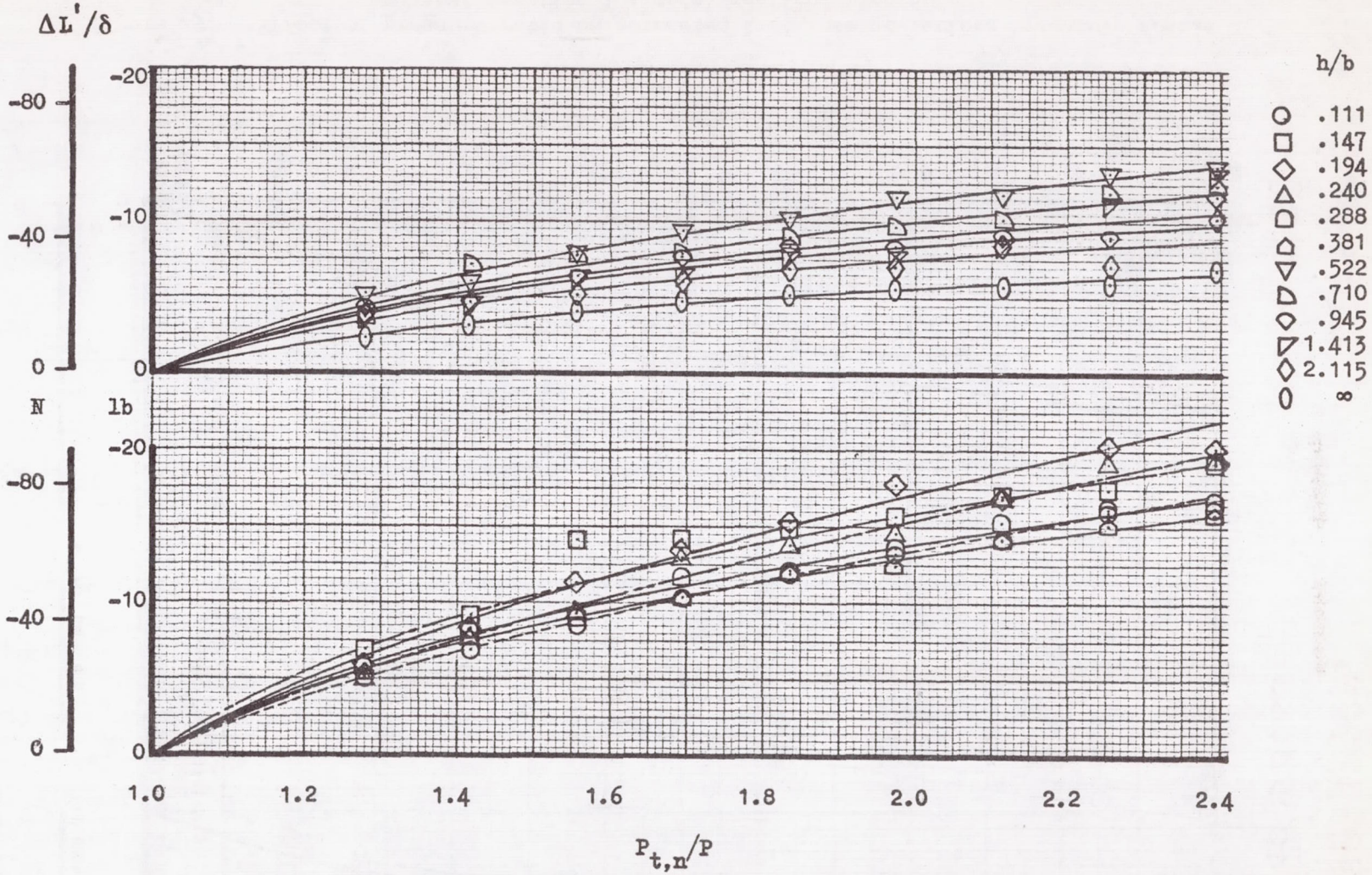

Figure 28.- Effect of pressure ratio on corrected lift loss at various heights. Nozzle configuration 9; model configuration 5.

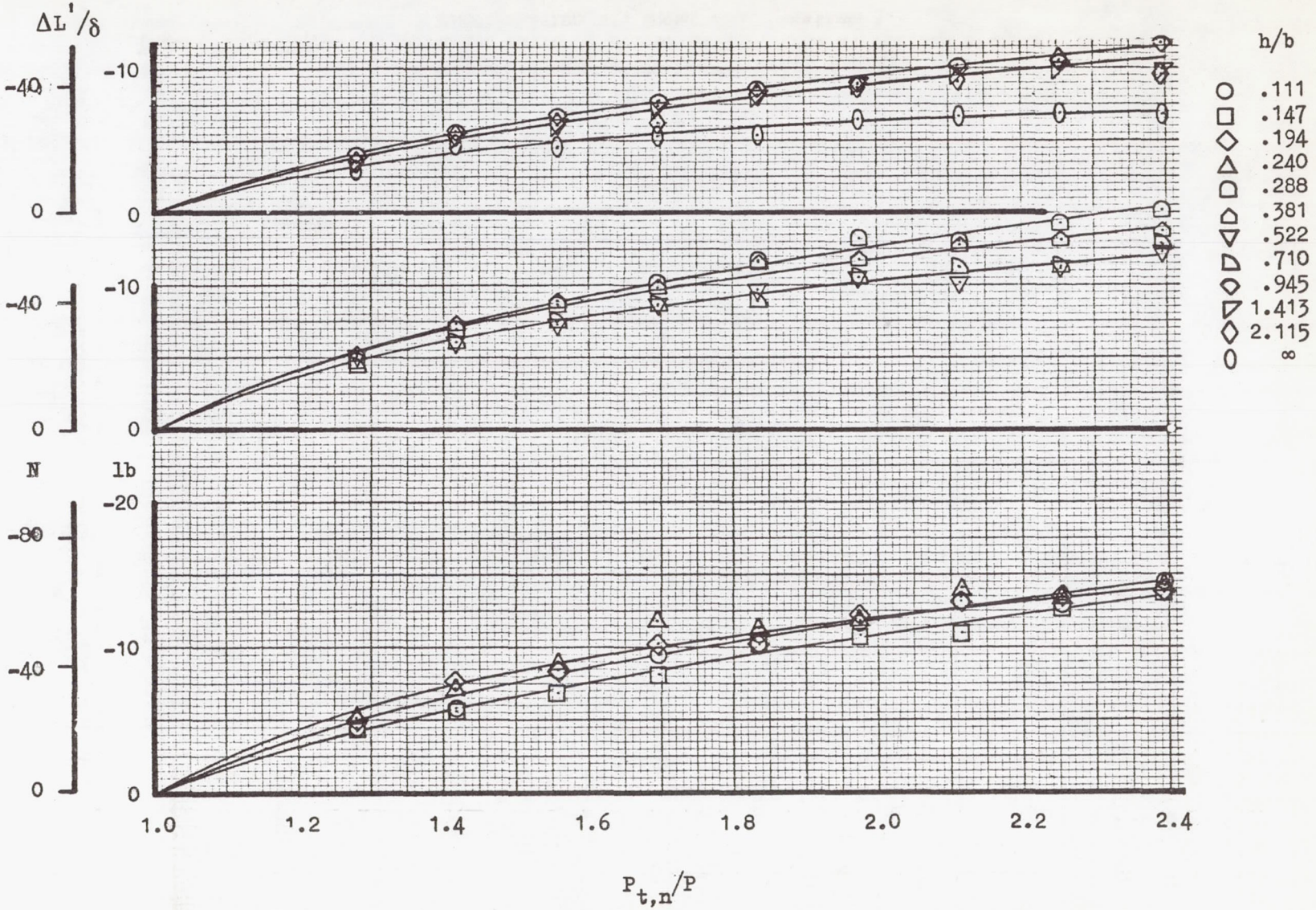

Figure 29.- Effect of pressure ratio on corrected lift loss at various heights. Nozzle configuration 10; model configuration 5.

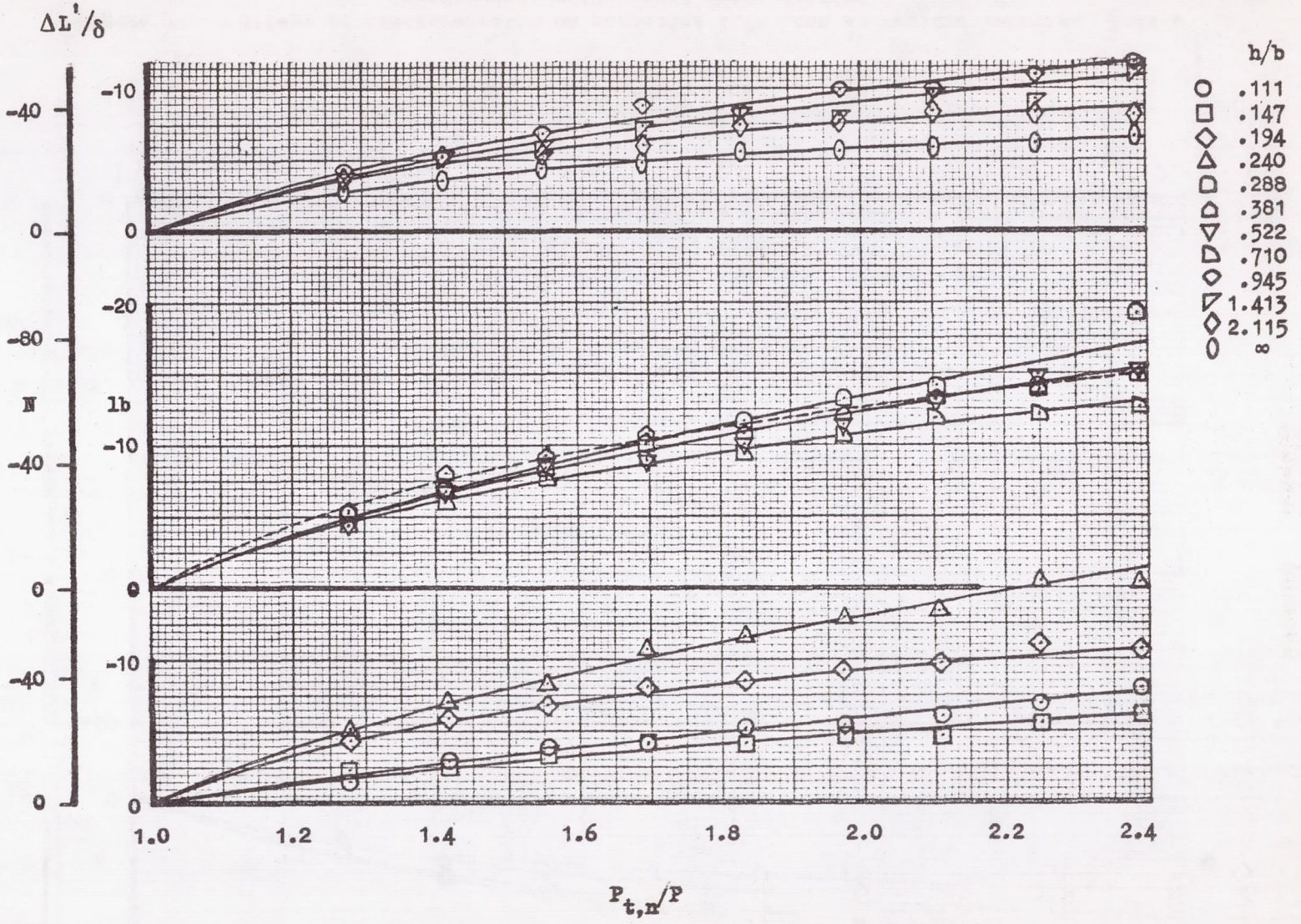

Figure 30.- Effect of pressure ratio on corrected lift loss at various heights. Nozzle configuration 12; model configuration 5.

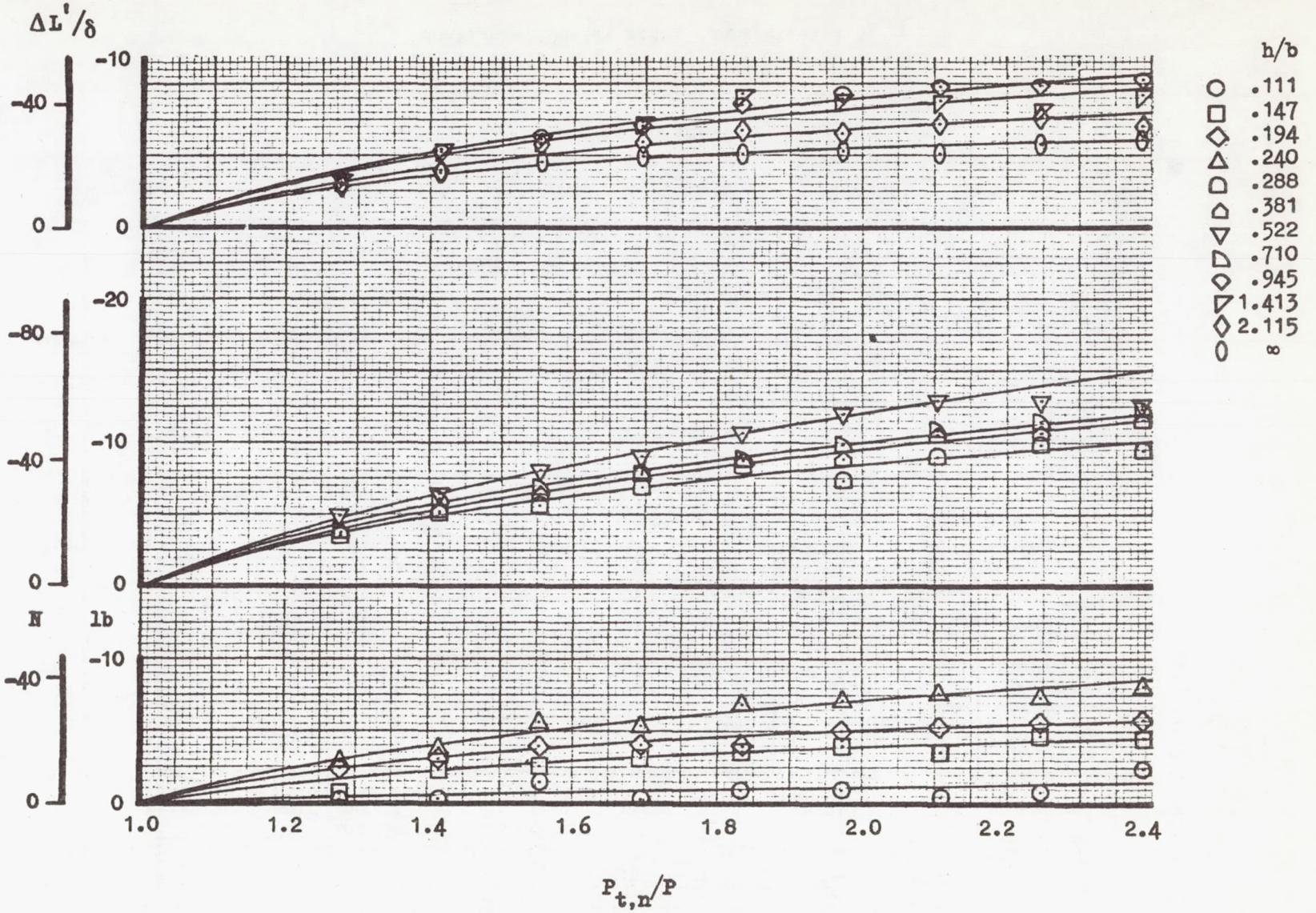

Figure 31.- Effect of pressure ratio on corrected lift loss at various heights. Nozzle configuration 13: model configuration 5.

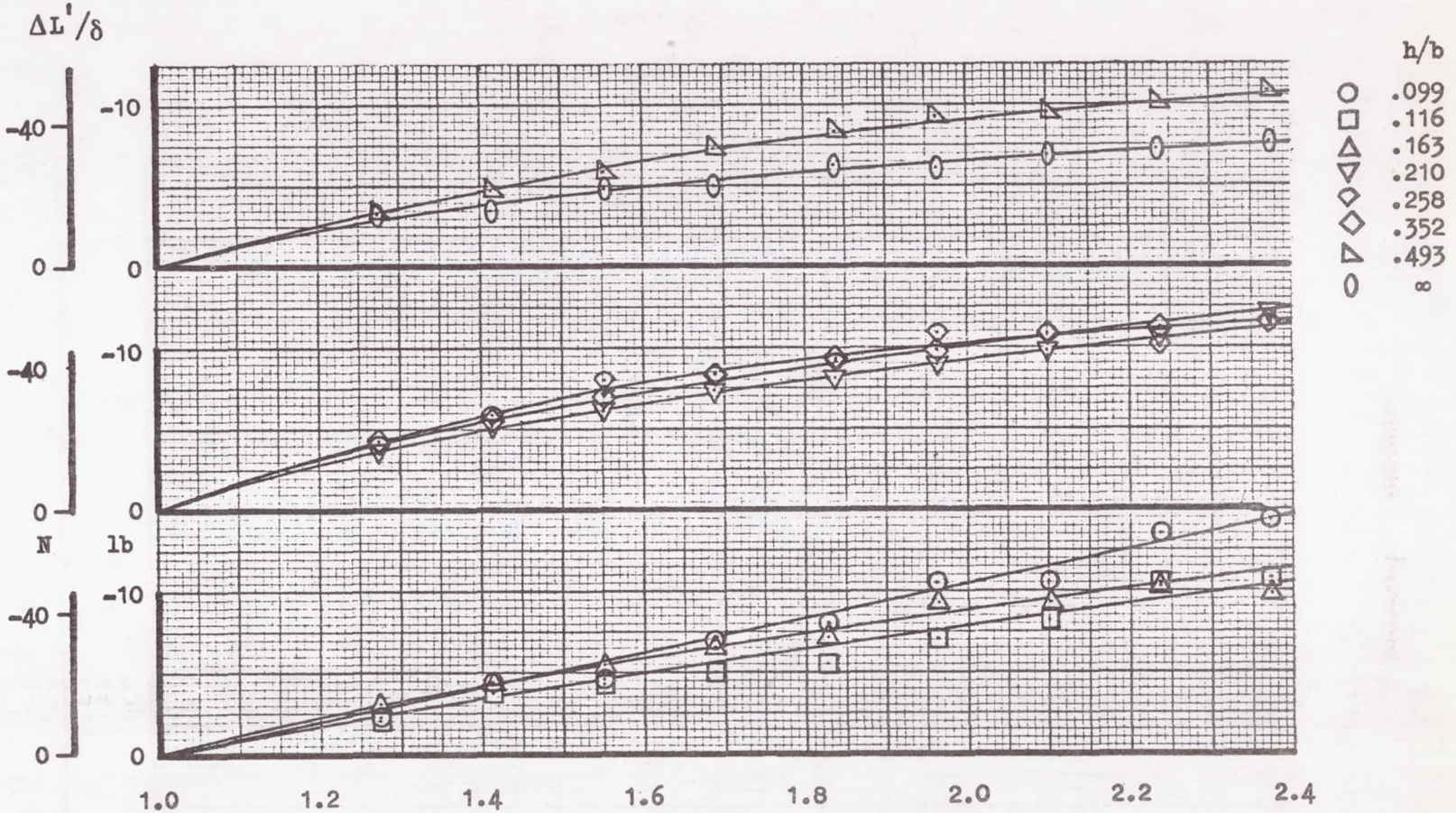

$P_{t,n}/P$

(a) Model configuration 5.

Figure 32.- Effect of pressure ratio on corrected lift loss at various heights. Nozzle configuration 21.

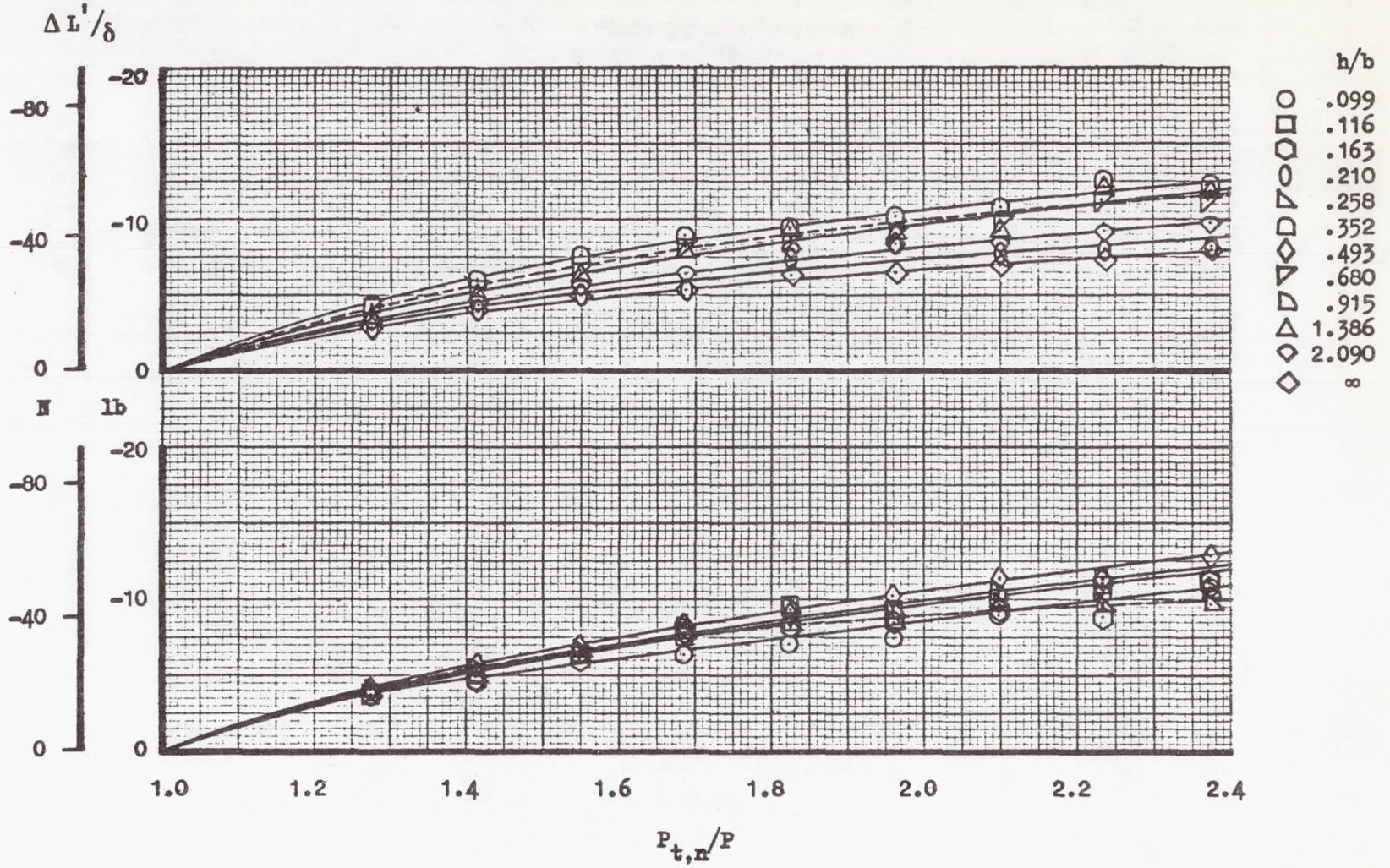

(b) Model configuration 7.

Figure 32.- Continued.

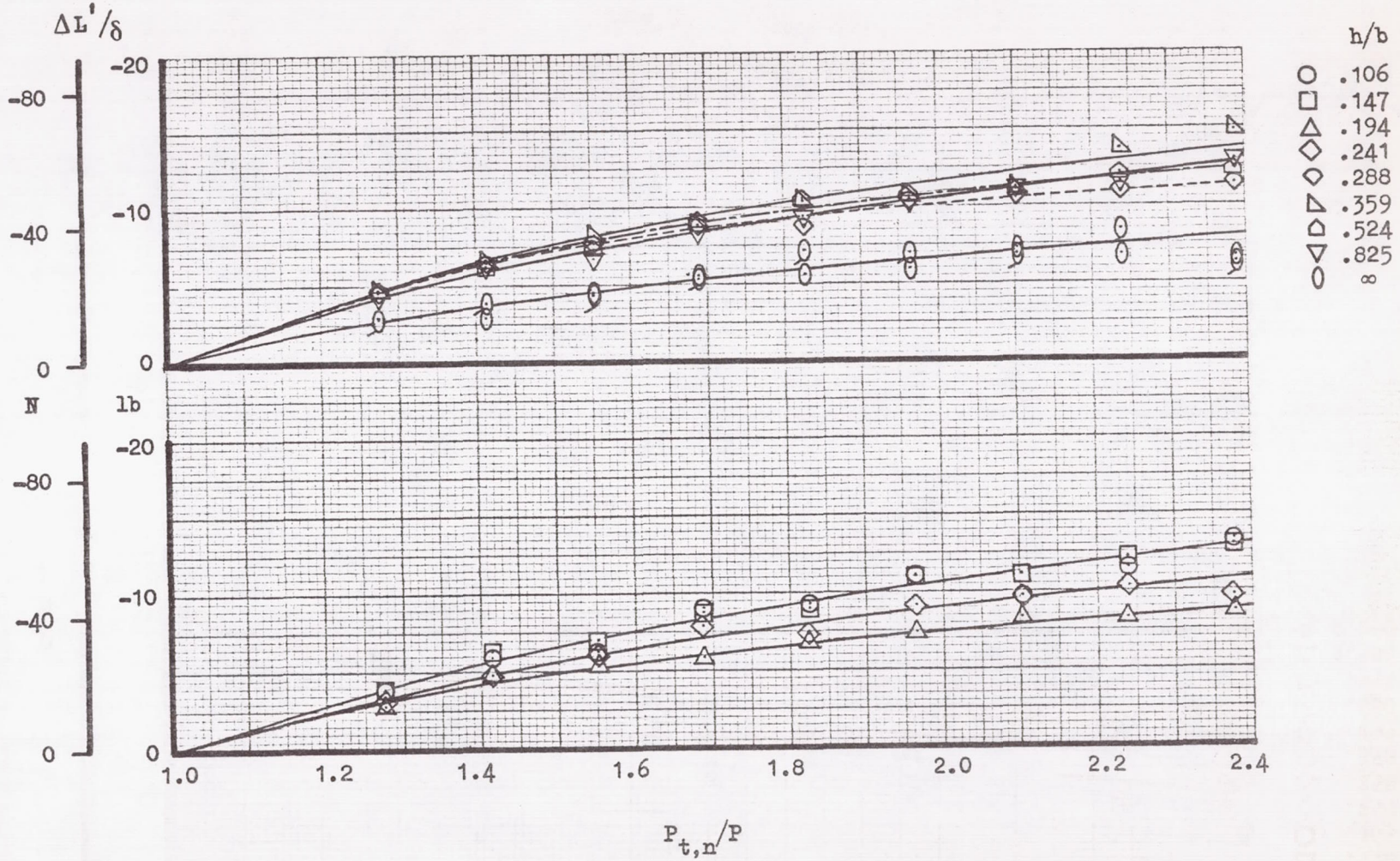

(c) Model configuration 8.

Figure 32.- Continued.

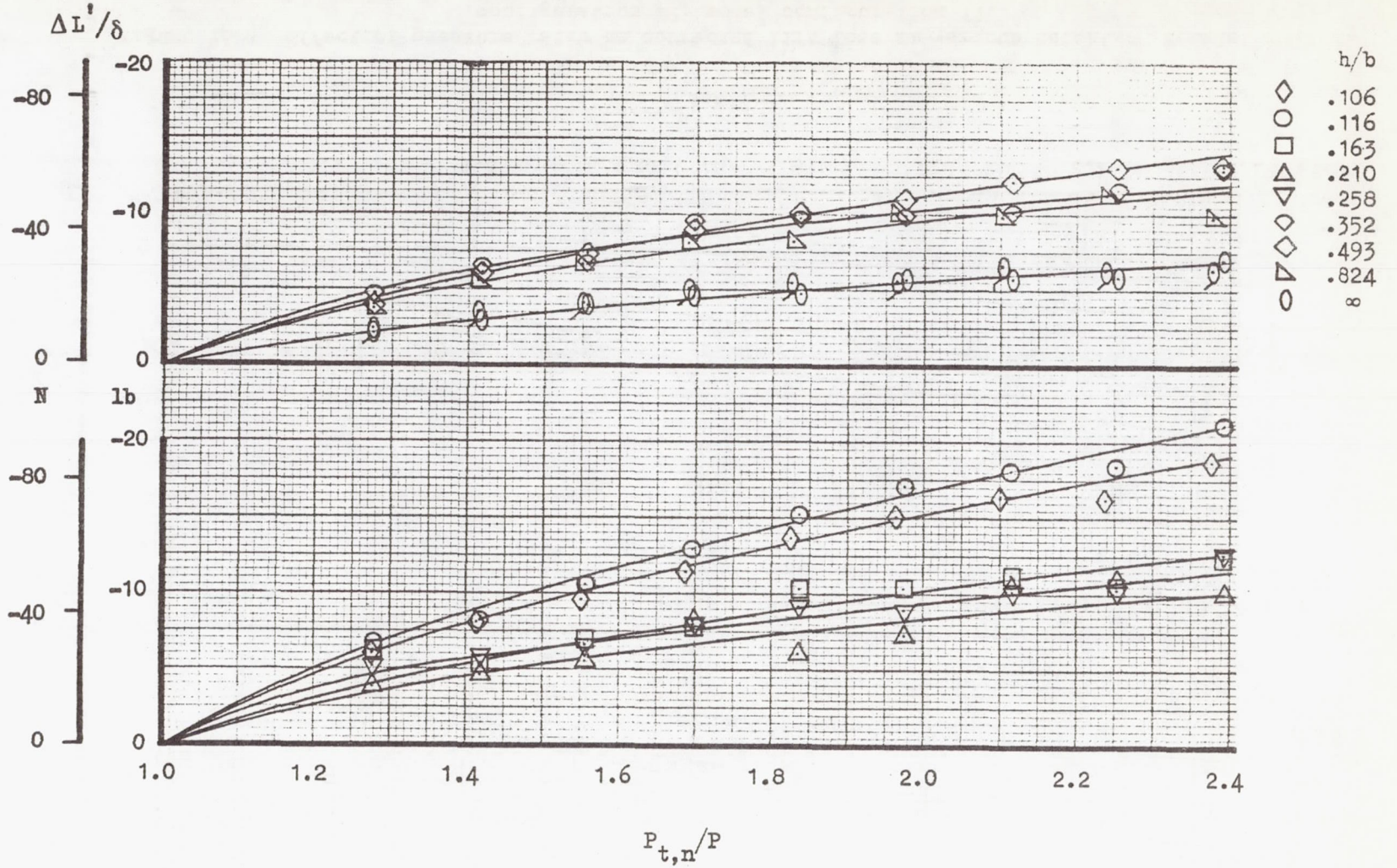

(d) Model configuration 9.

Figure 32.- Concluded.

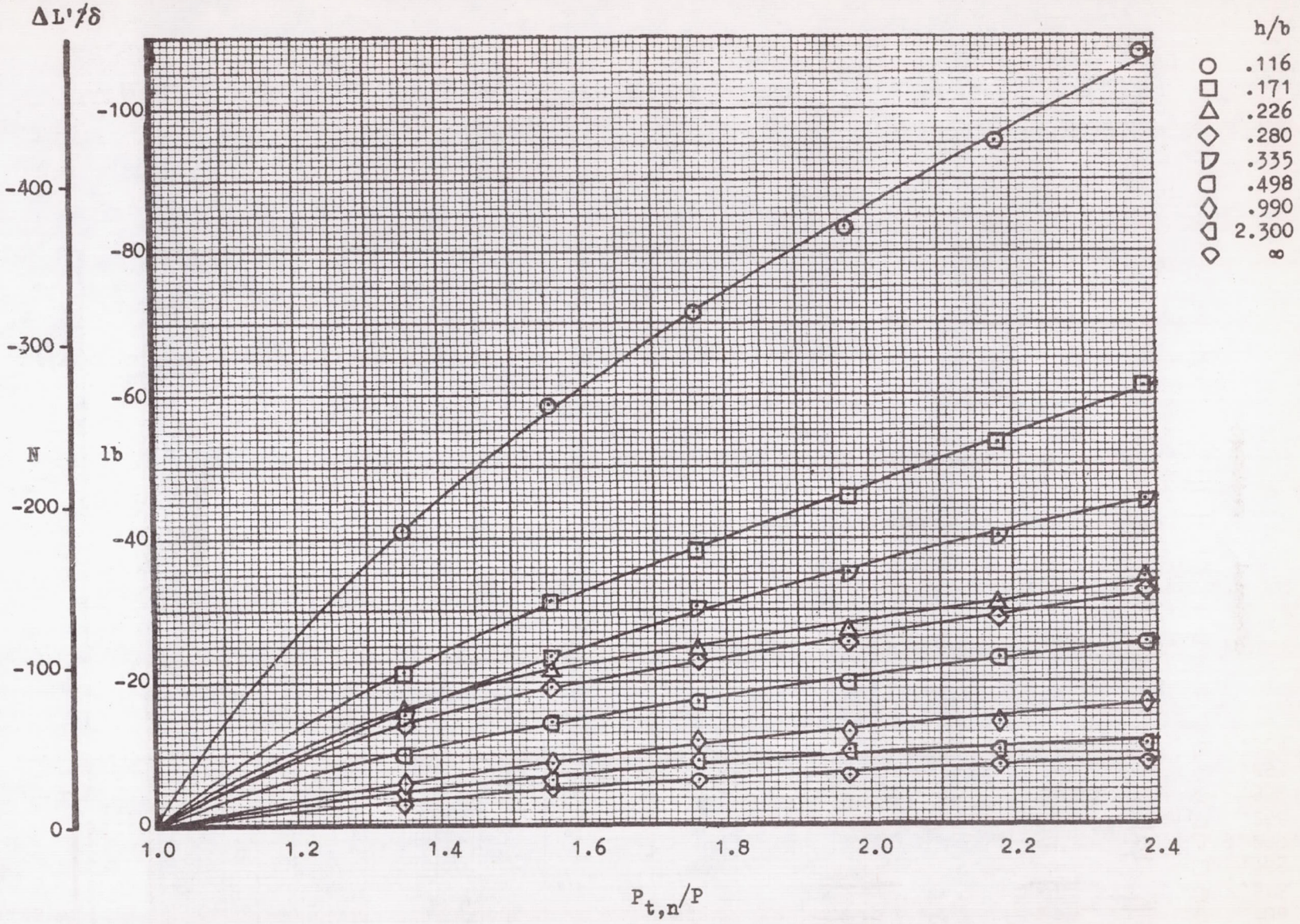

Figure 33.- Effect of pressure ratio on corrected lift loss at various heights. Nozzle configuration 22; model configuration 11.

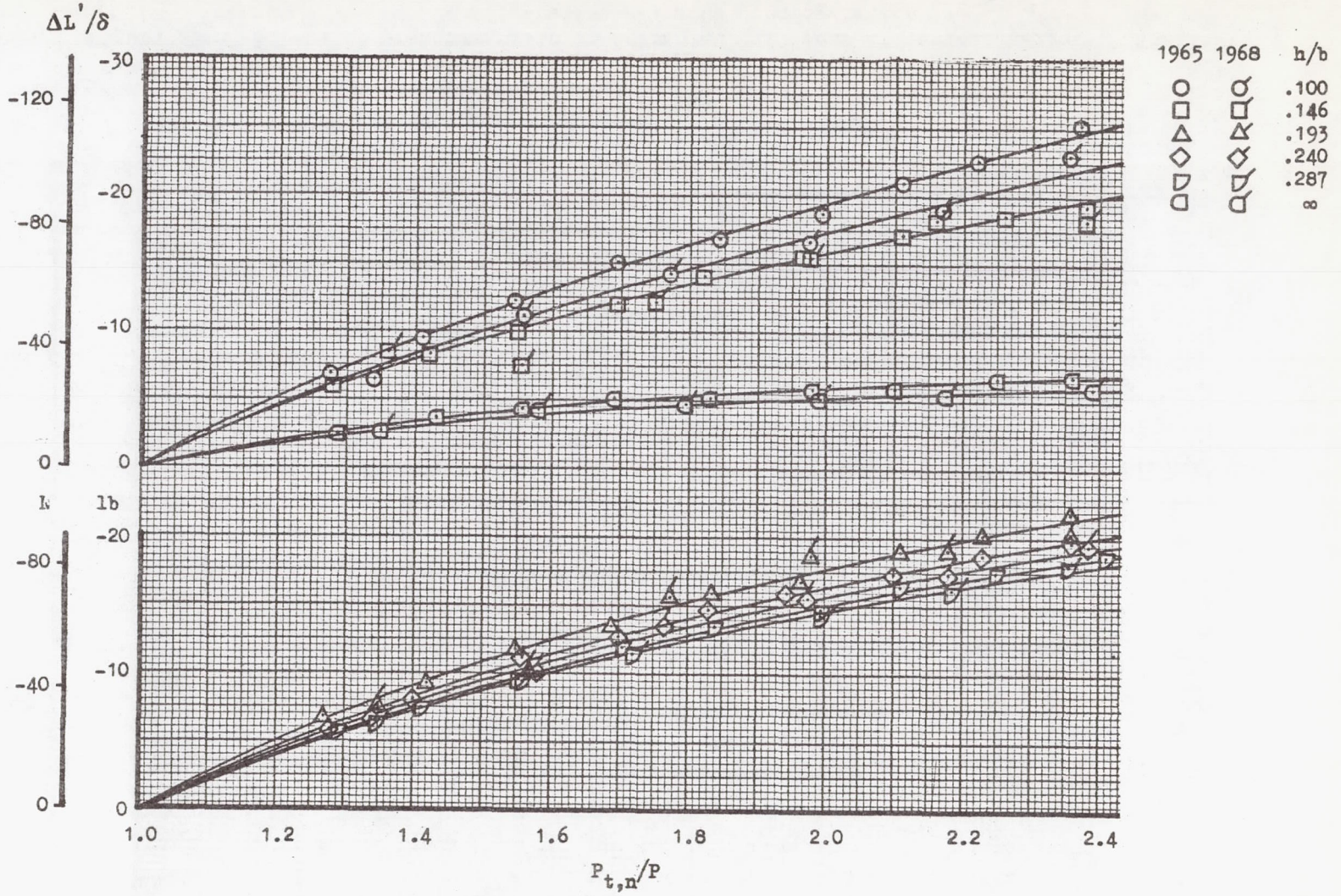

(a) Nozzle configuration 2.

Figure 34.- Comparison of 1965 and 1968 lift loss data. Model configuration 1.

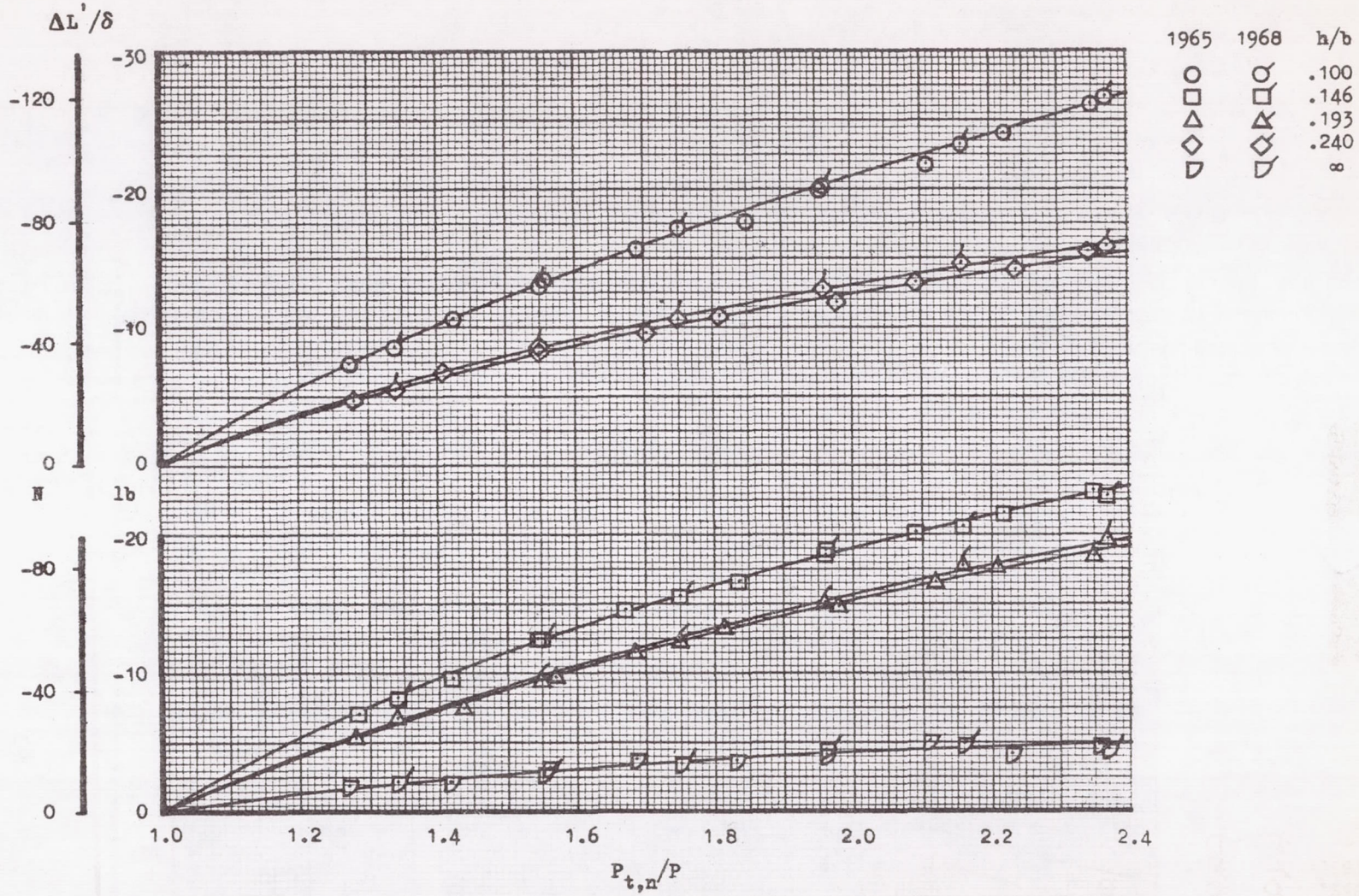

(b) Nozzle configuration 6.

Figure 34.- Continued.

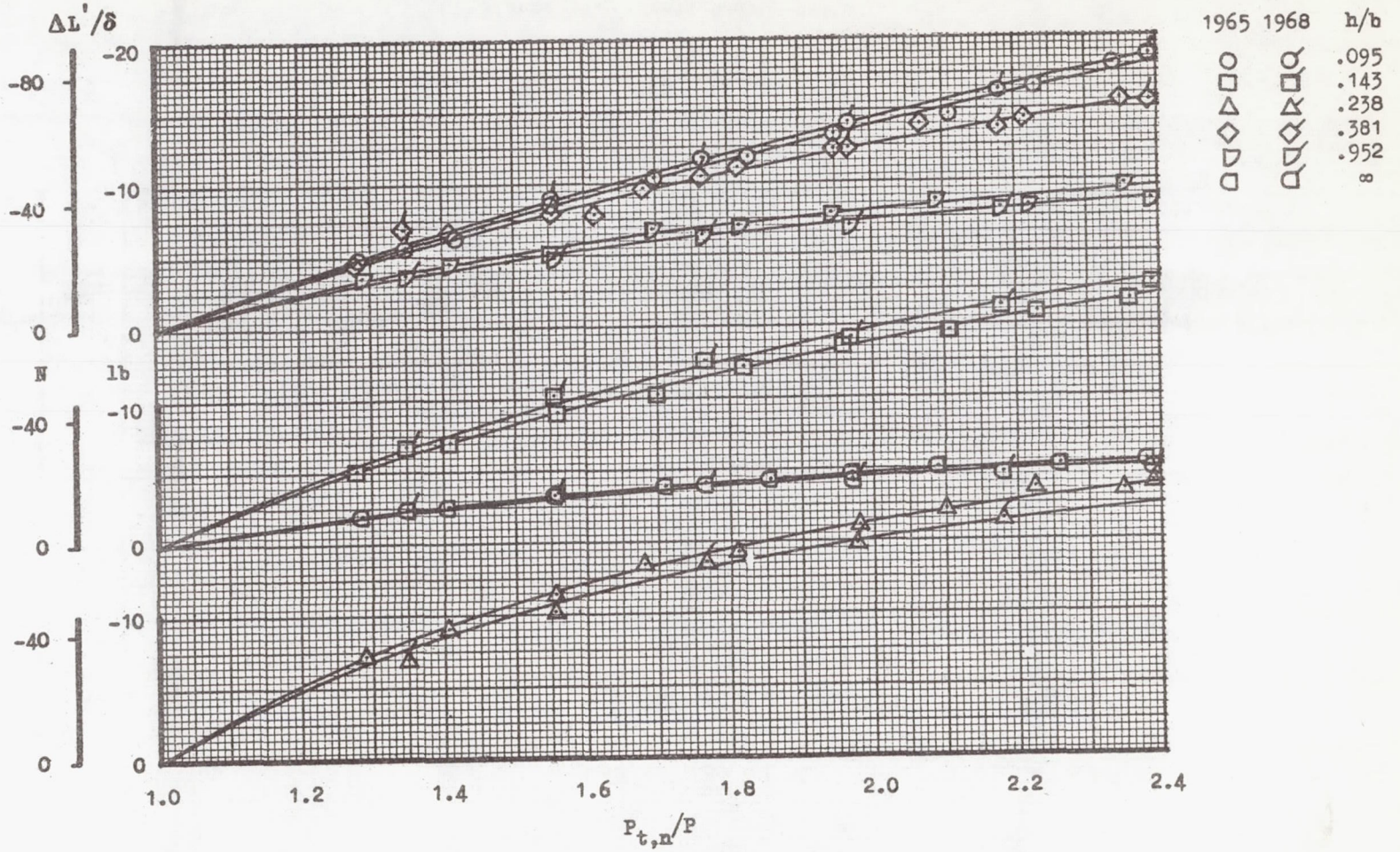

(c) Nozzle configuration 7.

Figure 34.- Concluded.

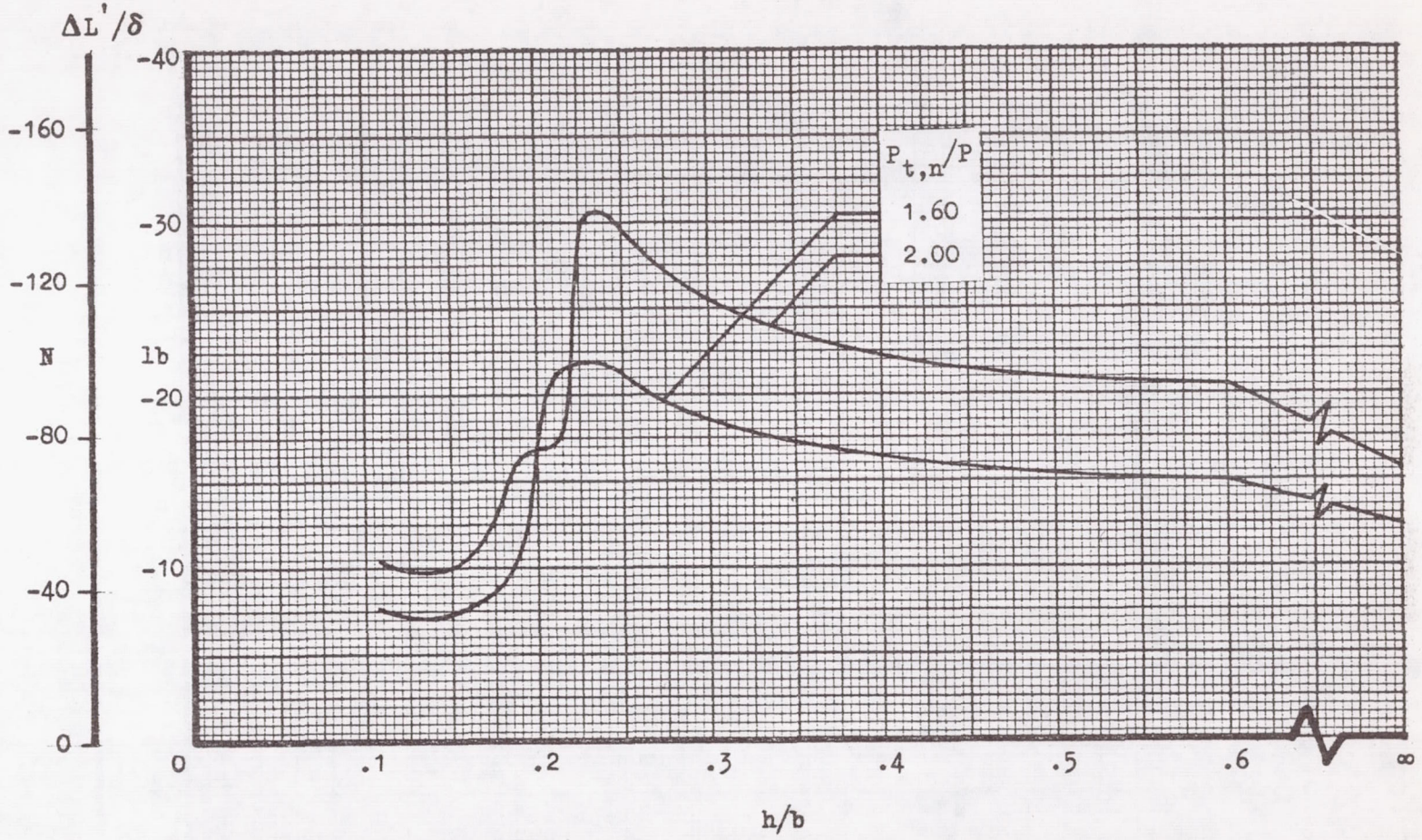

Figure 35.- Crossplot of figure 18(f) at pressure ratios bracketing lift loss break. Nozzle configuration 2; model configuration 6.

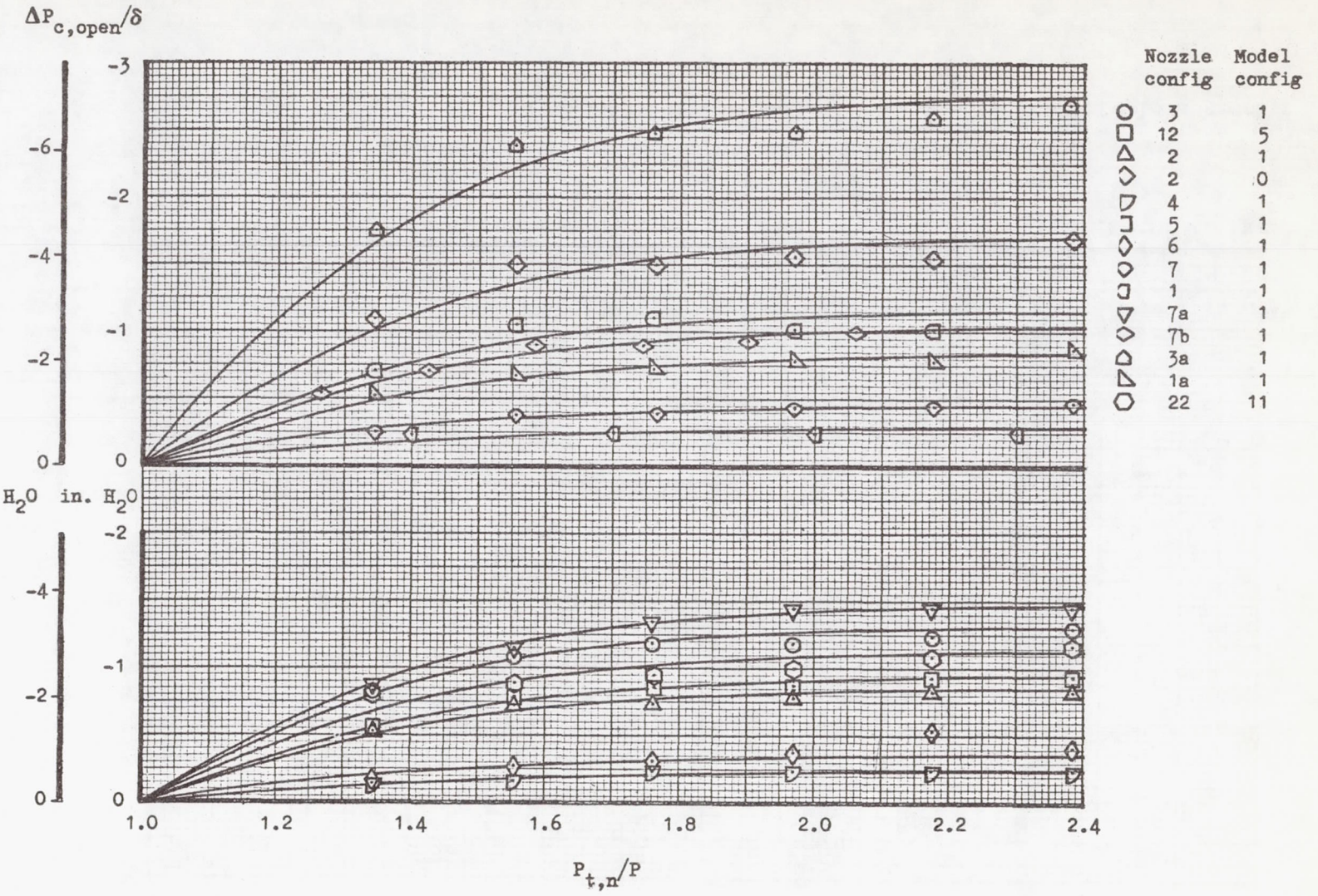

Figure 36.- Cavity pressures for all configurations. Cavity unsealed; no ground plane.

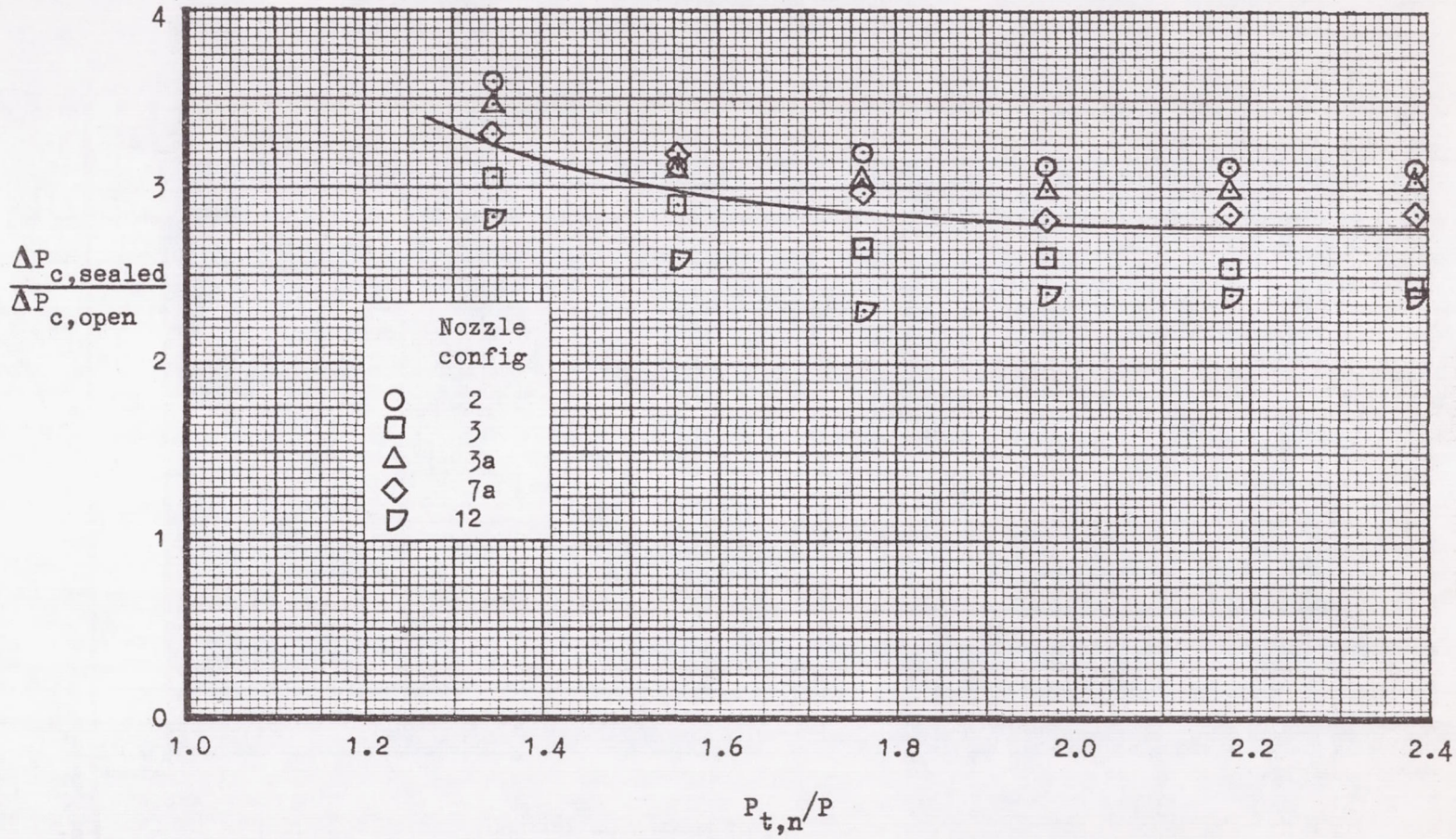

Figure 37.- Ratio of sealed-to-unsealed cavity pressure. No ground plane.

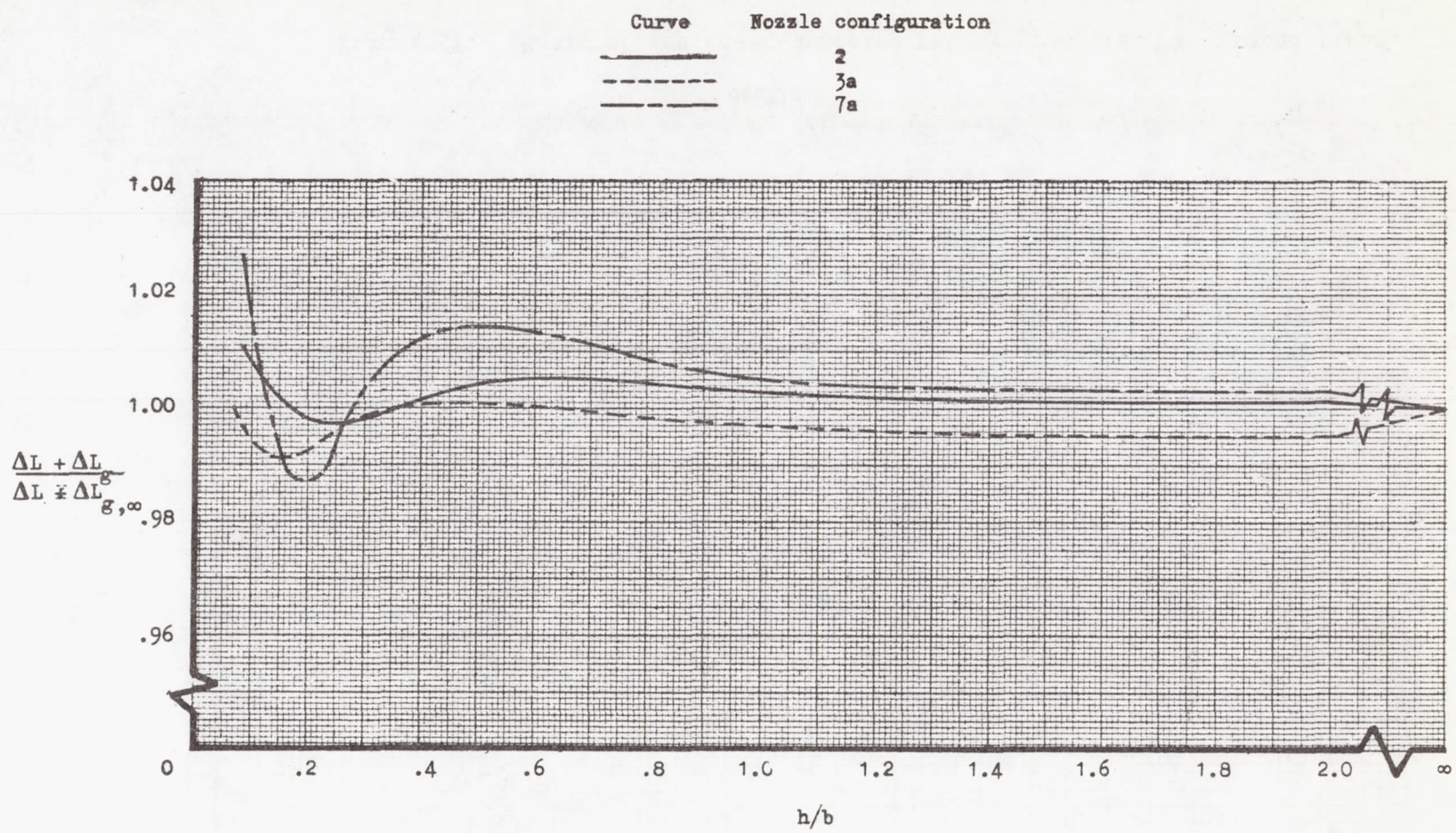

Figure 38.- Lift loss error introduced by neglecting height effect on gap correction. Model configuration 1.

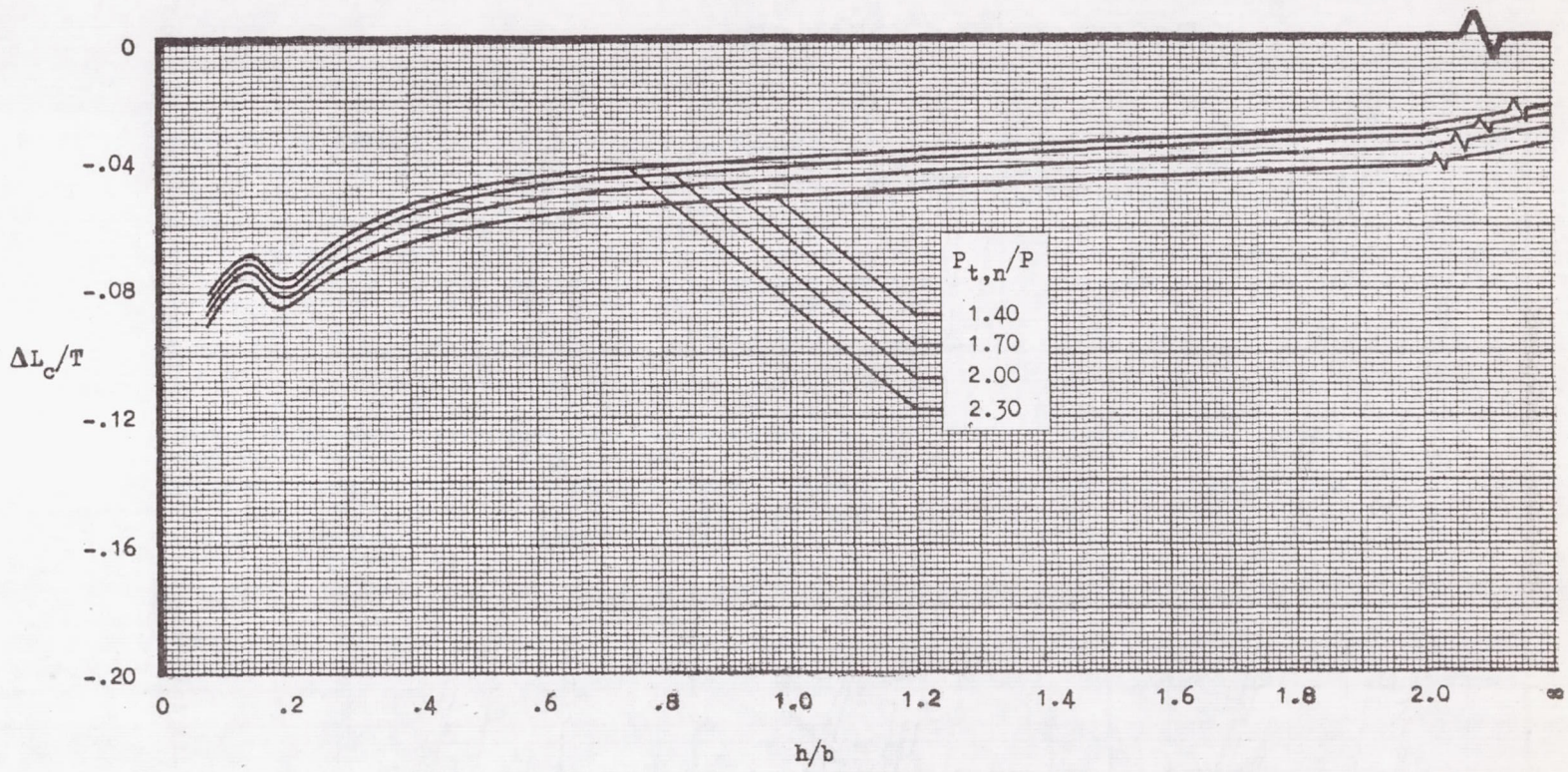

Figure 39.- Typical lift loss curves vs height, for various pressure ratios. Nozzle configuration 2; model configuration 1.

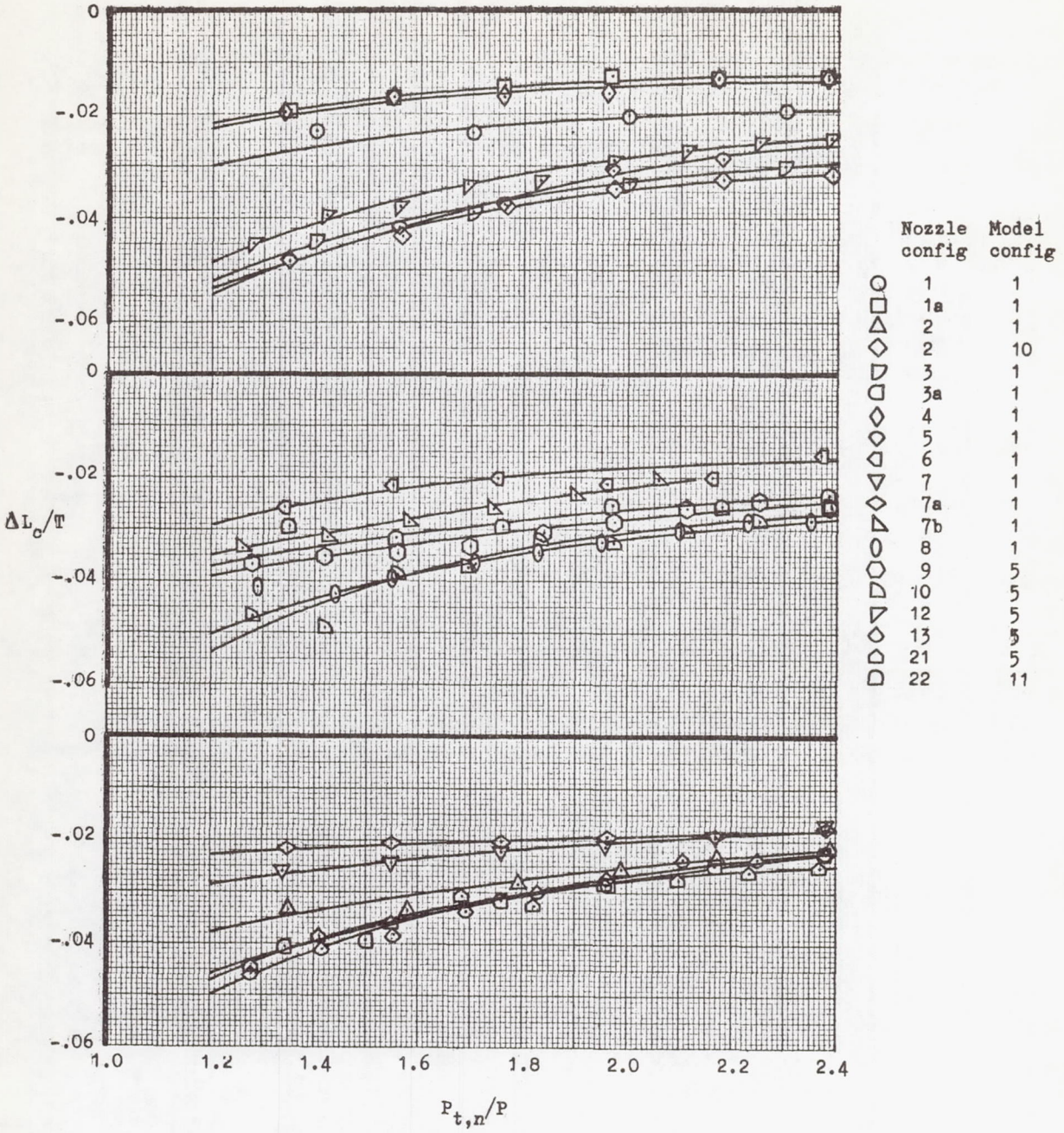

Figure 40.- Lift loss comparison for all configurations. No ground plane.

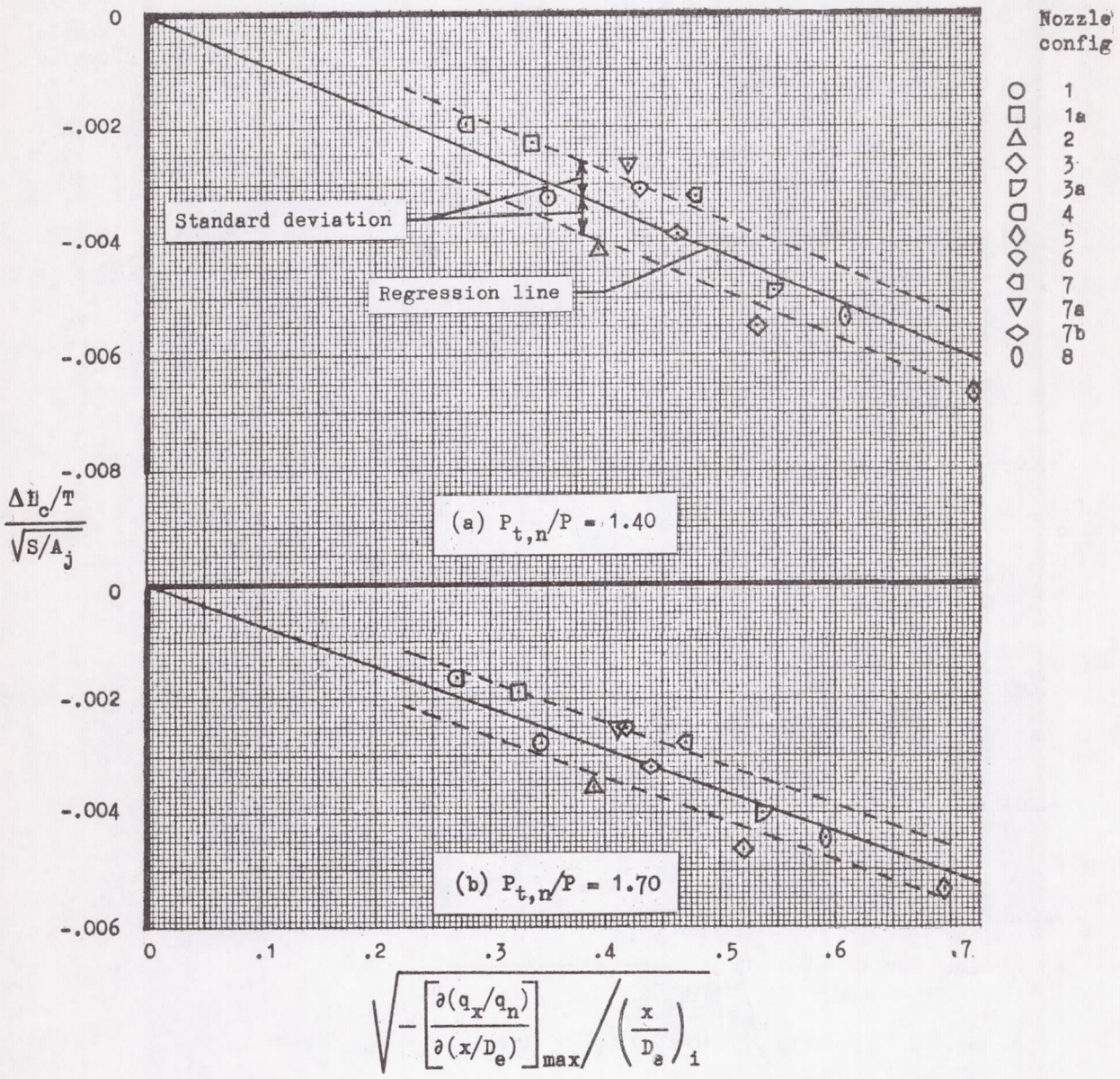

Figure 41.- Correlation of lift loss with jet decay parameter. Model configuration 1; h/b = ∞.

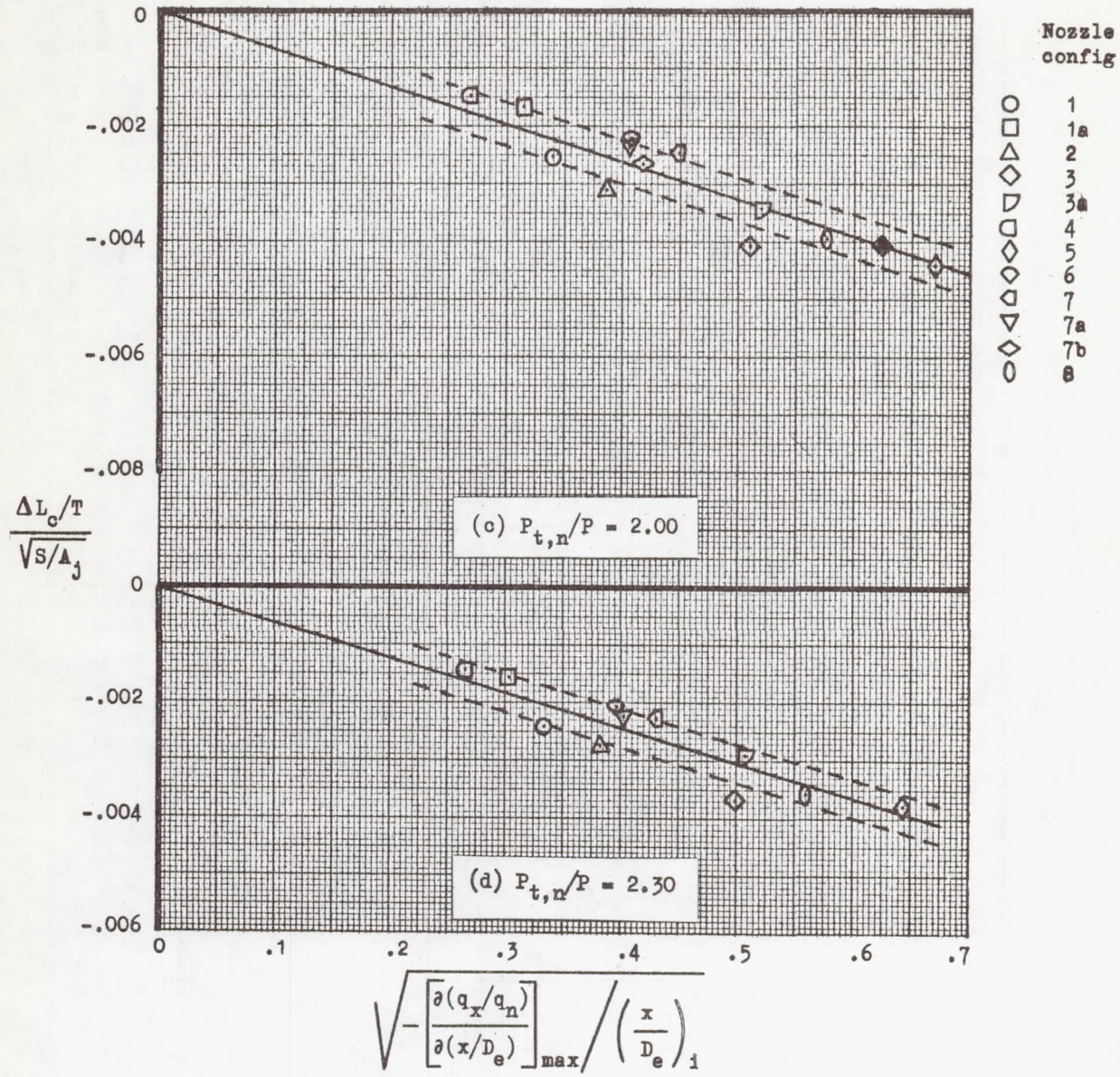

Figure 41.- Concluded.

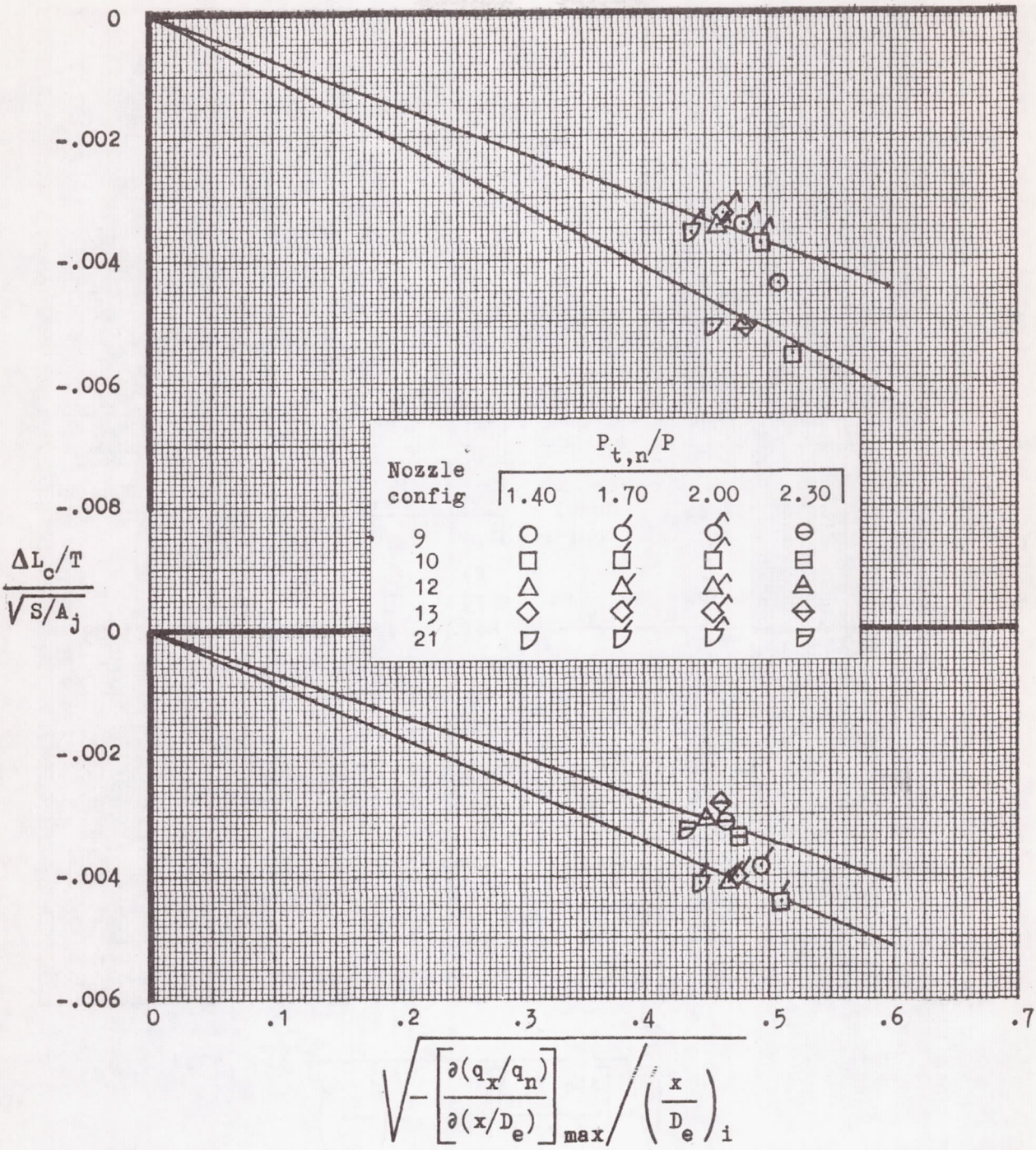

Figure 42.- Correlation of lift loss with jet decay parameter. Model configuration 5; h/b = ∞.

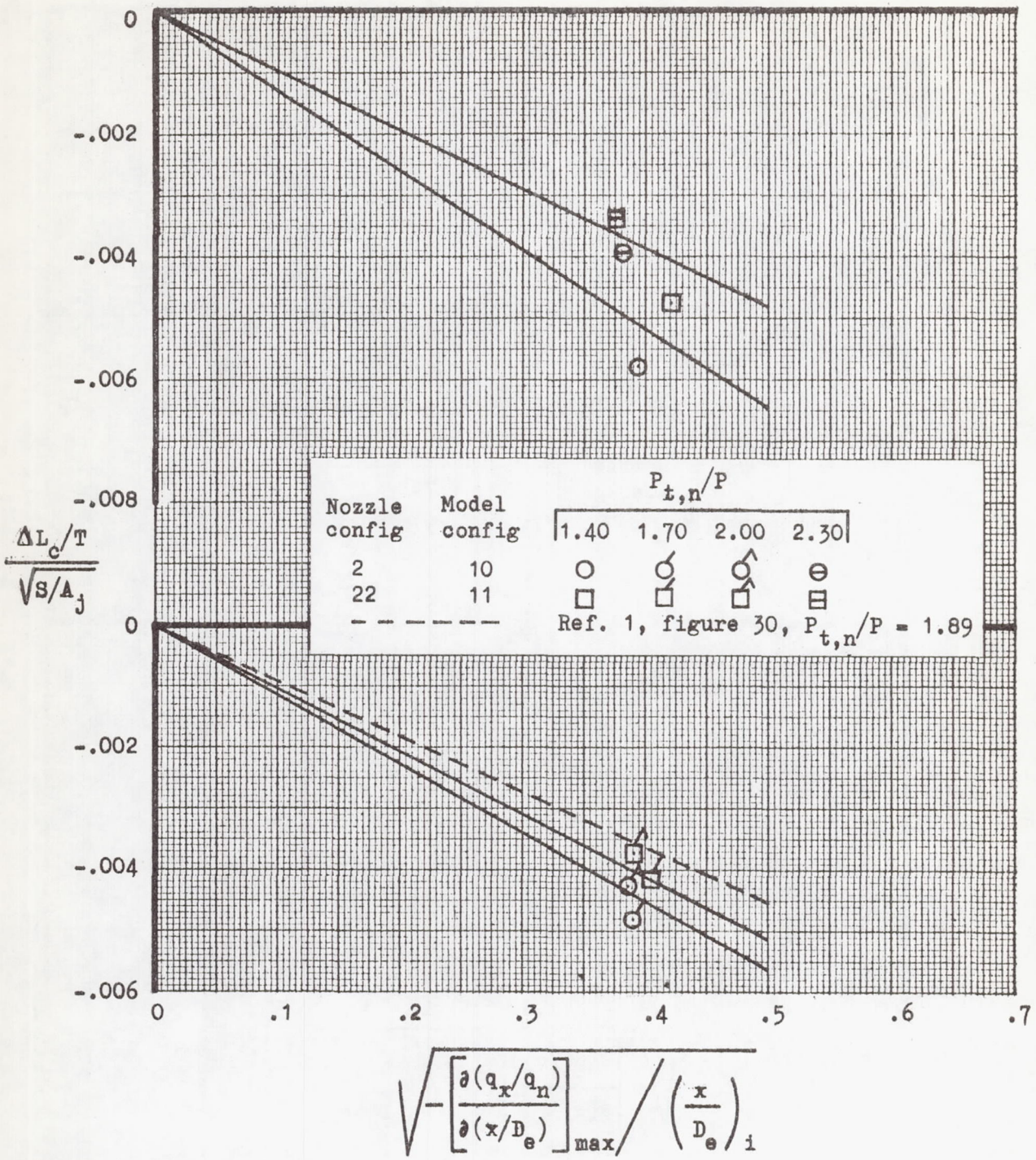

Figure 43.- Correlation of lift loss with jet decay parameter. Low-wing configurations; h/b = ∞.

Figure 44.- Refaired jet decay profile. Nozzle configuration 3; $P_{t,n}/P = 2.0$.

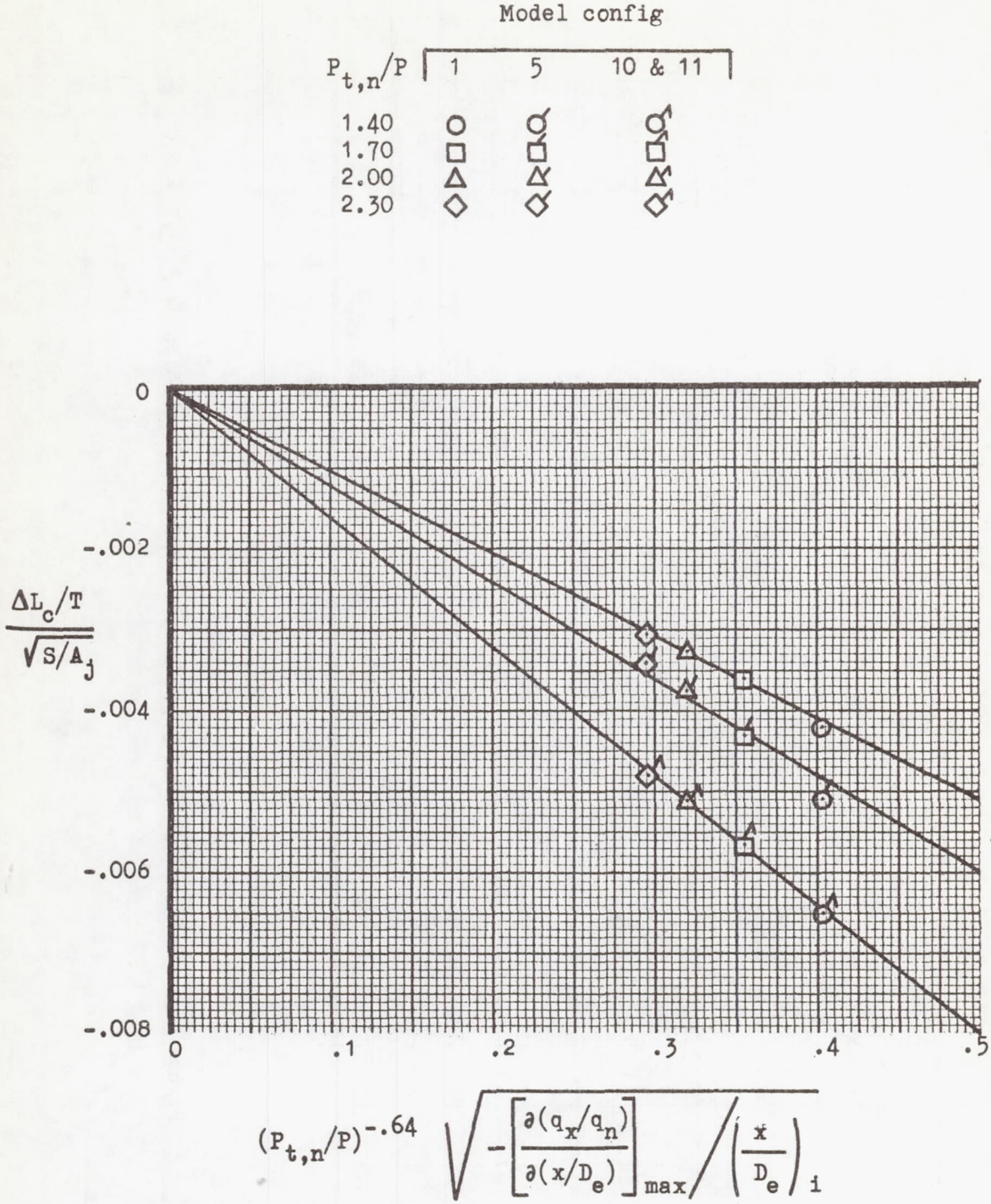

Figure 45.- Correlation of lift loss with nozzle pressure ratio and jet decay parameter; h/b = ∞.

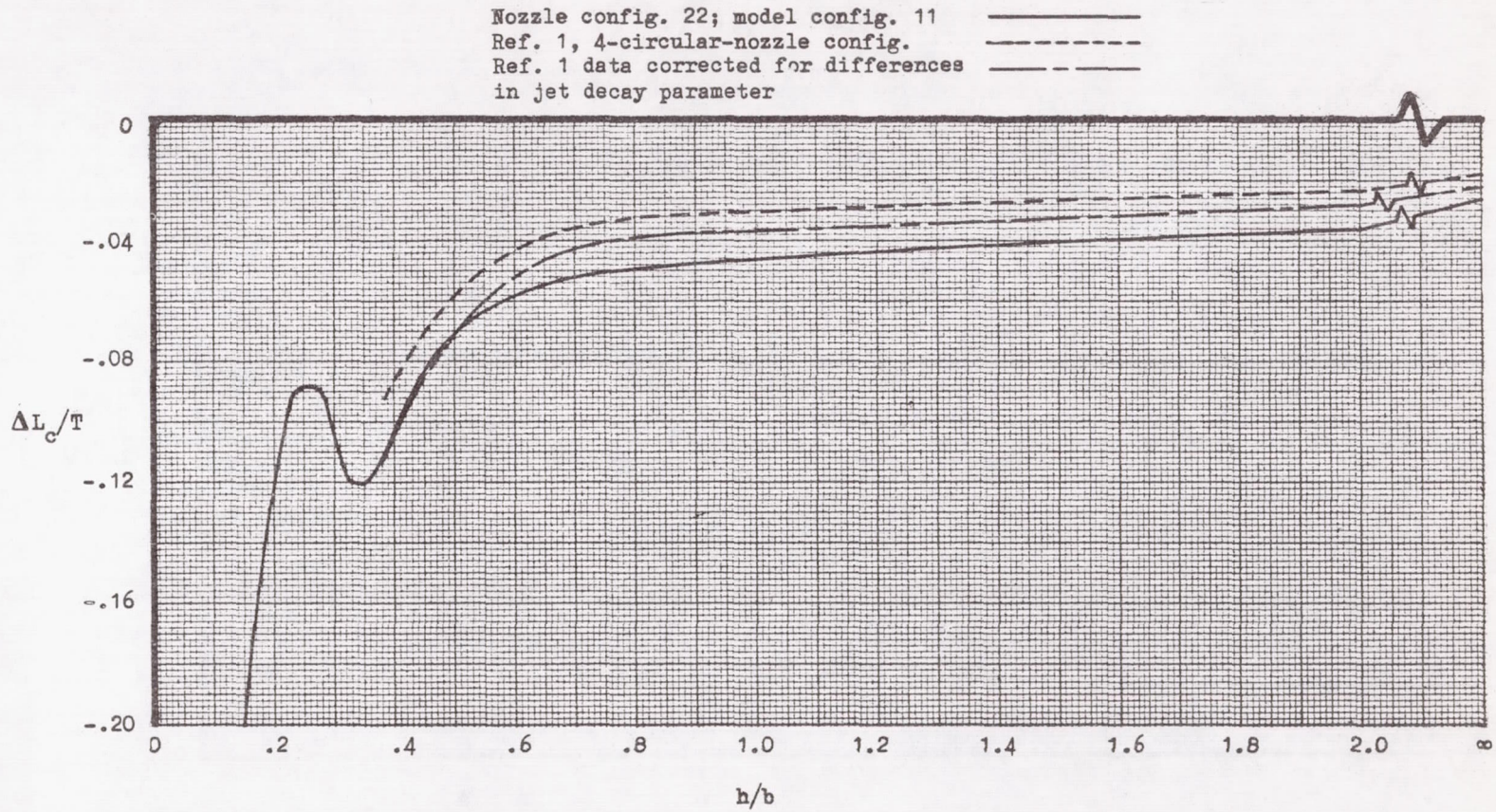

Figure 46.- Comparison of Lockheed and NASA results. $P_{t,n}/P = 2.08$.

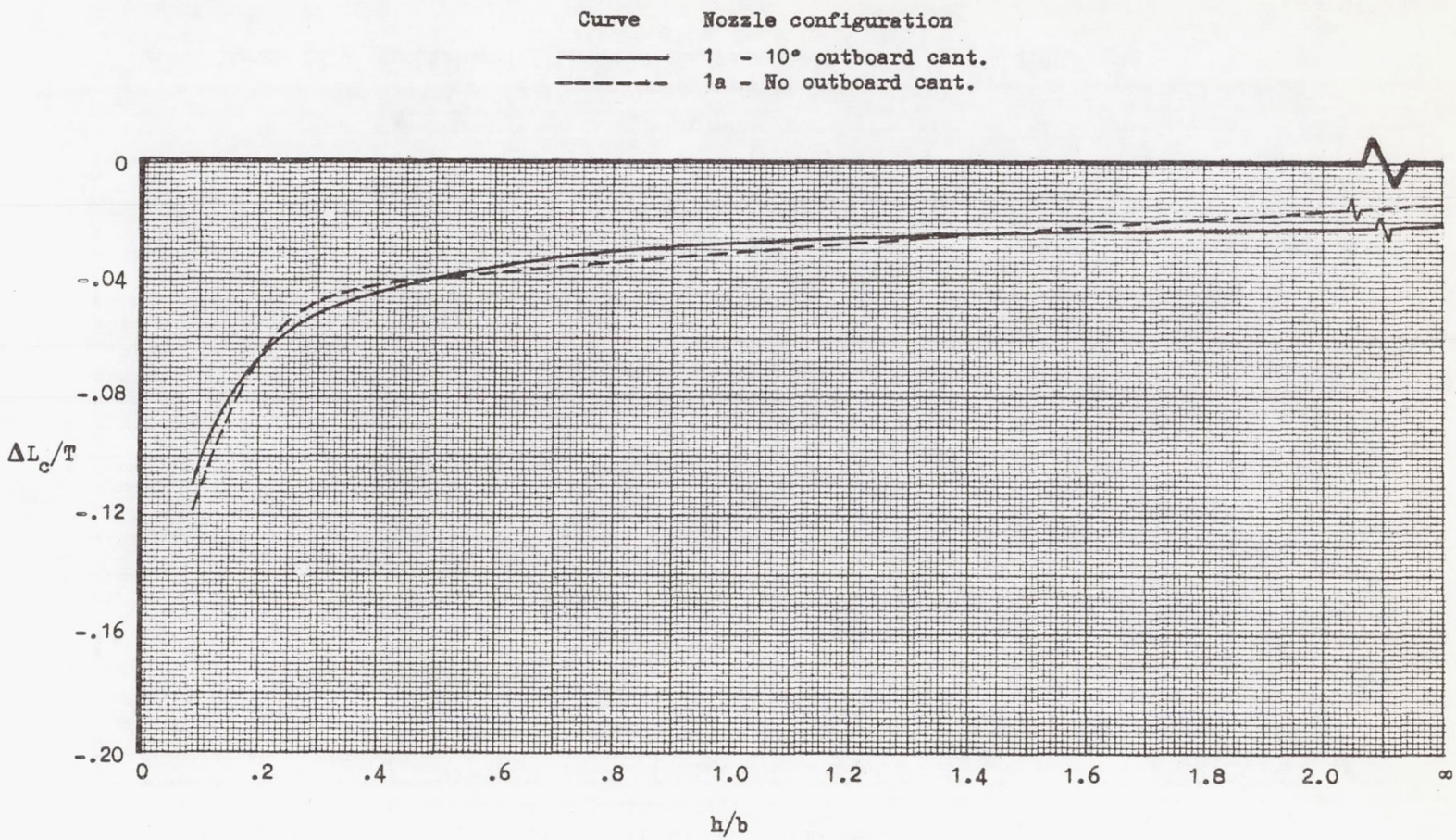

(a) 4 nozzles.

Figure 47.- Effect of nozzle outboard cant on lift loss. Model configuration 1; $P_{t,n}/P = 2.0$.

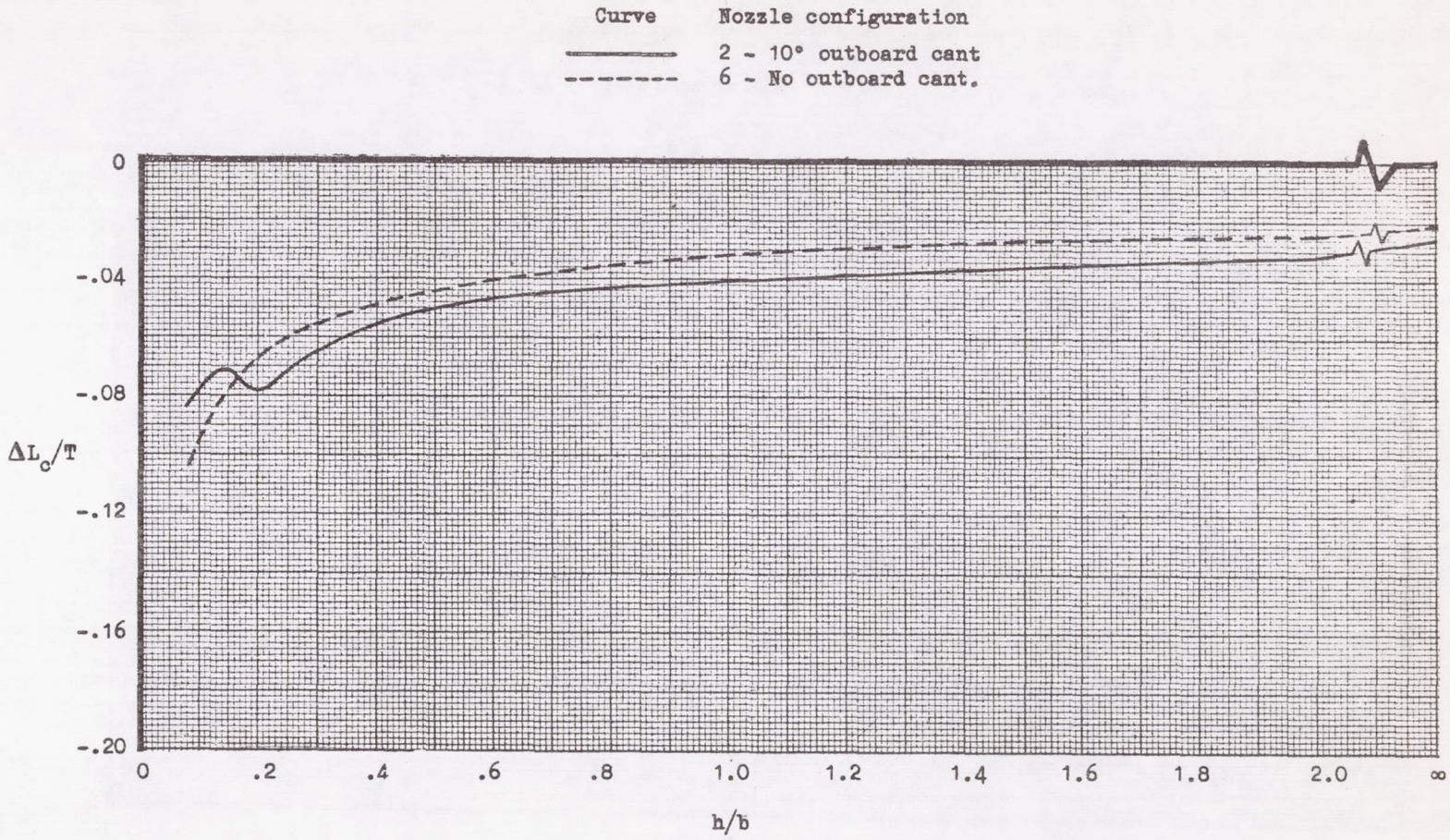

(b) 6 nozzles.

Figure 47.- Continued.

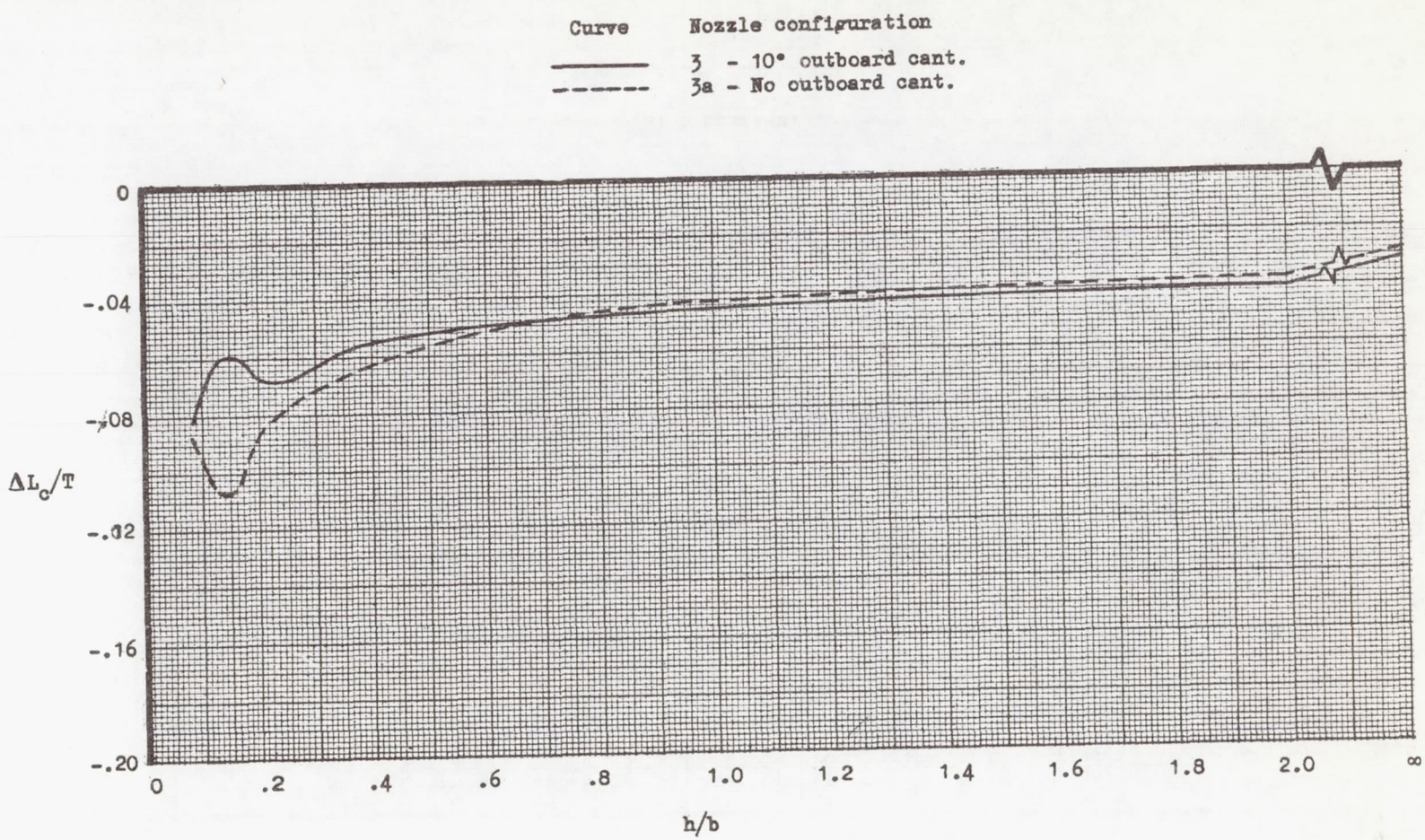

(c) 6 nozzles.

Figure 47.- Concluded.

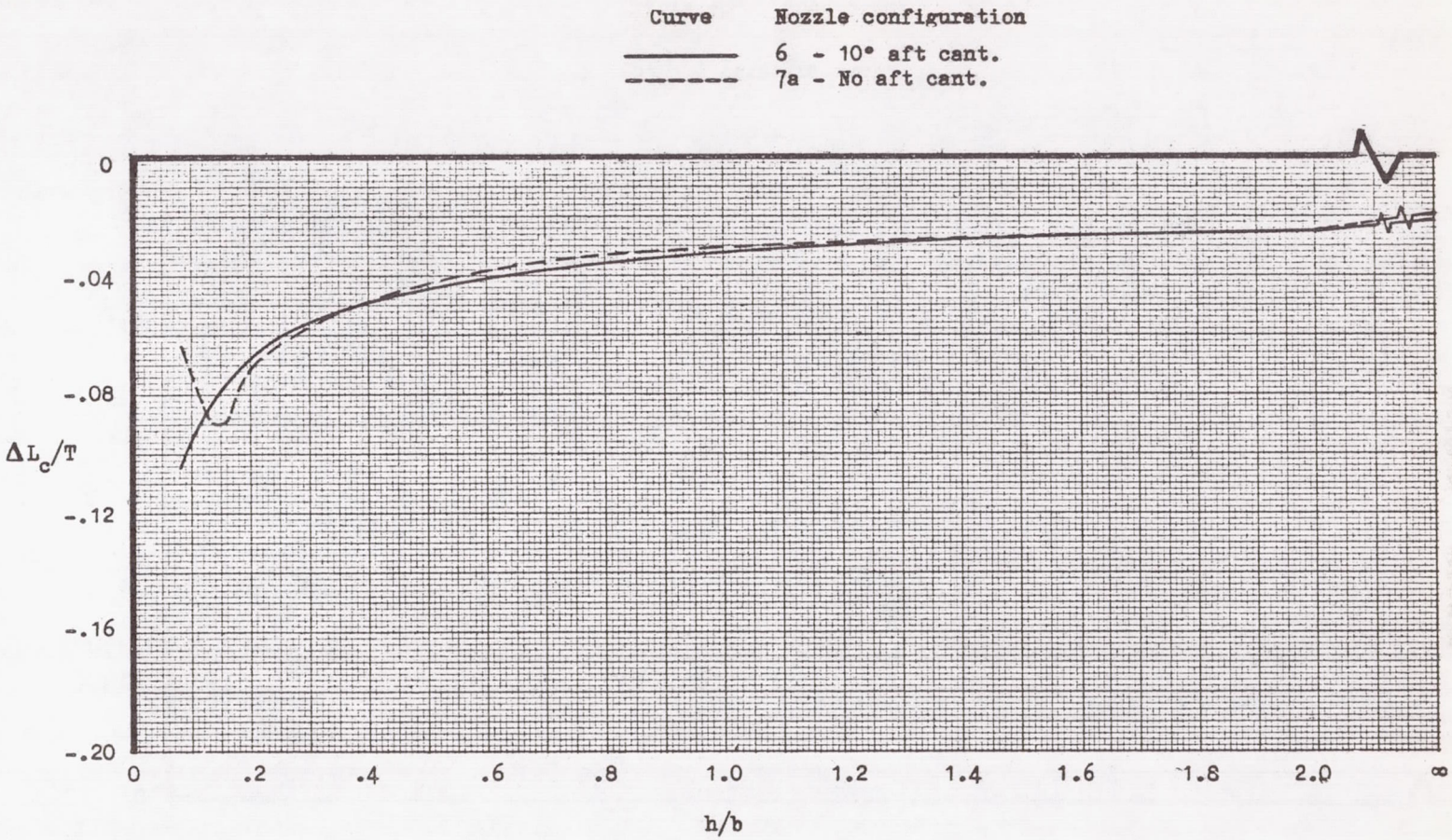

(a) No outboard cant.

Figure 48.- Effect of nozzle aft cant on lift loss. Model configuration 1; $P_{t,n}/P = 2.0$.

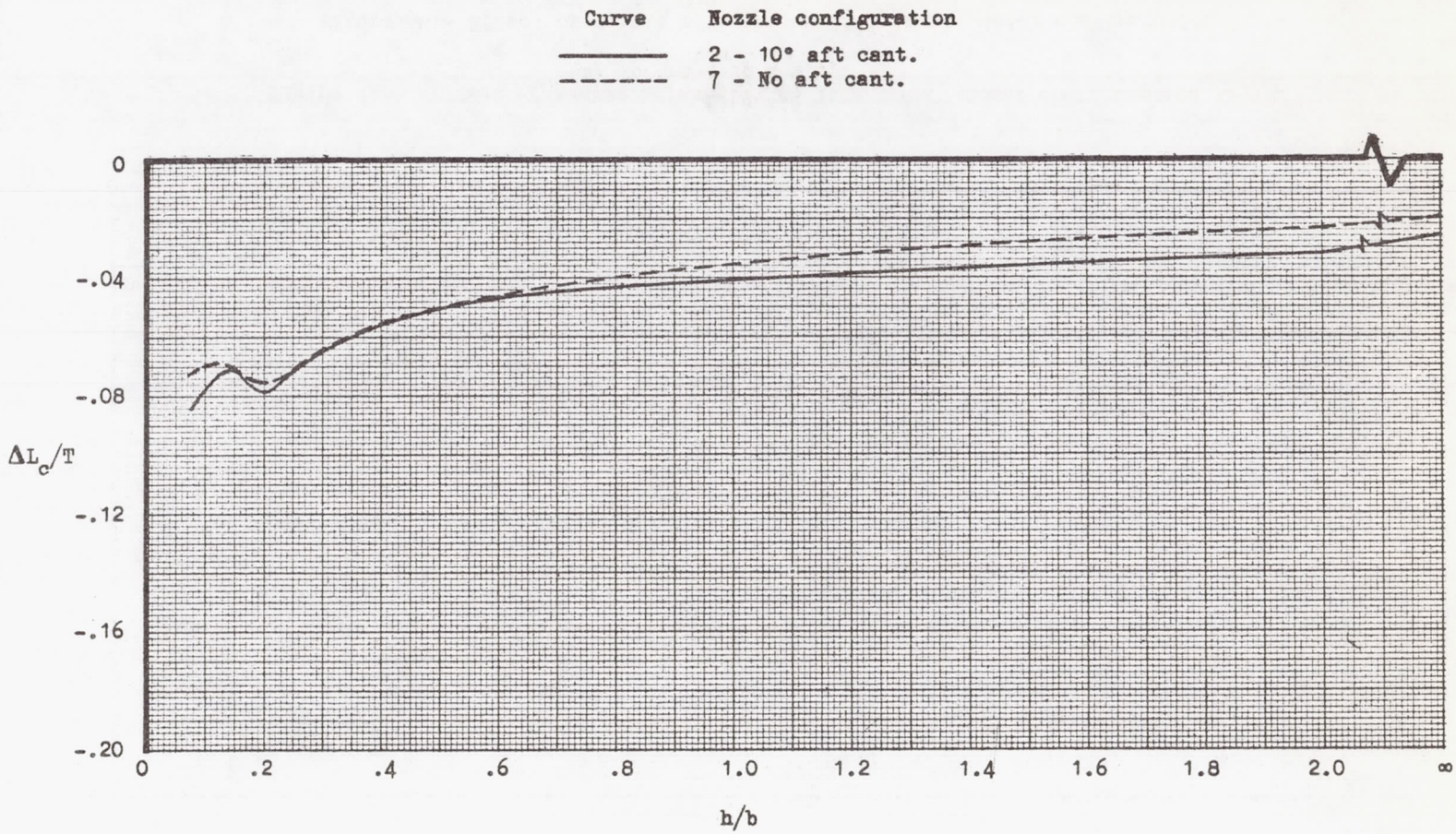

(b) 10° outboard cant.

Figure 48.- Concluded.

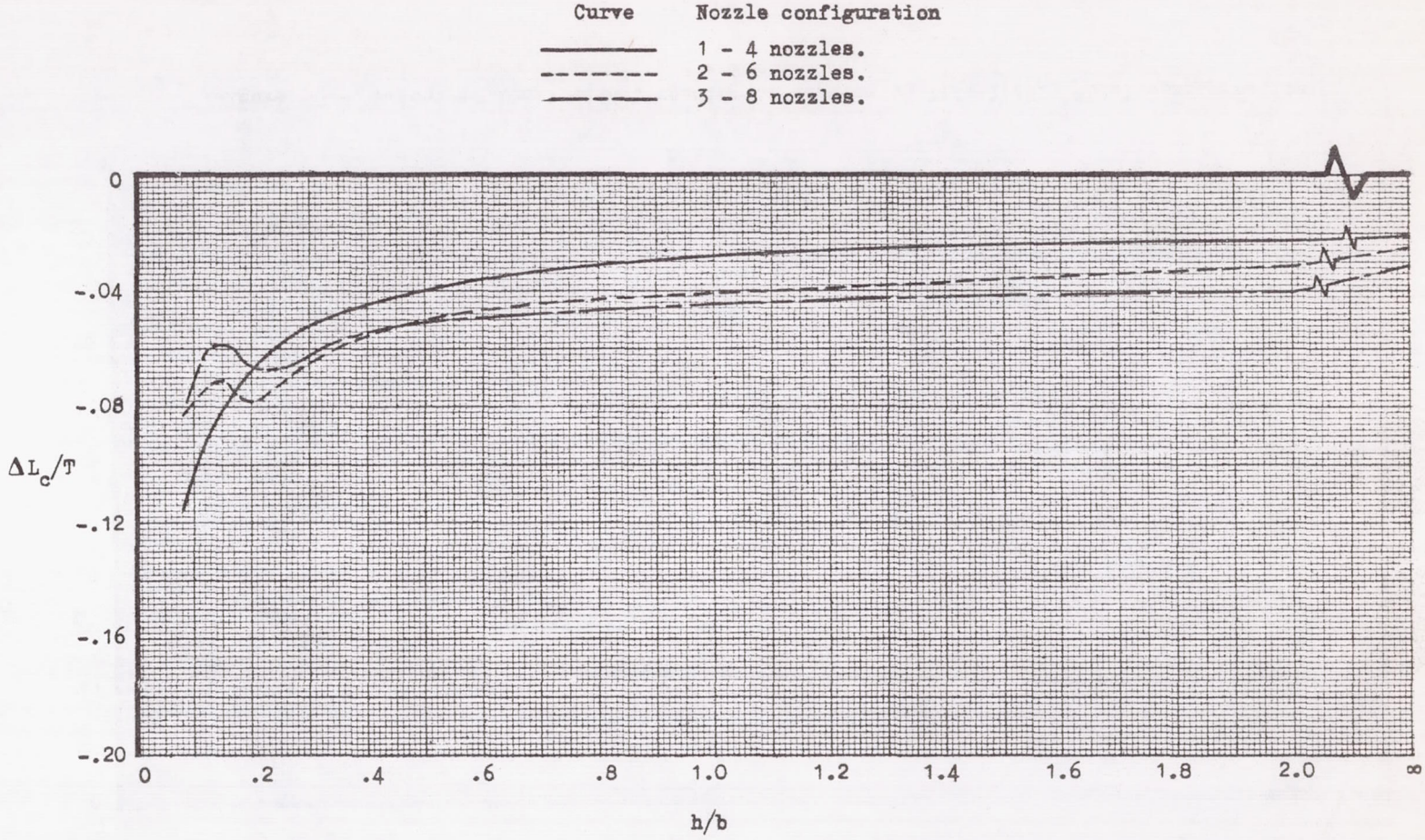

Figure 49.- Effect of number of nozzles on lift loss. Model configuration 1; $P_{t,n}/P = 2.0$.

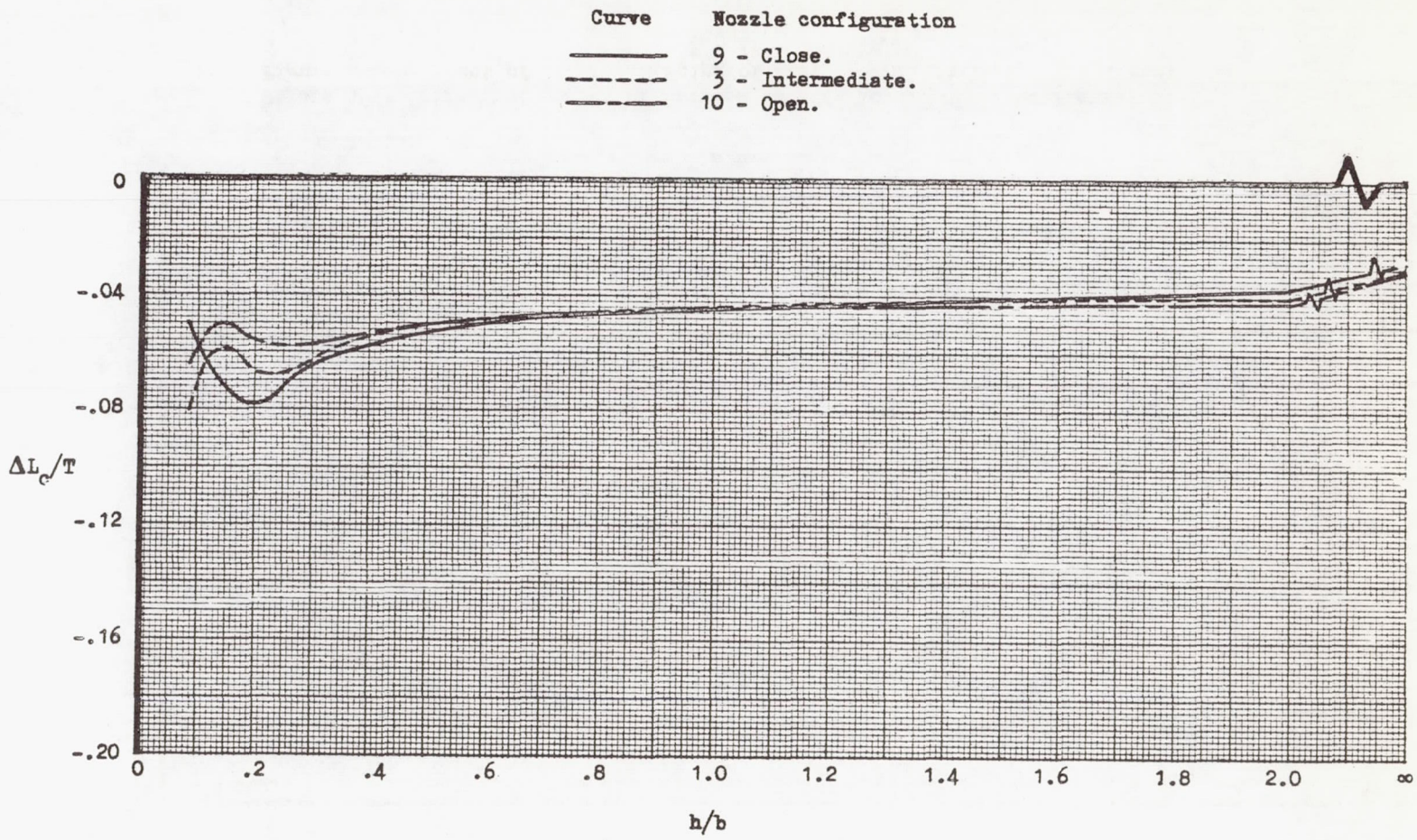

Figure 50.- Effect of longitudinal spacing of nozzles on lift loss. Model configuration 5; $P_{t,n}/P = 2.0$.

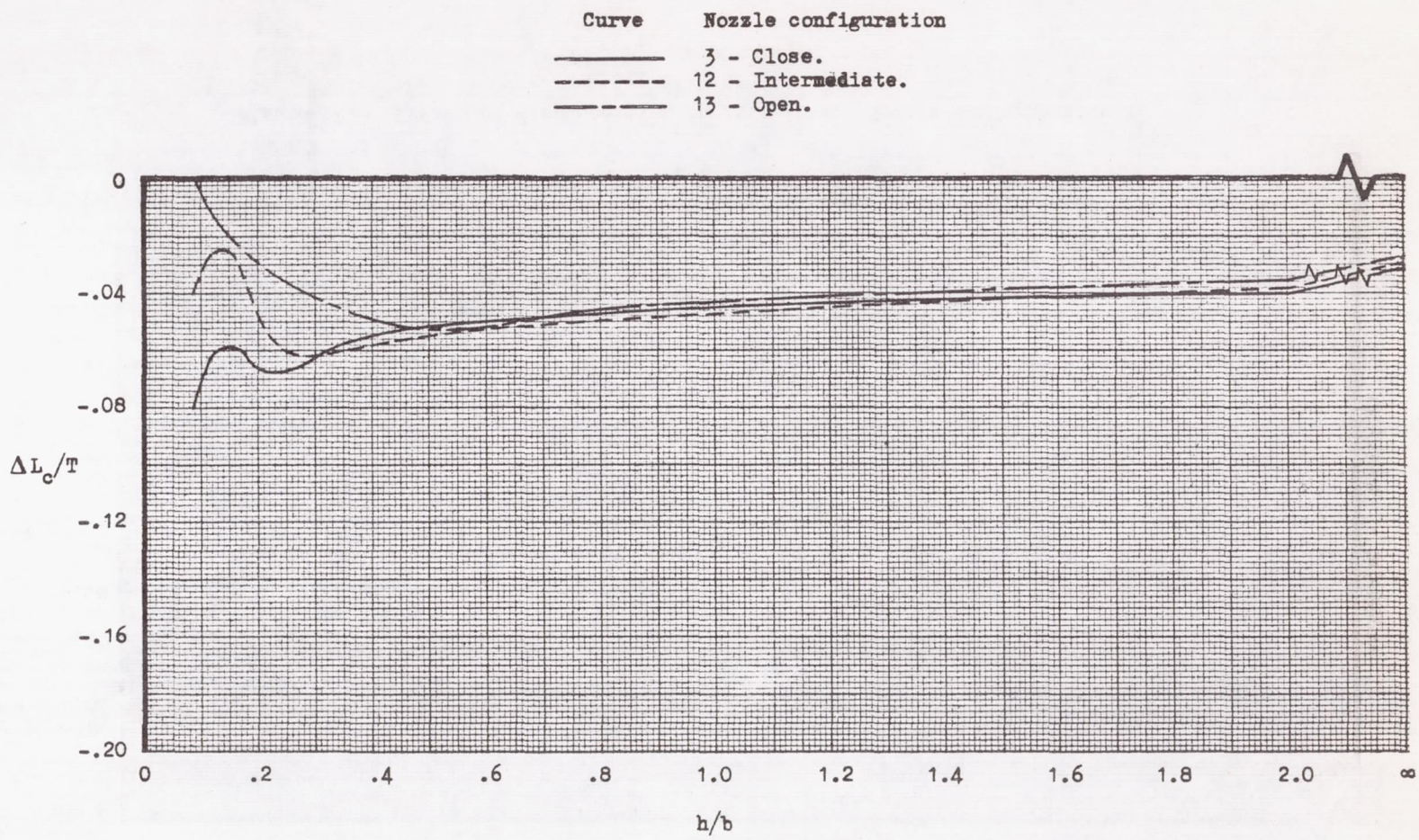

Figure 51.- Effect of lateral spacing of nozzles on lift loss. Model configuration 5; $P_{t,n}/P = 2.0$.

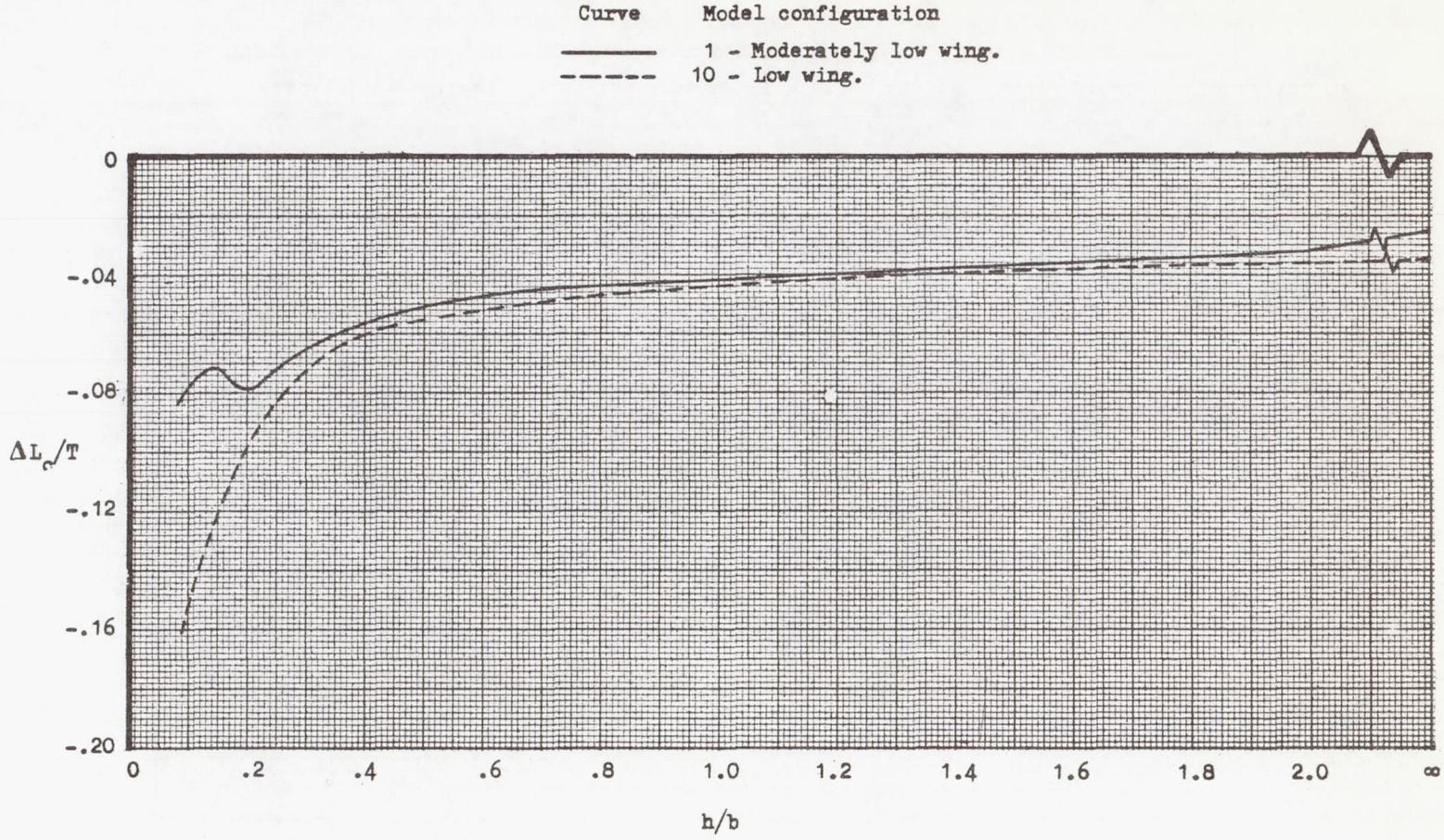

Figure 52.- Effect of wing position on lift loss. Nozzle configuration 2; $P_{t,n}/P = 2.0$.

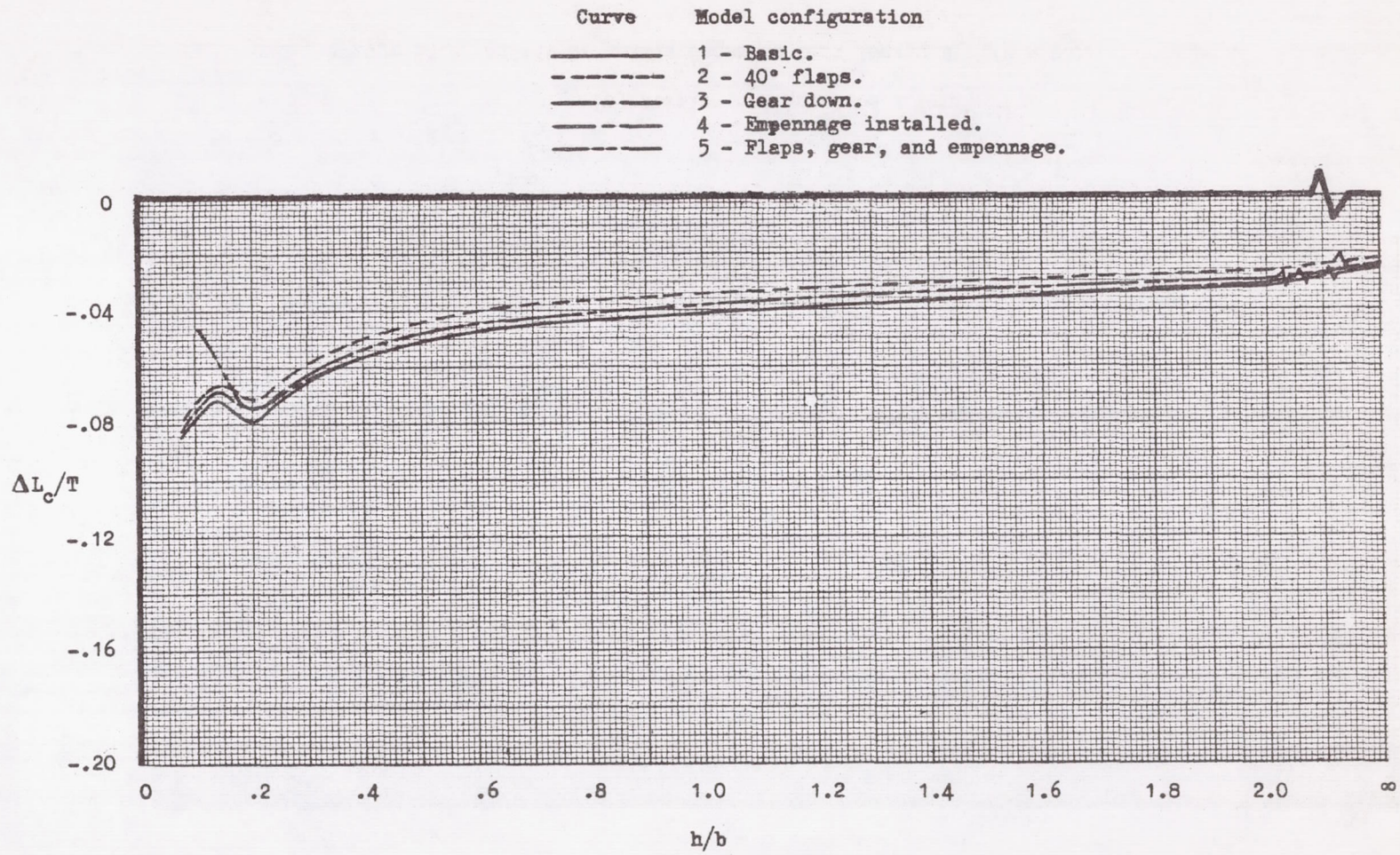

Figure 53.- Effect of airframe components on lift loss. Nozzle configuration 2; $P_{t,n}/P = 2.0$.

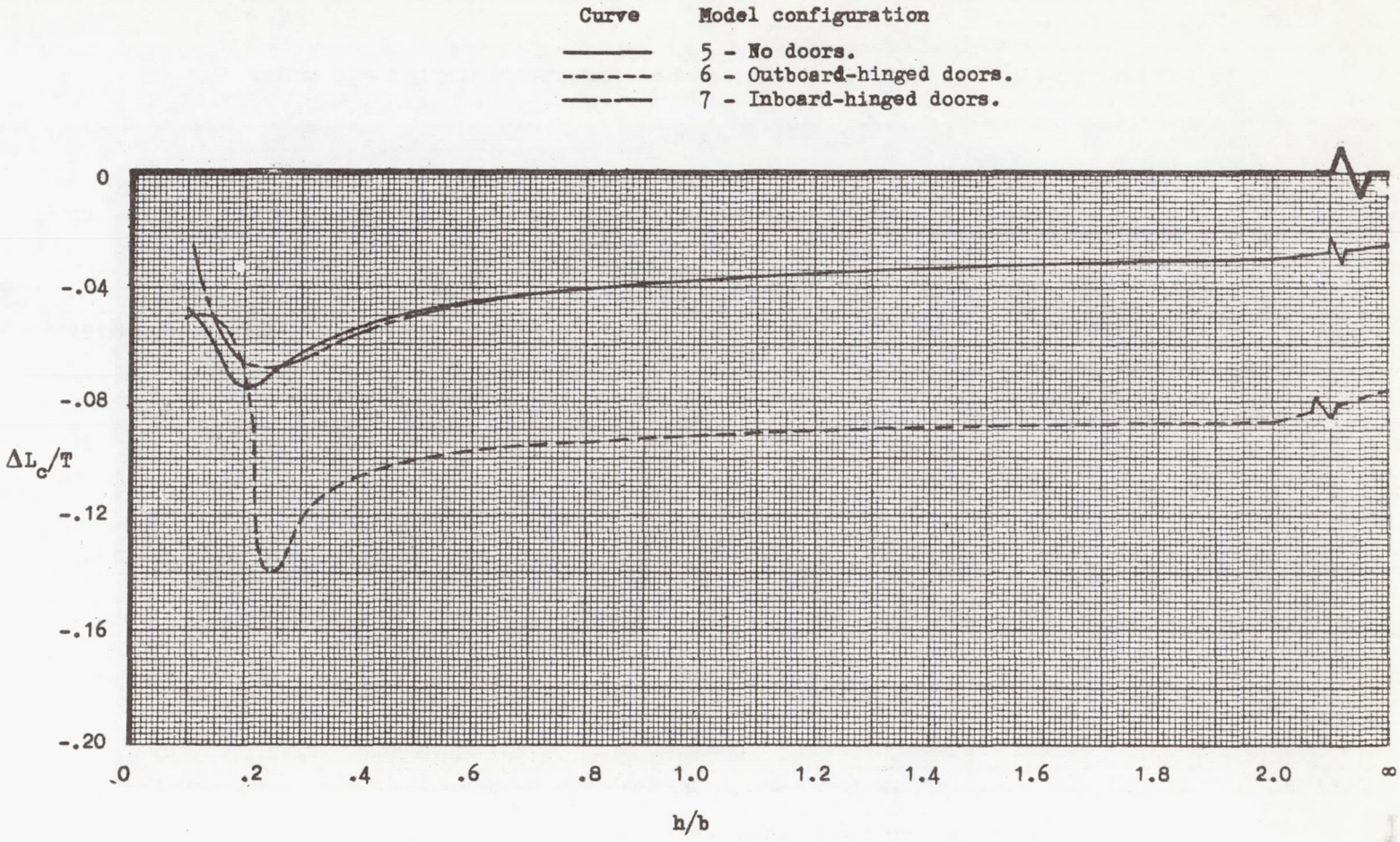

(a) Nozzle configuration 2.

Figure 54.- Effect of nozzle doors on lift loss. $P_{t,n}/P = 2.0$.

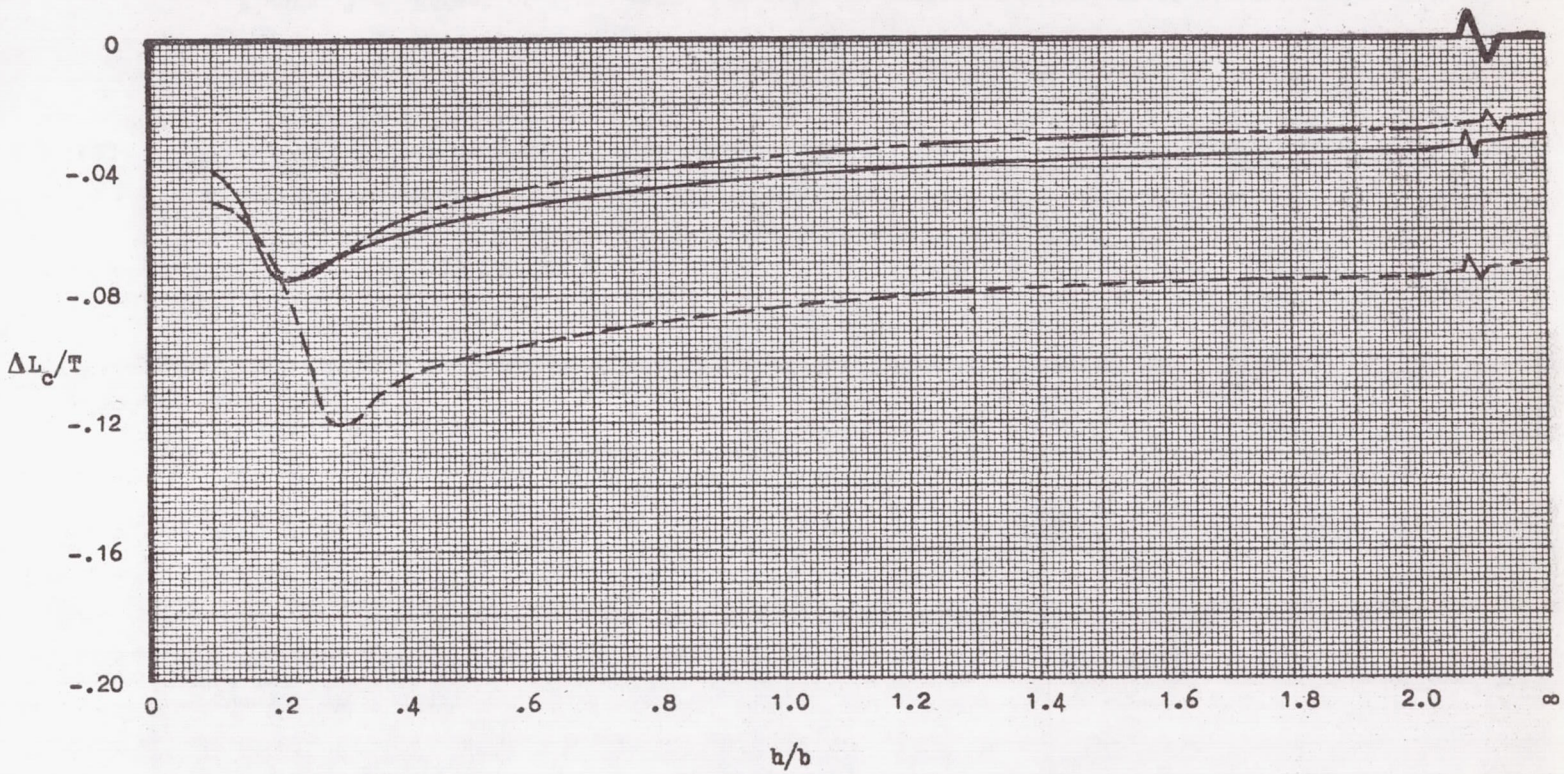

(b) Nozzle configuration 8.

Figure 54.- Concluded.

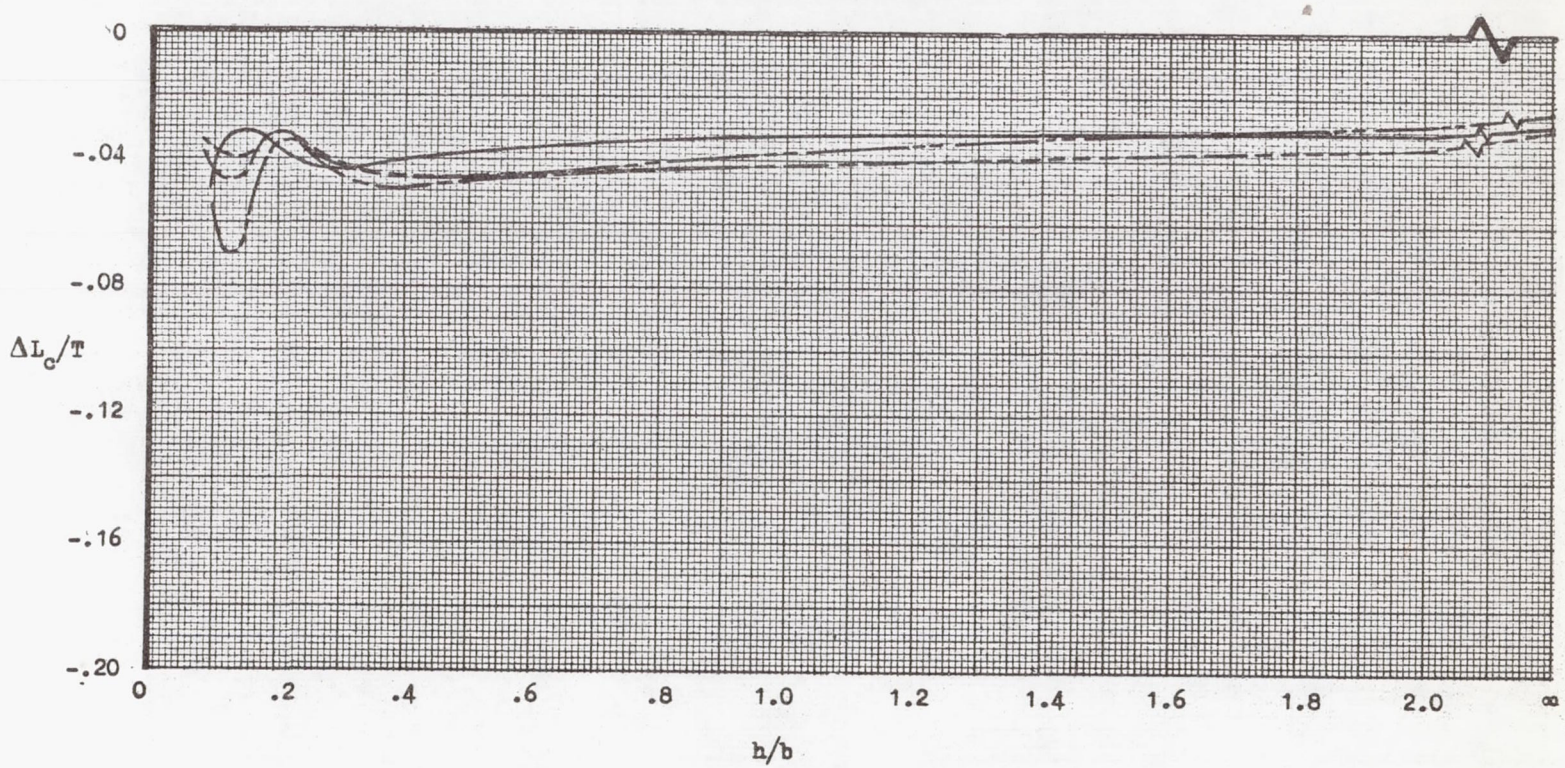

Figure 55.- Effect of flap, gear, and door deployment on lift loss of complete aircraft. Nozzle configuration 21; $P_{t,n}/P = 2.0$.

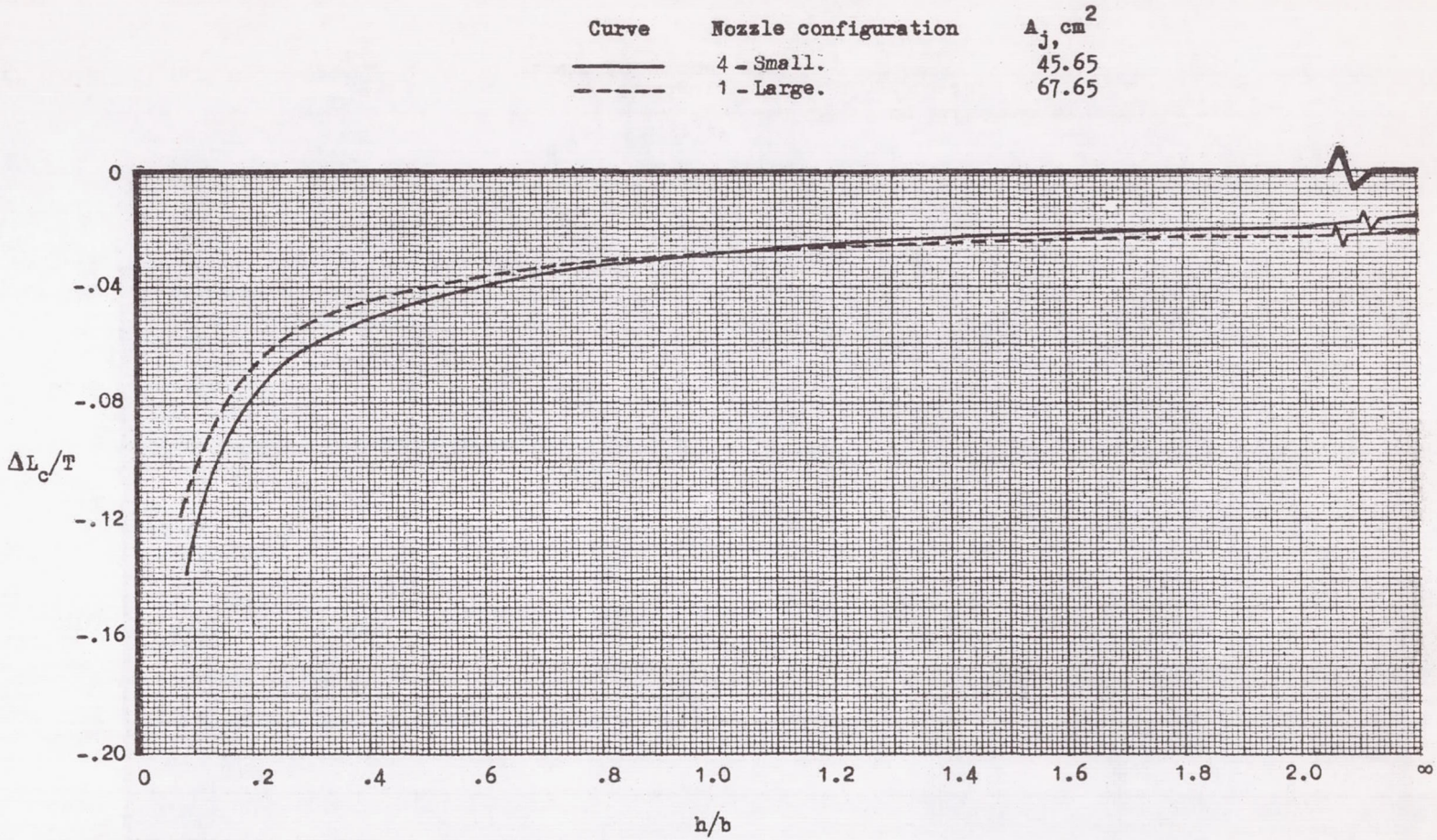

(a) 4 nozzles.

Figure 56.- Effect of total nozzle area on lift loss. Model configuration 1; $P_{t,n}/P = 2.0$.

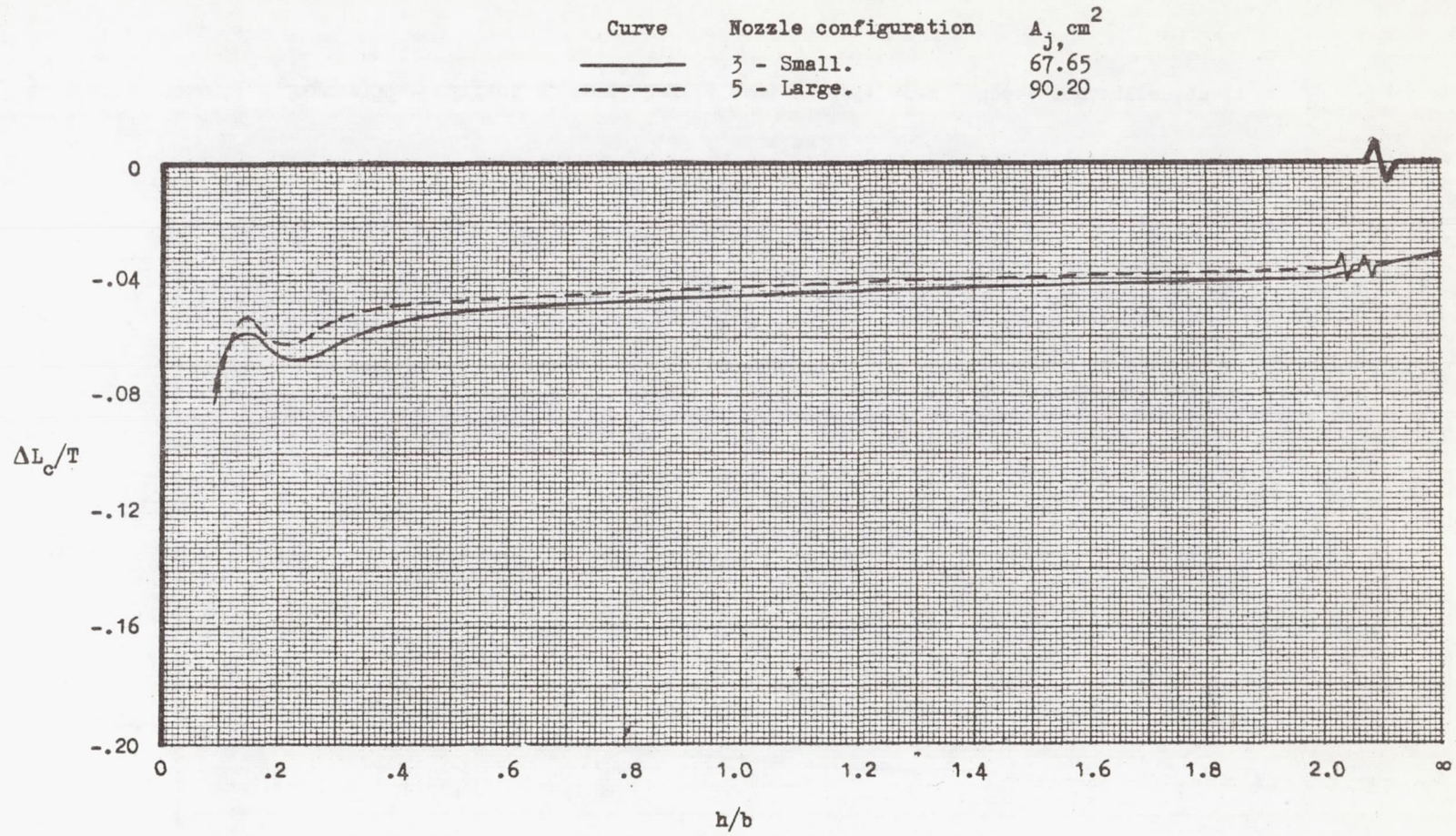

(b) 8 nozzles.

Figure 56.- Concluded.

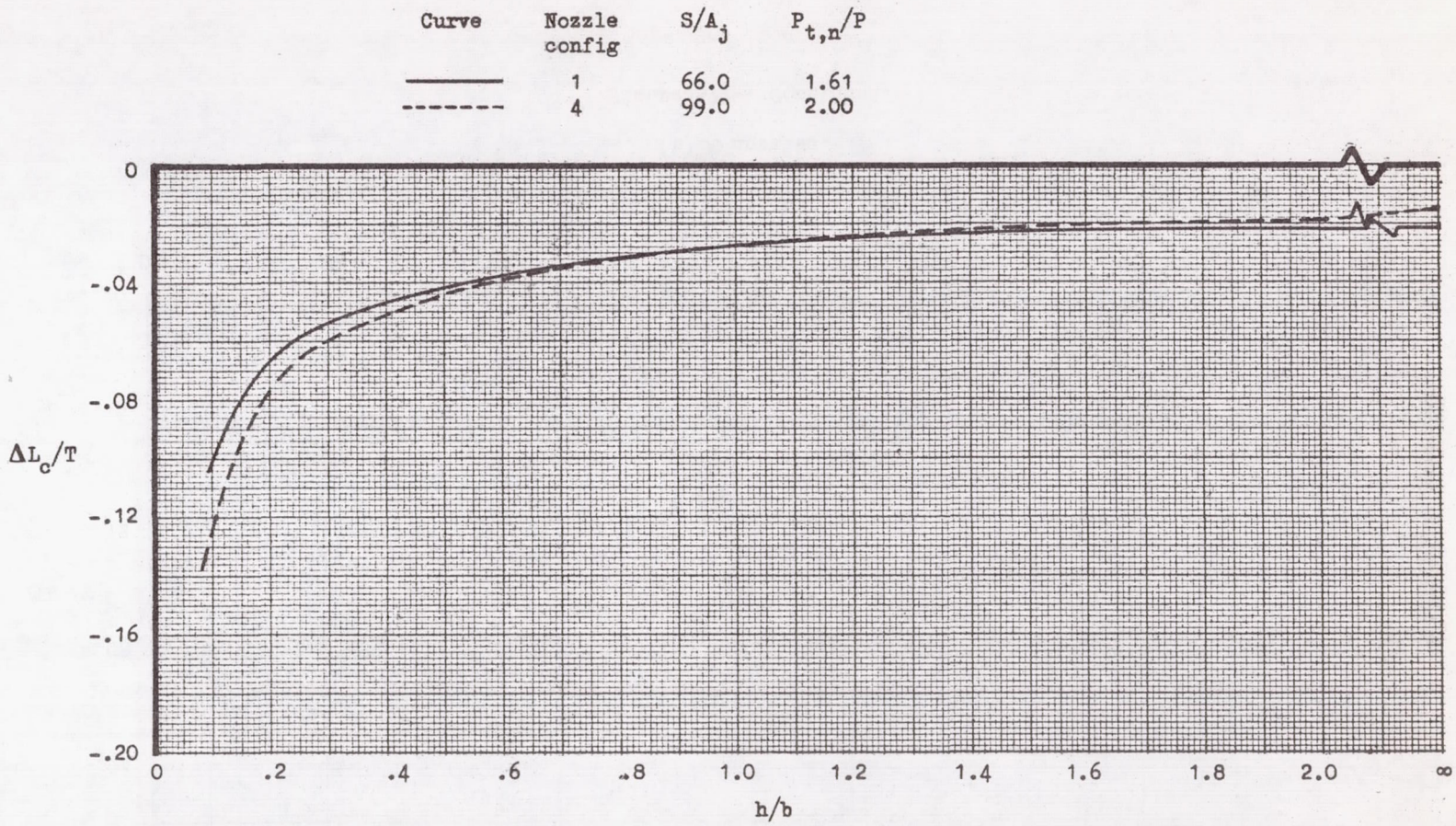

(a) 4 nozzles.

Figure 57.- Effect of pressure ratio on lift loss at constant thrust. Model configuration 1.

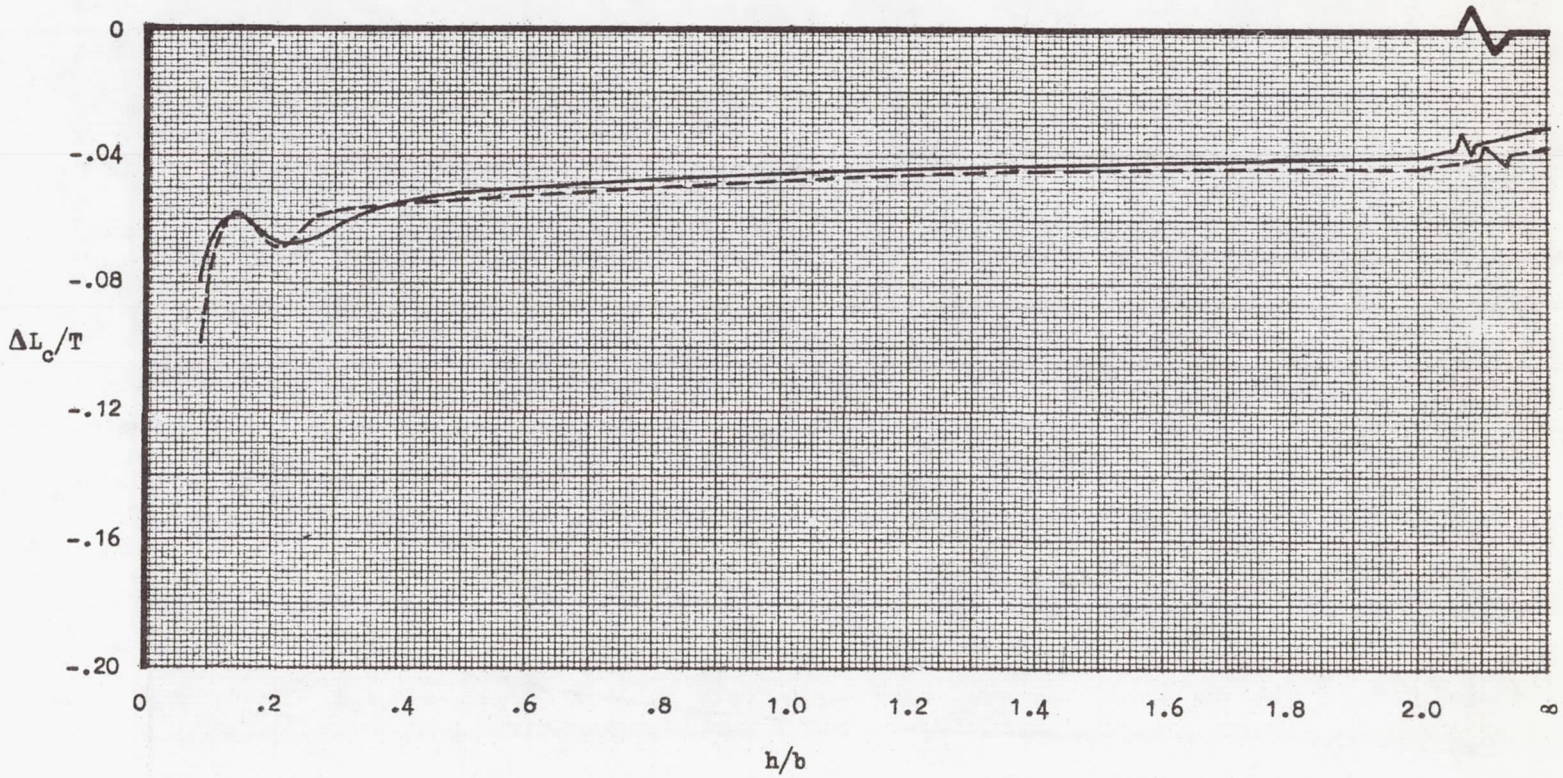

(b) 8 nozzles.

Figure 57.- Concluded.

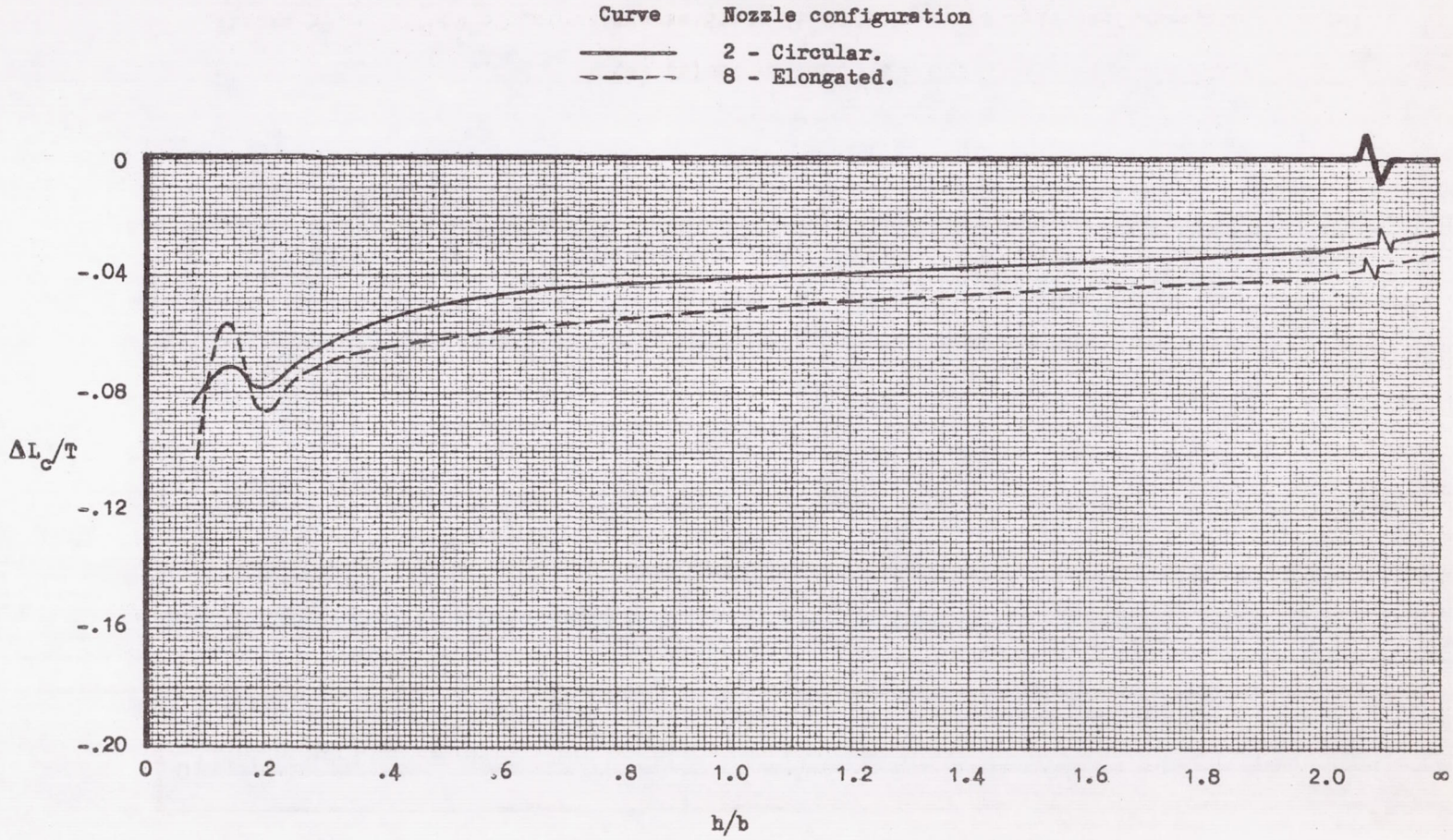

Figure 58.- Effect of nozzle aspect ratio on lift loss. Model configuration 1: ~~$P_{t,n}/P = 2.0$.~~

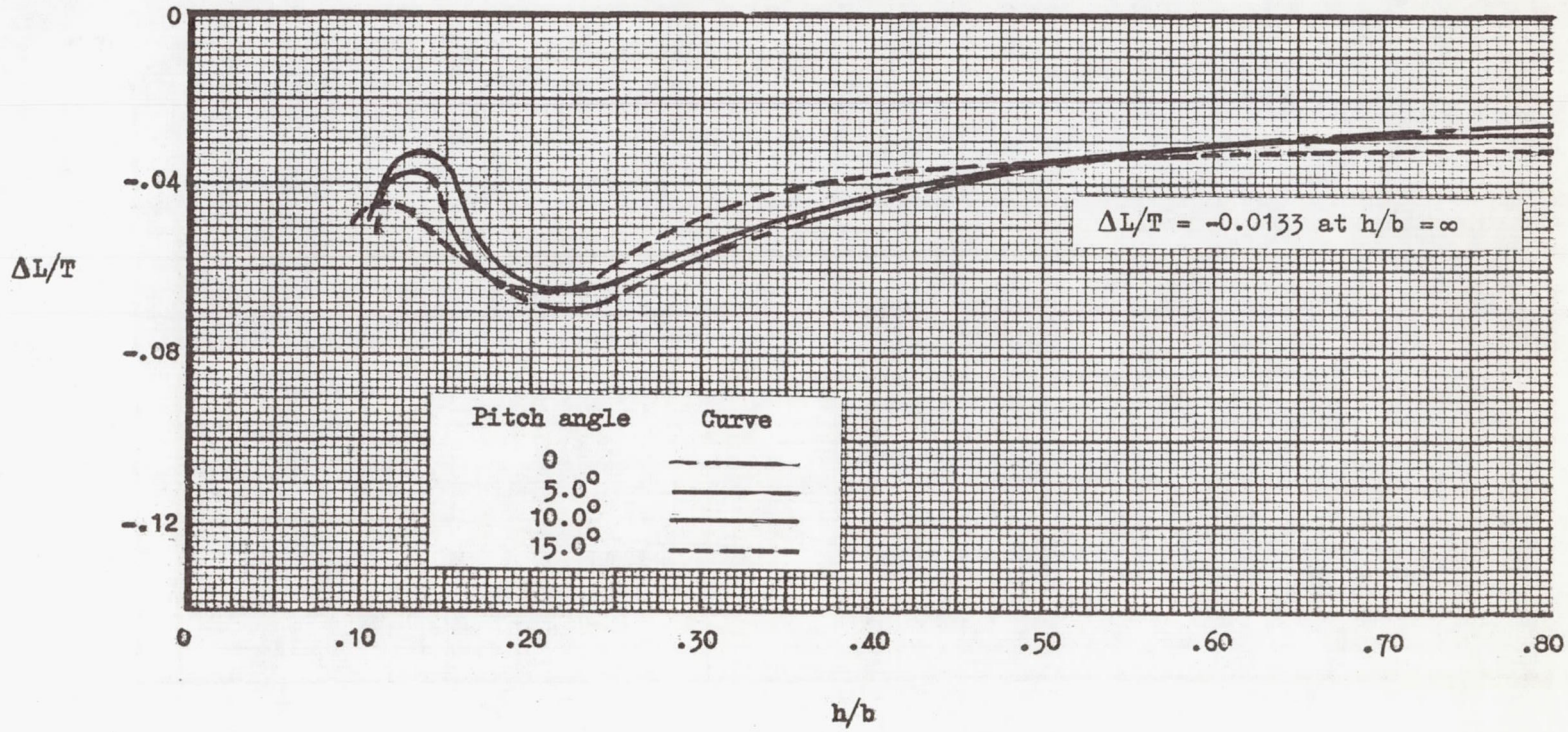

(a) Effect of α; $\phi = 0°$.

Figure 59.- Effect of height and attitude on lift loss. Nozzle configuration 8; model configuration 7; $P_{t,n}/P = 2.0$.

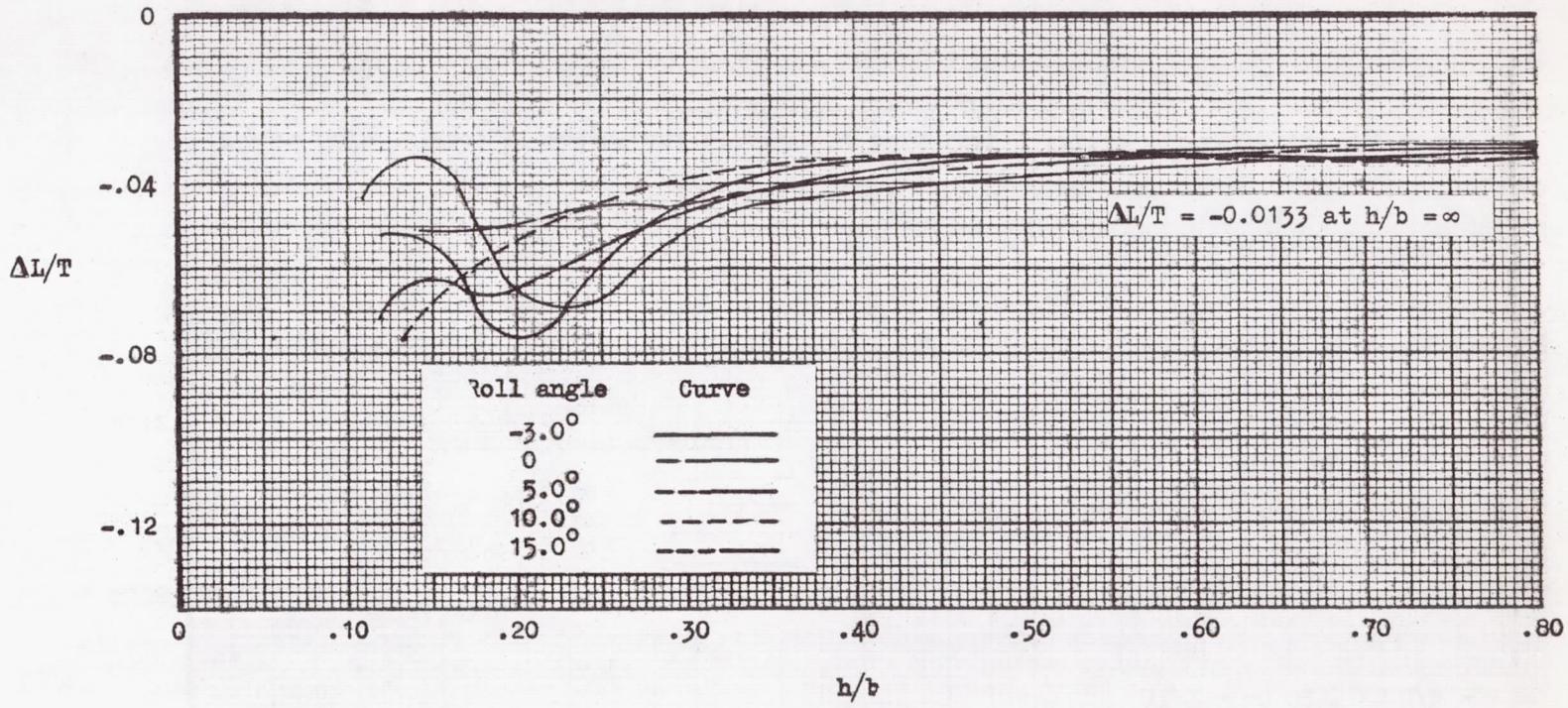

(b) Effect of ϕ; $\alpha = 10°$.

Figure 59.- Concluded.

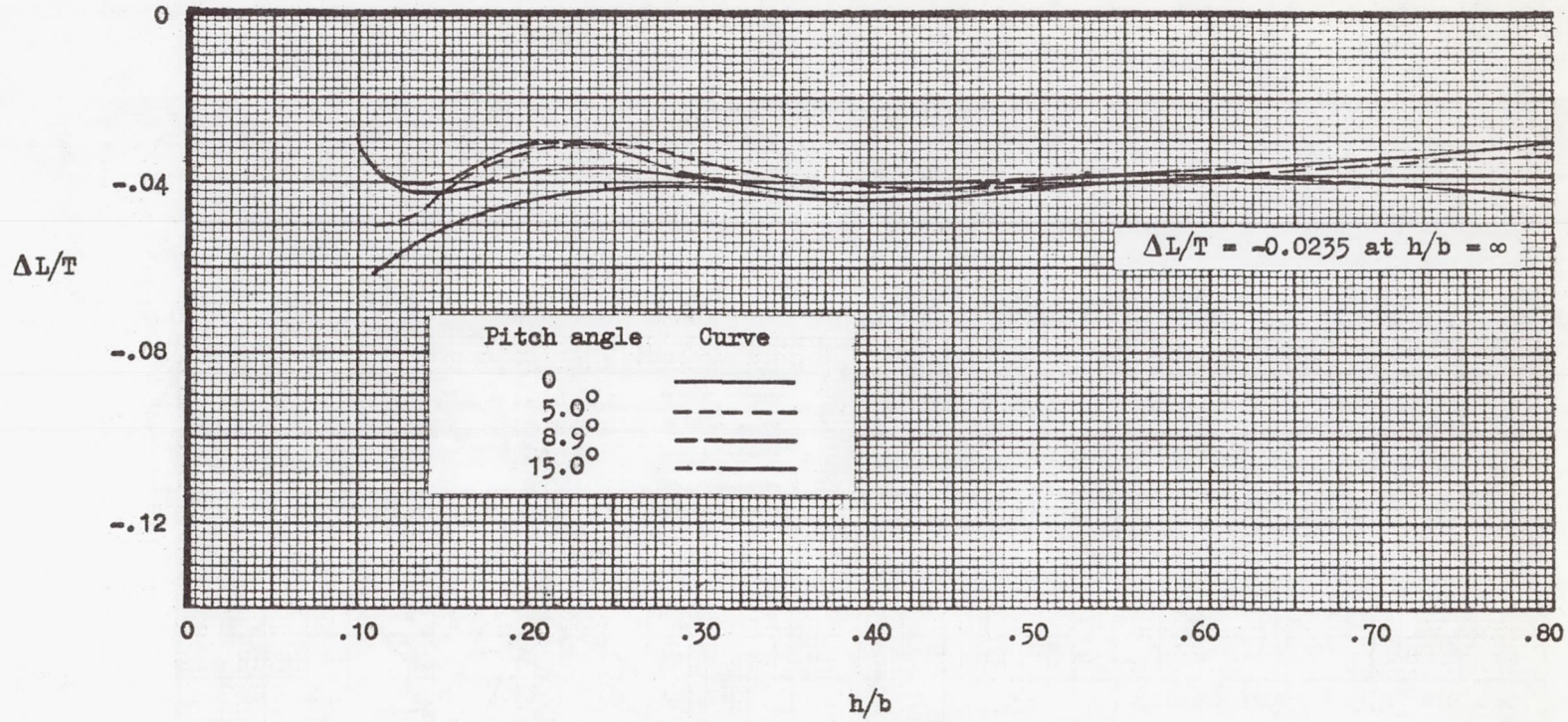

(a) Effect of α; $\phi = 0°$.

Figure 60.- Effect of height and attitude on lift loss. Nozzle configuration 21; model configuration 7; $P_{t,n}/P = 2.0$.

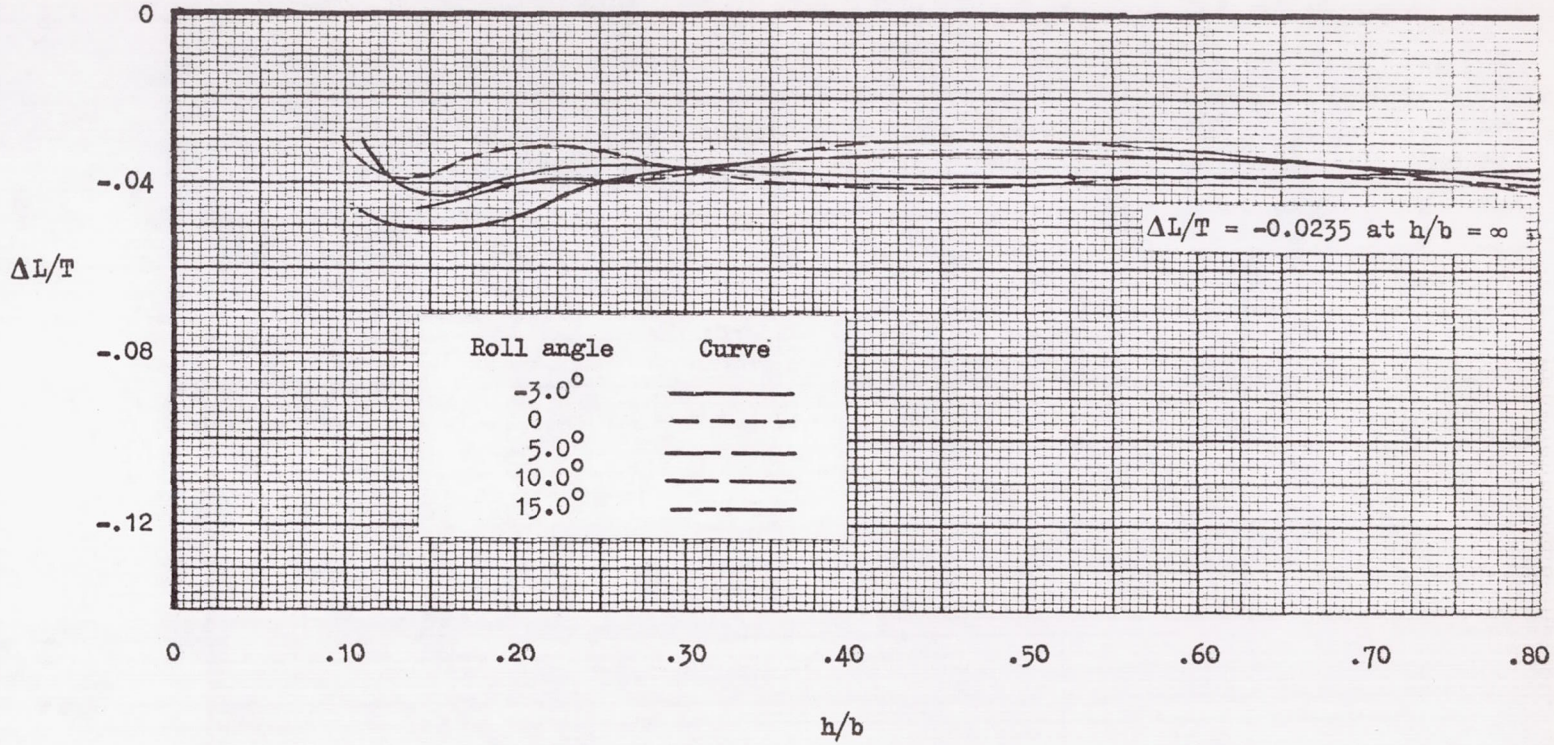

(b) Effect of ϕ; $\alpha = 8.9°$.

Figure 60.- Concluded.

NASA-Langley, 1969 —— 1